Heft 50
Neubiberg, 1997

Geodetic Activities
Juneau Icefield, Alaska
1981 - 1996

Edited by
Walter M. Welsch,
Martin Lang
and
Maynard M. Miller

SCHRIFTENREIHE

STUDIENGANG VERMESSUNGSWESEN
UNIVERSITÄT DER BUNDESWEHR MÜNCHEN

Heft 50
Neubiberg, 1997

Geodetic Activities
Juneau Icefield, Alaska
1981 - 1996

Edited by
Walter M. Welsch,
Martin Lang
and
Maynard M. Miller

SCHRIFTENREIHE

STUDIENGANG VERMESSUNGSWESEN
UNIVERSITÄT DER BUNDESWEHR MÜNCHEN

Printing was founded by:

- *Universität der Bundeswehr München, Neubiberg*
- *Amt für Militärisches Geowesen, Euskirchen*
- *Arbeitsgemeinschaft für Vergleichende Hochgebirgsforschung, München*

Number of Copies: 350

Produced at the Institut für Geodäsie der Universität der Bundeswehr München

Test processing: *Uwe G. F. Kleim, Martin Lang*

Desktop Publishing: *Uwe G. F. Kleim*

Graphic and cartographic processing: *Uwe G. F. Kleim, Tamas Nagy*

Reproduction techniques: *Amt für Militärisches Geowesen,*
Ernst Gradischnig, Uwe G. F. Kleim

Print: *Universitätsdruckerei der Universität der Bundeswehr München, Neubiberg*
Amt für Militärisches Geowesen, Euskirchen

Responsibility for the publication series:
The Vice Dean Studiengang Vermessungswesen
der Universität der Bundeswehr München

Suppliers:

Universität der Bundeswehr München
Fakultät für Bauingenieur- und Vermessungswesen
Studiengang Vermessungswesen

D-85577 Neubiberg

ISSN 0173 - 1009

Table of Contents

Appendices

Preface 1

The Juneau Icefield Research Program (JIRP) was organized in 1946 to pursue long-term research on interrelationships of scientific disciplines necessary to understand the total environment of arctic and mountain regions. The Summer Institute of Glaciological and Arctic Sciences was organized in 1959 to provide combined academic and field training, both at the graduate and undergraduate level, so essential to the solution of these multivariate problems. The aim is total systems competence in potential polar and mountain scientists and practical field training for geologists, hydrologists, geophysicists, atmospheric scientists, resource planners, ecologists, and – last but not least – surveyors. The program is in cooperation between the University of Idaho's Glaciological and Arctic Sciences Institute and the Foundation for Glacial and Environmental Research, Juneau, Alaska. The environmental science aspect is cooperative with the University of Alaska and the University of Idaho.

In a two months period (July and August) students have the opportunity to observe and study dynamic geo-processes in a region of existing glaciers and rugged mountain terrain, and to appreciate the inter-science investigational approach in the field studies appicable not only to pristine wilderness regions but to scientific assessments of environmental problems even in rural and urban areas. Participants attend lectures at pertinent field sites, participate in demonstrations with instruments and materials in the field, and take and record scientific measurements under supervision or via their own scientific competence as part of long-range research from high-elevation and continental periglacial areas to low-level temperate and maritime regions.

The Institute of Geodesy of the Bundeswehr University in Munich, Germany, joined the Juneau Icefield Research Program in 1981. Since then members of this institute and of other co-operative institutions have taken care of the scientific and practical field training in geodesy and surveying. The scientists and field instructors participated in the program are listed in Table 1.

From 1988 on (with the exception of 1995) *Scott McGee*, US Fish and Wildlife Service and Foundation for Glacial and Environmental Research, has supported the surveying work and the students' field training. The surveying program conducted by these scientists and the students interested in surveying work has covered a variety of subjects. The yearly repeated main task has been monitoring the surface velocities of some of the major glaciers of the Taku-Llewellyn glacier system at distinguished cross-glacier profiles mainly in the vicinity of Camp 10 and Camp 18. Glacier flow velocities can be used for different purposes. It is interesting to study the flow rates as such, to compare the velocity profiles of

Table 1: Scientists and field instructors participated in the Juneau Icefield Research Programm

Year	Name
1981	Prof. Dr.-Ing. *W. M. Welsch* [1)]
1982	Dipl.-Ing. *H. Rentsch* [2)]
1983	Prof. Dr.-Ing. *H. Rüther* [3)] Prof. Dr.-Ing. *W. M. Welsch* [1)]
1985	Dr.-Ing. *H. Heister* [1)] Prof. Dr.-Ing. *W. M. Welsch* [1)] Dipl.-Ing. *H. Rentsch* [2)] *M. Welsch*
1986	Dipl.-Ing. *N. Kersting* [1)]
1987	Dipl.-Ing. *K. Blachnitzky* [4)]
1988	Dipl.-Ing. *K. Blachnitzky (†)* [4)] Prof. Dr.-Ing. *W. M. Welsch* [1)]
1989	Dipl.-Ing. *M. Lang* [1)]
1990	Dr.-Ing. *H. Heister* [1)] Prof. Dr.-Ing. *W. M. Welsch* [1)] Prof. Dr. *H. Papo* [5)]
1991	Dipl.-Ing. *M. Lang* [1)]
1992	Prof. Dr.-Ing. *W. M. Welsch* [1)]
1993	Dr.-Ing. *C. Heipke* [6)] Dipl.-Ing. *M. Lang* [1)]
1994	Dipl.-Ing. *D. Beineke* [7)]
1995	Dipl.-Ing. *M. Lang* [1)] Prof. Dr. *H. Papo* [5)]
1996	Prof. Dr.-Ing. *W. M. Welsch* [1)]
1997	Dipl.-Ing. *M. Lang* [1)]

1) Bundeswehr University Munich, Germany
Institute of Geodesy
2) Bavarian Academy of Sciences, Munich, Germany
Commission for Glaciology
3) University of Cape Town, Rondebosch, South Africa
4) Bavarian Ordnance Survey, Munich, Germany
5) Israel Institute of Technology, Haifa, Israel
6) Technical University Munich, Germany
Institute of Photogrammetry
7) Bundeswehr University Munich, Germany
Institute of Photogrammetry and Cartography

different glaciers, to draw conclusions from their diversity, and to find clues from the alterations of the flow patterns over the years as to the reaction of the glaciers due to climatic changes. The velocity profiles were also applied to support and to calibrate a dynamic glacier model of Taku Glacier. Based on the flow law of glaciers developed by glaciologists and glaciophysicists mass flow rates were calculated as a contribution to the mass balance of the profiles; from principal strain rates stresses were derived and correlated with the crevasse patterns of the glaciers' surface.

The technique applied was polar point positioning and intersection by theodolite and electronic distance measurements. As reference frames local networks were established around the camps. Attempts were made to interconnect these individual, isolated networks with each other. However, in the circumstances given the trials were not successful. The whole situation changes drastically when the surveying work was supported by satellite aided measurements. From 1992 on the radio signals of the Global Positioning System (GPS) were used for all kinds of surveying tasks. Surveying, observations as well as calculations, became much more enjoyable, no longer so tedious for the students (and the supervisors), the work was pushed ahead, weather was no longer an obstacle. If with terrestrial means half a dozen of profiles, consisting of some 80 points or so, could be observed and evaluated in a two or three weeks period, now up to or even more than 300 points were

measured within ten days. The progress is more than amazing, it's fascinating! Especially real time applications speed up the operations. Apart from the new momentum, real time GPS has still more advantages to offer. It is now possible to find exactly the point positions of the last year's survey poles in no time, one can place a GPS receiver on the glacier's surface and literally watch the glacier moving – and even prove whether the glacier moves smoothly of by jerks. With the help of a helicopter the badly broken ice of the Taku terminus can be stepped on and recorded in much shorter time and much more accurately than it could before by terrestrial means. It has been easy to interconnect the local survey points around the camps to an overall network covering the whole icefield and even to integrate this network to the global network system of the International Geodynamic Service (IGS) making use of the Internet to get hold of the observations of permanent GPS-station as remote as Yellow Knife (Northwest Territories, Canada), Fairbanks (Alaska, USA), and Penticton (British Columbia, Canada). The new possibilities this high-tech surveying has to offer contribute much to an enjoyable and successful work for everybody involved.

A specific problem has always been to record the high-rate velocity of the inaccessible Vaughan-Lewis Icefall near Camp 18. The only reasonable solution could be achieved by applying terrestrial photogrammetry. This technique was also used for other unique tasks like monitoring the loss of volume of Lake Linda which uses to drain off all the sudden every year, or to sketch the pattern of the crevasses of Gilkey Glacier.

The publication in hand contains contributions about Alaska and the Juneau Icefield Program as an introductory information in general as well as some basic treaties on the phenomenon and the geodetic analysis of glacier flow for a better understanding of specific theoretical aspects. The main part documents essential results of the geodetic measurements carried out over the years as a source for further investigations by other disciplines involved in glaciological research. Some of the articles are reprints of former publications in scientific periodicals, some others are especially prepared for this booklet. The reader may consider that most of the observations were carried out by students not too familiar with geodesy and surveying but always eager to learn and ready for fieldwork and action. The work could not have been carried out without them.

We wish to dedicate this publication to our friend and colleague Dipl.-Ing. *Klaus Blachnitzky* who lost his live on the Icefield in fulfillment of his dedication to science and education.

The editors

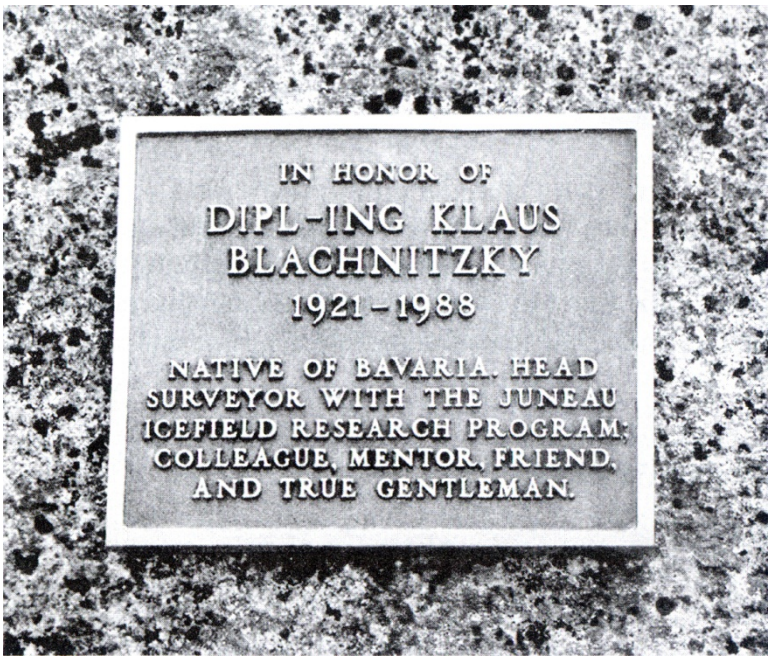

Preface 2

The motto of the Juneau Icefield Research Program is *„Books – Nature – Action"*. It describes completely how the founder and promoter of this unique project, Prof. Dr. *Maynard M. Miller*, thinks geo-sciences should be performed. The combination of the three elements is the previous way of learning and teaching. It is perfected on the Icefield. We are grateful to Prof. *Miller* that he has provided the opportunity for us to participate in this valuable kind of academic education.

We feel also indepted to his wife, Mrs. *Joan Miller*, who has supported us in many invaluable ways over all the years. But not only us – she has supported *Mal* and the whole program, too. *„We couldn't do without Joan. She is our official greeter, front office, purchasing agent, secretary-administrator, diplomatic liaison with the Air National Guard and the Governor's office, and a host of other things", Mal* says. *Joan* is the *„soul"* of the program.

Martin Lang
Walter M. Welsch

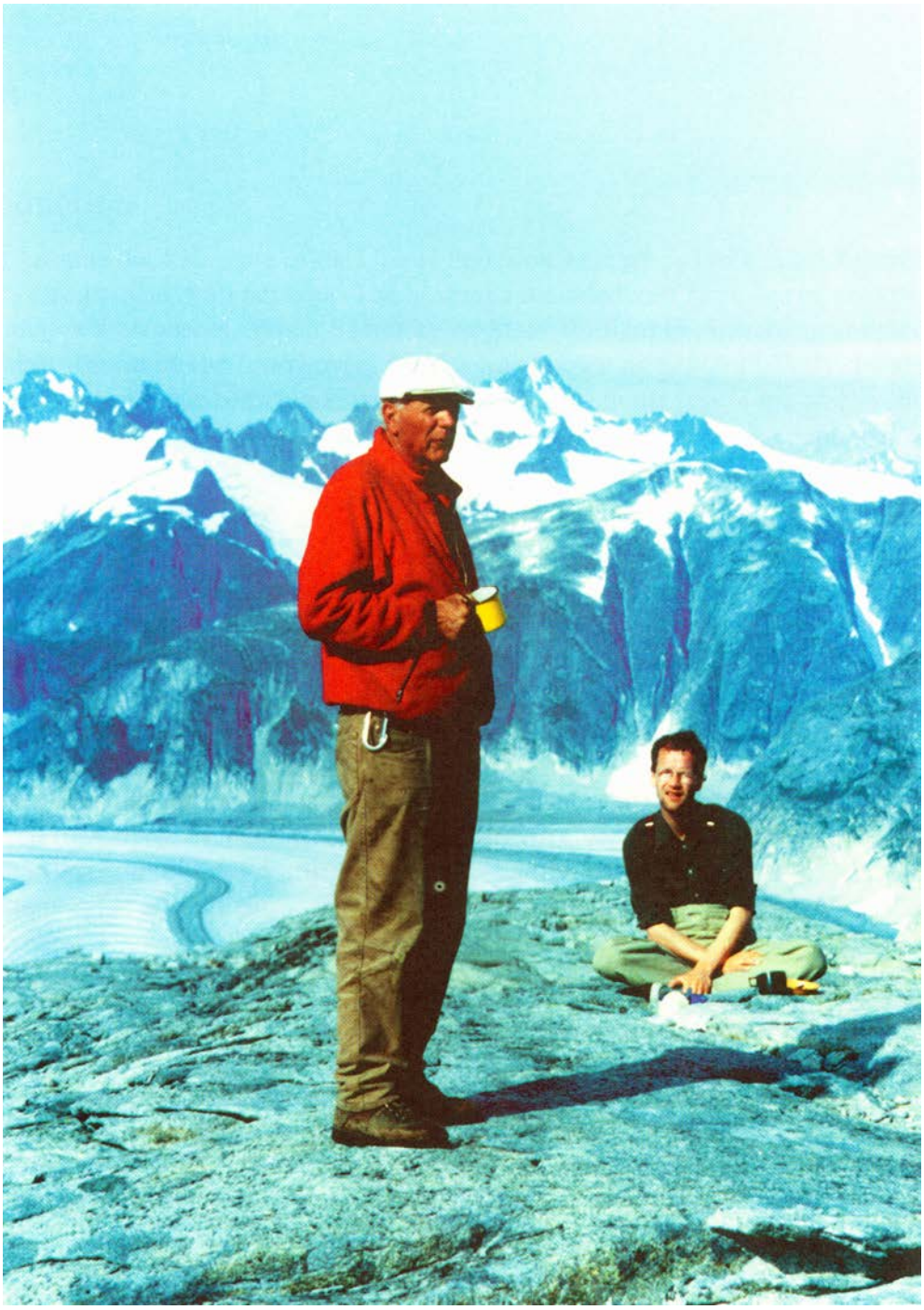

Photo M. Lang, 1993

M. M. Miller

Maynard M. Miller

Alaska [1)]

1. Introduction

When it became the 49th state of the United States on January 3, 1959, Alaska increased the nation‘s size by nearly 20 per cent. The new area included vast stretches of unexplored land and untapped resources. When Secretary of State William H. Seward negotiated its purchase from Russia in 1867, however, Alaska was known as Seward's Folly. Its settlement and exploitation have been hindered by its distance from the rest of the nation and by geographic and climatic impediments to travel and communications; Alaska continues to be the country‘s last frontier. More than half of the state‘s inhabitants live in the Greater Anchorage area. The capital is Juneau, 922 kilometers to the southeast in the panhandle region.

Alaska lies at the extreme northwest of the North American continent and is the largest peninsula on the Western Hemisphere. Its 1,530,700 square kilometers include some 38,830 square kilometers of fjords and inlets, and its three faces to the sea have about 54,400 kilometers of indented tidal coastline and 10,620 total kilometers of coast fronting the open sea. It borders the Arctic Ocean on the north and northwest, the Bering Strait and the Bering Sea on the west, and the Pacific Ocean and Gulf of Alaska on the south. The land boundaries on the east cut across some 1,850 kilometers of high mountains to separate the state from the Canadian Yukon Territory and British Columbia province. Rimming the state on the south is one of the Earth‘s most active earthquake belts. In the Alaska Range north of Anchorage, Mount McKinley (Denali), at 6,194 meters, is the highest peak in North America.

The question of development versus preservation has been heightened by commercial and ecological uses of land: the Alaska Highway gas-pipeline project, native Alaskans‘ land claims, noncommercial whaling by native peoples, and related matters. The conflicts between conservationists and petroleum companies over the Trans-Alaska Pipeline, which runs from the oil-rich North Slope on the Arctic Ocean to Valdez in the south, was a continuation of the century-long effort to find a balance between conservation and development in this enormous land.

2. Physical and Human Geography

2.1 The Land

The immense area of Alaska has a great variety of physical characteristics. Nearly one-third of the state lies within the Arctic Circle and has perennially frozen ground (permafrost) and treeless tundra. The southern coast and the panhandle at sea level are fully temperate regions. In these latter and in the adjoining Canadian areas, however, lies the world‘s largest expanse of glacial ice outside Greenland and Antarctica. Off the extreme western end

[1)] Encyclopaedia Britannica, 15th Edition, Vol. 29, Encyclopaedia Britannica International, London *[1990];* p. 188 and p. 431-435

of the Seward Peninsula, Little Diomede Island, part of Alaska, lies in the Bering Strait only 4 kilometers from Soviet-owned Big Diomede Island; both countries have shown a tacit tolerance of unintentional airspace violations, which are common in bad weather.

2.1.1 Relief

Alaska is composed of nine distinct physiographic and environmental regions. Much of the mainland panhandle region, a narrow strip of land 40 to 80 kilometers wide lying east and south of the St. Elias Mountains, is composed of the Boundary Ranges. There are several large icefields, and the peaks include Mount St. Elias (5,491 meters), from whose summit the Alaska-Yukon border swings due north. The western extension of this mountain chain is the Chugach Range, a giant arc at the northern-most edge of the Gulf of Alaska. Many remote valleys and high ridges are still unexplored, and the relief and glaciation inhibit exploitation. The coast is characterized by frequent and intense oceanic storm systems that have produced dense rain forests on the coastal mountain flanks. In the valleys rivers produce devastating annual floods often associated with excessive snowmelt and glacial meltwaters.

The region of the south coastal archipelago and the Gulf of Alaska islands includes the Alexander Archipelaga in the panhandle region, with 11,000 islands, plus Kodiak Island and its satellites south of Cook Inlet. These islands, extensions of the southern region, are lower, less rugged, and less glaciated. All receive heavy rain and are affected by waters warmed by the Kuroshio Current.

The Aleutian region includes the narrow Alaska Peninsula, which forms the south shoreline of Bristol Bay, and the 1,770-kilometer-long Aleutian chain that separates the North Pacific from the Bering Sea. The chain includes 14 large islands, 55 significant but smaller ones, and thousands of islets. The largest are Unimak, Unalaska, and Umnak. On the occasionally clear summer days, active volcanoes and such glacier-covered peaks as symmetrical Shishaldin Volcano (2,857 meters) on Unimak can be seen. Such magnificent views represent the Aleutians at their scenic best. Usually, however, the weather is wet and stormy, the winds horizontal and cutting, and the first fog all-pervading.

The broad Alaska Range region connects the Aleutian Range across the southern third of mainland Alaska to the Wrangell Mountains, which abut against the vast complex of the St. Elias Mountains. The Wrangell Mountains have large active volcanoes and high valley glaciers. The flanks of this subarctic range are largely tundra-covered.

The low-lying interior basin region between the Alaska Range in the north and the Chugach-Wrangell-St. Elias mountains to the south and east enjoys a relatively temperate climate. The lower valleys contain good farmlands, and it is there that most of the people of Alaska live.

The central plains and tablelands of interior Alaska constitute a vast region west and north of the Alaska Range; they reach as far north as the Brooks Range. The area is rolling and dissected by numerous streams tributary to the Yukon and Kuskokwim rivers. The plains extend from the Canadian border to Norton Sound, the Seward Peninsula, the Yukon delta, and south to the northern rim of Bristol Bay on the Bering Sea. The region is characterized by river flats and truncated upland tablelands. With abundant game, it is an important nesting ground for waterfowl, including great numbers of migrating birds.

A major mountain chain running west to east in the area north of the central plains and extending from the sea nearly to the Yukon border, the Brooks Range gradually slopes


ALASKA
ARCTIC OCEAN
BEAUFORT SEA
CHUKCHI SEA
BERING SEA
BRISTOL BAY
GULF OF ALASKA
PACIFIC OCEAN
RUSSIA
UNITED STATES
CANADA
YUKON TERRITORY
Barrow
Point Hope
Prudhoe Bay
Kotzebue
Nome
Teller
Taylor
Council
Galena
Ruby
Tanana
Fort Yukon
Circle
Hot Springs
Manley
Fairbanks
Eagle
Ophir
Rampart
Kantishna
McGrath
Bethel
Delta Junction
Dawson City
Denali
Talkeetna
Glennallen
Anchorage
Palmer
Valdez
McCarthy
Kenai
Hope
Whittier
Cordova
Seward
Homer
Seldovia
Togiak
Dillingham
Aleknagik
Naknek
King Salmon
Pedro Bay
Port Lions
Kodiak
KODIAK ISLAND
ALASKA PENINSULA
Chignik
Sand Point
Yakutat
Haines
Skagway
Juneau
Hoonah
Tenakee
Sitka
Kake
Petersburg
Wrangell
Klawock
Hollis
Ketchikan
Hyder
Inuvik
Fort McPherson
Carmacks
Whitehorse
QUEEN CHARLOTTE ISLANDS
N
1"
0
160 miles
Scale of Miles

ALASKA

northward to a narrow linear coastal plain bordering the Arctic Ocean and westward to lower hills north of Kotzebue Sound. There are few high Arctic glaciers, and the area is semiarid. The lower flanks and valleys are tundra-covered, with permafrost features.

The coastal lowland north of the Brooks Range, sometimes called the North Slope, is the home of great herds of caribou. The environment is truly polar, with the sea waters along the coast frozen eight months of the year and the ground permanently frozen except for a thin zone of summer melting. It is treeless, and, in summer, grasses and Arctic alpine flowers abound. The National Petroleum Reserve-Alaska is located in the western sector, while the Prudhoe Bay oil fields and part of the Arctic National Wildlife Refuge occupy the eastern sector.

The islands of the Bering Sea represent a small but unique Arctic maritime environment, typified by St. Lawrence, Nunivak, and St. Matthew islands and the Pribilof group. These tundra-covered islands are surrounded by sea ice in winter and serve as protected refuges for the world‘s largest herds of fur-bearing seals and sea otters, as well as sea lions and walrus. A large herd of domesticated reindeer is tended by Eskimos on Nunivak Island.

2.1.2 Climates

Five general climatic zones may be delineated in Alaska, excluding the great mountain ranges.

Southern coastal and southeastern Alaska, the Gulf of Alaska islands, and the Aleutians have average temperature ranges in the summer of 4° to 16°C and in the winter of 4° to -7°C. Rainfall varies locally from 1,525 to 4,065 millimeters, and the panhandle and southern islands are covered with Sitka spruce, hemlock, and other evergreens. The Cordova-Valdez region and parts of the west central panhandle have the state‘s highest precipitation, 5,100 millimeters or more. At Valdez 5,100 millimeters of snow is not uncommon. Precapitation is less in the Aleutians, but even there about 250 rainy days occur annually.

The interior basin ranges from 7° to 24°C in summer and -7° to -23°C in winter. The region is drier than the coast and only slightly colder in winter, with Anchorage receiving about 635 millimeters of precipitation annually. The pleasant conditions and proximity to the sea have helped to make the area the centre of the state‘s population.

The islands and coast of the Bering Sea have summer temperatures of 4° to 24°C and winter temperatures of -7° to -23°C. Tempering influences of the Pacific dissipate north of the Pribilof Islands, and Arctic sea ice often reaches this area.

The central plains and uplands range from 7° to 24°C in the summer and -23° to -34°C in the winter. Average rainfall is 255 to 510 millimeters, though less than 255 millimeters is common.

The ameliorating effects of the Arctic Ocean keep temperatures of the North Slope at 2° to 13°C in the summer and -21° to -29°C in the winter – less severe than those of the interior plains. About 130 millimeters of precipitation nonetheless remain on the ground as snow for some eight months of the year. The 24-hour sunlight of summer can produce strong buildups of radiant energy, sending temperatures to 32°C. The deep chill of winter, however, maintains the permafrost character of the High Arctic zone. Ice clogs the northern coast nine months of the year, while ice fog frequently extends southward to Fairbanks.

2.1.3 Settlement Patterns

A large percentage of Alaskans live in the southern interior basins araund Anchorage; most of the remainder live in the interior plains around Fairbanks or in the panhandle region, where Juneau is the major city and the administrative centre of the state. Tiny pockets of people are scattered in small villages, the most sparsely occupied being the Arctic plains, the Bering shores, and the Aleutians. Many frontier conditions persist: a male-to-female ratio of 5 to 1 in 1910 has been reduced to near equality, but in many places bars are as numerous as churches.

2.2 The People

English, Russian, Spanish, and French place-names reflect early European exploration, but equally prominent are dozens of names from the pre-Western era. The name Alaska itself is derived from the Aleut *alaska* and the Eskimo *alakshak*, both meaning „mainland".

Long before Bering's voyages the Tlingit Indians lived in the southern and southeastern coastal area; the Aleuts on the Aleutian Islands and the Alaska Peninsula; and the Eskimos on the Bering shore and the Arctic Ocean coast. The interior natives were the Tinneh Indians, whose language was Athabascan, that of the Plains Indians of the interior continent to the south. The Indian groups are presumably descendants of the earliest immigrants across the Bering Land Bridge from Asia, perhaps more than 15,000 years ago, and they reflect the migratory wave that reached as far as the southern extremity of South America as early as 10,000 years ago. Eskimos and Aleuts appear to be much later immigrants, having arrived probably in boats made of animal skins, perhaps 8,000 to 3,000 years ago. All groups have been involved in the debates and adjudications over public land grants.

The first wave of immigration from the „Lower 48" – which occurred in the decade before World War I was an aftermath of the gold rush – was a response to Alaska's initial concentration on its mineral, fish, and timber resources. The discovery of oil fields and the emergence of Alaska as an international air crossroads added impetus to the influx of the 1940s and '50s and construction of the Trans-Alaska Pipeline to that of the 1960s and '70s. By 1980 only about 20 per cent of the white population of the state was born in Alaska.

Of the current population about one-seventh are Eskimos, Aleuts, and Indians. The remaining citizenry include military personnel and their families and a melting pot of mixed American, Russian, Filipino, Japanese, Chinese, and other nationalities.

2.3 The Economy

The Alaskan economy is conditioned strongly by the state's frontierstage of development, but its formerly inadequate tax base for state and municipal growth ended with the development of the North Slope oil fields. High costs of labor and transportation and complicated environmental and land-use constraints still tend to discourage outside investment. Nonetheless, development of the state's natural resources has assisted markedly in the transition from a federal military to a commercial self-supporting economic base.

2.3.1 Government

Alaska's economy has been dominated by government since territorial days. From 1940 to 1960 the federal government invested nearly $ 2,000,000,000 in the development of

military bases in Alaska. Nothing else in Alaska‘s history has produced such long-term results, bringing thousands of residents into the territory and creating jobs and a vast array of transportation and communications facilities extending to remote corners of the state. Combined with state and local government, the defense installations continue to add much to Alaska‘s economy.

2.3.2 Agriculture

Only a small sector of Alaska‘s economy is agricultural, but a viable instate market is still under development. More than 1,200,000 hectares of tillable land are available for farming, but much clearing has yet to be done. Most acreage is near Anchorage and on the Kenai Peninsula, though there is some near Fairbanks, and stock ranching is practiced on Kodiak and Unimak islands. As a result, all farm products are sold locally, and most foods must be imported, tremendously increasing the cost of living. Closure of the Homestead Act, ending settlement of the native land claims issue, has further curtailed development of new land. In spite of a short growing season, the long hours of summer sunlight are adapted to the production of oats, barley, potatoes, hay, and cool-climate vegetables. Live-stock and greenhause crops are also successful.

2.3.3 Fishing, Forestry, and Furs

Alaska‘s most constant source of revenue is derived from fishing. Fish are found mostly in waters off the southern coasts, salmon being of especial importance. The centre of the world‘s salmon-packing industry is at Ketchikan, on Kodiak Island, and at Bristol Bay ports in the southern Bering Sea. Fleets also bring in quantities of herring, cod, pollack, and halibut, as well as Dungeness, king, and Tanner crabs. International fishing of Alaska‘s waters is regulated by the 200-mile-wide exclusive economic zone and the U.S.-Canadian Pacific Salmon Treaty (1985), which assigns ownership of fish to the country in which they spawn.

Most of Alaska‘s timber resources are in the Tongass and Chugach national forests, in the panhandle and on the southern coast, respectively. Timber is produced mainly for export to Asia, with the pulp of Ketchikan and Sitka exported to Japan.

Pribilof sealskins represent more than half of the state‘s annual fur production. Other furs, largely from controlled farms, are processed as well. The production of reindeer hides from a herd on Nunivak Island is managed by the Alaska Native Association.

2.3.4 Power

Alaska‘s immense waterpower reserve is virtually untapped. The largest project is at Lake Eklutna, near Anchorage. A hydroelectric development near Juneau delivers power to the panhandle area, and another project on the Kenai Peninsula is planned to deliver power to the central and southern regions. Most other communities depend on diesel and coal plants to produce much of the required municipal power.

2.3.5 Mining

Petroleum was first extracted and refined between 1917 and 1933, but the development of the Kenai oil field in 1961 made the petroleum and natural gas industry Alaska‘s most important mineral production. Oil seeps were known as early as the 1880s in the North Slope region, which today has become a field of major economic importance to both the state and the nation. Alaska ranks second only to Texas in oil production.

Since 1880 hard-rock ore minerals have been mined in Alaska, about 95 per cent of which yield gold, copper, zinc, and silver. Prospecting continues, with modern scientific technology and aerial exploration. The areas of maximum mineral potential lie in the panhandle, the Chugach and Alaska ranges, and the Seward Peninsula at locations unlimited by environmental regulation.

Alaska‘s gold production declined drastically after World War II, but the mining of gold especially and of zinc, silver, and lead began to rebound in the 1980s. Copper mining as a major industry ended with the closing of the Kennecott Mine in 1938, although there are new prospects elsewhere. Coal has remained an important industry. Another important activity is the extraction of sand, gravel, and clay to serve the construction industry.

2.3.6 Tourism

Alaska has had an upsurge of tourism. Travelers arrive mainly by air or sea and can now cover large areas by airplane and road. The influx is partly the result of the 500-passenger, 100-car ferries that operate as the Alaska Marine Highway. One ferry system connects Kodiak with mainland Seward and the Alaska Railroad, another links Cordova and Valdez, and a third serves panhandle communities from Ketchikan to Skagway, with service also from Prince Rupert, British Columbia, and Seattle, Wash.

2.3.7 Transportation

High costs of transportation continue to sap Alaska‘s economic development, largely because the major transportation links, both internal and external, are by air, which provides the fasted way to cross Alaska‘s great distances and formidable terrain. Two dozen airlines serve Alaska, with daily service for passengers and cargo from the Lower 48 and Canada, Europe, Hawaii, Korea, and Japan. Some 800 airfields, seaplane bases, and emergency strips are in use, and only few villages are without service at least by bush pilots. Most of the state‘s roads are surfaced. The Alaska Highway and its Haines and Skagway cutoffs connect Alaska‘s internal road network to the outside and provide relatively easy access for tourists. A 669-kilometers haul road from Fairbanks to Prudhoe Bay connects with the existing highway system to provide an overland route from the ice-free southern ports to the Arctic Ocean. The public, however, is restricted to the southern half of this highway and may use it only in the summer.

The government-owned Alaska Railroad runs for about 800 kilometers, linking Seward, Anchorage, and Fairbanks. Ocean shipping connects Seattle, Vancouver, and the trans-Canada railhead of Prince Rupert to towns in the panhandle and westward to Cordova, Valdez, Seward, and Kodiak. Ocean vessels also run during the ice-free midsummer months to Nome and Barrow and to the oil regions of the Arctic coast. A natural gas pipeline connects the Kenai gas fields and Anchorage, and the Trans-Alaska Pipeline delivers North Slope oil to ice-free tanker terminals at Valdez.

In the mid-l950s the Alaska Communication Cable was installed between Seattle and Alaska. Radiotelephones connect all interior communities.

2.4 Administration and Social Conditions

2.4.1 Government

The state constitution was adopted in 1956. The governor and lieutenant governor are the only executive officers and are elected for four-year terms. The 40-member House of

Representatives and 20-member Senate are elected for terms of two and four years, respectively. The Supreme Court has a chief justice and four associate justices. A three-member court of appeals was established in 1980. There are four district courts. A single federal district court sits alternately in Juneau, Anchorage, Fairbanks, and Nome.

Public financing is implemented through various personal income, property, sales, and business taxes, including petroleum-based severance taxes and mining rents and royalties. As a part of the Act of Admission, Congress granted Alaska certain revenues from the sale of furs and of federal lands.

State and borough governments have difficulty in providing the usual range of services because of the limited extent of the economy and a high unemployment rate. The vast area and the difficult terrain increase these problems.

The U.S. Bureau of Indian Affairs (BIA) assists Alaska‘s natives in achieving economic and social self-sufficiency. Despite a number of helpful programs, many of Alaska‘s natives suffer from unemployment, low income, and poverty. The native peoples were educated first by missionary groups, though by the time of statehood the BIA had assumed most of the responsibility for education. Funds are provided for vocational training and the development of job opportunities and for welfare, social work, and medical and health needs. The BIA also assists natives in organizing their villages under federal and state laws. Some oil revenues from native lands have been applied in self-help programs. Settlement of the native land claims in 1971 improved their economic plight by placing 17,600,000 hectares of federal land into the native entitlement.

2.4.2 Education

Education is compulsory through the eighth grade or until age 16 and is administered by a state board and a commissioner of education. Correspondence study is available for high school work through the State Department of Education. There are several federal schools on military bases. The University of Alaska, founded as a land-grant institution in 1917, operates campuses at Fairbanks, Anchorage, and Juneau. There are several community colleges, including those at Sitka, Ketchikan, Kenai, and Valdez. Alaska Pacific University in Anchorage, Alaska Bible College in Glennallen, and Sheldon Jackson College in Sitka are private institutions.

2.4.3 Health and Welfare

The elderly, dependent children, and the blind are aided by the state, and a special fund benefits sick and disabled fishermen. The state also operates a psychiatric hospital, a tuberculosis treatment centre, a youth camp, and a prison.

Medical and health clinics and hospitals available to the general public are provided by municipal and borough governments or private agencies, or are run as church-operated facilities. Health Standards have been raised markedly since 1950 through visits by U.S. Public Health Service nurses and doctors to the remote villages. The large number of airfields, the radio communications network, and the extensive use of bush pilots operating throughout the state make it possible for most persons, even in the remote villages, to reach medical facilities when there is serious need. There are modern hospitals located in Fairbanks, Anchorage, Juneau, and Ketchikan.

2.5 Cultural Life

Alaska‘s past, including the arts and crafts of its native peoples, is a major influence in Alaskan culture. Juneau is the site of the state‘s historical library and state museum. The university has a large museum, as do other communities, including Sitka, Haines, Valdez, and Nome. Eminent Alaskan artists have included both whites and Eskimos. Native ivory and wood carving are well known, and the nearly lost art of totem carving has been revived in part through private and public stimulus.

Wildlife refuges and ranges abound throughout Alaska, with more than 30,800,000 hectares managed by the U.S. Fish and Wildlife Service. The federal Bureau of Land Management also holds about 10,000,000 hectares for waterpower development.

In 1980, more than 41,600,000 hectares were designated for national parks, preserves, wildlife refuges, and wilderness areas, adding to the 2,000,000 already so established. The Alaskan national parks are notably spectacular. Denali (formerly Mount McKinley) National Park and Preserve (1917) has an abundance of wildlife, including brown and grizzly bears, caribou, and moose. Katmai National Park and Preserve (1918), on the Alaska Peninsula, includes the Valley of Ten Thousand Smokes, an area of active volcanoes that in 1912 produced one of the world‘s most violent eruptions. Glacier Bay National Park and Preserve (1925) has magnificent fjords, as well as glaciers that have retreated extensively in the 20th century. Sitka National Historic Park (1910), with a large totem pole collection, commemorates the stand of the Tlingits against early Russian settlers. The Tangass and Chugach national forests in the southeast and south central regions, respectively, are also federal public land reserves. The U.S. Department of the Interior has continued to study the need for withdrawing further regions from public domain into reserves.

The sporting industry, including guide and outfitter services and boat charters, continues to be a colorful activity. Alaska provides the nation‘s only significant Arctic wilderness, and much research is done in glacier, mountain, tundra, atmospheric, ionospheric, and polar oceanography fields by federal, state, university, and private agencies. For example, the University of Alaska carries out extensive research on Arctic problems through its Geophysical Institute, Institute of Marine Science, Institute of Arctic Biology, and other groups. Since 1946 the Juneau affiliate of the Foundation for Glacier and Environmental Research, in cooperation with the National Science Foundation, the University of Idaho, and the University of Alaska, has sponsored a glaciological and environmental research and field sciences training program on the Juneau Icefield.

3. History

3.1 Explorations

As early as 1700, native peoples of Siberia reported the existence of a huge piece of land lying due east. An expedition appointed by the Russian tsar and led by a Danish mariner, Vitus Bering, in 1728 determined that the new land was not linked to the Russian mainland, but because of fog it failed to locate North America. On Bering‘s second voyage, in 1741, the peak of Mount St. Elias was sighted, and men were sent ashore. Sea otter furs taken back to Russia opened a rich fur commerce between Europe, Asia, and the North American Pacific Coast during the ensuing century.

3.2 Early Settlement

The first European settlement was established in 1784 by Russians at Three Saints Bay, near present-day Kodiak. It served as Alaska‘s capital until 1806, when the Russian-American Company, organized in 1799 under charter from the emperor Paul I. moved its headquarters to richer sea otter grounds in the Alexander Archipelago at Sitka. The company governed Alaska until its purchase by the United States in 1867. Alaska‘s first governor (then termed chief manager), Aleksandr Baranov, was an aggressive administrator whose severe treatment of the native Indians and Eskimos led in 1802 to a massacre at Sitka.

A period of bitter competition among Russian, British, and American fur traders was resolved in 1824 when Russia granted equal trade rights for all. The near extinction of the sea otter and the political consequences of the Crimean War (1853-56) were factors in Russia‘s willingness to sell Alaska to the United States. The Russian minister made a formal proposal in 1867, and, after much public opposition, the purchase was approved by the U.S. Congress and the U.S. flag was flown at Sitka on October 18, 1867.

3.3 Political Growth

As a U.S. possession Alaska was governed by military commanders for the War Department until 1877. During these years there was little internal development, but a salmon cannery built in 1878 was the beginning of what became the largest salmon industry in the world. In 1884 Congress established Alaska as a judicial land district, federal district courts were established, and a school system was initiated.

In 1906 the first representative to Congress, a nonvoting delegate, was elected, and in 1912 Congress established the Territory of Alaska, with an elected territorial legislature. Alaskans voted in favor of statehood in 1946 and adopted a constitution in 1955. Congressional approval of the Alaska statehood bill in 1958 was followed by formal entry into the Union in 1959.

3.4 Mining Booms

Other significant events in Alaska‘s history included early gold discoveries on the Stikine River in 1861, at Juneau in 1880, and on Fortymile Creek in 1886, and later the stampede to the Atlin and Klondike placer goldfields of adjoining British Columbia and Yukon Territory in 1897-1900. Gold discoveries followed at Nome in 1898 and at Fairbanks in 1903. The gold rush made Americans aware of the economic potential of this previously neglected land. The great hard-rock gold mines in the panhandle were developed, and in 1898 copper was discovered at McCarthy. Gold dredging in the Tanana River valley was begun in 1903 and continued until 1967.

3.5 Economic Growth

A dispute between the United States and Canada over the boundary between British Columbia and the Alaska panhandle was decided by an Alaska Boundary Tribunal in 1903. The U.S. view that the border should lie along the crest of the Boundary Ranges was accepted and boundary mapping was completed in 1913. Between 1898 and 1900 a narrow-

gauge railroad was built across White Pass to link Skagway and Whitehorse in the Yukon, and shortly afterward the Cordova-to-McCarthy line was laid up the Copper River. Another railway milestone, and the only one of these still operating, was the 866-kilometers Alaska Railroad connecting Seward with Anchorage and Fairbanks in 1923. In 1935 the government encouraged a farming program in the Matanuska valley near Anchorage, and dairy herds and crop farming became established there, as well as in the Tanana and Homer regions.

In 1942, during World War II, Japanese forces invaded Agattu, Attu and Kiska islands in the Aleutian chain and bombed Dutch Harbor on Unalaska. This aggression prompted the construction of large airfields as well as the Alaska Highway linking Dawson Creek, British Columbia, and Fairbanks with more than 2,400 kilometers of road. Both proved later to be of immense value in the commercial development of the state.

During the 20th century nearly 40 earthquakes measuring at least 7.25 on the Richter scale have been recorded in Alaska. The devastating earthquake on March 27, 1964 (8.4 on the Richter scale) affected the northwestem panhandle and the Cook Inlet areas, destroying parts of Anchorage; a tsunami that followed wiped out Valdez; the coast sank 9.75 meters at Kodiak and Seward; and a 4.9-meters coastal rise destroyed the harbor at Cordova.

Oil and natural gas discoveries in the Kenai Peninsula and offshore drilling in Cook Inlet in the 1950s created an industry that by the 1970s ranked first in the state‘s mineral production. In the early 1960s a pulp industry began to utilize the forest resources of the panhandle. Major paper-pulp mills were constructed at Ketchikan and Sitka, largely to serve the Japanese market. The discoveries in 1968 of petroleuro on lands fronting the Arctic Ocean gave promise of relief for Alaska‘s economic lag, but problems of transportation across the state and to the Lower 48 held up exploitation of the finds. In 1969 a group of petroleum companies paid the state nearly $ 1,000,000,000 in oilland revenues, but the proposed pipeline across the eastem Brooks Range, interior plains, and southem ranges to Valdez created heated controversies among industry, government, and conservationists. In November 1973 a bill passed the U.S. Congress that made possible construction of the pipeline, which began in the following year. The completed 122-centimeter pipeline, 1,262 kilometers long, came into operation on June 20, 1977. As a result, oil flows freely from the Prudhoe Bay oil field on the Arctic coast to the ice-free harbor at Valdez, whence tankers transport it to U.S. West Coast ports. Further development of Alaska‘s petroleum reserves depends upon economic factors and the issue of high production costs in the hostile Arctic environment. In 1989 the oil tanker *Exxon Valdez* ran off course in Prince William Sound, causing the most disastraus oil spill in North American history and inflicting incalculable darnage on the area‘s marine ecology and local economy.

Maynard M. Miller

The Juneau Icefield Research Program and its Surveying Mission

1. Introduction

In documentation of details of modern glacier fluctuations, the disciplines of surveying and geodesy are of paramount importance. Nowhere is this better illustrated than in the long-term and on-going Juneau Icefield Research Program (JIRP) in Alaska and northern British Columbia, Canada.

The Juneau Icefield (Fig. 1) embraces about 3,000 km^2 of interconnected highland glaciers, composing what is the fifth largest icefield in the western hemisphere. Because of its unique location in the S.E. Alaska Panhandle on the northwest coast of North America, it is a prototype of Alaskan mountain glaciation and global glacio-climatic pulsations. Here the blocking highs of continental air masses vie with cyclonic intensities of the North Pacific atmospheric lows in an interaction zone that reflects even the most minor of storm front shifts. The extensive glacial networks in the linear ranges along this coast, including the Juneau Icefield (p. 31), lie in that zone and hence serve as sensitive monitors of world-wide climatic oscillations and perturbations.

Investigation of the prototype Juneau Icefield glaciers began in 1946, prompted by the Committee on Glaciers of the American Geophysical Union, with field work directed by *Maynard M. Miller*. Surveying and photogrammetric expertise was added by *William R. Latady*. In that summer, reconnaissance aerial photography and ground surveys were made of key glacier termini *[MILLER, 1947]*. In 1947, additional glacier surveys were accomplished, a field plan organized and an integrated network of research camp locations on the icefield was selected *[MILLER, 1948, 1949]*.

In 1948, JIRP received sponsorship from the American Geographical Society, through the cooperative efforts of *W.O. Field*. In that summer, the first field camp sites in the network were occupied and associated research initiated on the icefield‘s upland névés. An access route, used by the 8-person 1948 expedition, was pioneered up the ridge between East and West Twin Glaciers *[MILLER, 1949]*. Air drops of supplies were provided by U.S. Naval aircraft, operating from the Kodiak Naval Air Station.

In 1949, the Juneau Icefield Research Program fielded a team of 27 scientists, and constructed its first permanent buildings for the main field station at Nunatak Chalet (Camp 10; p. 31), in the highland source area of the Taku Glacier. In that year also, JIRP received a 10-year research contract with the U.S. Office of Naval Research *[FIELD and MILLER, 1950; MILLER and FIELD, 1951]*. In 1959, the American Geographical Society contract with the Office of Naval Research was completed. Since 1955, JIRP has been carried forward under the aegis of the Foundation for Glacier and Environmental Research, Seattle, Washington, with summer headquarters in Juneau, Alaska. In subsequent years, the program has established a network of 18 permanent field stations across the icefield. These

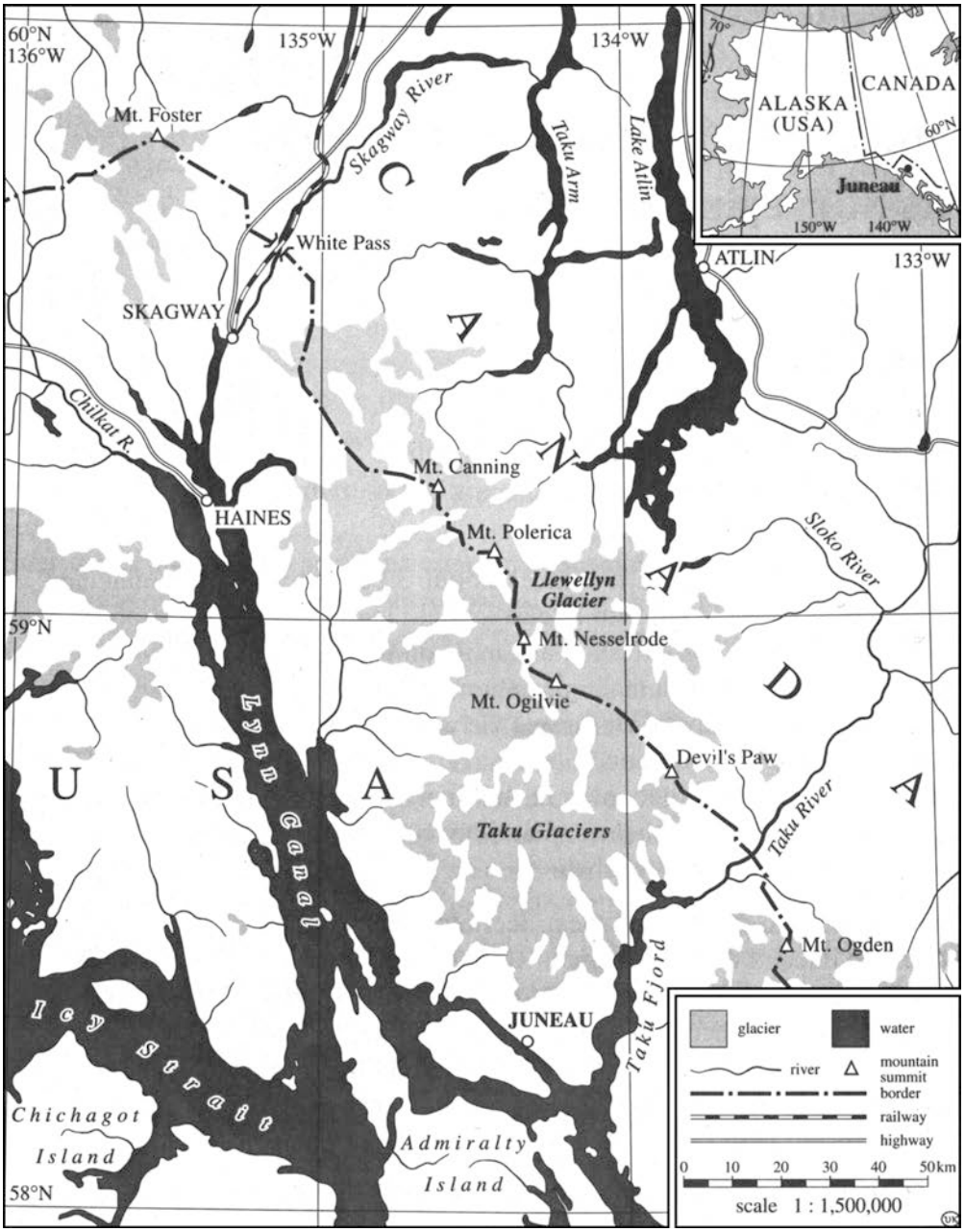

Fig. 1: The Juneau Icefield, Alaska

are comprised of metal-sheeted and insulated buildings, oversnow vehicle garages, messing and dormitory facilities, field libraries, laboratory work spaces and so forth.

Support has also been achieved through contracts with the U.S. National Science Foundation (NSF), the Army Research Office, the Federal Office of Water Resources Research (U.S. Department of Interior), NASA, the U.S. Forest Service, the State of Alaska, the National Geographic Society and other agencies, including Columbia University, Michigan State University, the University of Idaho and the University of Alaska Southeast in the United States; Queens University, the Survey Engineering Department of the University of New Brunswick and the Nova Scotia and Land Survey Institute in Canada; the Survey Department at the University of New South Wales, Australia; the Institute of Low Temperature Science at Hokkaido University; the Institute for Geography at Salzburg University,

Austria; the Institute of Photogrammetry at the University of Bonn and, very importantly, the Institute of Geodesy at the Bundeswehr University in Munich, Germany.

There have now been nearly 50 years of continuous research and field science training on the Juneau Icefield. Since 1959, JIRP has also been allied academically with the Glaciological and Arctic Sciences Institute for training field scientists and supported with some 56 continuing contracts and grant awards from the National Science Foundation and another 23 from the U.S. Army Research Office, as well as periodic support from the National Geographic Society *[MILLER, 1967]*. From 1955 to 1959, the program was also allied with Columbia University. From 1959 to 1974, the Institute was headquartered at Michigan State University, East Lansing, MI. The Institute has been under the academic aegis of the University of Idaho, Moscow, ID since 1975. Over the past half century, over 700 students have received academic credit for their participation through these universities.

The NSF programs supporting student training in recent years have changed the original purely research aim of this pioneering activity, but a number of published papers, monographs and open file research reports continue to document JIRP scientific results. Since 1960, the Glaciological Institute field training program has been recorded in annual reports. A JIRP publication series began in the 1940s with a set of yearly monographs published by the American Geographical Society for the Office of Naval Research and other supporting and cooperative agencies. These and subsequent issues include reports in various field disciplines and reference survey and mapping program results from projects carried on through the years. Some of the key publications that note JIRP survey data and analyses are listed at the end of this contribution. Included in this list are a few selected reports of historical significance with respect to JIRP‘s on-going programs.

It is planned that JIRP‘s primary aims in the next century will continue to be both basic research as well as experimental training of future field scientists and leaders in education and science. In this regard, between 1948 and 1994, some 70 academic theses and a number of professional publications have documented JIRP results in a variety of earth science disciplines. These investigations have also represented continuing strong liaison with scientists from over 50 universities in the U.S., Canada, China, Nepal, Japan, Argentina, Peru, South Africa, Australia, New Zealand, the United Kingdom, Norway, France, Austria, Germany, Czechoslovakia, Poland and other European countries.

2. A Prototype Glacier/Climate/Survey Model

The Alaskan glacial coast extends for 1,450 kilometers from Ketchikan in the extreme southeast corner of the Panhandle to Anchorage at the head of Cook Inlet in the central southern sector. Here glaciers of all morphogenetic types occur with a great range in size, length, elevation and geographic position. The fluctuational patterns in three key sectors are shown in Fig. 2, representing examples from the Prince William Sound area of the Chugach Range near Anchorage to the Yakutat Bay area of the St. Elias Mountains, and the Taku River District in the Alaskan Panhandle.

In the heart of this region is the Juneau Icefield to lie between Lat. 58°30´ and 59°N. The icefield shares half of its area in Alaska and the other half in bordering areas of northern British Columbia and Canada‘s Yukon Territory. The ultimate headwaters of the Yukon River lie at the crest of this icefield - in the Mount Noose (Camp 8) sector.

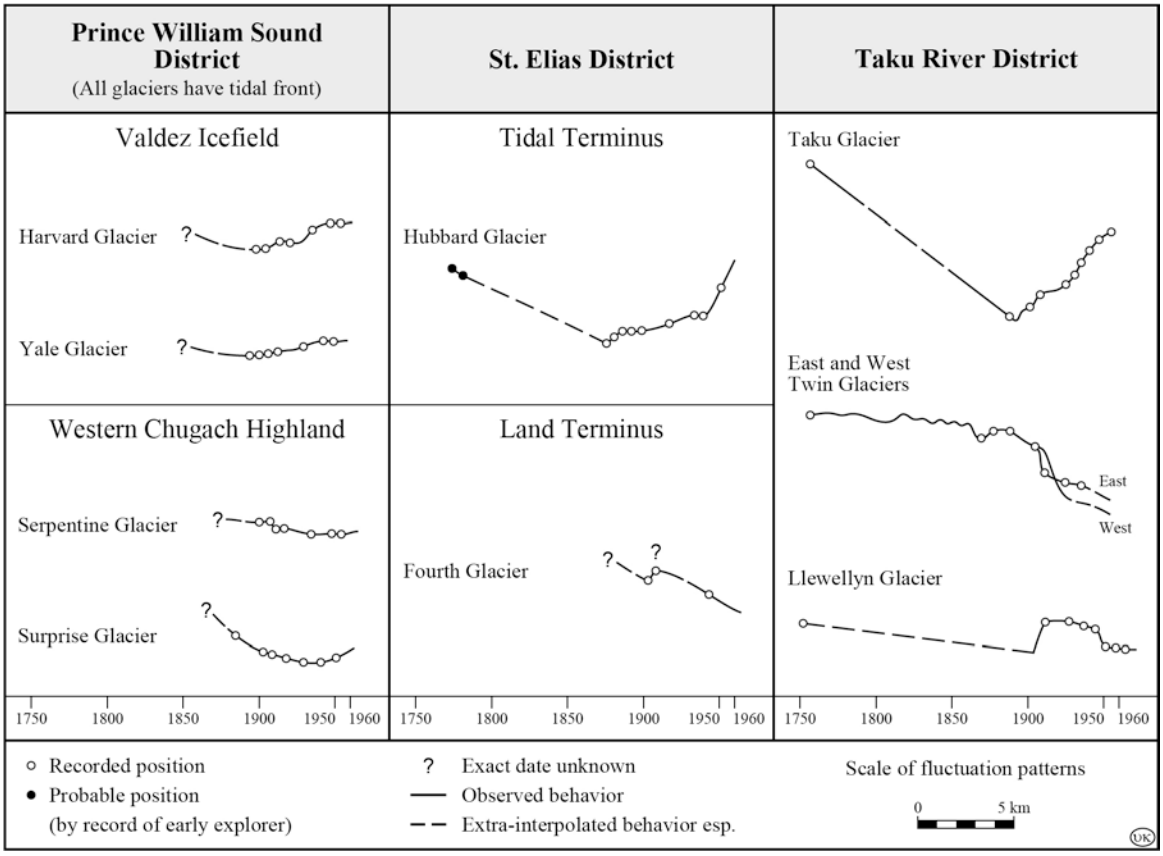

Fig. 2: Fluctuation patterns of Alaskan glaciers

Positioned in the Northern Boundary Range of the Alaska-Canada Coast Mountains, the Juneau Icefield is the most readily accessible icefield from a major center of expeditionary supply, in this case Alaska‘s capital, Juneau. The most usual access route for our participants today is via a trail to the Ptarmigan and Lemon Creek Glaciers and from there on ice to Camp 17 (p. 31).

For nearly 50 years, systematic and consecutive annual records of the fluctuations of the main glaciers on the icefield have been obtained by JIRP, with a chronology of earlier positions derived from early explorer charts, historical ground photos, aerial photographs and field studies in geomorphology, dendrochronology, lichenometry, soil science and radiocarbon dating of moraines. These data provide a unique record covering the Little Ice Age and extending from the 1400s to the present.

With respect to the timing of glacial regime changes, the right-hand section of Fig. 2 illustrates an apparently out-of-phase advance and retreat of adjoining glacier systems emanating from the southern edge of the Juneau Icefield. The upper picture on page 33 illustrates the lower area and terminal sector of the largest glacier, the Taku, which as a total system embraces over 700 km^2 of area. Climatological details of major accumulation shifts have been considered elsewhere *[MILLER, 1956, 1963, 1985]*. In general, the lower névés of the Taku Glacier system (from elevations of 900 to 1,500 m) experienced positive mass balance during the last half of the 19th and the first two decades of the 20th century, as have its upper névés (from 1,500 to 2,100 m) since the 1920s. Currently, the mean equilibrium line altitude (ELA) on this glacier lies at 1,000 m.

Juneau Icefield – Scale 1:300,000

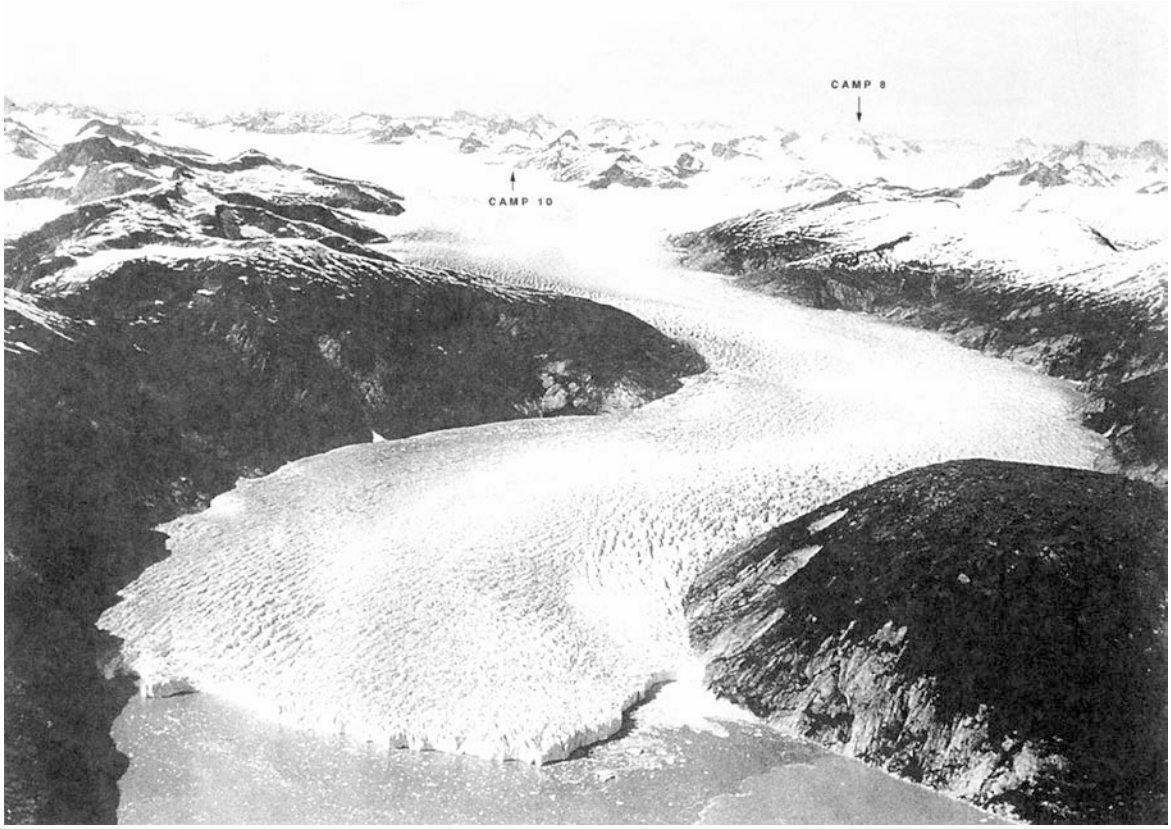

Archives M. Miller

Terminus position of Taku Glacier 1929

Photo M. Lang, 1989

Terminus position of Hole-in-the-Wall Glacier 1989

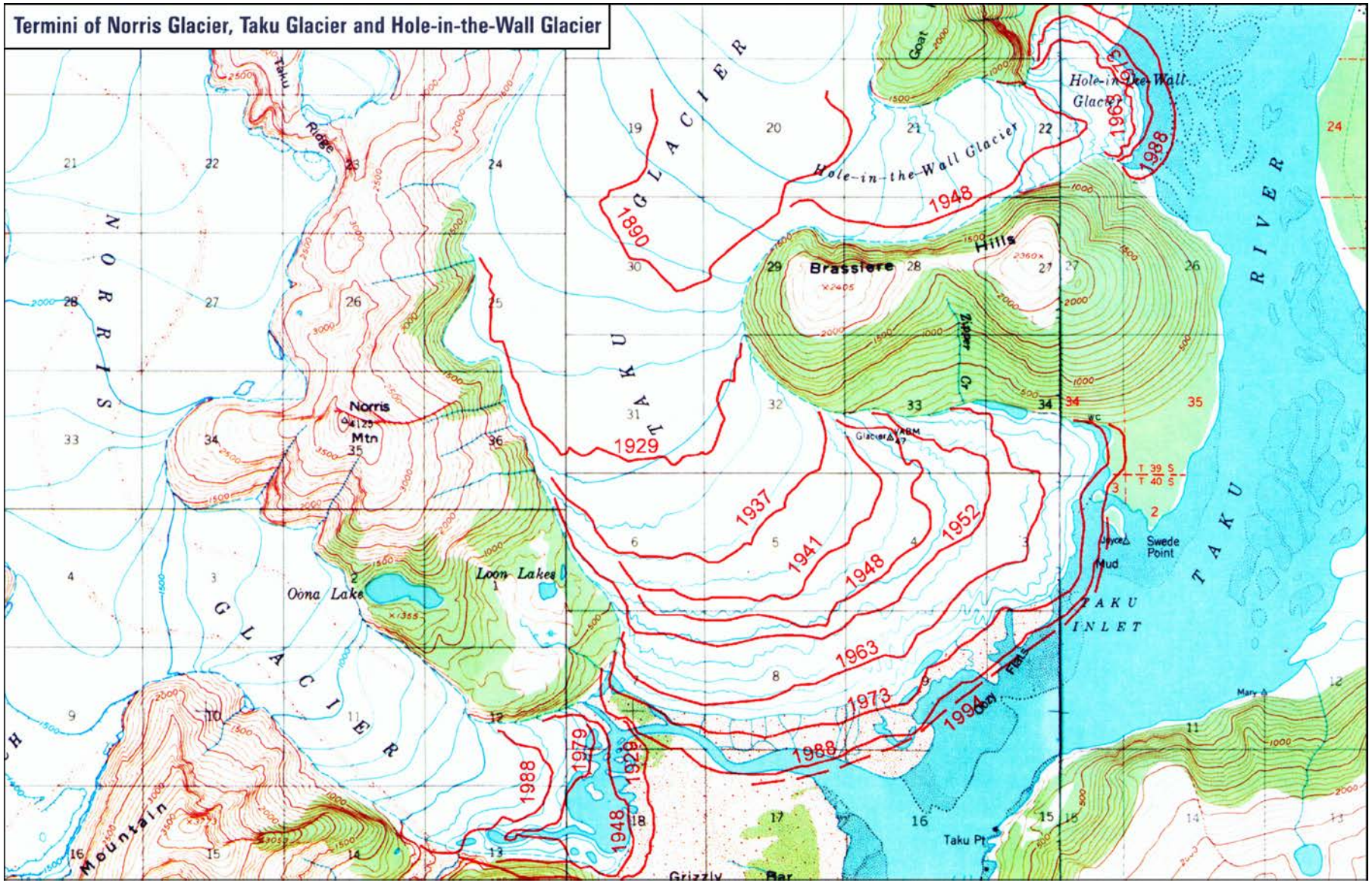
Termini of Norris Glacier, Taku Glacier and Hole-in-the-Wall Glacier
NORRIS GLACIER
TAKU GLACIER
TAKU RIVER
TAKU INLET
Hole-in-the-Wall Glacier
Hole-in-the-Wall Glacier
Brassiere Hills
Norris Mtn
Loon Lakes
Oona Lake
Mountain
Taku Ridge
Zipper Cr
Swede Point
Taku Pt
Grizzly Bar
Goat
Mary
1890
1929
1937
1941
1948
1952
1963
1973
1979
1988
1994

In contrast, the Llewellyn Glacier (upper right corner of p. 31), located in a comparably sized area in the northeastern sector of the icefield, flows in the interior continental region from a névé adjacent to the crestal névés of the Taku Glacier. Together, these two comprise a transection glacier system straddling the Juneau Icefield. In combination, they extend for a distance of over 120 kilometers and represent an area of more than 1,000 km^2. The Llewellyn Glacier received the heaviest accumulation on its lowest névés during the last two decades of the 19th and the first two decades of the 20th century.

Since the 1920s, negative regimes have prevailed throughout this large inland and climatologically subcontinental glacier system. Here the current mean ELA is at 1,500 m, some 500 m higher than on the maritime Taku Glacier. The similarly maritime Mendenhall and Norris Glacier systems adjoining to the west, and also the Twin Glaciers to the east (p. 31), received their most substantial net accumulation at lower elevations during the first half of the 18th century, as did the lower névés of the Taku Glacier system. With the exception of the Taku Glacier, each of these glaciers has been in retreat during this century.

3. Physiographic Considerations

The seemingly disparate advancing behavior of the Taku Glacier (pp. 33 and 35) has been referred to as an anomaly by *HEUSSER et al. [1954]*. This term is misleading because we have not been dealing with an anomaly per se but a consequence of natural flow differences conditioned by the area-elevation character of adjacent glacier systems. As well, there has been significant control on the terminal position by a massive underwater push moraine in Taku Fjord and a plug of bottom sediment pushed against the distal wall of the fjord (p. 35). Since 1948, this has shallowed the water and shielded the front, precluding loss by tidal calving.

This phenomenon and the effect of tidewater iceberg production at the termini of other tidal glacier fronts in south and southeastern Alaska have been well recognized as factors complicating the climatological interpretation of surveyed fluctuation patterns *[MILLER, 1955]*. In a sense, this replicates the situation pertaining on land termini where fjord calving does not occur. Such differences in the physiographic constraints on termini underscore the need for total glacier system assessments and where possible continued periodic geodetic surveys where regimen changes are being monitored.

Flow differences in the upper reaches of the large Juneau Icefield glaciers is illustrated by the hypsometric curves in Fig. 3. On these graphs, the main surface areas of the Mendenhall, Lemon Creek and Llewellyn Glaciers are all shown to lie at elevations of 800-1,500 m, whereas the present main névé of the Taku Glacier is between 1,100-1,500 m, with a crestal sector up to 1,900 m.

This morphological configuration caused the climatic amelioration of the later stages of the Little Ice Age (during the 1800s and early 1900s) to raise the mean freezing level at least 600 m from where it was in the 18th Century. The zone of maximum snowfall was correspondingly raised. This is because heaviest snowfall occurs at elevations close to the freezing level, where ambient air temperatures are at or slightly below freezing.

On higher elevation surfaces which lie well above the freezing level, available moisture drops off rapidly and snowfalls are lighter. At lower elevations, below the freezing level, the snow turns to rain. Thus, on this icefield during periods of maximum accumulation over

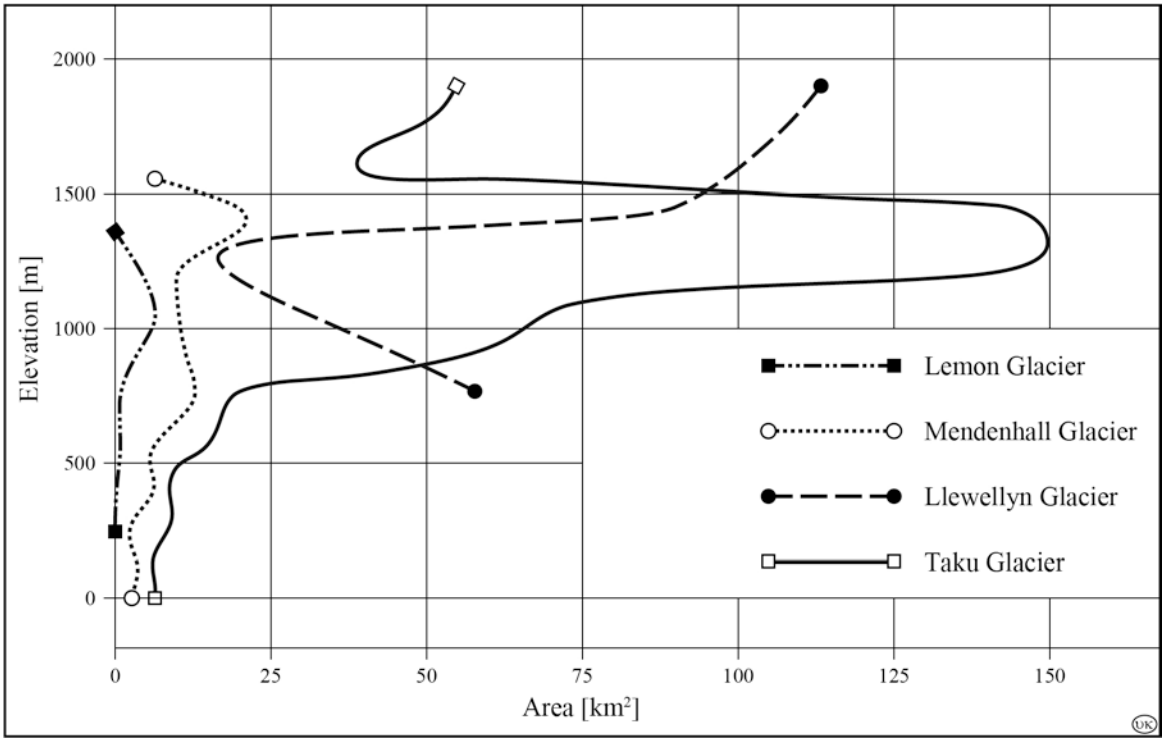

Fig. 3: Hypsometric curves showing the area-elevation characteristics of the main Icefield glaciers

many decades, accumulation on affected névés has caused substantial thickening. This has produced some changes in surface flow rates and related mass transfer of ice down the main trunk glaciers of the icefield.

4. Mass Balance and Flow Lag Determinations

Mass transfer exchanges in the Taku Glacier have been calculated using seismic depth records *[POULTER et al., 1950; MILLER et al., 1994]*, but yearly changes in this parameter have not been detailed. In advance of that, we have made the simplifying assumption that in each case where there is a significant increase in thickening-induced longitudinal stress, there is a flow between the incidence of strong accumulation on the highland névés and later allied advances of the termini of the glaciers involved. To determine this flow lag requires carefully repeated surface movement surveys using theodolites, EDMs and GPS equipment. From the periodic (although not always annual) records on selected transects available through the JIRP program, a general analysis can be made. It is desirable, however, to systematize this kind of data acquisition on an on-going annual basis.

On the Mendenhall Glacier, where only cursory surveys have been attempted, the flow lag is estimated at 80 years from the zone of maximum snowfall on its largest surface area (i.e., at its highest elevations between 1,000 and 1,600 m). Again, this is the number of years required for a significant accumulation increase to pass down valley to the terminus – a useful record only possible by repeated surface stake surveys *[McGEE, 1993]*.

More continuous data to present have been obtained on the Taku Glacier *[LANG and WELSCH, 1997]*, from its highest névé to its terminal discharge zone. Based on these survey records, the flow lag from the crestal zone is approximately 67 km/150 years (≈ 450 m/year). About 80 years are required for ice transfer from the large intermediate

elevation nourishment zone to the terminus (pp. 31 and 33). Thus, frontal variations of the Taku Glacier today largely reflect retention of increased snowfall on its prime source areas many decades ago and during quite different climate conditions than at present.

The flow lag interpretations, noted above, are drawn from annual surveyed surface velocity rates on the Taku Glacier over the past 45 years, abetted by annual measurements in firn test-pits and from crevasse stratigraphy on the prime accumulation plateaus. To elaborate on levels of maximum accumulation, comparative measurements have also been made during periods of individual storms *[MILLER, 1956]*. These reveal shifting elevation zones of maximum accumulation. The cumulative effect has been documented in the annual JIRP test-pit and crevasse stratigraphy reports. It is exemplified by the net accumulation and ELA trend plots for the Taku Glacier's main névé in Fig. 4.

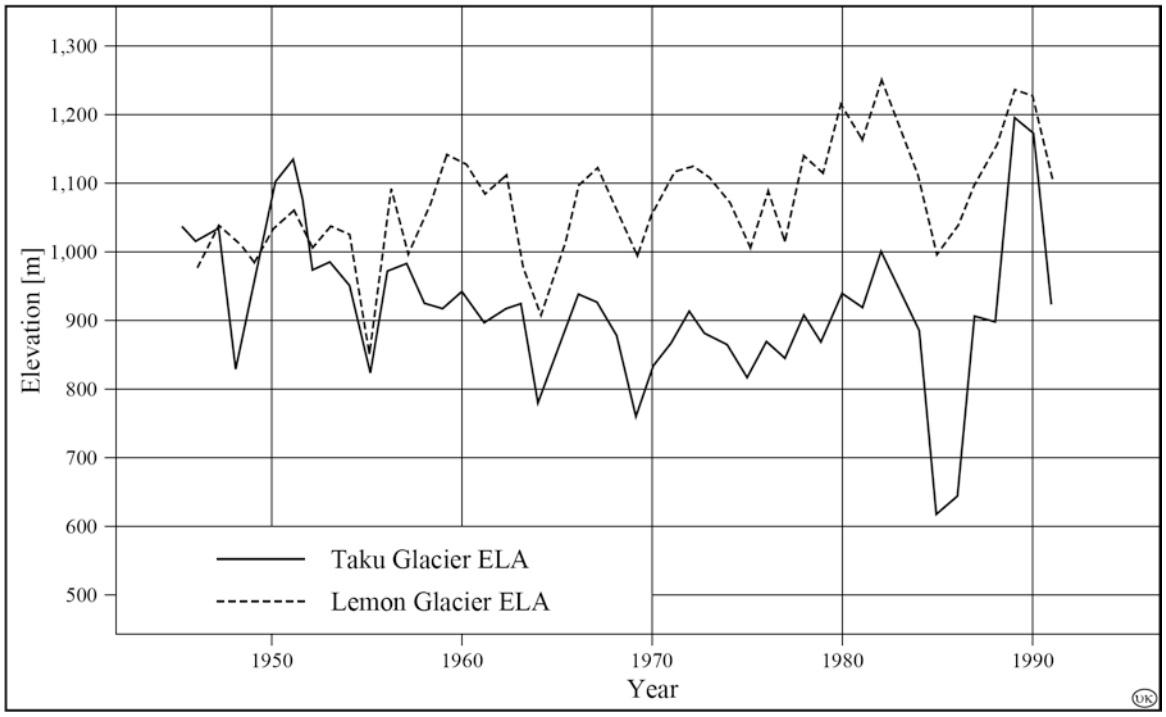

Fig. 4: Variations of the ELA on the Taku and Lemon Glaciers

5. Secular Trends in Icefield Regime

The regimen changes for the maritime sector of the icefield during the first half of this century are illustrated in the generalized accumulation trend plots for the total Taku Glacier system given in Fig. 5. Here, for the years 1900 to 1955, we see a significant increase in higher elevation net retained accumulation (in crestal Regime Zone A) since the decade 1910-20, with a notable decrease in net accumulation at lower elevations such as on the main névé (Regime Zone B).

Only the first half of this century is noted in the figure, as for those years it is doubtful that man-made atmospheric pollution effects or ozone-hole influences pertain. In Fig. 4, the accumulation and ELA record from 1955 to present may have received such influence. Viewed as a continuum, these figures reveal strong changes throughout this century, although with several recent large fluctuations. Interpretation of these fluctuations is beyond the scope of this present survey emphasized report.

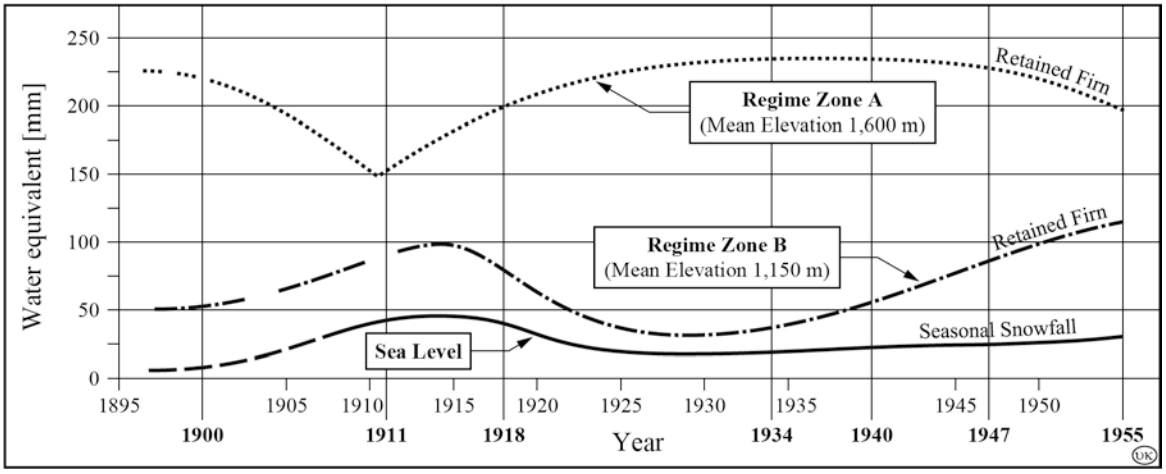

Fig. 5: Net accumulation trends for the Juneau Icefield (dashed lines are interferred)

The lowering ELAs from 1946 to 1986 (noted in Fig. 4) are inverse to the trend of accumulation increases on the upland névés, also shown in Fig. 4. The lowered ELAs on the Taku Glacier are also interpreted as due to a broadened area of thickening of the annual firn pack which has outweighed increased net losses in the ELA sector by climatic warming. All of this may be a consequence of the Greenhouse Effect which, since the early 1960s, is more widely considered to have been superimposed on the natural climatic oscillations *[MILLER, 1985]*.

Observations on marginal scour zones and trimlines of the Little Ice Age Maximum on the lower Taku Glacier with respect to present glacier surfaces show that a dominant concurrent thickening of solid ice has also occurred in this century in areas below the ELA, as well as on the lowermost névés. This may be attributed to an increase in mass transfer at intermediate elevations on the glacier. For example, at the 1,100 m level, the result has been a 20 m rise of the glacier‘s surface near the Camp 10 nunatak since the 1940s. Also documented are terminal thickening and advance of the Taku Glacier and its distributary tongue, the Hole-in-Wall Glacier (p. 33 and 35). Today these termini are close to the maximum advanced position they held in the Little Ice Age in the 18th Century, and are more advanced than at any other time in the past 8,000 years *[MILLER, 1963; EGAN, 1971]*. In general, the Taku Glacier system remains healthy in contrast to lower névé glaciers on the icefield. These have been experiencing strongly negative regimes.

As previously noted, the Taku Glacier terminal advance is partly attributed to frontal blocking by massive submarine push moraines in the fjord (p. 35), but it is dominantly the result of climatic conditions which have produced continuing positive mass transfer from the glacier‘s source névés. To recapitulate, the climatological factor in this regime relates to a pronounced upward shift of freezing level in modern times. This resulted in raised elevation of the zones of maximum accumulation in the mid-1900s, significantly repeating the pattern that occurred in the mid to late 1800s. The contrast is dramatic when compared with the preceding conditions of maximum cooling in the Alaskan Little Ice Age from the late 1400s to the late 1600s, which produced universal advances of the termini of the main trunk Juneau Icefield glaciers.

At that coolest Neoglacial time, average freezing levels were at least 500 m lower than the mean ELA we have observed over the past 50 years. With this, there was also a coastward shift in the mean position of the Arctic Front. Proof lies in the presence of well-delineated

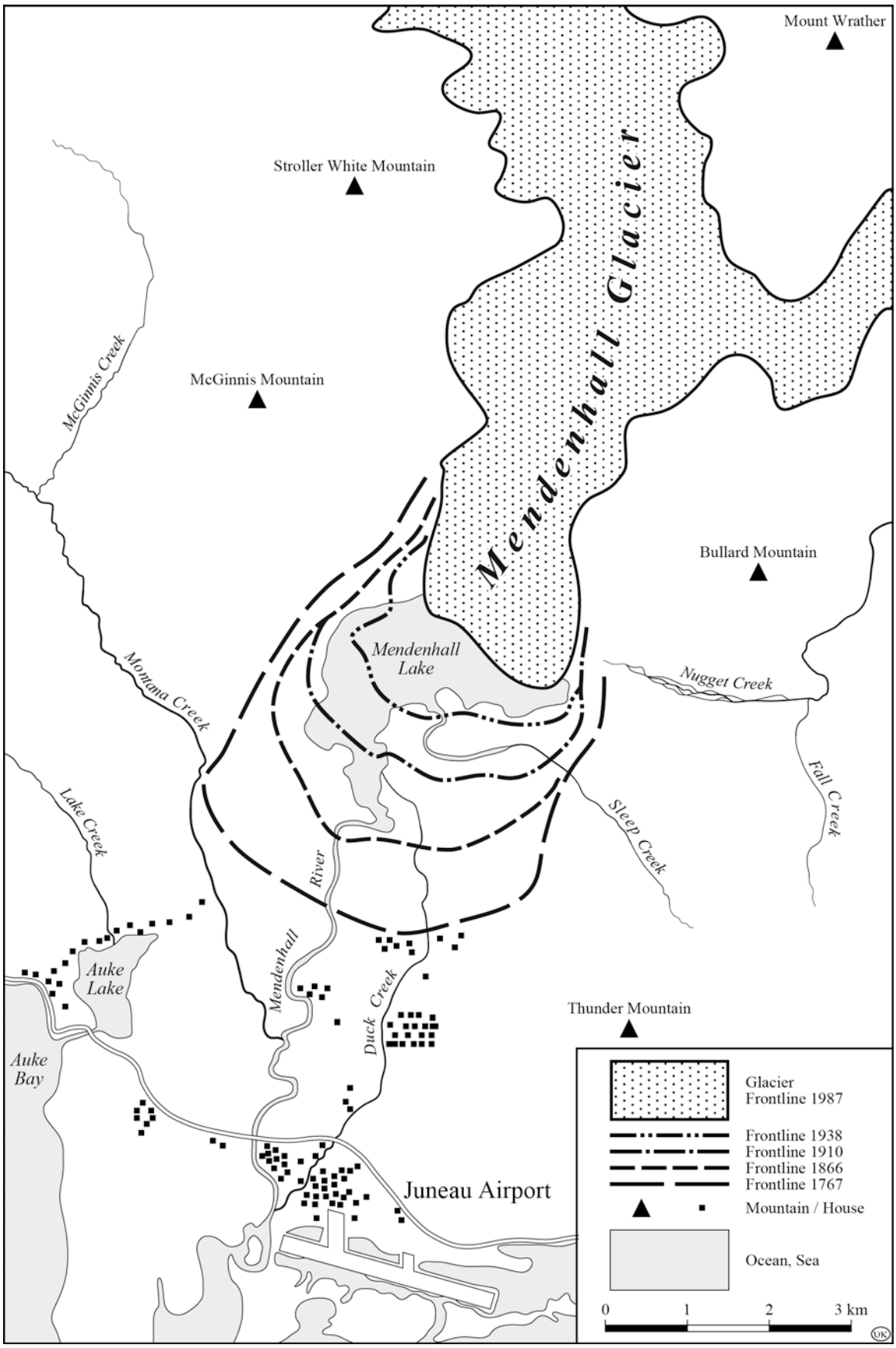

Fig. 6: Receding Mendenhall Glacier

1700s trimlines and wide marginal scour zones, extending high up on valley walls at the termini of the receding Mendenhall, Lemon Creek and Norris Glaciers and the East and West Twin Glaciers (at the icefield's western and southern margins, p. 31 and Fig. 6).

The advance of the Taku Glacier terminus over the past 100 years, and its distributary Hole-in-Wall Glacier, has been well documented in historic records, and since the 1920s by periodic ground and aerial photography and field mapping. More recently, repeated satellite imagery has helped to maintain a general record of annual ELA changes, although the image resolution is not yet adequate to detect minor net changes in terminal position. Increased application of GPS surveys in the Taku Glacier's terminal area are underway to provide that more precise information.

6. Early JIRP Survey Records, Annual Flow Variations, and Strain-rate Surveys

An example of the early upper level survey records on the Taku Glacier is noted in Figure 6. This plot, based on 1950s surveys, represents flow lines in the confluence zone close to the ELA and reveals the integration of stress fields in the main tributaries feeding from the highland névés. Over these past four decades, the ELA has been quite unstable, shifting upward to as high as 1,190 m, and downward to as low as 610 m (Fig. 4). Since 1970, the ELA has averaged at the 910 meter level, about half-way between the positions of Movement Profiles II and IV in Figure 7.

We have also found that the configuration of across-glacier transects of down-glacier flow at the mean high level of the Taku Glacier's ELA have varied annually since the 1940s. This is shown with successive plots from Movement Profile IV (MP IV), given in Fig. 8. These compare flow rates in 1949, 1950 and 1952 and also those in 1986, 1987 and 1988. Such survey records, if accurately taken, have significant glacio-climatic import and help to delineate and document significant changes and trends in glacier mass balance. With today's GPS equipment used year after year at the same locations, it is also possible to measure surface elevation changes with high accuracy, giving a new dimension to mass balance determinations *[PELTO and MILLER, 1990; LANG, 1991, 1993, 1995; McGEE et al., 1995; LANG and WELSCH, 1997]*. Extensive surveys of glacier strain-rates have also been conducted. Examples are the application of embedded wire strain gages, allied to theodolite and terrestrial photogrammetry surveys, on the Cathedral Massif Glacier at Camp 29 (p. 31). These data are reported by *WARNER and CLOUD [1974]* and in the topographic and glacier forefield map published by *SLUPETZKY et al. [1988]*. A further use of terrestrial photogrammetry is illustrated by the surface flow map and digital terrain model analysis of the icefall and wave-ogives of the Vaughan Lewis and Gilkey Glaciers by *RENTSCH et al. [1997]* and by the theodolite strain-rate surveys of *McGEE [1990]* and *LANG and WELSCH [1997]*.

The down-glacier horizontal displacement of the top of the 10B borehole over the successive years 1950-53 was surveyed to be 692 meters (Fig. 7 and 9). On this southerly flow direction in even the short 3-year interval, surveyed velocities increased from 0.61 to 1.3 m/day. A 1.4° surface gradient was measured at the 1953 position compared to 1.0° in 1950, which implies that the borehole was moving from an area of some extension to greater extension. This may relate to increased strain-rate on the longitudinal stress trajectory due to substantially increased up-glacier load stress between 1950 and 1953. This is a good

example of the value of supporting mass balance and precise strain-rate measurements which can be made at any glacier site to clarify the absolute role of slope angle in the flow law.

In 1993, exactly 40 years after the 1953 pipe survey, and after four intervening decades of burial by successive annual increments of firn-pack, the drill platform became exposed

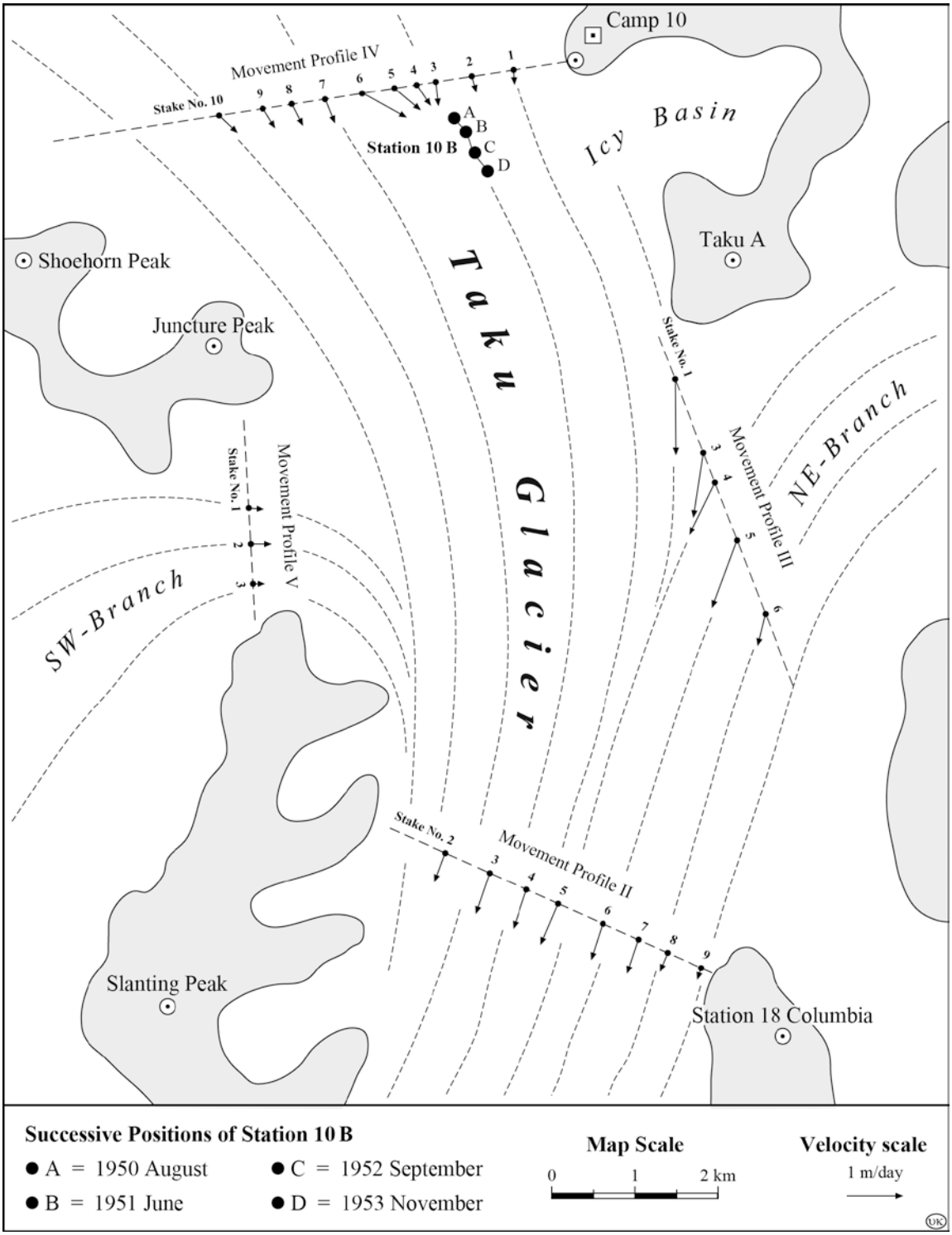

Fig. 7: Movements on Taku Glacier 1950 - 1953

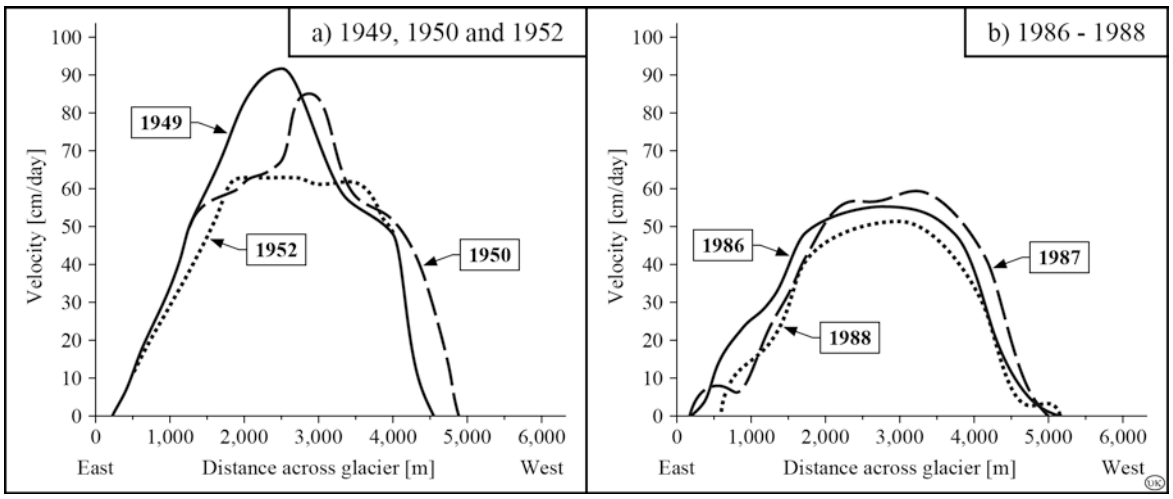

Fig. 8: Main velocities on Profile IV 1949 - 1952 and 1986 - 1988

by ablation near the 1993 ELA. In August of that year, a GPS positioning of the platform revealed it to be 11 km down-glacier from its 1953 location. The position was in mid-glacier, about 1.7 km due west of Station Columbia (Survey Station 18 in the SE corner of Fig. 7). From this unique four decade record a mean flow in the confluence zone of 300 m/year is calculated.

The narrowing of the main glacier down-valley from the 1993 platform site results in a 50 per cent increase in surface ice flow velocity, based on comparing surveys between MP IV and MP II (Fig. 7). Therefore, the platform henceforth should be displaced down-glacier at 450 m/year.

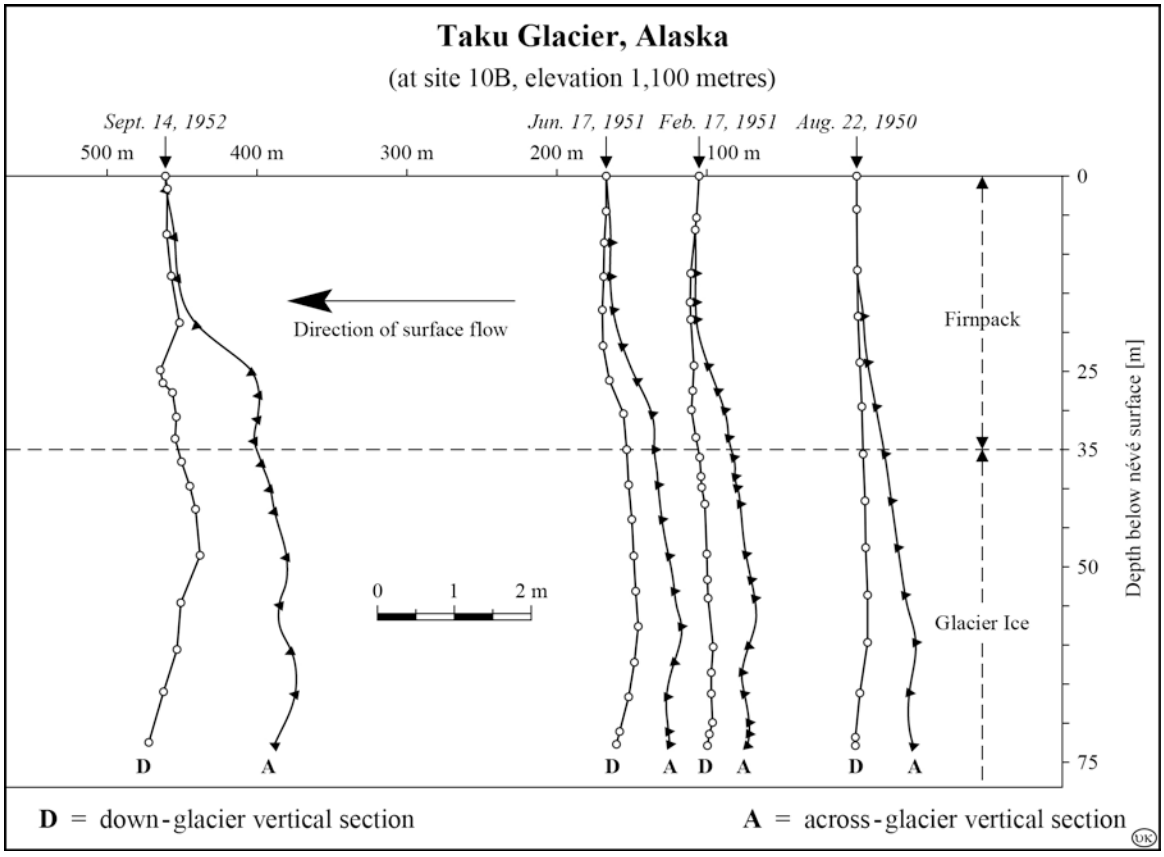

Fig. 9: Vertical velocity profile

As the present platform location is 11 km up-glacier from the most receded (1890) terminal position in Taku Fjord (p. 35), a flow lag of 24 years may be expected. To this we add the measured 40 years displacement between MP IV and MP II and the measured 14 flow lag years between MP IV and the mean elevation of névé Regime Zone B (1,150 m, noted in Fig. 5). This results in a total flow lag of 78 years, the time for ice to flow from Névé Zone B to the glacier terminus.

This flow lag appears to corroborate the 80-year lag previously calculated in our 1950s surveys. This adds credence to the determination of even short-term flow records, especially in situations where the channel morphology is simple and without large changes in gradient. This kind of geometry typifies the Taku Glacier system.

7. Conclusion

Reports on subsequent survey data, key records and analyses, including mapping projects and other strain rate studies using GPS, are presented in the remaining chapters of this monograph. Some of these annually made measurements reveal added details of variations in the continuum of surface flow. In this contribution, we have interpreted these measurements to relate to significant changes in mass balance on the broad and smooth surfaces of upper névés of the Juneau Icefield. In such cases, the climatological importance of survey-based research is further emphasized.

It is noteworthy that many of these later investigations have been accomplished with the cooperation of Prof. Dr.-Ing. *Walter Welsch* and his colleagues from Munich with the excellent assistance of our student participants, many of them supported by U.S. National Science Foundation, Army Research Office and Foundation for Glacier and Environmental Research field grants.

Because of his close involvement with JIRP in recent years, Prof. *Welsch* and *M. Lang* have edited reports as a summary compendium of JIRP survey results in more recent years. Most of these surveys have been supported by the National Science Foundation and Foundation for Glacier and Environmental Research contracts with JIRP.

The Taku, Lemon Creek, Vaughan Lewis, Llewellyn and Cathedral Massif Glaciers topographic mapping projects between 1958 and 1994 have been supported by the American Geographical Society and the National Geographic Society *[CASE, 1958; AMERICAN GEOGRAPHICAL SOCIETY, 1960; KONECNY, 1966; RENTSCH et al., 1990; MILLER et al., 1994]*.

References cited

AMERICAN GEOGRAPHICAL SOCIETY [1960]: Lemon Creek Glacier, Alaska. Nine Glacier Maps, Northwestern North America, to accompany nine separate map sheets on scale of 1:10,000. Special Publication No. 34, Map 1. American Geographical Society, New York

CASE, J. B. [1958]: Mapping of Glaciers in Alaska. Photogrammetric Engineering, Vol. 24, Falls Church, VA.; p. 815-821

EGAN, C. P. [1971]: Contribution to the Late Neoglacial History of the Lynn Canal and Taku Valley Sector of the Alaskan Boundary Range, Juneau Icefield Region. Thesis (Ph. D.), Michigan State University; 200 pp.

FIELD, W. O. and MILLER, M. M. [1950]: The Juneau Icefield Research Project. The Geographical Review, Vol. XL, No. 2, New York; p. 179-190

HEUSSER, C. J., SCHUSTER, R. L. and GILKEY, A. K. [1954]: Geobotanical Studies on the Taku Glacier Anomaly. The Geographical Review, Vol. XLIV, No. 2, New York; p. 224-239

KONECNY, G. [1966]: Application of Photogrammetry to Surveys of Glaciers in Canada and Alaska. Canadian Journal of Earth Sciences, Vol. 3, No. 6, Ottawa; p. 783-798

LANG, M. [1991]: Report on the Geodetic Activities during the 1991 Juneau Icefield Research Program Field Season. JIRP Survey Report, 1991. Juneau Icefield Research Program, Foundation for Glacial and Environmental Research, Juneau; Bundeswehr University Munich, Germany

LANG, M. [1993]: Report on the Geodetic Activities during the 1993 Juneau Icefield Research Program Field Season. JIRP Survey Report, 1993. Juneau Icefield Research Program, Foundation for Glacial and Environmental Research, Juneau; Bundeswehr University Munich, Germany

LANG, M. (ed.) [1995]: Geodetic Activities during the 1995 Juneau Icefield Research Program Field Season. JIRP Survey Report, 1995. Juneau Icefield Research Program, Foundation for Glacial and Environmental Research, Juneau; Bundeswehr University Munich, Germany

LANG, M. and WELSCH, W. M. [1997]: Movement Vector and Strain Rate Determination for the Taku Glacier System. - In: *WELSCH, W. M., LANG, M. and MILLER, M. M. (eds.):* Geodetic Activities, Juneau Icefield, Alaska, 1981-1996. Schriftenreihe des Studiengangs Vermessungswesen, Heft 50, Universität der Bundeswehr München, Neubiberg ; p. 91-116

MARCUS, M. G., CHAMBERS, F., MILLER, M. M. and LANG, M. [1995]: Recent Trends in Lemon Creek Glacier, Alaska. Physical Geography, Vol. 16, No. 2, Silver Springs, MD.; p. 150-161

McGEE, S. R. [1990]: Surface Strain Rates Measurements on the Gilkey Glacier, Juneau Icefield, Alaska, 1989. JIRP Survey Report, 1989. Juneau Icefield Research Program, Foundation for Glacial and Environmental Research, Juneau

McGEE, S. R. [1993]: Fundamentals of Glacier Surveying. JIRP Survey Report, 1993. Juneau Icefield Research Program, Foundation for Glacial and Environmental Research, Juneau

McGEE, S. R. (ed.) [1995]: Geodetic Activities during the 1994 Juneau Icefield Research Program Field Season. JIRP Survey Report, 1995. Juneau Icefield Research Program, Foundation for Glacial and Environmental Research, Juneau

MILLER, M. M. [1947]: Alaskan Glacier Studies, 1946. The American Alpine Journal, Vol. VI, No. 3, New York; p. 339-343

MILLER, M. M. [1948]: Glacier Surveys in the Tetons and Aerial Survey of Alaskan Glaciers, 1947. Appalachia, June 1948, Boston; p. 110-115

MILLER, M. M. [1949]: 1948 Season of the Juneau Icefield Research Project. The American Alpine Journal, Vol. VII, No. 2, New York; p. 185-191

MILLER, M. M. [1955]: Observations on the Regimen of the Glaciers of Icy Bay and Yakutat Bay, Alaska, 1946-1947. FGER Special Report. Foundation for Glacier and Environmental Research

MILLER, M. M. [1956]: The Glaciology of the Juneau Icefield Southeastern Alaska. Ph. D. dissertation, Cambridge University, England

MILLER, M. M. [1963]: Taku Glacier Evaluation Study. Conducted for the State of Alaska, Department of Highways, in cooperation with the U.S. Department of Commerce, Bureau of Public Roads; n. p.

MILLER, M. M. [1967]: Alaska's Mighty Rivers of Ice. National Geographic, February 1968, Washington; p. 194-217

MILLER, M. M. [1985]: Recent Climatic Variations, their Causes and Neogene Perspectives. - In: *SMILEY, C. J. (ed.):* Late Cenozoic History of the Pacific Northwest: Interdisciplinary Studies on the Clarkia Fossil Beds of Northern Idaho. Proceedings of a Symposium organized for the 1979 Annual Meeting of the Pacific Division of the American Association for the Advancement of Science, held at the University of Idaho, Moscow, Idaho. Pacific Division of the American Association for the Advancement of Science, California Academy of Science, San Francisco, California; p. 357-414

MILLER, M. M. and FIELD, W. O. [1951]: Exploring the Juneau Ice Cap. Office of Naval Research, Department of the Navy, NAVEXOS P-510; p. 7-15

MILLER, M. M., MARCUS, M. G., LANG, M. and CHAMBERS, F. [1994]: Lemon Creek Glacier, Alaska, Map, Scale 1 : 10.000. Foundation for Glacial Environmental Research and Arizona State University in cooperation with the National Geographic Society

MILLER, M. M., SPRENKE, K., BENEDICT, T., ADEMA, G., AUERBACH, D., PRUIS, M. and VOLKENING, L. [1994]: Preliminary Report of the 1994 Seismic Surveys on the Juneau Icefield, Alaska. JIRP Geophysical Report, 1994. Juneau Icefield Research Program, Foundation for Glacial and Environmental Research, Juneau

PELTO, M. S. and MILLER, M. M. [1990]: Mass Balance of the Taku Glacier, Alaska from 1946 to 1986. Northwest Science, Vol. 64, No. 3, Washington; p. 121-130

POULTER, T. C., ALLEN, C. F. and MILLER, S. W. [1950]: Seismic Measurements on the Taku Glacier. Sponsored by American Geographical Society, New York, as part of their Juneau Ice Field Research Project, summer of 1949. Stanford Research Institute Special Publication, Stanford; 12 pp.

RENTSCH, H., WELSCH, W., MILLER, M. M. and HEIPKE, C. [1997]: Digital Terrain Models as a Tool for Glacier Studies. - In: *WELSCH, W. M., LANG, M. and MILLER, M. M. (ed.):* Geodetic Activities, Juneau Icefield, Alaska, 1981-1996. Schriftenreihe des Studiengangs Vermessungswesen, Heft 50, Universität der Bundeswehr München, Neubiberg; p. 171-184

SLUPETZKY, H., GRUBER, W. and MAUELSHAGEN, L. [1988]: 1:5.000 Scale Map: Cathedral Massif Glacier System, Atlin Wilderness Park, NW British Columbia, Canada. Zeitschrift für Gletscherkunde und Glazialgeologie, Band 24, Heft 2, Innsbruck; p. 125-136

WARNER, G. and CLOUD, G. [1974]: Measurement of Surface Strain Rates in Glaciers using Embedded Wire Strain Gages. Experimental Mechanics, Vol. 14, No. 1, Brookfield Center; p. 24-28

Further References

BLACHNITZKY, K. [1987]: Report on the Geodetic Activities during the 1989 Juneau Icefield Research Program Field Season. JIRP Survey Report, 1987. Juneau Icefield Research Program, Foundation for Glacial and Environmental Research, Juneau; Bundeswehr University Munich, Germany

BYERS, C., DAELLENBACH, K. K., MARKLILLIE, J. R., McGEE, S. R. and PETER-SON, E. [1988]: Results of the Summer 1988 Surveying Program. Conducted under the Auspices of the Juneau Icefield Research Program. JIRP Survey Report, 1988. Juneau Icefield Research Program, Foundation for Glacial and Environmental Research, Juneau

COLE, J. [1993]: Surveyed Ablation Rates on the Juneau Icefield, Summer, 1993. JIRP Open File Survey and Glaciology Report, 1993. Juneau Icefield Research Program, Foundation for Glacial and Environmental Research, Juneau

DAELLENBACH, K. K. [1989]: Strain Rate Analysis of Glacier Flow in the Taku Glacier, 1987-1988. Senior thesis, Department of Mechanical Engineering, Oregon State University

FRIEDMANN, A. and MILLER, M. M. [1992]: Glacier Surface Velocities and Ablation Rates on the Taku Glacier System, Juneau Icefield, Alaska. JIRP Open File Survey and Glaciology Report, 1992. Juneau Icefield Research Program, Foundation for Glacial and Environmental Research, Juneau

HEISTER, H. [1985]: Adjustment of Network at Camp 10, Juneau Icefield, Alaska. JIRP Survey Report, 1985. Juneau Icefield Research Program, Foundation for Glacial and Environmental Research, Juneau; Bundeswehr University Munich, Germany

JANOCH, J. M. [1982]: Glacier Movement Surveys on the Juneau Icefield, 1982. JIRP Survey Report, 1982. Juneau Icefield Research Program, Foundation for Glacial and Environmental Research, Juneau

KAUFMANN, M. [1992]: Surface Velocities, Strain Rates and Ice Flux on the Taku Glacier and Tributaries, Juneau Icefield, Alaska. JIRP Survey Report, 1992. Juneau Icefield Research Program, Foundation for Glacial and Environmental Research, Juneau

KERSTING, N. [1986a]: Densification of the Gilkey Network 1985 and 1986. JIRP Survey Report, 1986. Juneau Icefield Research Program, Foundation for Glacial and Environmental Research, Juneau; Bundeswehr University Munich, Germany

KERSTING, N. [1986b]: Determination of the Taku Glacier Movement, Juneau Icefield, Alaska, 1986. JIRP Survey Report, 1986. Juneau Icefield Research Program, Foundation for Glacial and Environmental Research, Juneau; Bundeswehr University Munich, Germany

LANG, M. [1989]: Report on the Geodetic Activities during the 1989 Juneau Icefield Research Program Field Season. JIRP Survey Report, 1989. Juneau Icefield Research

Program, Foundation for Glacial and Environmental Research, Juneau; Bundeswehr University Munich, Germany

MARTY, M. [1983]: Surface Movement on the Vaughan Lewis Glacier. JIRP Survey Report, 1983. Juneau Icefield Research Program, Foundation for Glacial and Environmental Research, Juneau

McGEE, S. R. [1989]: Surface Flow Rates in the Taku Glacier System, 1987-1988. Senior thesis, Alaska Pacific University

NYGREN, K. [1989]: Lemon Creek Glacier Remapping Project, 1989. JIRP Open File Report, 1989. Juneau Icefield Research Program, Foundation for Glacial and Environmental Research, Juneau

PORCHER, J. [1990]: Some Aspects of Glacier Movement and Documented Surface Observations, Juneau Icefield, Alaska. JIRP Survey Report, 1990. Juneau Icefield Research Program, Foundation for Glacial and Environmental Research, Juneau

RAY, T. K. [1984]: Surface Flow Survey of the Taku Glacier, 1984. JIRP Survey Report, 1984. Juneau Icefield Research Program, Foundation for Glacial and Environmental Research, Juneau

RENTSCH, H. [1982]: Local Survey Network and Movement Surveys, Lemon and Ptarmigan Glacier, Juneau Icefield, Alaska. JIRP Survey Report, 1982. Juneau Icefield Research Program, Foundation for Glacial and Environmental Research, Juneau; Bundeswehr University Munich, Germany

STEVENS, J. [1993]: Surface Movement Comparisons on the Matthes and Upper Vaughan Lewis Glaciers. JIRP Survey Report, 1993. Juneau Icefield Research Program, Foundation for Glacial and Environmental Research, Juneau

WELSCH, W. M. [1984]: Adjustment of Taku and Gilkey Networks, Juneau Icefield, Alaska. JIRP Survey Report, 1984. Juneau Icefield Research Program, Foundation for Glacial and Environmental Research, Juneau; Bundeswehr University Munich, Germany

Robert P. Sharp

The Flow of Glaciers [1)]

1. Differences in the Speed of Flow as Measured Along a Line Across a Glacier

Glaciers differ from other bodies of landborne ice in their ability to flow. This distinguishing behavior has long fascinated scientists and alymen alike, even to the point of a humorous treatment by the redoubtable *Mark Twain*. Records of surface-velocity measurements on valley glaciers go back at least 200 years.

Early investigators in the Alps showed that straight lines of markers laid across a glacier were, in due time, deformed into parabolic curves (Fig. 1a). Much later, repeated photo-

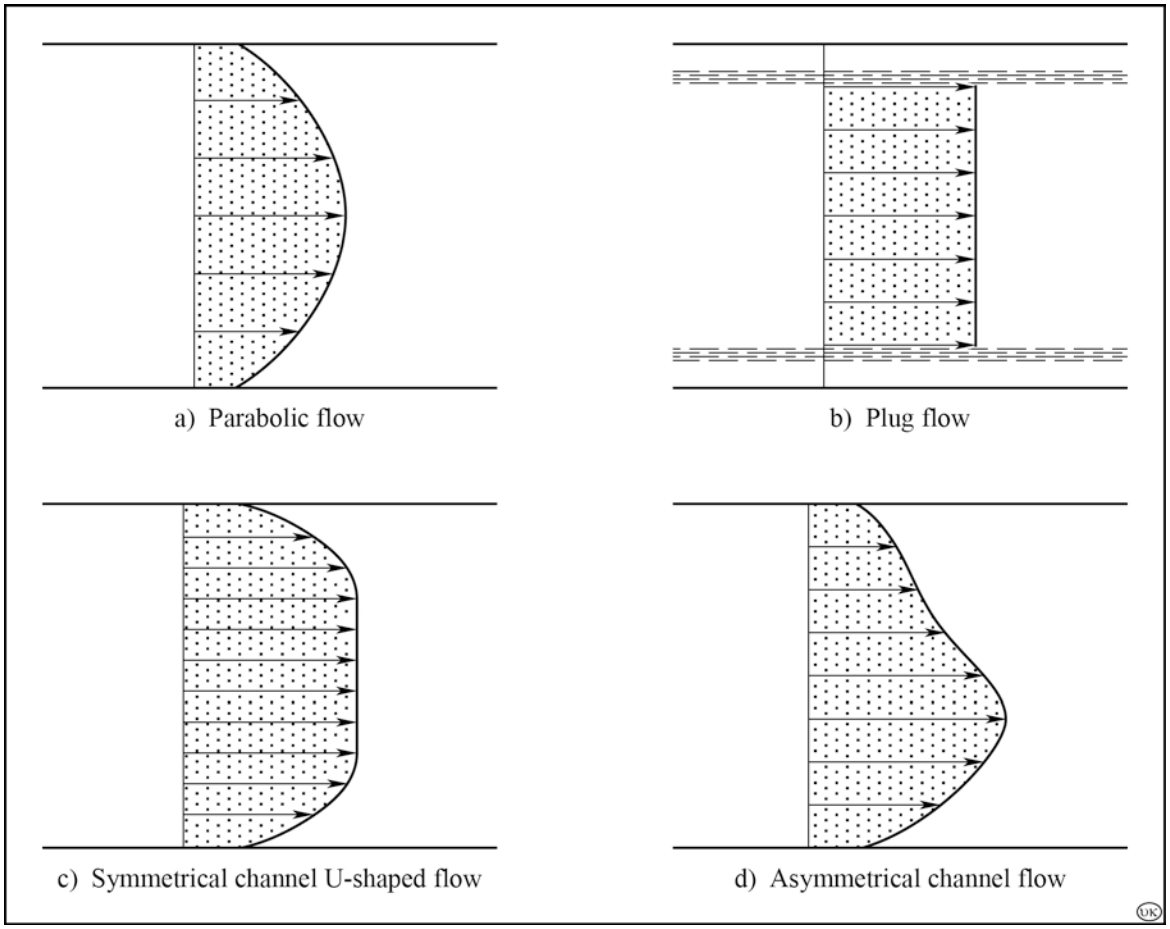

Fig. 1: Different types of surface-velocity distribution along traverse profiles across valley glaciers

1) *SHARP, R. P. [1960]:* Glaciers. Condon Lectures, Oregon State System of Higher Education, Eugene, Orgeon; p. 34-47

graphs of some rapidly flowing glaciers in the Himalayas showed that the entire central parts of these glaciers move with a uniform velocity past marginal zones of nearly stationary ice. In these glaciers the change from essentially no movement to maximum movement occurs within narrow zones near the margins of the glacier (Fig. 1b). This mode of movement has been called plug flow, because the central part moves as a plug past essentially stationary borders.

Measurements of surface velocity using more closely spaced markers suggest that the flow curve across many valley glaciers is intermediate between the parabolic and plug-flow types. As shown by this curve, which for want of a better term we shall call U-shaped, the central part of the glacier moves at a nearly uniform velocity, and the transition to slower movement near the valley walls occurs rapidly in narrow marginal zones (Fig. 1c). Velocity profiles across the Saskatchewan, the Blue and other glaciers (Fig. 2 and 3) suggest that this sort of transverse velocity curve is probably the most common, although for some reason we tend to overlook this fact.

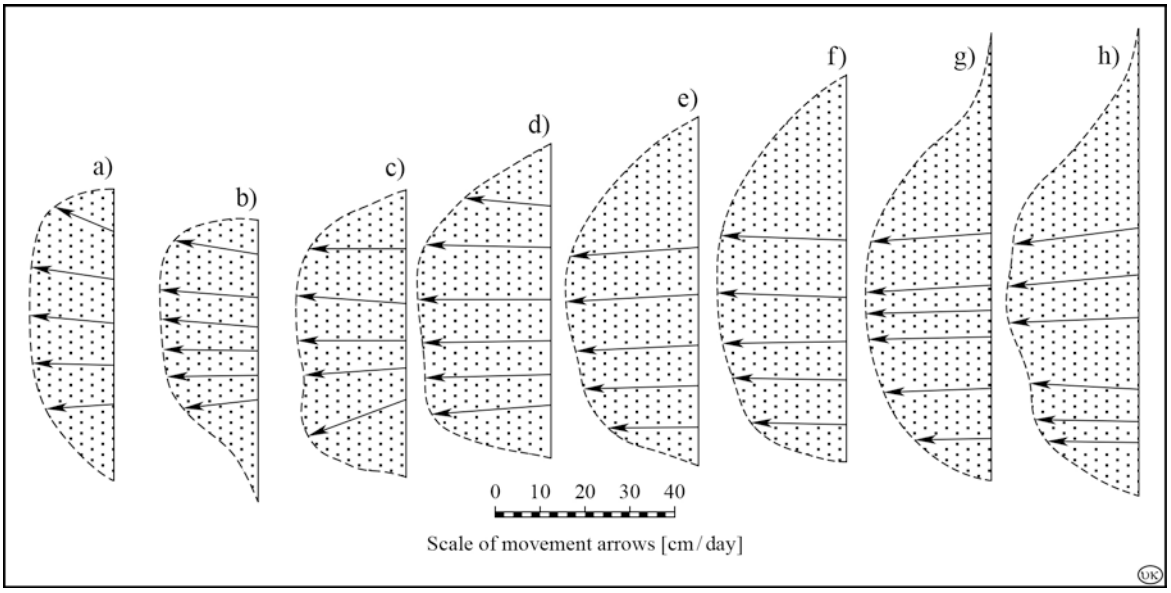

Fig. 2: Horizontal component of surface velocity along a series of transverse profiles from firn edge (h) nearly to terminus (a) of Blue Glacier as measured in 1957-58. Note decrease of velocity near terminus and flow toward margins in terminal region (a).

In evaluating the meaning of the shape of a transverse velocity curve, one must remember that the surface velocity is strongly influenced by the thickness of the glacier and the steepness of its slope. Variations in either or both factors affect the shape and symmetry of the velocity curve. Since the surface velocity is greatest where the ice is thickest, other influences being equal, one would expect that a channel with a U-shaped cross section would produce a U-shaped velocity curve. It does, but a parabolic channel can also yield a U-shaped velocity curve. This happens because of the manner in which ice yields to stress.

To understand this matter it is helpful to make a plot showing the difference in rates at which various substances yield to different degrees of stress. This is known as a stress and rate-of-strain diagram. On such a diagram (Fig. 4), we have plotted the relationships for

three types of material, a, b and c. „a" is a so-called Newtonian fluid, such as water, in which the rate of yielding (strain) increases in a steady, regular manner as the stress (force per unit area) is increased. This gives a straight line of constant slope on the diagram. „b" is a perfectly plastic substance that doesn't yield at all until a certain threshold value of stress is exceeded, after which it theoretically yields at an infinite rate. It gives a straight horizontal line on our plot. „c" is ice which yields at a changing rate as the stress increases, and this produces a curved line on our plot. This behavior is sort of half way between that of the plastic and viscous materials, and for this reason some people refer to ice as a pseudo-plastic or quasi-viscous substance. If ice behaved as a Newtonian viscous fluid, the transverse surface velocity curve would reflect rather faithfully the cross-section shape of the glacier's channel. The U-shaped velocity curve of a glacier flowing in a parabolic channel is thus a reflection of the fact that the yielding curve of ice under the increasing stress caused by increasing thickness has the shape of a half-U (Fig. 4c).

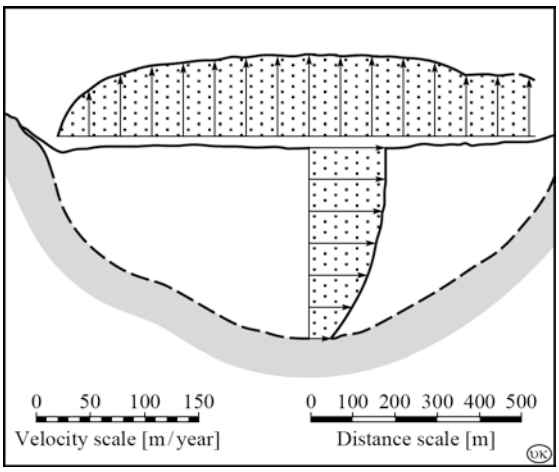

Fig. 3: Measured transverse surface velocity profile (horizontal component) on Saskatchewan Glacier and calculated vertical velocity profile. To get proper picture, reader should imagine velocity profiles folded back so they are perpendicular to plane of the page.

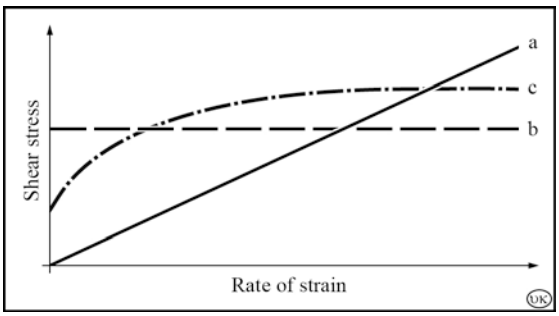

Fig. 4: The relationship of rate of strain to stress for a Newtonian viscous material (a), a perfectly plastic substance (b), and ice (c), as determined by laboratory experiments.

2. Magnitude and Variations of Flow Velocity

Everyone seems to be interested in the speed of glacier movement. Unless otherwise specified, the figures cited below refer to the maximum surface velocity near the center. Many valley glaciers flow with a speed of 0.3 to 0.6 meters per day. In steep reaches, the movement can be 3 or even 6 meters per day, and over icefalls it may be still greater. Velocities up to 40 meters per day have been measured on the huge outlet glaciers of the Greenland Ice Sheet. Sudden short-lived advances of valley glaciers have occurred in the Himalayas, the Andes, and Alaska for which velocities of 30 to 115 meters per day have been estimated. During a brief advance in 1937, the Black Rapids Glacier in Alaska may have attained a velocity of 75 meters per day. These spectacular speeds are truly exceptional, and most of the glaciers that we see move only a few decimeters per day at most.

Seasonal variations in the movement of valley glaciers have been recorded. It is commonly stated that movement in the accumulation area is greater during winter because of the increased load of snow. Conversely, the flow is supposedly greatest in the ablation area during summer because of warmer temperatures and a copious supply of meltwater. These

statements may well represent oversimplifications, and the causes are not necessarily those specified. Seasonal variations in glacier movement need much more study.

Some measurements have been made suggesting that glaciers experience variations in velocity within periods of a few hours or days. Although such movements are often erratic, in some instances a regular diurnal cycle is said to exist, and variations in flow appear to be related to changes in weather conditions. Some of the earlier measurements made may not have been rigorously controlled, and others are possibly not accurate enough to justify the conclusions reached. However, it is certain that variations of small magnitude do occur, but apparent relationships to variations in temperature or other meteorological elements have not yet been satisfactorily explained in terms of cause and effect. It seems that major storms, particularly those with heavy rain, can have a marked temporary effect on velocity, but the reasons for this are not yet known. Short-time variations of glaciers flow constitute an interesting facet of glaciological research worthy of more study than is has yet received.

3. Basal Slip and Internal Flow

The surface movement is produced by slippage of the ice over its floor and by internal flow within the glacier (Fig. 5). Basal slip may account for most of the movement of thin, warm, thick glaciers lying on gentle slopes. Adequate testimony to the existence of basal slippage is given by the ice-scoured bedrock surfaces across which glaciers have moved.

Attempts to determine the proportionate contributions of internal flow and basal slip have been made by boring vertical holes into glaciers and measuring the subsequent deformation of pipes left in the holes. Investigations of this type have been undertaken on glaciers in the Alps, Alaska, Canada and the United States. Fig. 6 presents vertical velocity profiles, or flow curves, obtained from holes in the Malaspina and Blue Glaciers. These curves show that the surface is carried along by movement of the underlying ice and that the differential rate of flow increases with depth.

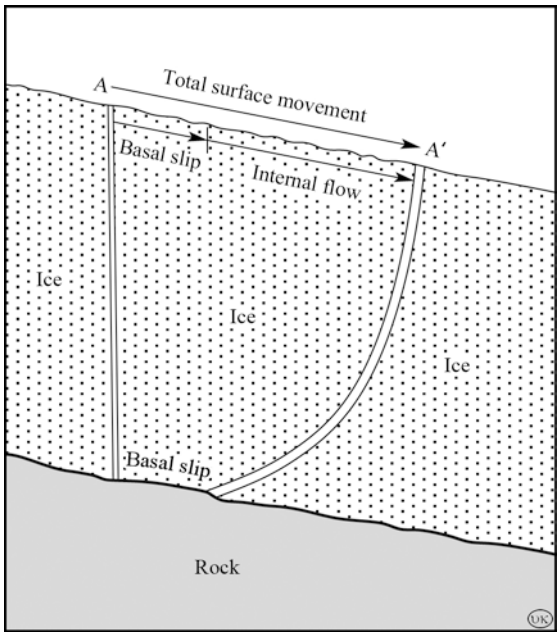

Fig. 5: Sketch illustrating that surface movement on a glacier is produced partly by slip on the floor at its base and partly by internal deformation.

About 20 years ago much attention was given a hypothesis suggesting that ice at depth in a sheet resting on a flat surface would be squeezed out or extruded by the weight of the overlying material, more or less like paste from a tube. Initially, this concept was favorably regarded in some quarters, but physicists have since shown on theoretical grounds that extrusion flow is not only unlikely but indeed downright impossible in most glaciers. Data from boreholes on the Jungfraujoch in Switzerland and the Malaspina Glacier indicate that extrusion flow does not occur in these two bodies, although it should if the concept were valid.

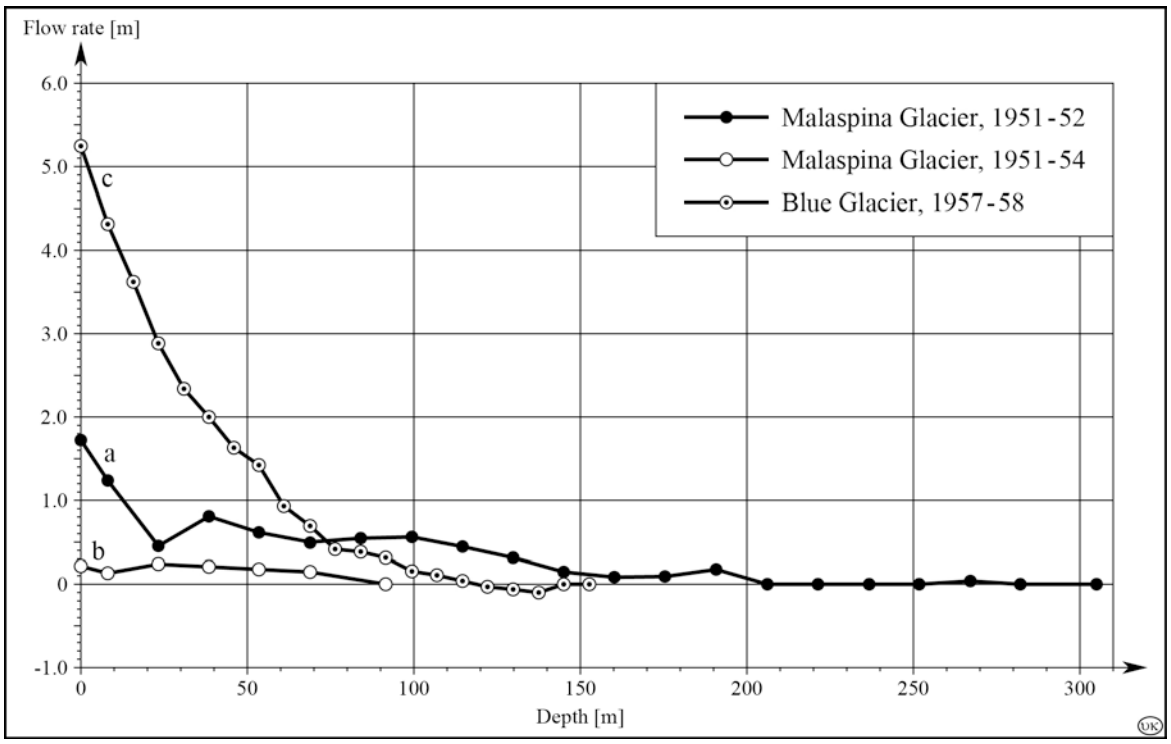

Fig. 6: Deformation by glacier flow of pipes in deep borehoples.

a: Malaspina Glacier 300-meter hole, 1951-52;

b: Upper 100 meters of the Malaspina hole, 1951-54;

c: Blue Glacier, 1957-58.

All glaciers show maximum movement at the surface but greater differential movement with depth. Curve „b" demonstrates that measurable deformation occurs within ice close to the surface in a period of 3 years. If extrusion flow were a valid concept, its effects would show in curve „a", which they do not. Note horizontal scale is exaggerated with respect to vertical scale.

4. The Actual Direction of Flow

For some reason most of us are inclined to think of the flow of a glacier as parallel to its surface. In most parts of the glacier the true direction of movements is *not* parallel to the surface, and most of the values reported for surface velocities represent only that part of the motion that is parallel to the horizontal plane of a map.

Many years ago the American glaciologist *Harry Fielding Reid* deduced that the actual directions of flow in a valley glacier should be obliquely downward in the accumulation area and obliquely upward in the wastage area. He arrived at this conclusion partly through the realization that the snow layer added each year in the accumulation area is wedge-shaped, thickest at the glacier head and thinning to an edge at the snowline. A somewhat similar wedge, thickest near the terminus, is removed each year in the wastage area. Clearly, a glacier could maintain its surface profile most easily in the face of these wedge-shaped changes by movements oblique to rather than parallel to the surface. The component of downward movement, *with respect to the surface*, should increase toward the head of the glacier, and the component of upward movement, should increase toward the terminus. Flow in the vicinity of the annual snowline should be essentially parallel to the surface.

Measurements of the absolute directions of movement made in the ablation areas of the Saskatchewan and Blue Glaciers show that it is generally slightly upward *with respect to the surface* but *not* with respect to the horizontal (Fig. 7). With exceptions, the upward angle increases slightly towards the terminus. Nowhere is the angle large, and diagrams drawn by *Reid* and others after him, including myself, probably err in showing the flow lines as rising to steeply. They may also be incorrect in indicating movement upward from the horizontal. Unfortunately, corresponding data on actual directions of movement have not yet been obtained from the accumulation areas of these glaciers.

As viewed in a horizontal rather than a vertical plane the direction of flow is also not always directly downglacier. The direction of flow is controlled primarily by the direction of slope of the ice surface. Most valley glaciers have a slightly convex transverse profile in the wastage area caused by greater melting along the margins. Because of this, some flow of ice obliquely toward the margins should be expected, and has been recorded on the Saskatchewan and Blue Glaciers (Figs. 2 and 8). This direction of flow enables glaciers to replace ice destroyed by marginal melting and helps maintain the transverse profile. One should expect to find just the reserve relationship above the annual snowline in places of exceptionally heavy marginal accumulation, and inward flow from margins has been recorded in such situations.

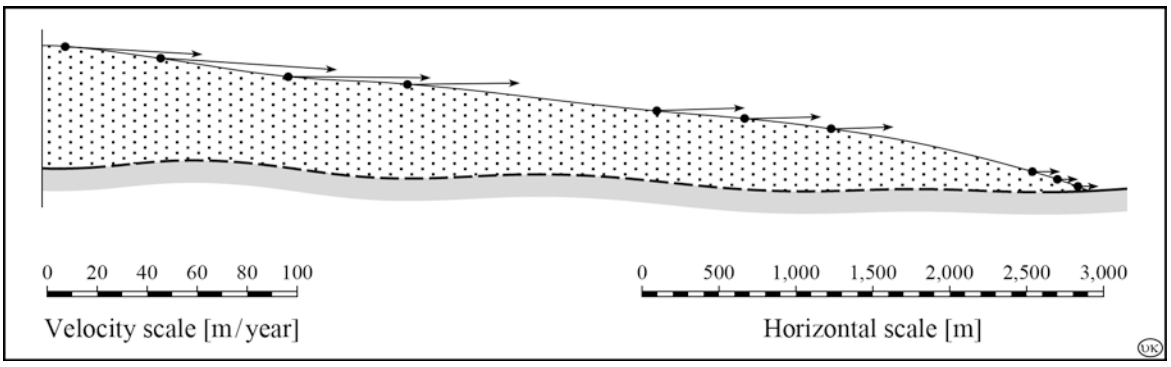

Fig. 7: True direction and amount of flow as recorded along a central flowline in the Saskatchewan Glacier. Note that flow directions are slightly upward with respect to the glacier surface and that movement is much slower near the terminus.

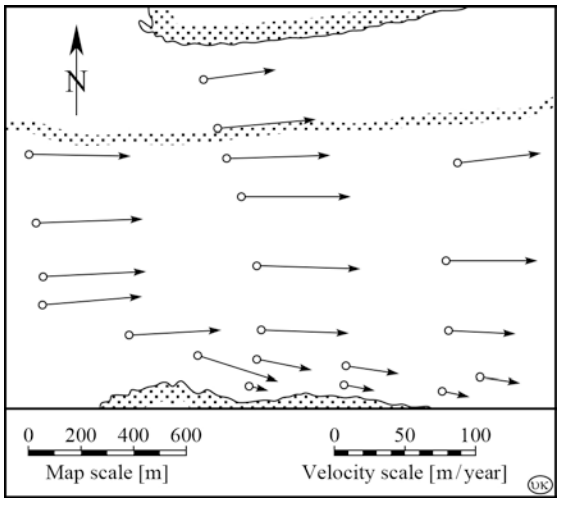

Fig. 8: Arrows indicate horizontal component of annual surface movement on Saskatchewan Glacier about 3 kilometers below firn edge. Note flow obliquely toward south margin, presumably because of excessive ablation and local widening of the valley.

5. Longitudinal Variations in Flow

The largest volume of ice being handled by a glacier is at the annual snowline. This must be so, for the total amount of ice increases progressively to the snowline because of accumulation and progressively decreases below it through wastage. In a glacier of uniform cross section and uniform longitudinal slope, the surface velocity must also have its greatest value at the annual snowline. In such a glacier the average velocity should increase from the head of the glacier to the snowline and decrease from there to the terminus. Few glaciers are of uniform cross section and slope, but allowing for irregulations in both factors, a decrease in surface velocity downglacier from the snowline is shown by both the Saskatchewan and Blue Glaciers (Figs. 2 and 8). Corresponding data above the snowline are lacking.

Actually, much larger and more abrupt changes in velocity are caused by variations in channel characteristics, particularly slope. What happens when a glacier slows down over a gentle reach in its course? The ice farther upglacier doesn't know anything about this, except possibly for a local *„back water"* effect, and its keeps moving along at its usual pace pouring material into the gentler reach. The result is that ice tends to pile up in the gentle reach, and the glacier becomes thicker until it can handle the discharge at the slower velocity. Rivers of water do the same thing, slow flowing parts are deep. This behavior in glaciers has been termed *„compressive flow"* by *John Nye* of Bristol, England, who has demonstrated on a mathematical and physical basis, how and why it occurs. One should not be misled by the term *„compressive"*. Ice in glaciers is to all intent and purpose essentially an incompressible solid. Except for elimination of air bubbles the ice remains unchanged in density, the only compression that occurs is a shortening of a unit ice which is balanced by its increase in thickness.

Nye has also demonstrated that steep reaches with accelerating velocity produce an extension of the glacier, with a reduction in thickness and the formation of crevasses. This he designates *„extending flow"*. It occurs, for example, as a glacier descends an icefall, and the ice becomes several times thinner than it was above. It is also badly crevassed. In the *„plunge pool"*, at the base of the icefall, extreme compressive flow occurs, and the ice builds up to a thickness several times that in the icefall, the crevasses are forced shut, and the broken ice debris that has fallen into them is severely squeezed.

Practically all glaciers undergo at least a modest degree of extending and compressive flow because of differential accumulation and wastage. However, the areas of strong compression and extension are related to abrupt changes in longitudinal gradient. The concept of these types of flow developed by *Nye* is one of the most useful ideas to have appeared in glaciology in decades. It helps immeasurably in understanding glacier behavior and in interpreting the structures seen within them.

6. Surges in Glaciers

For many years it has been known that bulges of increased thickness descend through valley glaciers at a velocity several times the normal speed of flow. We now realize that many of the recorded erratic and sudden advances of glacier snouts are the result of the arrival of such bulges at the glacier terminus. The movement of a bulge through the Nisqually Glacier on Mount Rainier in Washington, has been under observation now for nearly 15 years. The events attending its arrival at the terminus, if it gets that far, are awaited with interest.

A theoretical analysis of the behavior of waves in glaciers suggests that the bulges, better termed surges, should move with velocities about 3 to 8 times greater than the normal speed of flow. Surge velocities about 4 times normal have actually been observed. It appears that a general disturbance in the headwaters can generate a series of surges. Those of high velocity overtake and enforce slow-moving surges so that the phenomenon which ultimately arrives at the terminus may have some of the characteristics of a shock wave. Perhaps, this is one reason why the behavior of the glacier snout is so unusual. Surges need not be limited to valley glaciers. Our experiences suggest that one moved through the borehole site on the Malaspina Glacier, a piedmont ice sheet, between the summers of 1953 and 1954.

The general tendency is to attribute surges to episodes of increased accumulation in the headwater. This possibility is supported by the behavior of glaciers in the Yakutat Bay area of Alaska following the powerful Yakutat Bay earthquakes in 1899. Many of these glaciers experienced sudden short-lived advances a few years after the earthquakes. Various line of reasoning led to the conclusion that this behavior was best explained by the movement of surges through these glaciers, and it was postulated that these surges were generated by the large amounts of snow avalanched onto the headwaters of the glaciers by the earthquakes. Many other spectacular, short-lived advances, seemingly unrelated to earthquakes or even to known periods of exceptional accumulation, have been reported from Alaska, the Alps, the Andes and the Himalayas.

In this regard the recent behavior of Muldrow Glacier draining off the east slopes of Mt. McKinley in Alaska is particularly informative. The lower reach of this glacier has been relatively inactive, even locally stagnant, for a long time. Suddenly during the winter of 1956-57 it showed a spectacular renewal of activity, and the terminus advanced rapidly. Morainal features on the upper part of the ice tongue also moved downward rapidly. The important thing is that there is no reason to attribute this behavior to a sudden increase in accumulation of either earthquake or meteorological origin. Following the advance, it was noted that the ice level in the upper reaches of several of the important tributaries of the Muldrow system had dropped by several meters. The volume of ice supplied by this drop is about right to account for the advance and expansion of the lower part of the glacier. It looks as though the Muldrow Glacier had slowly been accumulating material for many years, up to a certain threshold amount. At this point a sudden evacuation from the accumulation area began to occur which gave rise to a surge or series of surges that moved rapidly downglacier and ultimately produced the great changes in the lower reaches. This is not a new concept by any means, but the recent Muldrow Glacier behavior is one of the best documented cases on record.

The behavior of surges in glaciers is currently a topic of high interest in glaciology. We need more observation of this phenomenon in the field to support the excellent theoretical treatments made by *Weertman, Nye* and others.

7. The Mechanics of Movement

Ice is clearly a solid substance, but it is equally clear that large bodies of ice will flow with great facility, given time. Just how does ice flow, what are the detailed mechanics of the process, and do several different mechanism contribute to the total effect? Or is it likely that different mechanism play the dominant role under different conditions? Glaciologists have struggled with these problems for a long time, so let us review briefly their thoughts on these matters.

Adjustments between grains have long been highly regarded as a possible means of glacier flow. This involves the movement of individual grains (crystals) past one another as might occur in a bean bag or a sack of lead shot (Fig. 9b). Intergranular adjustments could occur freely and easily in loose snow or firn, and studies of changes in crystallographic orientation of firn grains indicate that such adjustments are common in early stages of the compaction process. However, are they equally common in solid glacier ice made up of crystals firmly grown together? The possibility of intergranular adjustments in such material cannot be hastily dismissed in view of the extended time available and the assistance afforded by local pressure melting and vapor transfer. However, some glacier ice consists of crystals so intimately and completely loose. They are held together in the manner of a three-dimensional jig-saw puzzle. Furthermore, the strong preferred crystallographic orientation found in glacier ice suggests that intergranular shifting is minimal. For these reasons, intergranular adjustments are no longer so highly regarded as a major mechanism of solid flow in glaciers. They may be the principal means by which snow deforms, and they could contribute in limited degree to glacier flow under proper conditions.

A once-favored mechanism of flow depends upon local and temporary changes of ice to the liquid or vapor phases (Fig. 9c). The thought is that local stresses, crystal configuration or energy distribution cause some of the ice to melt or vaporize. This vapor or liquid is then supposed to move a short distance before reverting to the solid state, thus effecting a transport of material. Changes of phases could promote intergranular adjustments, and the homogenization of oxygen isotopes that occurs within glaciers is one reason of thinking that such changes may occur. However, the movement of the liquid would probably be controlled by capillarity, and there is no obvious reason why either it or the vapor should move predominantly in a downglacier direction. Furthermore, laboratory tests show that ice

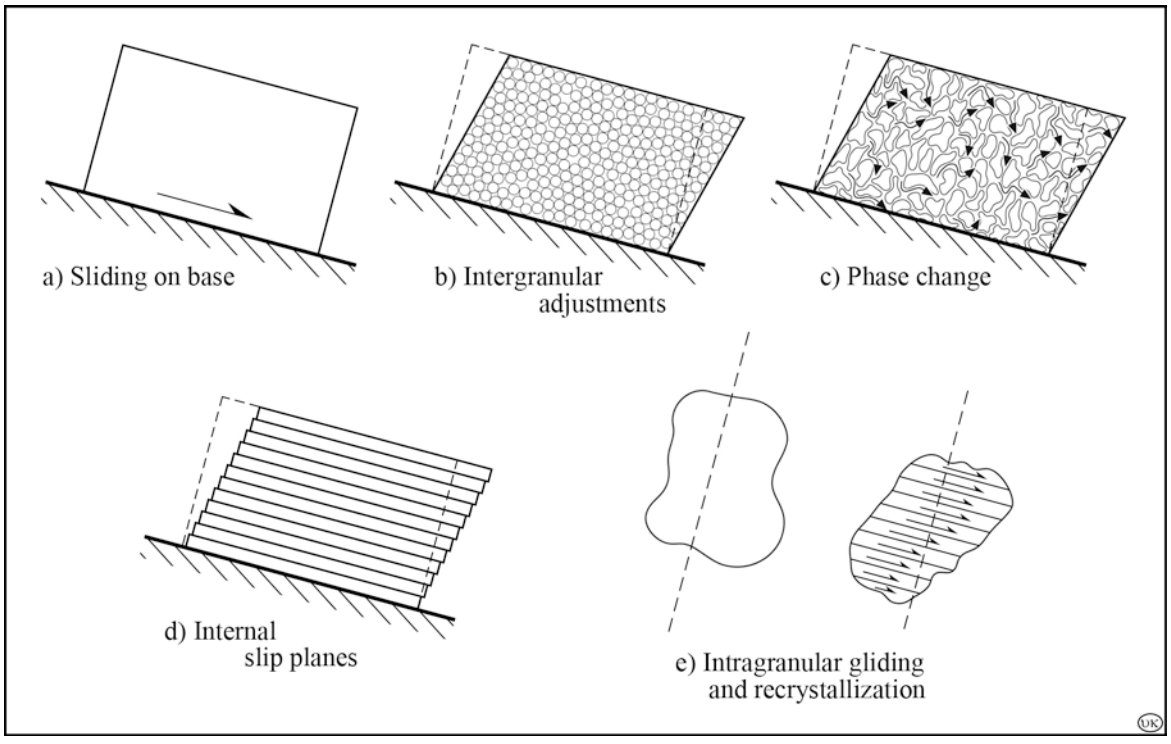

Fig. 9: Sketches illustrating various possible mechanisms of glacier movement

can be made to flow at temperatures well below those at which pressure melting would occur. The phase-change mechanism may function, but it is probably not of major importance in most situations.

A solid body can be deformed by a series of small displacements along a multitude of closely spaced parallel planes (Fig. 9d). Slippage of the individual playing cards within a deck affords a good analogy. Structures observed in glaciers suggest that such slip displacements occur locally, and on a limited scale, but the phenomenon does not appear pervasive enough of of sufficient magnitude to account for most glacier movement.

This brings us to a final possibility which currently is highly regarded. It holds that ice flows principally because of adjustments that occur within the individual ice crystals (Fig 9e). This is known as *intragranular* yielding as compared to *intergranular* adjustments; the two should not be confused. It has long been known that an ice crystal yields easily to shear stress by gliding along the basal crystallographic plane. This is a process which does not destroy the solidity or coherence of the material and does not alter or disrupt the internal atomic arrangement of the crystal. Its occurence has been demonstrated repeatedly by laboratory experiments. The fact that crystals in a glacier display a strongly preferred orientation is taken as evidence in support of intracrystalline yielding as a principal mechanism of glacier flow. Continued internal gliding of the crystals would eventually distort them into grossly elongated shapes unlike anything usually seen in glaciers. Therefore, it is postulated that a progressive recrystallization accompanies the intracrystalline gliding, and that this maintains the crystals in their roughly equidimensional form. Recrystallization of this type has been demonstrated in the laboratory, and it is one of the mechanisms by which crystals arrange themselves into the proper orientation for yielding by intracrytsalline gliding. This need not be the only mechanism of solid flow in glacier ice, but it is currently regarded as one of major significance.

Arne Friedmann

The Ice Flux and Dynamics of Taku Glacier, Juneau Icefield, Alaska

Through geophysical sounding of several transects of the Taku Glacier System it was possible to determine ten cross-sectional profiles of key locations on the glacier. By multiplying the cross-sectional area of a profile with the mean yearly glacier velocity the flux through such a profile can be calculated. Ten profiles were examined and the highest flux was found at Profile II near the **E**quilibrium **L**ine **A**ltitude (ELA) with $6.7 \cdot 10^8$ m^3/a. The Matthes Glacier is transporting the largest ice volume into the Main Glacier, approximately as much as the Demorest Glacier and the NW-Branch together. The SW-Branch and the smaller tributaries contribute only a negligible ice volume to the Main Taku Glacier. A comparison of the actual flux and the balance flux shows that ice thickness is increasing over the whole glacier length. It was also revealed that ice thickness at Profile VII, determined by the gravity method, is incorrect and Profiles VIa and V were found to be too small. All other ice thickness profiles were proofed to be correct.

1. Introduction

The Juneau Icefield in southeast Alaska covers an area of about 4,000 km^2 and consists mainly of interconnected highland valley glaciers in the Northern Boundary Range at the Canada/Alaska border. The Taku Glacier System is a fairly large (710 km^2) temperate tidewater glacier, which is composed of several tributary glaciers. The four largest ones are the Matthes Glacier, the Demorest Glacier, the NW-Branch and the SW-Branch (Fig. 1). It has a total length of 59 km and its lower part splits into two tongues, the short Hole-in-the-Wall-Glacier terminus and the board lobe of the Main Taku terminus. Both end near tidewater in the Taku River Valley or the Taku Inlet respectively. The Taku Glacier has a strong positive mass balance (AAR: 0.88 – **A**ccumulation **A**rea **R**atio (AAR) is the percentage of a glacier's total area above the ELA) nand has advanced 7.3 km since 1899, but stagnates since 1989 (p. 35).

Over the last four decades glacier surface velocities were measured yearly by the Juneau Icefield Research Program (JIRP) on several selected profiles (Fig. 2) on which occasionally in some years geophysical ice thickness soundings were carried out. The best set of ice thickness data was obtained by using seismic techniques in the years 1993 and 1994 by *BENEDICT et al. [1993, 1994]*.

2. Methods

Ice flux was calculated on several profiles of the Taku Glacier System by *NIELSEN [1957], MILLER [1963]* and on Profile IV by *DAELLENBACH and WELSCH [1990]*. These works did not include the new ice depth data gained in the years 1993 and 1994.

In this article the new data set will be used for the first time to calculate the ice flux through all classic profiles (Fig. 2) of the Taku Glacier System.

The ice flux through a glacier profile depends mainly on its cross-sectional area (given by ice thickness and glacier width) and the mean velocity of the ice passing through it *[PATERSON, 1994]*. The following equations are used for the ice flux calculations:

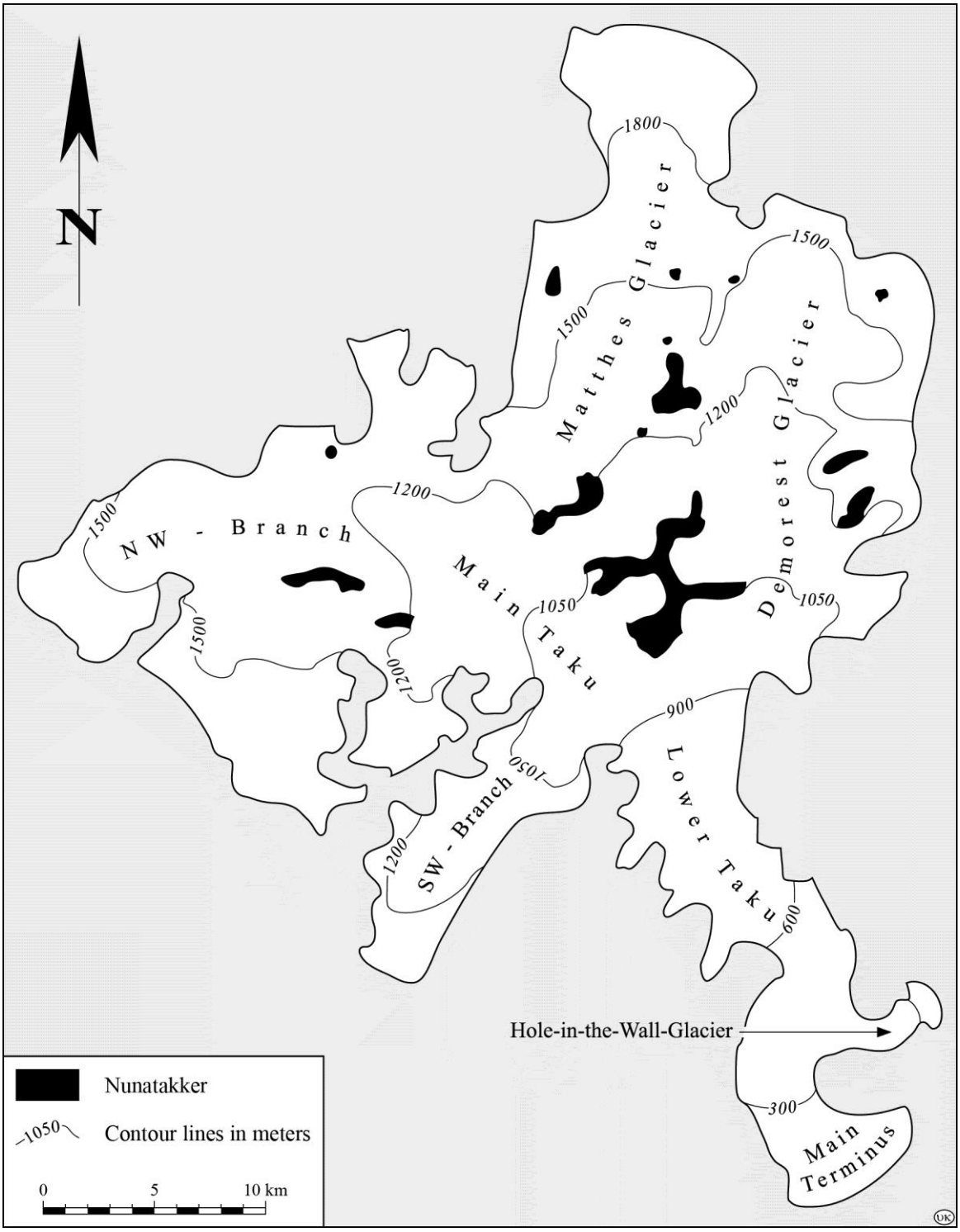

Fig. 1: The Taku Glacier with its four major tributary glaciers

$$Q_x = A_x \cdot u_M \,, \qquad [1]$$

$$Q_x = A_x \cdot u_M \cdot \rho \,. \qquad [2]$$

Q denotes the ice flux trough profile x, A_x is the respective cross-sectional area, ρ is the density of ice and u_M describes the mean yearly glacier surface velocity averaged over the glacier width. Equation 1 gives the ice flux in m^3 per year (m^3/a) and equation 2 in kg

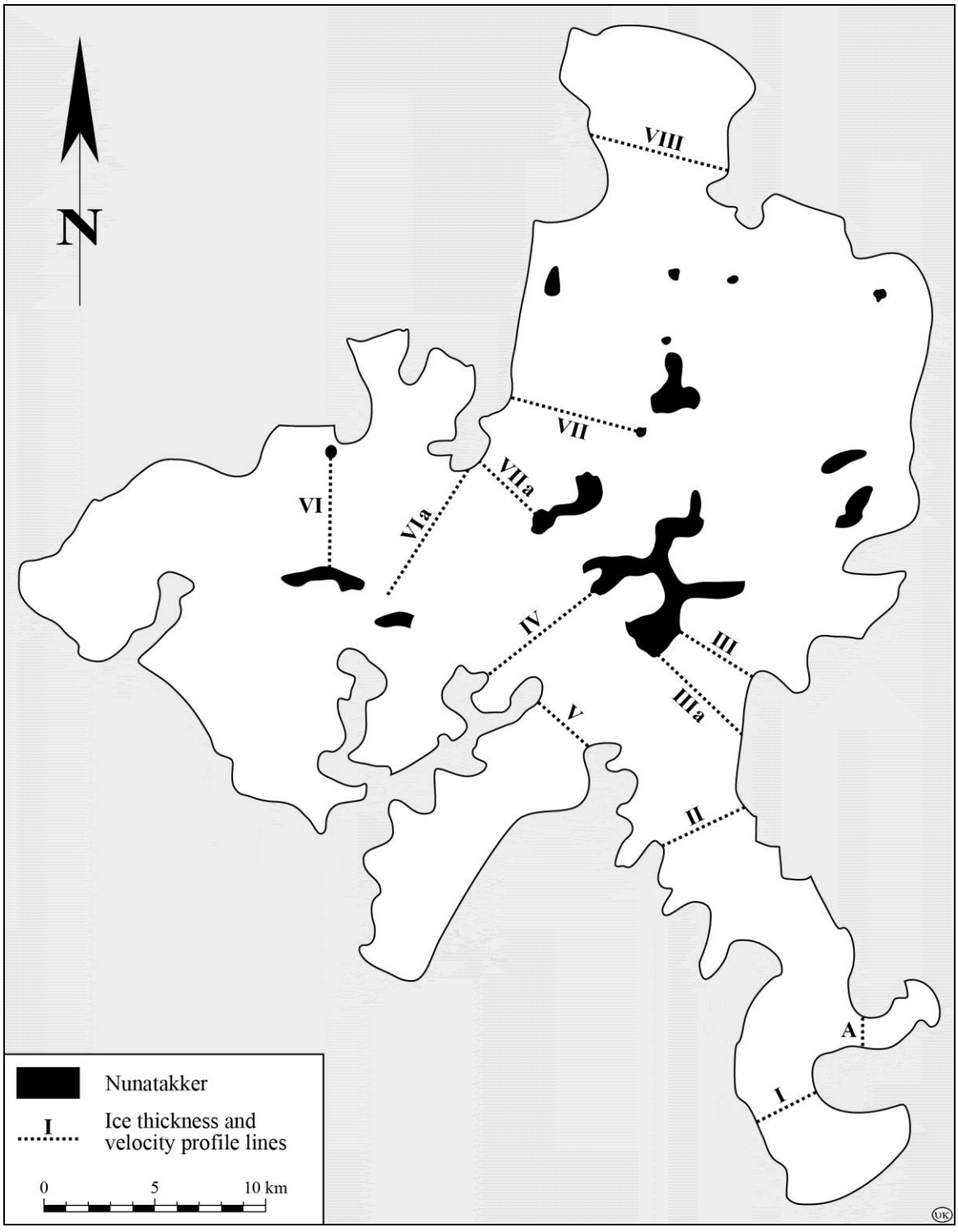

Fig. 2: The individual ice thickness and velocity profiles of the Taku Glacier System

water equivalent per year (kg/a). Following *NYE [1965]* the mean yearly surface velocity matches the mean yearly velocity integrated over the ice thickness by 2 percent for profiles with $W>2$. W, a scaling factor introduced by *NYE [1965]*, is defined as

$$W = \frac{\frac{1}{2} w}{h} \quad . \qquad [3]$$

The half-width of the glacier profile is described by $\frac{1}{2}w$ and h denotes ice thickness. On Taku Glacier there are three profiles with $W>2$. The surface velocity will therefore be scaled in these three profiles by the appropriate factor as given by *NYE [1965]*. The flux of all other profiles is calculated using the measured surface velocity per day multiplied by 365 to give the yearly mean value.

The cross-sectional areas A_x of the ice thickness profiles were either determined planimetrically or by using the equation

$$A_x = h_M \cdot w \qquad [4]$$

h_M represents the mean ice thickness and w denotes the width of the glacier profile.

Balance flux is calculated following *RAYMOND [1980]*. The accumulation rate b per unit time t is integrated over the surface area A above the profile x, which can be expressed by the equation

$$Q_b(x,t) = \int_{A_x} \frac{\partial b}{\partial t} \cdot \mathrm{d}A \; . \qquad [5]$$

The mean balance velocity $V_b(x)$ in m/a can be found likewise for profile x *[CLARKE, 1987]*:

$$V_b(x) = \frac{Q_b(x)}{A_x} \quad . \qquad [6]$$

The actual ice velocity $V_a(x)$ through a cross-sectional profile x is given by

$$V_a(x) = \frac{Q_a(x)}{A_x} \qquad [7]$$

where Q_a is the actual flux.

The instruments used to measure glacier surface velocities were the Global Positioning System (GPS) or theodolites with Electronic Distance Meters (EDM) *[FRIEDMANN, 1992]*. The surface velocities were measured over a period of a few weeks in July and August over the last years by the Juneau Icefield Research Program (JIRP). The data comes mostly from *LANG [1991, 1993], WELSCH [1992]* and *BEINEKE [1994]*. The resulting glacier movement was multiplied by 365 to achieve the yearly velocity. This is well justified, because no basal sliding occurs at the Taku Glacier with the exception of Profile I. Year-round stake measurements by *MILLER [1963]* in the 1950s and 1960s show, that the summer velocity field closely resembles the winter velocity distribution. The velocity pattern of the Taku Glacier System is mainly parabolic or U-shaped with a high velocity zone in the center of the glacier *[FRIEDMANN, 1992]*. The velocity data used to calculate the ice flux is given in Table 1 and the partially interpolated mean yearly velocity distribution on the Taku Glacier System is shown in Fig. 3.

Ice thickness was measured employing seismic techniques by *BENEDICT et al. [1993, 1994]* on Profiles I, II, IV, VIIa and VIII. Profile IIIa was determined by *POULTER et al. [1950]* and is the only not yet newly resurveyed profile. The other profiles were sounded using the gravity method: Profile VII by *BENEDICT [1984]*, Profile VIa and V by *ISBELL [1984]*. Profile A of the Hole-in-the-Wall-Glacier was taken from the topography of the USGS map (1890) of the Taku area. The ice thickness profiles can be verified by the flux

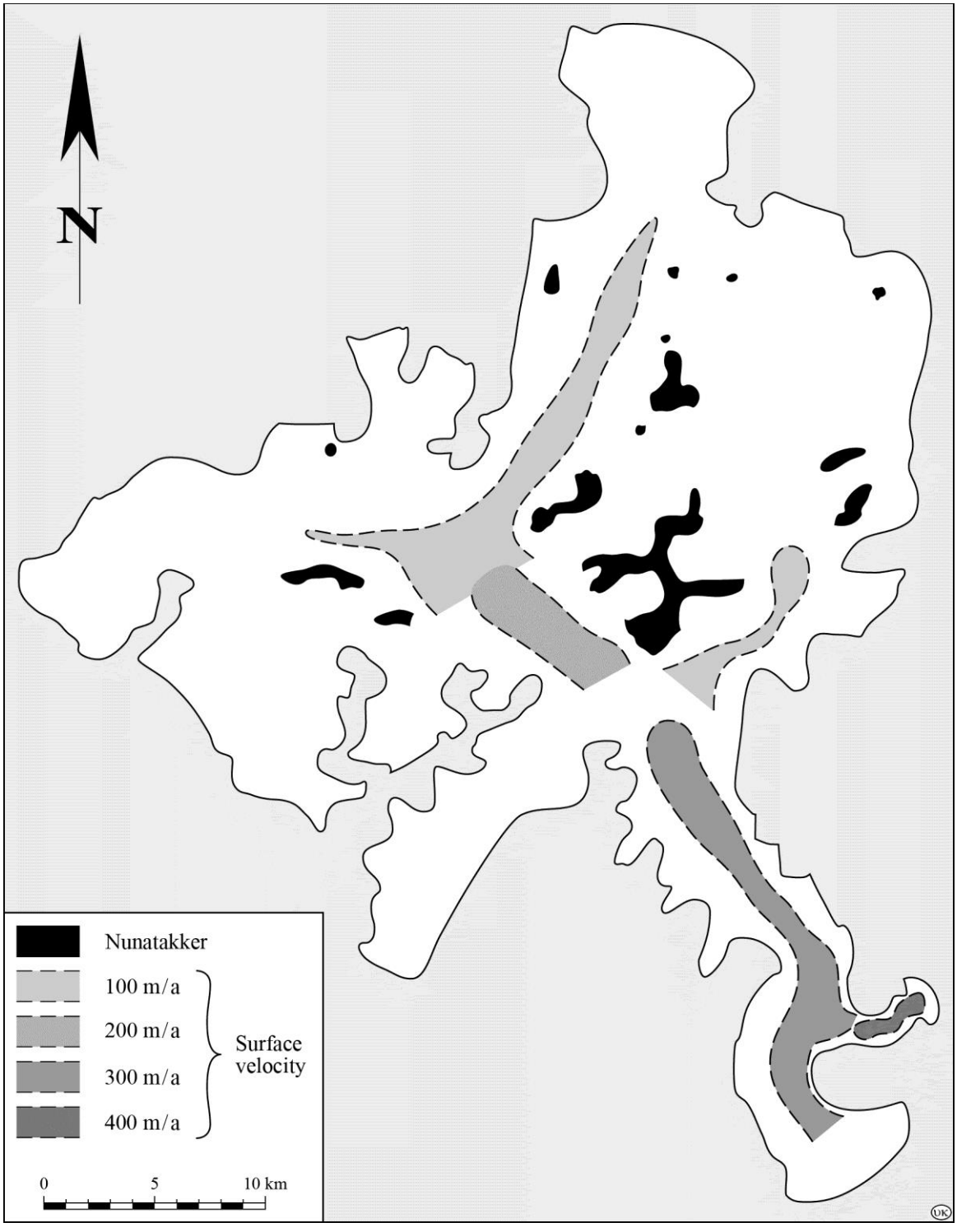

Fig. 3: Partially interpolated glacier surface velocities in m/a on the Taku Glacier System

calculations. The partially interpolated ice thickness distribution of the Taku Glacier System can be detected in Fig. 4 and the resulting cross-sectional areas of the respective profiles are listed in Table 2.

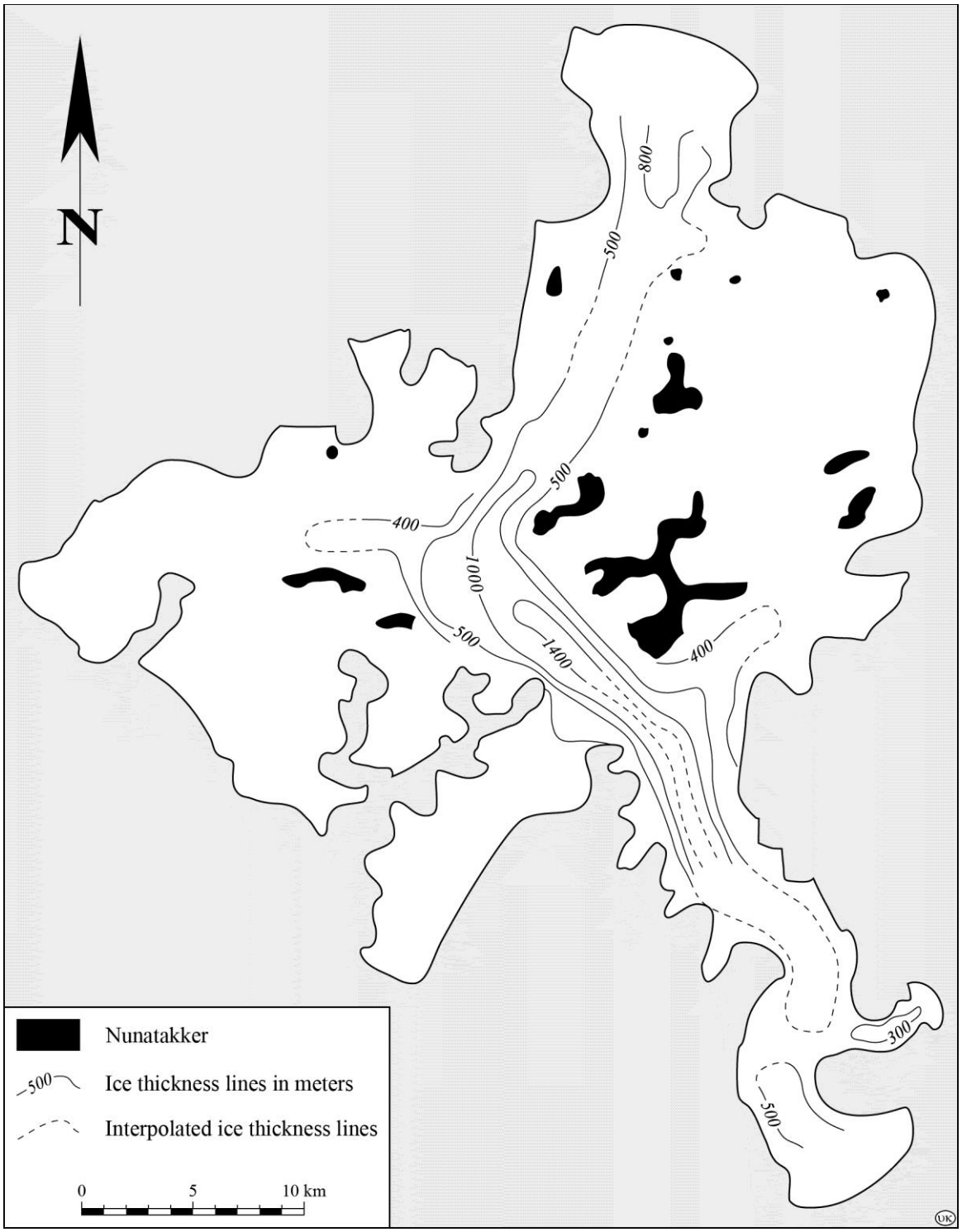

Fig. 4: Ice thickness distribution in meters on the Taku Glacier System

Table 1: Mean glacier surface velocities used in the flux calculations for the individual profiles

Profile	Mean yearly glacier surface velocity u_M [m/a]
A	219
I	219
II	223
III / IIIa	88
IV	128
V	26
VIa	84
VII	95
VIIa	120
VIII	42

Table 2: Mean glacier surface velocities used in the flux calculations for the individual profiles

Profile	Cross-sectional area [$m^2 \cdot 10^6$]
A	0.5010
I	1.2874
II	3.0000
III / IIIa	1.7250
IV	3.9100
V	0.5500
VIa	1.2400
VII	(1.7000)
VIIa	2.2500
VIII	2.0250

3. Results and Discussion

The results of the 1994 ice flux calculations are presented in Table 3. It is shown, that the Matthes Glacier transports the largest ice volume into the Main Taku Glacier. The flux of the Demorest Glacier and the NW-Branch is also a substantial contribution to the Main Glacier, whereas the flux of the SW-Branch is negligible.

In Profile IV 60% of the ice volumes comes from the Matthes Glacier, 25% from the NW-Branch and 15% from other sources. Profile II near the ELA has the highest ice flux of the Taku Glacier System with $6.7 . 10^8$ m^3/a. It is composed by 24% of Demorest Glacier ice and by 76% of ice from Profile IV. The Matthes Glacier always occupies the over 1,400 m deep central portion of the valley. 58% of the ice from Profile II arrive at Profile I and A. Thereof 72% flow to the Main Taku Icefront and 28% into the Hole-in-the-Wall-Glacier. In Profile A 70% of the ice volume comes from the Demorest Glacier and 30% is composed of ice from the Matthes Glacier. The errors of the ice flux calculations are 10%, which results mainly from uncertainties in the velocity data and the cross-sectional areas of the profiles.

3.1 Balance Flux

To interpret the dynamics of the Taku Glacier it is useful to compare the actual ice flux of the year 1994 (Table 3) with the balance flux. The balance flux at the ELA gives the ice volume, which would transport the total yearly accumulation into the ablation area. This situation would represent a model glacier exactly in balance. In reality most glaciers are out of balance. Is the balance flux at the ELA lower than the actual flux, more ice will be transferred into the ablation area than snow fell on the accumulation area. The glacier looses mass.

In the opposite case, if the balance flux is higher than the actual flux, not the whole yearly accumulation will be transported into the ablation zone. The surplus will lead to ice thickness increases.

As can be seen in Table 4 the balance flux and actual flux of the Taku Glacier are not identical. The glacier is not in balance. Less ice is transported out of the accumulation area as snow fell, which will result in an ice thickness increase. For the calculation of the balance flux the mean accumulation rates over the last 40 years on the Taku Glacier System as given by *PELTO and MILLER [1990]* were used rather than the data of 1994. Since the cross-sectional areas of all glacier profiles are constant and the mean velocities did not vary much since the late 1950s *[FRIEDMANN, 1996]*, the ice flux of the year 1994 will approximately represent the mean yearly flux over the last 40 years. Therefore the difference between balance flux and actual flux will give the yearly ice surface rise above the relevant profile over the last 40 years.

Table 3: Ice flux through the profiles of the Taku Glacier System 1994

Profile	Ice flux [10^6 m^3/a]	Ice flux [10^6 m^3/d]	Ice flux [10^9 kg/a]	Ice flux [10^9 kg/d]
A	110	0.30	100	0.27
I	280	0.77	257	0.70
II	670	1.80	614	1.68
III / IIIa	150	0.41	138	0.38
IV	500	1.37	450	1.23
V	14	0.04	126	0.03
VIa	105	0.29	945	0.26
VII	(240)	(0.66)	(216)	(0.59)
VIIa	270	0.74	243	0.67
VIII	85	0.23	765	0.21

Table 4: Comparison of actual flux and balance flux on the Taku Glacier System

Profile	Q_b [10^6 m^3/a]	Q_a [10^6 m^3/a]	V_b [m/a]	V_a [m/a]	ΔQ [10^6 m^3/a]	ΔV [m/a]	Z_G [m/a]
A	–	110	–	219	–	–	–
I	–	280	–	219	–	–	–
II	810	670	270	223	140	47	0.235
III / IIIa	200	150	116	88	50	28	0.33
IV	591	500	151	128	91	23	0.275
V	40	14	73	26	26	47	(0.58)
VIa	246	105	197	84	141	113	(0.97)
VII	260	(240)	104	95	20	9	0.165
VIIa	291	270	130	120	21	10	0.15
VIII	90	85	44	42	5	2	0.14

The mass increase $M(x)$ per unit time t in an area can be written after *RAYMOND [1980]* in the form

$$\frac{\mathrm{d}M(x)}{\mathrm{d}t} = Q_b(x) - Q_a(x) \; . \qquad [8]$$

The resulting ice surface level rise z in the area x is given by

$$z_x = \frac{\Delta Q}{F} \; . \qquad [9]$$

Herein ΔQ is the difference between Q_b and Q_a and F is the area above the respective profile.

Most profiles of the Taku Glacier System show a slightly higher value for the balance flux than the actual flux. This points to a small but steady increase in ice volume over the last 40 years. A marked difference between actual and balance flux can be seen in Profile VIa and V, which might indicate an incorrect ice thickness profile or mass balance data for this area.

3.2 Mass Balance Implications

The mass balance of the year 1994 was below average but still positive. The flux through the Profiles I and A adds up to $3.9 \cdot 10^8$ m^3/a, which represents 58% of the flux through Profile II. Therefore 42% of the ice volume was melted away. This would lead to an ablation rate of 7 m/a in the 40 km^2 large glacier area between Profile II and I/A (= 61% of the ablation area beneath Profile II). By comparing this value with the ablation rates given by *PELTO and MILLER [1990]* and *NIELSEN [1957]* (3 - 5 m/a), 7 m/a is very high. This might lead to the fact that ablation could have increased in the last years or that the data of these authors are wrong.

If the terminus beneath Profile I and A is in balance (Taku Glacier stagnates since 1989) and the whole flux of $3.9 \cdot 10^8$ m^3/a melts, the mean ablation rate in the 25 km^2 large terminus area would be 15.6 m/a. *NIELSEN [1957]* and *PELTO and MILLER [1990]* give for the same area an ablation rate of 9.5 - 10.5 m/a. The same discrepancy as described earlier results. There are two error sources: the flux through Profiles I and A is too high or the ablation rates increased since the measurements of *PELTO and MILLER [1990]*. The flux through Profiles I and A has a maximum error of $\pm 0.5 \cdot 10^8$ m^3/a, which is not enough to explain the difference. Also it is not very likely that the ablation rates increased over 5 m/a in the last years.

Another explanation was suggested by *MOTKYA [1995]:* he states, that the terminus area is not in balance and the ice surplus is used to increase ice thickness. The Taku Glacier is thought to erode downwards into the fjord sediments, which leads to ice thickness increases that cannot be detected at the glacier surface. This seems to be a very likely explanation for the current superficial stagnation of the Taku Glacier. Further it might explain why tidewater glaciers in general advance slowly into a fjord during their advance phase.

3.3 Verification of Ice Thickness Measurements

By calculating the actual and balance ice flux for individual profiles on the Taku Glacier System the ice thickness measurements at these profiles can be cross-checked. Thereby it

was found that the measured ice thickness of Profile VII (cross-sectional area ca. 1,700,000 m^2) is far too low. The calculated flux would only be $1.6 \cdot 10^8$ m^3/a, which is much too small when compared to the reliably determined flux through Profile VIIa a few kilometers down-glacier. A flux of $2.4 \cdot 10^8$ m^3/a (calculated from accumulation data and surface velocities of 1994) would predict an approximate cross-sectional area of 2,500,000 m^2, which would represent the real situation very closely (Table 1 and 2).

Also Profile VIa shows a large difference between outgoing flux and yearly accumulation on its surface area. Therefore the cross-sectional area of Profile VIa seems to be too small or the reported accumulation data too high.

Ice thickness Profile V of the SW-Branch seems to be a little too small, but the low flux does not influence the dynamics of the Taku Glacier anyway.

Profiles IIIa/III represent a combination of the cross-sectional area determined at the location of Profile IIIa and the reliable glacier surface velocities measured at Profile III, located approximately 1 km upstream of Profile IIIa. The calculated ice flux is correct even in comparison to its proportion in the flux through Profile II.

4. Conclusions

The flux of the whole Taku Glacier System was established and the importance of the individual tributary glaciers to the dynamics of the Main Taku Glacier was revealed. All major tributary glaciers except the SW-Branch contribute substantially to the Main Glacier, whereby all the ice of the Demorest Glacier flows into the Hole-in-the-Wall-Glacier and the Main Taku terminus is formed solely by ice of the Matthes Glacier. The Matthes Glacier is the only real tidewater glacier of the Taku Glacier System. Its fluctuations influence all the other glaciers of the Taku System, which imposes the characteristic advance – retreat cycle also on them.

The comparison of balance flux and actual flux near the ELA (Profile II) results in a mean yearly ice thickness increase of 0.235 m/a (Table 4) in the accumulation area. This is in good agreement with measured ice level rises over the last 45 years in the accumulation area by *FRIEDMANN [1996]* and *LANG [1993]*. The whole Taku Glacier System has an ice volume exceeding 300 km^3 *[FRIEDMANN, 1996]*.

The ablation rates in the ablation area might have increased over the last years and the glacier probably eroded fjord sediments which leads to „hidden“ ice thickness growth as proposed by *MOTKYA [1995]*. The results of the flux calculations show the Taku Glacier System as a dynamic tidewater glacier in its advance phase with a balance flux higher than the actual flux resulting in net ice volume increase over the whole glacier length.

Acknowledgments

I would like to thank Prof. *Maynard M. Miller*, former director of the Juneau Icefield Research Program (JIRP) and Prof. Dr. *Walter M. Welsch*, leader of the Surveying program of JIRP very much for their support of my work. The logistical support of the Foundation for Glacier and Environmental Research (FGER) in the years 1992 and 1994 is gratefully acknowledged.

References

BEINEKE, D. [1994]: Preliminary Results of the 1994 Glacier Surveys on the Juneau Icefield. JIRP Survey Report, 1994. Juneau Icefield Research Program, Foundation for Glacier and Environmental Research, Juneau; Bundeswehr University Munich, Germany

BENEDICT, R. [1984]: Gravity Survey on the Matthes Glacier, Juneau Icefield, Alaska. JIRP Open File Report, 1984. Juneau Icefield Research Program, Foundation for Glacier and Environmental Research, Juneau

BENEDICT, T., SPRENKE, K., GILBERT, G., STIRLING, J. and MILLER, M. M. [1993]: New Seismic Depth Profiles on Taku Glacier, 1993, Juneau Icefield, Alaska. JIRP Open File Report, 1993. Juneau Icefield Research Program, Foundation for Glacier and Environmental Research, Juneau

BENEDICT, T. and SPRENKE, K. [1994]: Preliminary Results of the Seismic Invcestigations on the Taku Glacier, Alaska, 1994. JIRP Open File Report, 1994. Juneau Icefield Research Program, Foundation for Glacier and Environmental Research, Juneau

CLARKE, G. K. C. [1987]: Fast Glacier Flow: Ice Streams, Surging and Tidewater Glaciers. Journal of Geophysical Research, Vol. 92, Ser. B, No. 9, Washington; p. 8835-8841

DAELLENBACH, K. K. and WELSCH, W. M. [1990]: Determination of Surface Velocities, Strain and Mass Flow Rates of the Taku Glacier, Juneau Icefield, Alaska. Zeitschrift für Gletscherkunde und Glazialgeographie, Vol. 26, No. 2, Innsbruck; p. 169-177

FRIEDMANN, A. [1992]: Glacier Surface Velocities and Ablation Rates on the Taku Glacier System, Juneau Icefield, Alaska, USA. JIRP Survey Report, 1992. Juneau Icefield Research Program, Foundation for Glacier and Environmental Research, Juneau

FRIEDMANN, A. [1996]: Das Taku-Gletschersystem (Juneau Icefield, Alaska): Seine Dynamik und Fluktuationen. Univ. Diss. 1995. Freiburger Geographische Hefte, Heft 50. Albert-Ludwigs-Universität Freiburg, Institut für Physische Geographie, Freiburg; 148 pp.

ISBELL, W. [1984]: Gravity Depth Profiles, Taku Glacier, 1984. JIRP Open File Report, 1984. Juneau Icefield Research Program, Foundation for Glacier and Environmental Research, Juneau

LANG, M. [1991]: Report on the Geodetic Activities during the 1991 Juneau Icefield Research Program Field Season. JIRP Survey Report, 1991. Juneau Icefield Research Program, Foundation for Glacier and Environmental Research, Juneau; Bundeswehr University Munich, Germany

LANG, M. [1993]: Report on the Geodetic Activities during the 1993 Juneau Icefield Research Program Field Season. JIRP Survey Report, 1993. Juneau Icefield Research Program, Foundation for Glacier and Environmental Research, Juneau; Bundeswehr University Munich, Germany

MILLER, M. M. [1963]: Taku Glacier Evaluation Study. Conducted for the State of Alaska, Department of Highways, in cooperation with the U.S. Department of Commerce, Bureau of Public Roads; n.p.

MOTKYA, R. J. [1995]: Department of Natural Resources, Division of Geological and Geophysical Surveys, Fairbanks, Alaska, 99775-7320, USA. Personal communication

NIELSEN, L. [1957]: Preliminary Study on the Regimen and Movement of the Taku Glacier, Alaska. Bulletin of the Geological Society of America, Vol. 68, Boulder; p. 171-180

NYE, J. F. [1965]: The Flow of a Glacier in a Channel of Rectangular, Elliptic or Parabolic Crosssection. The Journal of Glaciology, Vol. 5, No. 41, Cambridge; p. 661-690

PATERSON, W. S. B. [1994]: The Physics of Glaciers. 3rd edition. Pergamon, Oxford; 480 pp.

PELTO, M. S. and MILLER, M. M. [1990]: Mass Balance of the Taku Glacier, Alaska from 1946 to 1986. Northwest Science, Vol. 64, No. 3, Washington; p. 121-130

POULTER, T. C., ALLEN, C. F. and MILLER, S. W. [1950]: Seismic Measurements on the Taku Glacier. Sponsored by American Geographical Society, New York, as part of their Juneau Icefield Research Project, summer of 1949. Stanford Research Institute Special Publication, Stanford; 12 pp.

RAYMOND, C. F. [1980]: Temperate Valley Glaciers. – In: *COLBECK, S. C. (ed.):* Dynamics of Snow and Ice Masses. Academic Press, New York; p. 79-139

SENSTAD, P. and RIFKIND, L. [1983]: 1983 Geophysical Depth Measurements using Seismic Reflections, Juneau Icefield, Alaska. JIRP Open File Report, 1983. Juneau Icefield Research Program, Foundation for Glacier and Environmental Research, Juneau

WELSCH, W. M. [1992]: Geodetic Data, JIRP Season 1992. Unpublished

Walter M. Welsch

Description of Homogeneous Horizontal Strains and some Remarks to their Analysis[1)]

The elastic deformations which a body undergoes by stresses applied to it are designated as strains. The description of stress and strain is made in elasticity which is in its simplest form based on *Hooke's* law; this means strain is proportional to stress, and the deformation of an ideally elastic body is uniform and homogeneous, in general small and reversible.

Many substances are elastic, including, to a certain extent, the crust of the earth. Overstressed beyond the limits of elasticity, however, fractures, faults and other non-elastic phenomena are observed.

The description and the analysis of deformations of the earth's crust have to be considered from this point of view. While geophysics has proceeded in this manner for a long time, geodesy has only recently started adjusting its advanced statistical techniques to take account of geotectonic problems. Nevertheless, the mathematical tools for analyzing homogeneous strains have long been available via the theory of affine transformation.

The following studies have two sources: firstly the theory of elasticity which deals with the description of homogeneous strain within the scope of continuum mechanics, e. g. *BECKER and BÜRGER [1975, pp. 41-52], HEITZ [1980, pp. 48-54], JAEGER [1969, pp. 20–48, 221-235], MEANS [1976, pp. 129-215], STEIN [1978, chapter 4], VERHOOGEN et al. [1970, pp. 482-489, 511-518]*; secondly references which treat the theory of affine transformation, e. g. *NÄBAUER [1961, pp. 354-368], WOLFRUM [1978, including the bibliography]*.

Since the concept of homogeneous strain is essentially a branch of geometry, all information which can serve the analysis of strain is included in the displacements of the points representing the body under investigation.

A rigid body movement displaces the body but does not distort it, but a distortion of the body creates displacements of the representative points, too. Thus, since a fixed reference system if often missing, one cannot easily decide if the point displacements were caused by a rigid body movement, or by a distortion or by both effects. One has to separate the deformation components. To clarify the terminology, by deformation the total movement pattern is meant, i. e. components of translation, rotation and distortion. The investigation of the distortion components themselves is the essential interest of strain analysis. In the sense of deformation interpretation, this involves a more complete analysis than is traditionally carried out. The traditional methods are performed as tests of similarity or congruence and show by statistical whether a point or a group of points has participated in a rigid body movement.

[1)] With reference to: Proceedings of the International Symposium on Geodetic Networks and Computations of the International Association of Geodesy, Munich, August 31 to September 5, 1981, Vol. 5 – Network Analysis Models. Veröffentlichungen der Deutschen Geodätischen Kommission bei der Bayerischen Akademie der Wissenschaften, Reihe B, Heft 258/V, München *[1982]*; p. 188-205

The following paragraphs describe the deformation of a strained body, firstly on the basis of the affine transformation of its displaced characteristic points, secondly with the help of distorted elements which also represent the body but are independent of the coordinate and reference system, and thirdly by the strain ellipse which is also known as *Tissot* indicatrix. Matrix notation is used throughout.

1. Affine Coordinate Transformation

The theory of elasticity is in its general representation so complicated that it is for practical use hardly applicable. In order to have a feasible concept one starts from a linear relation between the points representing the original and the deformed shape of the body. This is at the same time a definition of homogeneous strain and means that straight lines remain straight after deformation, and parallel lines remain parallel although their bearings may change. Homogeneous strain is therefore uniform at all points of the body and independent of its magnitude. For infinitesimal strain the relations become even simpler.

The linear relation of the deformation vector $\boldsymbol{x}'$ of the points of the deformed body to those points $\boldsymbol{x}$ of the original shape is represented by the transformation

$$\boldsymbol{x}' = \boldsymbol{F}\boldsymbol{x} + \boldsymbol{t} \qquad [1.1]$$

where (for a two-dimensional problem)

$\boldsymbol{x}'^{\mathrm{T}} = | x' \quad y' |$

$\boldsymbol{x}^{\mathrm{T}} = | x \quad y |$ vectors of coordinates

$\boldsymbol{t}^{\mathrm{T}} = | t_x \quad t_y |$ vector of translation elements

$$\boldsymbol{F} = \begin{vmatrix} \dfrac{\partial x'}{\partial x} & \dfrac{\partial x'}{\partial y} \\ \dfrac{\partial y'}{\partial x} & \dfrac{\partial y'}{\partial y} \end{vmatrix}$$ deformation matrix (rotation and distortion).

The vector of translation can be neglected in what follows, as it can easily be determined by a shift of the two groups of points. The elements of the $\boldsymbol{F}$-matrix are scalars and gradients which as derivatives of the position functions indicate how the old point coordinates are transformed to new ones (translation now neglected). The strain analysis is frequently carried out in tensor notation; here the tensor $\boldsymbol{F}$ is called the deformation gradient. This nomenclature can also be maintained in matrix notation. The diagonal elements represent the extensional or normal strains in the direction of the coordinate axes, the non-diagonal elements show the shearing strains in terms of the tangents of the shearing angles. Figure 1 may serve to illustrate the transformation.

For some purposes it is advantageous to introduce this displacement vector $\boldsymbol{u}$ which is defined as

$$\boldsymbol{u} = \boldsymbol{x}' - \boldsymbol{x} = (\boldsymbol{F} - \boldsymbol{I})\,\boldsymbol{x} = \mathrm{d}\boldsymbol{F} \cdot \boldsymbol{x}\,. \qquad [1.2]$$

Thus $\boldsymbol{F}$ is split

$$\boldsymbol{F} = \boldsymbol{I} + \mathrm{d}\boldsymbol{F}\,, \qquad [1.3]$$

where d$\boldsymbol{F}$ is called the displacement gradient.

In general, the deformation gradient $\boldsymbol{F}$ is not symmetric. However, it is regular, thus $\det\{\boldsymbol{F}\} > 0$. Therefore $\boldsymbol{F}$, as a second rank tensor, can be represented as the product of an orthogonal rotation matrix $\boldsymbol{R}$ and a symmetric distortion matrix $\boldsymbol{V}$

$$\boldsymbol{F} = \boldsymbol{R} \cdot \boldsymbol{V} \,. \qquad [1.4]$$

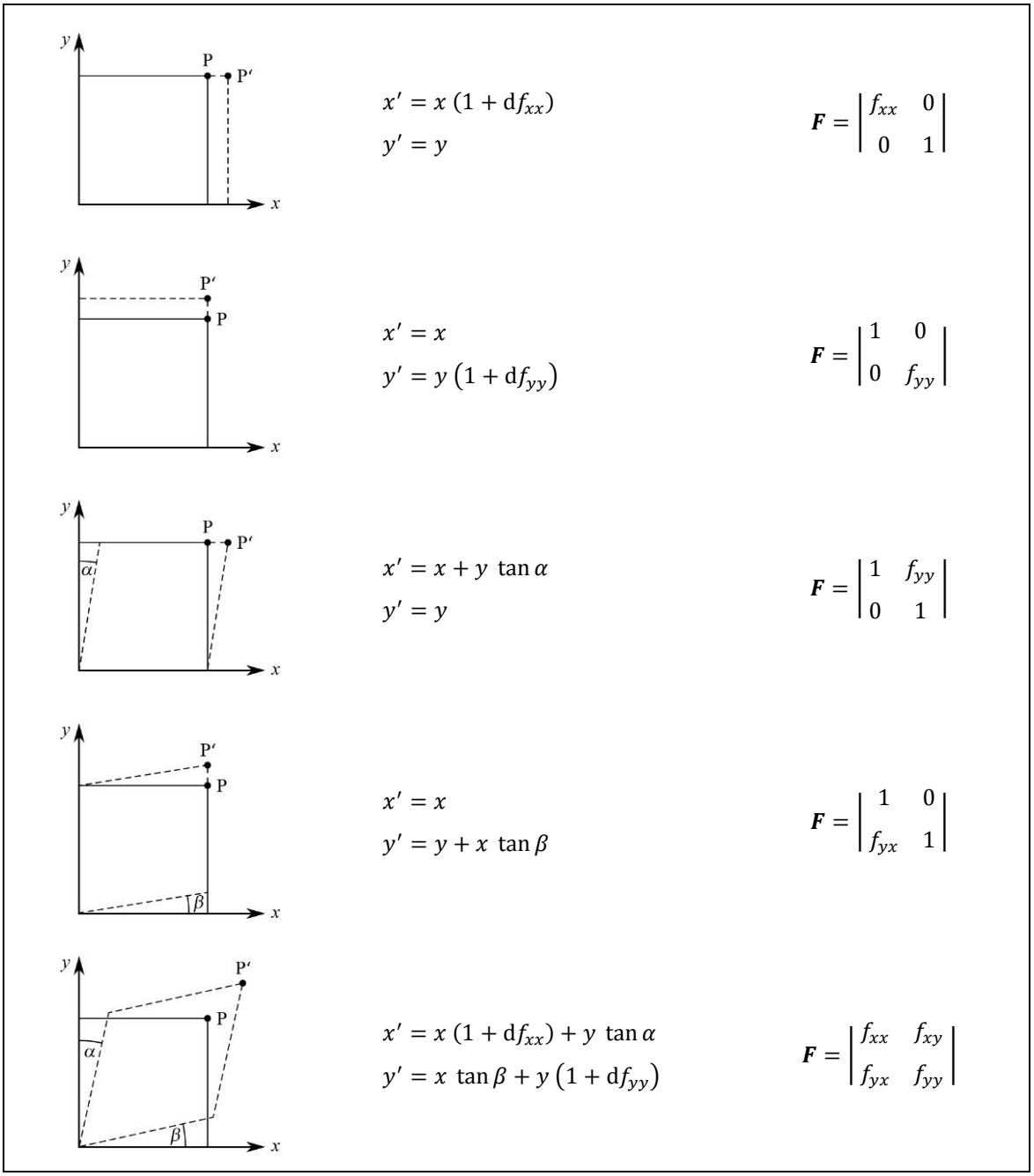

Fig. 1: Components of homogeneous strains
The coordinate system is chosen as is usual in continuum mechanics; bearings start from the x-axis, counterclockwise positive. Therefore no changes of the usual geodetic formulae have to be considered. However, in geotectonics the geodetic definition of bearings (starting from the y-axis, clockwise positive) is also followed.

$\boldsymbol{R}$ and $\boldsymbol{V}$ are determined by $\boldsymbol{F}$; $\boldsymbol{V}$ is given by

$$\boldsymbol{V} = \boldsymbol{R}^{-1}\boldsymbol{F} = \boldsymbol{R}^{\mathrm{T}}\boldsymbol{F} \qquad [1.5]$$

(because of orthogonality $\boldsymbol{R}^{-1} = \boldsymbol{R}^{\mathrm{T}}$).

If the angle of rotation is ω, then

$$\boldsymbol{R} = \begin{vmatrix} \cos\omega & \sin\omega \\ -\sin\omega & \cos\omega \end{vmatrix} \qquad [1.6]$$

and in detail

$$\boldsymbol{V} = \begin{vmatrix} f_{xx}\cos\omega - f_{yx}\sin\omega & f_{xy}\cos\omega - f_{yy}\sin\omega \\ f_{yx}\cos\omega - f_{xx}\sin\omega & f_{yy}\cos\omega - f_{xy}\sin\omega \end{vmatrix} = \begin{vmatrix} v_{xx} & v_{xy} \\ v_{yx} & v_{yy} \end{vmatrix} \qquad [1.7]$$

As $\boldsymbol{V}$ is symmetric, it follows

$$f_{yx}\cos\omega + f_{xx}\sin\omega = f_{xy}\cos\omega - f_{yy}\sin\omega\,, \qquad [1.8]$$

so that ω can uniquely be calculated from

$$\tan\omega = \frac{f_{xy} - f_{yx}}{f_{xx} + f_{yy}}\,. \qquad [1.9]$$

Though the distortion tensor $\boldsymbol{V}$ describes the strain components uniquely, some additional distortion tensors have been introduced. Here the *Cauchy*-tensor (there is some confusion about terminology in the international literature)

$$\boldsymbol{C} = \boldsymbol{F}^{\mathrm{T}}\boldsymbol{F} = \boldsymbol{V}^{\mathrm{T}}\boldsymbol{R}^{\mathrm{T}}\boldsymbol{R}\,\boldsymbol{V} = \boldsymbol{V}^{\mathrm{T}}\boldsymbol{V} \qquad [1.10]$$

(because of its orthogonality $\boldsymbol{R}^{\mathrm{T}}\boldsymbol{R} = \boldsymbol{I}$) and the *Green*-tensor

$$\boldsymbol{G} = \frac{1}{2}(\boldsymbol{C} - \boldsymbol{I}) \qquad [1.11]$$

should be mentioned. Both $\boldsymbol{C}$ and $\boldsymbol{G}$ are invariant with respect to rigid body movements.

The above formulae are valid for homogeneous distortions of any magnitude (finite strains). However, if the distortions and the parameters describing them are so small that their products and squares can be neglected without any influence on the results, then one speaks of infinitesimal strain. Considering this some simplifications can be made:

Using [1.11] and [1.10] it follows

$$\boldsymbol{G} = \frac{1}{2}(\boldsymbol{V}^{\mathrm{T}}\boldsymbol{V} - \boldsymbol{I})\,, \qquad [1.12]$$

and

$$\boldsymbol{V}^{\mathrm{T}}\boldsymbol{V} = \boldsymbol{I} + 2\boldsymbol{G}\,. \qquad [1.13]$$

If $\boldsymbol{G} << \boldsymbol{I}$ and therefore neglecting terms of second order, the infinitesimal (index *i*) distortion tensor $\boldsymbol{V}_i$ can be derived as

$$\boldsymbol{V}_i = \boldsymbol{I} + \boldsymbol{G}_i = \boldsymbol{I} + \boldsymbol{E} . \qquad [1.14]$$

In E, usually called the strain tensor, the infinitesimal strain components are given by

$$\boldsymbol{E} = \begin{vmatrix} e_{xx} & e_{xy} \\ e_{yx} & e_{yy} \end{vmatrix} . \qquad [1.15]$$

Using [1.3], [1.11] and [1.13] $\boldsymbol{E}$ can also be written as

$$\boldsymbol{E} = \frac{1}{2}(\mathrm{d}\boldsymbol{F} + \mathrm{d}\boldsymbol{F}^{\mathrm{T}}) , \qquad [1.16]$$

and the symmetry of $\boldsymbol{E}$ with $e_{xy} = e_{yx}$ can be seen.

If the rotation angle $\omega = \omega_i$ is small, the rotation matrix $\boldsymbol{R}$ [1.6] becomes

$$\boldsymbol{R}_i = \begin{vmatrix} 1 & \omega_i \\ -\omega_i & 1 \end{vmatrix} = \boldsymbol{I} + \mathrm{d}\boldsymbol{R}_i . \qquad [1.17]$$

Thus with infinitesimal strain an additive decomposition of $\boldsymbol{F}_i$ can be performed

$$\boldsymbol{F}_i = \boldsymbol{R}_i \cdot \boldsymbol{V}_i = \boldsymbol{R}_i + \boldsymbol{E} \qquad [1.18]$$

or

$$\mathrm{d}\boldsymbol{F}_i = \mathrm{d}\boldsymbol{R}_i + \boldsymbol{E}$$

and $$[1.19]$$

$$\boldsymbol{E} = \mathrm{d}\boldsymbol{F}_i - \mathrm{d}\boldsymbol{R}_i .$$

Furthermore using [1.16] one obtains

$$\boldsymbol{R}_i = \boldsymbol{I} + \frac{1}{2}(\mathrm{d}\boldsymbol{F} - \mathrm{d}\boldsymbol{F}^{\mathrm{T}}) , \qquad [1.20]$$

and immediately the angle of infinitesimal rotation

$$\omega_i = \frac{1}{2}(f_{xy} - f_{yx}) . \qquad [1.21]$$

This result follows also from [1.9] by series expansion.

By this means the decomposition of the deformation gradient $\boldsymbol{F}$ into the rigid body rotation $\boldsymbol{R}$ and the distortion $\boldsymbol{V}$ or $\boldsymbol{E}$ becomes possible.

By spectral decomposition the distortion tensor $\boldsymbol{V}$ can be transformed into the system of the principal strain axes

$$\boldsymbol{V} = \boldsymbol{S}\,\boldsymbol{\Lambda}\,\boldsymbol{S}^{\mathrm{T}} = \begin{vmatrix} \cos\Theta & -\sin\Theta \\ \sin\Theta & \cos\Theta \end{vmatrix} \cdot \begin{vmatrix} \lambda_1 & 0 \\ 0 & \lambda_2 \end{vmatrix} \cdot \begin{vmatrix} \cos\Theta & \sin\Theta \\ -\sin\Theta & \cos\Theta \end{vmatrix} . \qquad [1.22]$$

$\boldsymbol{\Lambda}$ characterizes the spectral, $\boldsymbol{S}$ the modal matrix, Θ the orientation of the principal axes system. Further details of this spectral decomposition will be given below. Here it should only be pointed out that the determinant of $\boldsymbol{\Lambda}$ is the ratio of the volume (area) of the body

after and before the decomposition. In the case of a pure distortion without dilatation the determinant tensor can be split again. In this case it is composed of a dilatation tensor (see paragraph 4)

$$\boldsymbol{K} = \begin{vmatrix} k & 0 \\ 0 & k \end{vmatrix} \qquad [1.23]$$

with

$$k = \det\{\boldsymbol{\Lambda}\}^{\frac{1}{2}}, \qquad [1.24]$$

and a pure distortion tensor

$$\boldsymbol{D} = \begin{vmatrix} \frac{\lambda_1}{k} & 0 \\ 0 & \frac{\lambda_2}{k} \end{vmatrix}. \qquad [1.25]$$

The determinant (as well as the trace) of a matrix is independent of both rigid body movements and principal axes transformations. Thus it can also be derived from other deformation matrices

$$\det\{\boldsymbol{\Lambda}\} = \det\{\boldsymbol{V}\} = \det\{\boldsymbol{F}\}, \qquad [1.26]$$

so that the spectral decomposition is not essential for computing the dilatation. Following these considerations a homogeneous deformation can be described in particular by

$$\boldsymbol{F} = \boldsymbol{R} \cdot \boldsymbol{K} \cdot \boldsymbol{V}^* \qquad [1.27]$$

with

$$\boldsymbol{V}^* = \boldsymbol{S}\,\boldsymbol{D}\,\boldsymbol{S}^{\mathrm{T}} = \boldsymbol{K}^{-1}\,\boldsymbol{V}. \qquad [1.28]$$

$\boldsymbol{V}^*$ is a measure of the pure distortion which is often the only interest.

Analogous reflections can be made with the decomposition of the strain tensor $\boldsymbol{V}_i$ in the case of infinitesimal strain.

The distortion of a body gas, of course, the consequence that several geometric elements, such as distances and angles, as well as the volume (area), are distorted. In the next paragraph these distortions will be investigated.

2. Distortion of Distances

The linear extension of any line is defined as

$$e = \frac{s' - s}{s}. \qquad [2.1]$$

s and s' are the line lengths before and after the deformation. If the lines were originally parallel to the axes of the coordinate system, the linear extensions are equivalent to the extensional strains e_{xx} and e_{yy}. By conversion

$$e + 1 = \frac{s'}{s} = m \qquad [2.2]$$

the scale factor *m* is obtained from the extension. The square of it

$$q = \left(\frac{s'}{s}\right)^2 = (1+e)^2 \qquad [2.3]$$

is called the quadratic elongation. This measure is more suitable in the case of finite strain.

In the following the relations between the line length distortion measures [2.1] and [2.3] and the distortion tensors of the first paragraph are shown.

The distance s between the two points $P_1(x_1, y_1)$ and $P_2(x_2, y_2)$ may be given. If the coordinate differences between those points are contained in the vector

$$\mathrm{d}\boldsymbol{x}^T = |\,\mathrm{d}x \quad \mathrm{d}y\,|, \qquad [2.4]$$

the square of the line length can be obtained from the scalar product $\mathrm{d}\boldsymbol{x}^{\mathrm{T}}\mathrm{d}\boldsymbol{x}$. This is valid before the deformation; afterwards the square of the distance is $\mathrm{d}'\boldsymbol{x}^{\mathrm{T}}\,\mathrm{d}'\boldsymbol{x}$. According to [1.1] and [1.10]

$$\mathrm{d}'\boldsymbol{x}^{\mathrm{T}}\,\mathrm{d}'\boldsymbol{x} = \mathrm{d}\boldsymbol{x}^{\mathrm{T}}\,\boldsymbol{F}^{\mathrm{T}}\,\boldsymbol{F}\,\mathrm{d}\boldsymbol{x} = \mathrm{d}\boldsymbol{x}^{\mathrm{T}}\,\boldsymbol{C}\,\mathrm{d}\boldsymbol{x} \qquad [2.5]$$

or in detail

$$s'^2 = \mathrm{d}'x^2 + \mathrm{d}'y^2 = \mathrm{d}x^2\,c_{xx} + 2\,\mathrm{d}x\,\mathrm{d}y\,c_{xy} + \mathrm{d}y^2\,c_{yy}\,. \qquad [2.6]$$

t being the original bearing of the line and with

$$\begin{aligned} \mathrm{d}x &= s\cdot\cos t \\ \mathrm{d}y &= s\cdot\sin t \end{aligned} \qquad [2.7]$$

[2.6] results in

$$s'^2 = s^2\left(c_{xx}\cos^2 t + 2\,c_{xy}\sin t\cos t + c_{yy}\sin^2 t\right) \qquad [2.8]$$

and according to [2.3]

$$q = c_{xx}\cos^2 t + c_{xy}\sin 2t + c_{yy}\sin^2 t\,. \qquad [2.9]$$

Using [1.11]

$$\boldsymbol{C} = 2\boldsymbol{G} + \boldsymbol{I} \qquad [2.10]$$

holds. Therefore [2.8] becomes

$$s'^2 = s^2\left(1 + 2g_{xx}\cos^2 t + 4g_{xy}\sin t\cos t + 2g_{yy}\sin^2 t\right). \qquad [2.11]$$

This formula is rigorous and is also valid for finite strain. In the case of infinitesimal strain the components $g_{ik} << 1$, and [2.11] can be written as a series expansion. Thus, using [1.14]

$$s' = s\left(1 + e_{xx}\cos^2 t + 2e_{xy}\sin t\cos t + e_{yy}\sin^2 t\right) \qquad [2.12]$$

and using [2.1]

$$e = e_{xx}\cos^2 t + e_{xy}\sin 2t + e_{yy}\sin^2 t\,. \qquad [2.13]$$

3. Distortion of Angles

The distortion of an angle between any two lines is defined as

$$g = \alpha' - \alpha \,. \qquad [3.1]$$

α' is the distorted and α the original angle.

Consider next the distortion of the bearing of the line between P_1 and P_2. The original bearing t is distorted due to the deformation to t'. Thus the change is

$$\begin{aligned} \mathrm{d}t \;&=\; t' - t \;=\; \arctan\frac{\mathrm{d}'y}{\mathrm{d}'x} - \arctan\frac{\mathrm{d}y}{\mathrm{d}x} \\ &=\; \arctan\frac{\mathrm{d}'y\,\mathrm{d}x - \mathrm{d}y\,\mathrm{d}'x}{\mathrm{d}'x\,\mathrm{d}x - \mathrm{d}'y\,\mathrm{d}y}\,. \end{aligned} \qquad [3.2]$$

With [1.1] this results in

$$\mathrm{d}t \;=\; \arctan\frac{f_{yx}\,\mathrm{d}x^2 - f_{xy}\,\mathrm{d}y^2 + \left(f_{yy} - f_{xx}\right)\mathrm{d}x\,\mathrm{d}y}{\mathrm{d}\boldsymbol{x}^{\mathrm{T}}\,\boldsymbol{F}\,\mathrm{d}\boldsymbol{x}}\,. \qquad [3.3]$$

If one splits from [3.3] the rotation according to [1.4] through [1.9] another formulation of the change $\mathrm{d}t'$ is obtained

$$\mathrm{d}t' \;=\; \arctan\frac{v_{xy}\,(\mathrm{d}x^2 - \mathrm{d}y^2) + \left(v_{yy} - v_{xx}\right)\mathrm{d}x\,\mathrm{d}y}{\mathrm{d}\boldsymbol{x}^{\mathrm{T}}\,\boldsymbol{V}\,\mathrm{d}\boldsymbol{x}}\,. \qquad [3.4]$$

This rigorous formula concludes the considerations for the case of finite strain.

Developing formulae for the infinitesimal strain one takes advantage of [1.14]. Therefore [3.4] becomes

$$\mathrm{d}t' \;=\; \arctan\frac{e_{xy}\,(\mathrm{d}x^2 - \mathrm{d}y^2) + \left(e_{yy} - e_{xx}\right)\mathrm{d}x\,\mathrm{d}y}{\mathrm{d}\boldsymbol{x}^{\mathrm{T}}\,(\boldsymbol{I} + \boldsymbol{E})\,\mathrm{d}\boldsymbol{x}}\,. \qquad [3.5]$$

Within the denominator

$$\mathrm{d}\boldsymbol{x}^{\mathrm{T}}\,(\boldsymbol{I} + \boldsymbol{E})\,\mathrm{d}\boldsymbol{x} \;=\; s^2\,(1 + e) \qquad [3.6]$$

the extension e can be neglected. Also neglecting quadratic terms when expanding in series, and using [2.7] the change of the bearing is

$$\begin{aligned} \mathrm{d}t' \;&=\; e_{xy}\,(\cos^2 t - \sin^2 t) + \left(e_{yy} - e_{xx}\right)\sin t\,\cos t \\ &=\; e_{xy}\cos 2t + \frac{1}{2}\left(e_{yy} - e_{xx}\right)\sin 2t\,. \end{aligned} \qquad [3.7]$$

The distortion of an angle the legs of which originally had the bearings t_1 and t_2 is given

$$\begin{aligned} g \;&=\; \alpha' - \alpha \;=\; (t_2' - t_1') - (t_2 - t_1) \;=\; \mathrm{d}t_2' - \mathrm{d}t_1' \;= \\ &=\; e_{xy}\,(\cos 2t_2 - \cos 2t_1) + \frac{1}{2}\left(e_{yy} - e_{xx}\right)(\sin 2t_2 - \sin 2t_1)\,. \end{aligned} \qquad [3.8]$$

The change (see Fig. 1)

$$\varphi \;=\; \alpha + \beta \qquad [3.9]$$

of the right angle φ between two lines originally parallel to the axes of the coordinate system becomes with

$$\gamma \;=\; \tan\varphi \qquad [3.10]$$

the measure of shearing strain.

Those two lines are defined by the original bearings t_1 with $\mathrm{d}y_1 = 0$ and t_2 with $\mathrm{d}x_2 = 0$. With these results the distortion φ can immediately be obtained as

$$\varphi \;=\; \arctan\left(-\frac{v_{xy}}{v_{yy}}\right) - \arctan\left(\frac{v_{xy}}{v_{xx}}\right) . \qquad [3.11]$$

Therefore the shearing strain [3.10] becomes

$$\gamma \;=\; \tan\varphi \;=\; \frac{v_{xy}\left(v_{xx} + v_{yy}\right)}{v_{xy}^2 - v_{xx}\cdot v_{yy}} . \qquad [3.12]$$

Using the identity

$$\frac{\pi}{2} - \arctan x \;=\; \arccos\frac{x}{\sqrt{1+x^2}} \qquad [3.13]$$

the distorted right angle φ' can be calculated from

$$\cos\varphi' \;=\; \frac{v_{xy}\left(v_{xx} + v_{yy}\right)}{\sqrt{\left(v_{xx}^2 + v_{xy}^2\right)\left(v_{yy}^2 + v_{xy}^2\right)}} \qquad [3.14]$$

or applying the distortion tensor $\boldsymbol{C}$, from

$$\cos\varphi' \;=\; \frac{c_{xy}}{\sqrt{c_{xx}\cdot c_{yy}}} . \qquad [3.15]$$

Consequently $\cos\varphi'$ represents the correlation coefficient between the distortion elements c_{xx} and c_{yy}.

In the case of infinitesimal strain, neglecting higher order terms as usual, and using the relations [1.11] and [1.14], [3.15] becomes

$$\cos\varphi_i' \;=\; 2\,e_{xy} , \qquad [3.16]$$

and with [3.10]because of $\varphi_i' = \frac{\pi}{2} - \psi_i$, $\cos\varphi_i' = \sin\psi_i \approx \tan\psi_i \approx \psi_i$

$$\gamma_i = \psi_i = 2\,e_{xy} . \qquad [3.17]$$

Therefore the shearing parameters $e_{xy} = e_{yx}$ (comp. [1.16]) represent half the distortion which is referred to as engineering shear, too.

4. Dilatation

Analogously to the linear extension [2.1] the dilatation as a measure of the distortion of an area is defined as

$$\mathrm{d}A \;=\; \frac{A' - A}{A} \qquad [4.1]$$

(A being the original area). In addition, the modulus m_A is defined as the ratio of the distorted and the original area, i. e.

$$m_A \;=\; \frac{A'}{A} \;=\; 1 + \mathrm{d}A\,. \qquad [4.2]$$

As shown above it can be derived from the determinant of the distortion matrix

$$m_A \;=\; \det\{\boldsymbol{\Lambda}\} \;=\; \det\{\boldsymbol{V}\} \;=\; k^2\,. \qquad [4.3]$$

The spectral matrix is composed of the eigenvalues λ_1 and λ_2 of the distortion matrix $\boldsymbol{V}$ which are at the same time the principal strains

$$\begin{aligned} \lambda_1 \;&=\; m_1 \;=\; 1 + e_1 \\ \lambda_2 \;&=\; m_2 \;=\; 1 + e_2\,. \end{aligned} \qquad [4.4]$$

Therefore the modulus

$$m_A \;=\; \lambda_1 \cdot \lambda_2 \;=\; m_1 \cdot m_2 \qquad [4.5]$$

is the product of the principal strains.

Neglecting products as usual, one obtains from [4.5] in the case of infinitesimal strain

$$m_{A_i} \;=\; 1 + e_1 + e_2\,. \qquad [4.6]$$

Therefore the infinitesimal dilatation

$$\mathrm{d}A_i \;=\; e_1 + e_2 \qquad [4.7]$$

is the sum of the principal strains.

5. Strain Ellipse

The principal strains, i. e. the elements of the spectral matrix, are related to the coordinate system of the principal axes the orientation of which is taken from the elements of the modal matrix. The principal strains and their orientation define immediately the strain ellipse. Analogously to the geodetic „point error ellipse“ the elements of the strain ellipse can also be calculated directly from the distortion tensor $\boldsymbol{V}$:

$$\begin{aligned} \lambda_1 \;&=\; m_1 \;=\; \frac{1}{2}\left(v_{xx} + v_{yy} + v\right) \;=\; 1 + e_1 \\ \lambda_2 \;&=\; m_2 \;=\; \frac{1}{2}\left(v_{xx} + v_{yy} - v\right) \;=\; 1 + e_2 \\ v \;&=\; \frac{2v_{xy}}{v_{xx} - v_{yy}} \;=\; \tan 2\Theta\,. \end{aligned} \qquad [5.1]$$

The principal quadratic elongations, i. e. the squares of the semi-axes of the strain ellipse, and also the orientation of the principal axes, can also be obtained by spectral decomposition of the distortion tensor $\boldsymbol{C}$.

The strain ellipse contains all the information which is needed for describing the various distortions.

If one replaces in [2.9] the component c_{ik} by the elements to be obtained from the spectral decomposition

$$\begin{aligned} c_{xx} &= m_1^2 \cos^2\Theta + m_2^2 \sin^2\Theta \\ c_{xy} &= (m_1^2 - m_2^2) \sin\Theta \cos\Theta \\ c_{yy} &= m_1^2 \sin^2\Theta + m_2^2 \cos^2\Theta \,, \end{aligned} \qquad [5.2]$$

the quadratic elongation of any line results in

$$q = m_1^2 \cos^2(t-\Theta) + m_2^2 \sin^2(t-\Theta) \,, \qquad [5.3]$$

$(t-\Theta)$ being the bearing of the line related to the principal axes system before the deformation.

With infinitesimal strain this becomes

$$e = e_1 \cos^2(t-\Theta) + e_2 \sin^2(t-\Theta) \,. \qquad [5.4]$$

Using the trigonometric relations

$$\begin{aligned} \cos^2 x &= \frac{1}{2}(1+\cos 2x) \,, \\ \sin^2 x &= \frac{1}{2}(1-\cos 2x) \end{aligned} \qquad [5.5]$$

[5.3] and [5.4] becomes

$$q = \frac{m_1^2 + m_2^2}{2} + \frac{m_1^2 - m_2^2}{2} \cos 2(t-\Theta) \qquad [5.6]$$

and

$$e = \frac{e_1 + e_2}{2} + \frac{e_1 - e_2}{2} \cos 2(t-\Theta) \,. \qquad [5.7]$$

There are a maximum and a minimum with $(t-\Theta) = 0°$ and $(t-\Theta) = 90°$. Amount and direction of the extremes are therefore given by the principal strains themselves.

If one wants to use the bearing $(t'-\Theta)$, i. e. the bearing of the line related to the principal axes system after the deformation, the formulae [5.3] and [5.6] remain valid, if one replaces the elements of the reciprocal strain ellipse

$$\begin{aligned} m' &= \frac{1}{m} \,, \\ q' &= \frac{1}{q} \,, \end{aligned} \qquad [5.8]$$

that means one considers the deformed shape the starting point. With infinitesimal strain the

small difference between the bearings of a line before and after the deformation is negligible so that in [5.4] and [5.7] $t = t'$.

The change of any bearing t can be derived from [3.4] using relations for the elements v_{ik} which are analogously to [5.2]:

$$\mathrm{d}t' = \arctan \frac{\frac{1}{2}(m_2 - m_1)\sin 2(t - \Theta)}{m_1 \cos^2(t - \Theta) + m_2 \sin^2(t - \Theta)} . \qquad [5.9]$$

With infinitesimal strain, i. e. $m_1 \approx m_2 \approx 1$, [5.9] becomes

$$\mathrm{d}t' = \frac{1}{2}(e_2 - e_1)\sin 2(t - \Theta) . \qquad [5.10]$$

[5.10] can also be derived from [3.7]. There is a maximum value of $\mathrm{d}t'$ with $(t - \Theta) = 45°$ and 135°, a minimal one with $(t - \Theta) = 0°$ and 90°. Using the elements of the reciprocal strain ellipse one can also take the bearing t' after the deformation with finite strain, while with infinitesimal strain the difference between t and t' can again be neglected.

The distortion of angles can be derived (see [3.8]) from the distortion of differences of bearings.

The dilatation has already been dealt with in the above paragraph, it equals the product of the semi-axes of the strain ellipse.

Finally, by transformation from the principal axes system to the original coordinate system according to [1.22], the distortion tensors can also be obtained.

6. Further Representations and Time Dependence

The notation used so far in describing horizontal strains has been defined as follows:

a) Extensional strain rates (Fig. 1):
   - e_{xx} rate of change of length per unit length in the direction of the x-axis, positive for extension,
   - e_{xy} rate of shear strain, (=e_{yx}), positive for right lateral shear (⇌),
   - e_{yy} rate of change of length per unit length in the direction of the y-axis, positive for extension;

b) Principal strain rates (par. 5):
   - e_1 maximum principal strain rate, rate of the greatest change of length per unit length,
   - e_2 minimum principal strain rate, rate of the smallest change of length per unit length, perpendicular to e_1,
   - Θ bearing of the direction of the maximum strain rate, counterclockwise from the x-axis.

Furthermore the following notation is used [Prescott et al., 1979]:

c) Strain rates when derived from triangulation networks:
   - $\gamma_1 = e_{yy} - e_{xx}$, the components e_{xx}, e_{yy} cannot be separated when using distortion of directions
   - $\gamma_2 = 2e_{xy}$ (= γ_i in [3.17]), defined as engineering shear,

$\Delta = e_{xx} + e_{yy}$ (= dA_i in [4.7]), rate of dilatation or change in area per unit area, positive for increase. The dilatation rate is necessary in order to determine the extensional strain rates individually;

d) Engineering shear related to the direction of the maximum shear rate:

$\gamma = (\gamma_1^2 + \gamma_2^2)^{\frac{1}{2}}$, also referred to as total shear (not identical with in [3.10]),

ψ bearing of the direction of maximum shear rate (see [5.10] and the following remarks; not identical to ψ in [3.9]);

e) Strain rates in a coordinate system related to the strike of the fault:
If β is the bearing of the horizontal normal to the strike of the fault, the strain rates γ_1', γ_2' are to be obtained from a transformation of γ_1, γ_2 by rotation β.

Depending on the purpose, commonly the extensional or the principal strain rates are used for greater clarity in presentation of results.

If one wants to relate the strain rates to a certain period of time, e. g. 1 year, the symbols are marked with a dot.

The dimension of all strain rates is microstrain [μ strain], i. e. pars in million (ppm), or microstrain per year [μ strain/yr] respectively.

7. Problems Involved in the Evaluation of Strain Parameters from Geodetic Data

The above paragraphs have shown that both the coordinate or the coordinate differences of repeatedly observed points and the differences of the observations between those points are functions of the same strain parameters. Conversely the strain parameters can be expressed as functions either of differences of coordinates or of differences of observations. In the case of redundancy they are to be estimated by least squares-adjustments.

Doing so, one question which arises is the equivalence of the results obtained from those different procedures. Another problem which should be considered is whether or not the results depend on the coordinate system and on the geodetic datum as a reference system. Furtheron, if one follows the usual procedure of geodetic deformation analysis one has to carry out two steps of evaluation; firstly a global statistical test of the significance of the displacements or observations differences, secondly the calculation of the strain parameters themselves, along with tests of their significance. The results of both steps should be discussed with respect to the above questions of equivalence and independence.

Consequently the following paragraphs will deal with some aspects of the geodetic analysis of strain parameters.

8. Transformation of Point Coordinates and Displacements, and their Covariance Matrices Considering Effects of the Assumed Geodetic Datum and Coordinate System

It is well known that adjusted point coordinates depend on the coordinate system and the chosen geodetic datum. This dependence is transferred to the point coordinate displace-

ments. As a consequence, a deformation cannot be described uniquely by point displacements. This problem is especially important if an object is to be monitored by a geodetic network which is as a whole established on the deformable body without any external reference.

However, as far as solely relative movements of points are concerned the coordinate system does not matter at all. Even the choice of the geodetic datum is not relevant. The only condition is that both the coordinate systems and the datums of the adjusted networks are in exact correspondence, which ensures that comparable coordinates and covariance matrices can be obtained. Modifying the coordinate system implies modifying the coordinate differences but not the point displacements, modifying the datum implies modifying the point displacements but not their relative information.

Transformation from one geodetic datum to any other can be carried out by so-called S–transformations *[VAN MIERLO, 1978]*. If $\boldsymbol{u}_1$ is the vector of the displacements of the n points of a network related to a specific geodetic datum with d degrees of freedom, and if $\boldsymbol{Q}_{u_1}$ is the corresponding covariance matrix, then the total variety of displacement vectors

$$\boldsymbol{u} = \boldsymbol{u}_1 + \boldsymbol{H} \cdot t \,, \quad \boldsymbol{Q}_u \qquad [8.1]$$

carries the same relative displacement information.

$\boldsymbol{H}$ consists of the coefficients, t of the d parameters of a similarity transformation:

$$\boldsymbol{H}^{\mathrm{T}} = \begin{vmatrix} 1 & 0 & 1 & 0 & \mathrm{L} \\ 0 & 1 & 0 & 1 & \mathrm{L} \\ -y_{01} & x_{01} & -y_{02} & x_{02} & \mathrm{L} \\ x_{01} & y_{01} & x_{02} & y_{02} & \mathrm{L} \end{vmatrix} \qquad [8.1a]$$

$$\boldsymbol{t}^{\mathrm{T}} = | \; t_x \quad t_y \quad \omega \quad m \; | \,, \qquad [8.1b]$$

where

x_{0i} , y_{0i} the center of gravity related approximate coordinates of network adjustments

t_x , t_y translation

ω rotation angle

m scale factor.

From the total [8.1] another displacement vector related to another datum can be selected by a rigid body transformation

$$\boldsymbol{u}_2 = (\boldsymbol{I} - \boldsymbol{H}\,(\boldsymbol{H}^{\mathrm{T}}\,\boldsymbol{I}_{\mathrm{s}}\,\boldsymbol{H})^{-1}\,\boldsymbol{H}^{\mathrm{T}}\boldsymbol{I}_{\mathrm{s}})\,\boldsymbol{u}_1 = \boldsymbol{D}_2\,\boldsymbol{u}_1 \qquad [8.2]$$

with

$$\boldsymbol{Q}_{u_2} = \boldsymbol{D}_2\,\boldsymbol{Q}_{u_1}\,\boldsymbol{D}_2^{\mathrm{T}} \qquad [8.3]$$

using a selective identity matrix $\boldsymbol{I}_{\mathrm{s}}$.

To obtain a particularly illustrative picture of the displacements for special purposes even the transformation matrix $\boldsymbol{H}$ can be modified *[PRESCOTT, 1981]*.

Occasionally it may be useful to adapt not only the datum but also the coordinate system to a specific deformation problem, e. g. by a rotation into the strike of a fault. With respect to this local coordinate system the point displacements are now given by

$$\bar{\boldsymbol{u}} = \boldsymbol{R}\,\boldsymbol{u} \qquad (\boldsymbol{R} \text{ rotation matrix}) \qquad [8.4]$$

with the covariance matrix

$$\boldsymbol{Q}_{\bar{u}} = \boldsymbol{R}\,\boldsymbol{Q}_u\,\boldsymbol{R}^{\mathrm{T}} . \qquad [8.5]$$

In some cases the retention of the chosen geodetic datum may require another datum transformation.

The above explanations might have illustrated that the representation (and also the eventual test of significance) of point displacements give certainly an obvious but in no case a unique description of the real deformations.

9. Coordinate System and Datum Invariant Test Statistics for Significant Deformations

Nevertheless, point displacements offer, of course, the possibility of testing for statistically significant deformations. Admittedly the proof of significance of the deformations is not so important to the analysis of strain as it is to the deformation analysis for surveying engineering purposes.

For the statement of statistical significance of deformations the quadratic form

$$q_{u_1} = \boldsymbol{u}_1^{\mathrm{T}}\,\boldsymbol{Q}_u^{-1}\,\boldsymbol{u}_1 \qquad [9.1]$$

is used, and form it the well-known „mean gap“ *[PELZER, 1971]* used in statistical variance tests is derived. The quadratic form is a coordinate system and datum invariant quantity. To prove this, according to [8.2] and [8.3] the quadratic form of the special solution $\boldsymbol{u}_2$ is derived from]9.1]:

$$\begin{aligned} q_{u_2} &= \boldsymbol{u}_2^{\mathrm{T}}\,\boldsymbol{Q}_{u_2}^{-1}\,\boldsymbol{u}_2 = \boldsymbol{u}_1^{\mathrm{T}}\,\boldsymbol{D}_2^{\mathrm{T}}\left(\boldsymbol{D}_2\,\boldsymbol{Q}_{u_1}\boldsymbol{D}_2^{\mathrm{T}}\right)^{-1}\boldsymbol{D}_2\,\boldsymbol{u}_1 \\ &= \boldsymbol{u}_1^{\mathrm{T}}\,\boldsymbol{Q}_{u_1}^{-1}\,\boldsymbol{u}_1 = q_{u_1} . \end{aligned} \qquad [9.2]$$

In the same way it can be shown that

$$q_{u_1} = q_{u_2} = q_u = q_{\bar{u}} . \qquad [9.3]$$

Therefore the quadratic form is an appropriate statistical indicator for the existence of significant deformations. The decompositions of these quadratic forms again lead, however, to datum variant statements.

The alternative is to investigate differences of corresponding observations. The basic requirement for this procedure is that there must be corresponding observations. That is, observations which do not exist in pairs cannot be analyzed. To avoid this loss of information the proposal is made here to use adjusted observations which can, by substitution, also be derived from adjusted coordinates. Thus pairs of comparable adjusted observations can always be obtained – and they carry the same information that adjusted coordinates do. Furthermore, observed as well as adjusted observations do not depend on the coordinate system or the geodetic datum.

If the vector

$$\mathrm{d}\boldsymbol{l} \;=\; \boldsymbol{L}\,\boldsymbol{u} \;\;,\;\; \text{order}\,\{\mathrm{d}\boldsymbol{l}\} \;=\; (2u-d,1) \qquad [9.4]$$

with the corresponding covariance matrix

$$\boldsymbol{Q}_{\mathrm{d}l} \;=\; \boldsymbol{L}\,\boldsymbol{Q}_u\,\boldsymbol{L}^{\mathrm{T}} \qquad [9.5]$$

represents the changes of a so-called basis-set of comparable adjusted observations which define just uniquely the shape of the network, then the quadratic form of those changes

$$\begin{aligned} q_l \;&=\; \mathrm{d}\boldsymbol{l}^{\mathrm{T}}\,\boldsymbol{Q}_{\mathrm{d}l}^{-1}\,\mathrm{d}\boldsymbol{l} \;=\; \boldsymbol{u}^{\mathrm{T}}\,\boldsymbol{L}^{\mathrm{T}}\big(\boldsymbol{L}\,\boldsymbol{Q}_u\,\boldsymbol{L}^{\mathrm{T}}\big)^{-1}\boldsymbol{L}\,\boldsymbol{u} \\ &=\; \boldsymbol{u}^{\mathrm{T}}\,\boldsymbol{Q}_u^{-1}\,\boldsymbol{u} \;=\; q_u\,. \end{aligned} \qquad [9.6]$$

It has the same value as the quadratic forms [9.3] and is, of course, datum invariant. It is also an appropriate statistical characteristic for deformations. Furthermore its decomposition gives some datum invariant information on observational changes which may be meaningful for characterizing the distortion of a network. An interpretation of the fact of invariance leads to the statement that the quadratic forms of both coordinate displacements and differences of observations can, unbiased by rigid body motions, indicate deformations.

10. Determination of the Strain Tensor Using Point Displacements and Observation Differences

The decompositions of quadratic forms lead to a localization of the deformations. Thus either datum dependent single points or a group of points, or datum independent single observations are withdrawn, and the rest of the network is congruent. But this procedure is by no means a description of the deformation.

In the case of crustal movements the strain tensor is, of course, the basic way of representing the deformations. A network established for monitoring deformations is much more sensitive to an averaging deformation characteristic like the homogeneous strain tensor than to detecting single point movements. And, in general of course, when analyzing strain one is not interested in detecting single point movements. This becomes relevant only when the strain tensor cannot explain the deformations adequately.

BRUNNER [1979] has treated in detail the determination of the strain tensor using point displacements of the „inner“ coordinate solution. But, somewhat in contradiction to his view point, the strain tensor can also be derived from any minimum constraint solution because it is an estimable quantity.

The full equivalence of strain determination from observation differences is shown by *BRUNNER et al. [1981]* assuming equivalent information is applied. Here the proposal of utilizing adjusted observations or analogous functions derived as substitutes, may help a little further. This procedure of strain determination may be advantageous because it is free of any translation and rotation effects.

The significance of the strain tensor as a whole, or of single tensor components can be tested by variance tests which have to be performed by means of the variances calculated from the coordinate differences which remain in each case *[CASPARY and SCHWINTZER, 1981]*. A subsequent rigid body transformation has no influence on these tests.

Theoretically the analysis of homogeneous strain is quite clear so far. But ideally homogeneous strain fields do not exist. There are always variations in the material properties from point to point and these lead ultimately to variations in the strain from point to point. The treatment of strain as homogeneous means averaging varying strains. In many cases this is justified and the only possible procedure. Nevertheless, the task is to interpret strain fields and strain accumulations to completely determine strain pattern in both space and time *[SAVAGE, 1979]*.

References

BECKER, E. and BÜRGER, W. [1975]: Kontinuumsmechanik – eine Einführung in die Grundlagen und einfache Anwendungen. Leitfäden der angewandten Mathematik und Mechanik, Band 20. Teubner-Studienbücher: Mechanik. Teubner, Stuttgart; 228 pp.

BRUNNER, F. K. [1979]: On the Analysis of Geodetic Networks for the Determination of the Incremental Strain Tensor. Survey Review – Directorate of Overseas Surveys, Vol. 25, No. 192, Staines Middlesex; p. 56-67

BRUNNER, F. K., COLEMAN, R. and HIRSCH, B. [1981]: A Comparison of Computation Methods for Crustal Strains from Geodetic Measurements. Tectonophysics, No. 71, Amsterdam; p. 281-298

CASPARY, W. and SCHWINTZER, P. [1981]: Bestimmung von Einzelpunktbewegungen und von Relativbewegungen zweier Netzteile in geodätischen Deformationsnetzen. Zeitschrift für Vermessungswesen, Vol. 106, No. 6, Stuttgart; p. 277-288

HEITZ, S. [1980]: Grundlagen, Dynamik starrer Körper. Mechnik fester Körper, Band 1. Dümmlers Typoscripts Geodäsie/Vermessungswesen. Dümmler Verlag, Bonn; 339 pp.

JAEGER, J. C. [1969]: Elasticity, Fracture and Flow, with Engineering and Geological Applications. 3rd Edition. Methuen's Monographs on Chemistry Subjects. Methuen, London; 268 pp.

MEANS, W. D. [1976]: Stress and Strain: Basic Concepts of Continuum Mechanics for Geologists. Springer, New York – Heidelberg – Berlin; 339 pp.

NÄBAUER, M. [1961]: Mathematische Grundlagen, Ausgleichungsrechnung und Rechenhilfsmittel. Jordan-Eggert-Kneißl, Handbuch der Vermessungskunde, Band 1. Metzlersche Verlagsbuchhandlung, Stuttgart; 808 pp.

PELZER, H. [1971]: Zur Analyse geodätischer Deformationsmessungen. Deutsche Geodätische Kommission bei der Bayerischen Akademie der Wissenschaften, Reihe C, Heft 164. Bayerische Akademie der Wissenschaften, München; 83 pp.

PRESCOTT, W. H., SAVAGE, J. C. and KINOSHITA, W. T. [1979]: Strain Accumulation Rates in the Western United States between 1970 and 1978. Journal of Geophysical Research, Vol. 84, Ser. B, No. 1, Washington; p. 5423-5435

PRESCOTT, W. H. [1981]: The Determination of Displacement Fields from Geodetic Data along a Strike Slip Fault. Journal of Geophysical Research, Vol. 86, No. 97, Washington; p. 6067-6072

SAVAGE, J. C. [1979]: Strain Patterns and Strain Accumulation along Plate Margins. Report of the 9th Geodesy/Solid Earth and Ocean Physics Research (GEOP) Conference „Applications of Geodesy to Geodynamics“, Columbus, Ohio, Oct. 1978. Reports of the Department of Geodetic Science, The Ohio State University, Columbus, Ohio, Report No. 280. International Association of Geodesy, American Geophysical Union, NASA, The Ohio State University, Department of Geodetic Science, Columbus, Ohio; p. 93-97

STEIN, E. [1978]: Einführung in die Elastizitätstheorie. Technische Universität Hannover, Lehrstuhl für Baumechanik, Hannover

VAN MIERLO, J. [1978]: A Testing Procedure for Analyzing Geodetic Deformation Measurements. II. International Symposium on Deformation Measurements and Geodetic Methods, Bonn 1978

VERHOOGEN, J., TURNER, F. J., WEISS, L. E., WAHRHAFTIG, C. and FYFE, W. S. [1970]: The Earth: an Introduction to Physical Geology. Holt, Rinehart and Winston, New York; 748 pp.

WOLFRUM, O. [1978]: Die Verzerrungseigenschaften der affinen Transformation. Allgemeine Vermessungsnachrichten, Vol. 85, No. 10, Karlsruhe; p. 367-374

Martin Lang and Walter M. Welsch

Movement Vector and Strain Rate Determination for the Taku Glacier System

1. Introduction

Surface velocities and strain rates are two of the key parameters to describe the behavior of a glacier. By means of standard surveying techniques these parameters can easily be determined. Using usual glaciological models significant secondary information can be derived. Since the foundation of the Juneau Icefield Research Program (JIRP) the survey work was mainly focused on the determination of surface velocities on various profiles of the Taku Glacier system. Beginning in the late seventies strain rates analysis *[WELSCH, 1997]* was adopted to standard surveying techniques in glaciology. Consequently the derivation of strain rates became another main topic of the JIRP surveying program in the following years.

2. Movement Profiles

2.1 Methodology

Wooden stakes with flagging material attached and set in a line across a glacier usually serve as point markers for the determination of glacial surface velocities. The movements of these flags represents the main flow characteristics of the glacier. Therefore the flags are set in a profile perpendicular to the estimated flow direction of the glacier. A spacing of 250 to 500 m depending on the width and the slope of the glacier turned out to be sufficient.

Up to the early nineties all profiles were surveyed using theodolite and electronic distance measurements. Thus the point coordinates were determined by either intersection or polar survey (epoch 0). After an appropriate period of time the measurements were repeated (epoch 1). The movements of the flags were calculated from the coordinate differences between the epochs. Taking into account that periods of good visibility on the Juneau Icefield are often very short, a simplified, time-saving method was chosen in some instances. By this method the point movement is derived from the change of angle (see Fig. 1), the distance measurement is not repeated in epoch 1. As a consequence only $ds' = s \cdot d\alpha$ can be derived. However, this quantity does not represent the real movement ds of the flag. When analyzing the velocity of the glacier

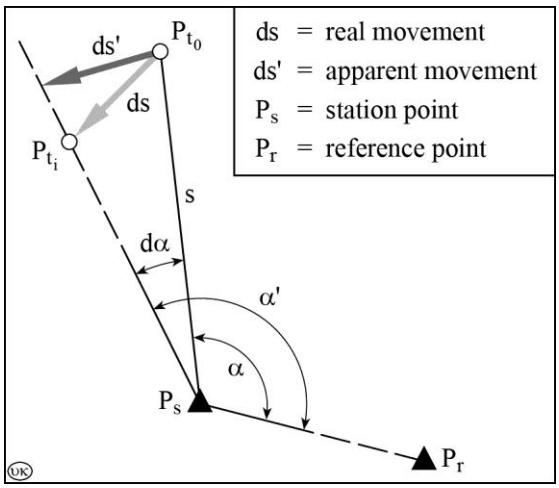

Fig. 1: Difference of real and apparent movement using a simplified survey setup

this fact has to be considered. Another drawback of terrestrial surveying techniques is the distance dependent accuracy of the results (e. g. about 10 cm for 5 km in distance).

GPS measurement techniques offer numerous advantages:

- greater time efficiency:
  using real-time GPS and motorized transport a typical profile can be measured in two or three hours only
- higher and distance independent accuracy:
  using differential GPS a position can be derived with a standard deviation of about 1 cm for baseline lengths shorter than 5 km
- the positions of the flags of former years can be re-established very accurately and in no time using real-time GPS:
  a more consistent comparison of movements and heights over the years is enabled
- the measurements are weather independent:
  in principle surveys can be carried out even under white-out conditions.

Since 1992 the use of GPS has consequently been intensified. More profiles per season and profiles in remote areas open up better research possibilities on the Icefield.

2.2 Results

2.2.1 Movements

The movement vectors shown in the plots on pages 97, 101, 103 and 107 represent the mean movements over the period 1986-1996 (see Appendix A). Small variations of the profile locations (up to 500 m) and the numbers of points per profile show no remarkable effects on the movement patterns and on the individual vectors. All the vectors derived by the simplified method (see Fig. 1) were no taken into account. Only the locations of Profile II were far apart from each other over the years. Therefore the location of both profiles and their movements are shown on the map, page 97. The locations of all profiles are shown on page 93; all point locations and movement vectors are listed in Appendix B.

2.2.1.1 Ablation Area of the Taku Glacier

Profile I is located on a line between Norris Mountain and Brassiere Hills on the lower Taku Glacier about 5 km above its present terminus. This profile was only in 1994 observed, however with less than two days between the epochs. The out-radiating movement pattern reflects the fact that the profile is situated on the last narrow cross-section above the terminus. The zone of maximum movement starts 800 m east of the Norris Mountain glacier border and continues for some 1.3 km ending 400 m in front of the bedrock of the Brassiere Hills. The velocity of the maximum movement zone is fairly consistent with an average of 85 cm/day and a maximum of 91 cm/day close to the western end indicating an asymmetrical channel flow. On the western end of the profile the movement vectors are orientated towards the margin of the glacier. This fact may be caused by two factors. First, the steep valley sidewalls are responsible for an increasing ablation rate towards the margin so that the glacier intends to compensate for the loss. Second, the still strong positive mass balance *[Pelto and Miller, 1990]* of the Taku Glacier leads to a convex height profile – this is typical for advancing glaciers. Despite the short timespan between the

Locations of the main movement profiles, Juneau Icefield

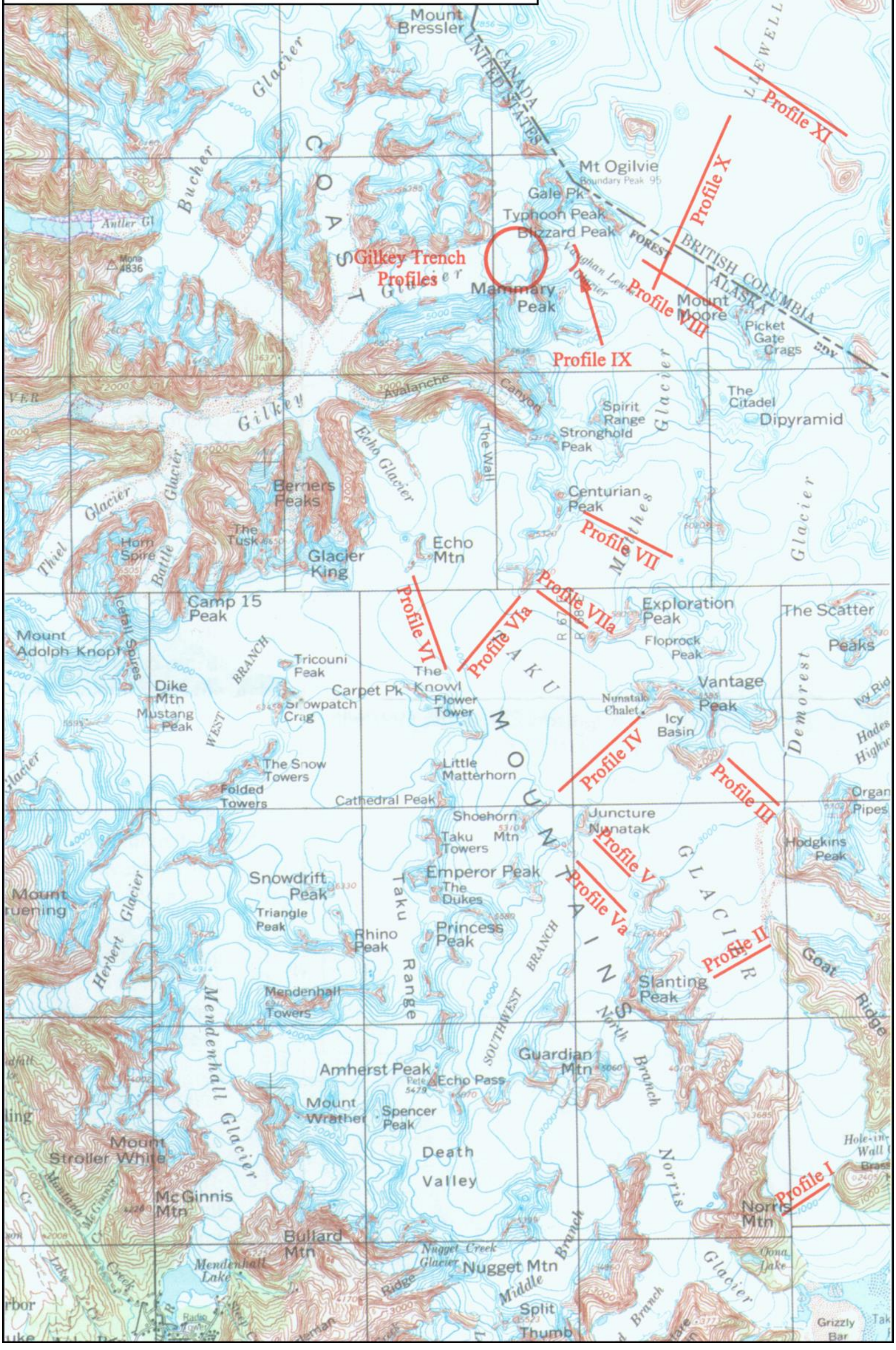

observation epochs the movement pattern is in surprisingly good accordance with the one observed in the early fifties *[MILLER, 1953]*. In Fig. 2 a fourth order polynom is the best fit to the data. The mean movement for Profile I is 65 cm/day.

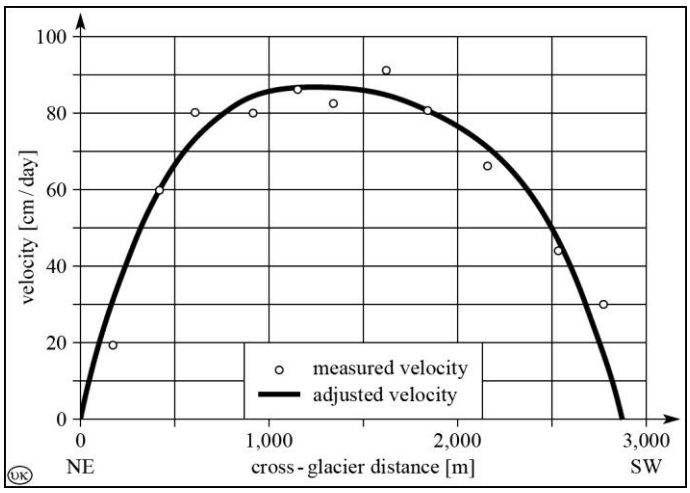

Fig. 2: Profile I: measured and adjusted velocities

Profile II has a location which varies from year to year. The location corresponds to the annual ELA. In 1993 the profile was located on a line from Slanting Peak to the northern end of Goat Ridge. Higher accumulation in the following winter required a shift of the profile some 1.5 km down glacier a year later.

The highest velocity of any profile on the Taku Glacier can be expected in Profile II for three reasons. All tributaries enter the main Taku above this line, second the ELA characterize the cross-section of highest mass transportation, and third the combination of a narrow glacier bed and a steep slope of about 2.5°.

The 1993 profile shows a highly uniform velocity in the central part of the glacier (80 cm/day to 85 cm/day). The 1994 profile, situated on a narrower section of the lower Taku Glacier reveals the highest velocity (= 93 cm/day). The variations on the central section of the profile are comparable to the 1993 profile (83 cm/day to 93 cm/day), see Fig. 3. The mean velocity (71 cm/day) of Profile II as found in 1994 is the highest of all Taku Glacier profiles. The mean velocity in 1993 (66 cm/day) equals that of Profile I.

Heavily crevassed and well defined shear zones can be seen on the margins of both profiles. In combination with the strong increase of the velocity in these marginal zones and the uniform velocity in the central part, a Block-Schollen-movement has to be considered for Profile II. *PILLEWITZER [1957]* mentions three causes for Block-Schollen-movements:

(1) vast firn or accumulation areas pushing the icemasses through narrow outlets (e.g. Greenland),

(2) high accumulation in relatively small areas producing large icemasses that are forced through small valleys (Karakorum glaciers and all advancing glaciers of alpine type),

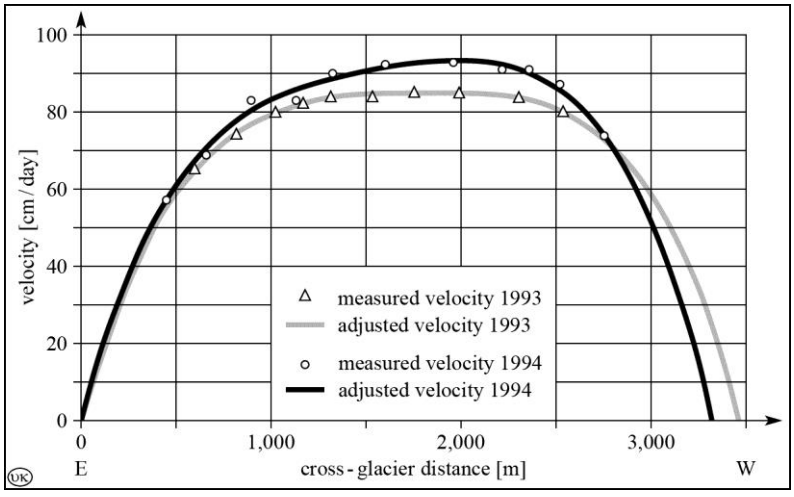

Fig. 3: Profile II: measured and adjusted velocities

(3) steep and high slopes of the accumulation areas where avalanches and icefalls create the Block-Schollen-movement of the float glacier tongues (e. g. some small glaciers of Jostedalsbre/Norway).

With some caution a combination of (1) and (2) can be seen for the Taku Glacier. Even the accumulation area of app. 600 km^2 has to be considered small as compared to the mighty Greenland glaciers (Jakobshavnbræ ~ 120,000 km^2 e. g.). The maximum accumulation in the past 40 years of about 1,500 mm water equivalent *[MILLER and PELTO, 1990]* reaches only some 10 percent of the more than 11,000 mm *[EDMAIER and JUNG-HÜTTL, 1996]* responsible for vigorously advancing glaciers in New Zealand. Nevertheless the Taku Glacier was advancing up to the early nineties; the latest survey of the terminal front in 1994 showed a small advance of some 50 m as compared to 1988/89, while in some parts the glacier front was stagnant, see page 33. According to *FINSTERWALDER [1950]* the ratio of the mean annual movement and the width of the glacier on a particular profile has to exceed 1 : 6 to characterize the movement as a Block-Schollen-type. Taking the maximum speed of both profiles (93 cm/day) as the mean velocity, yields a ratio of about 1 : 7. This is close to *FINSTERWALDER*'s statement. These reasons may give some evidence to the Block-Schollen-movement of Profile II.

A major setback remains: the velocity distribution in the marginal zones, which stretch over 700 m on both sides, cannot be measured because these areas are heavily crevassed. Thus the typical velocity profile of a Block-Schollen-flow across the whole glacier cannot be verified. In addition, best fit polynoms of fourth order reveal rather a sort of parabolic flow.

Summing up the preceding discussion, the flow in the area of both profiles has to be characterized as a transition form of parabolic and Block-Schollen-flow.

2.2.1.2 Main Taku Glacier and its Lower Branches (Demorest Glacier, SW-Branch)

Profile III between Taku A and Peak 4785 (a western side summit of Hodgkins Peak) allows to monitor the eastern accumulation area of the Taku Glacier mainly formed by the Demorest Glacier and its tributaries. In most of the recent summers this area was above the ELA. Movement surveys were conducted in 1987 and from 1991 to 1996.

The velocity pattern over the years is quite stable. The mean velocity of 20 cm/day was derived by a best fit fourth order polynom. It shows clearly a parabolic flow pattern. The 1987 and 1992 data were not taken into account. In 1987 a simplified method was used for the velocity determination and in 1992 a 20% higher velocity was observed, but due to the lack of additional data no reason for this anomaly could be found. Fig. 4 shows the measured and adjusted velocities.

Profile IV stretches from Camp 10 to the northeast ridge of Shoehorn Mountain. The significance of the profile is given by the fact that yearly movement surveys have been carried out here since the late 1940s creating one of the longest continuous velocity records of an individual glacier. Since 1993 the profile consists of two parallel lines approximately 300 m apart, the lower line representing the original location. This setup allows to gather a lot more parameters like strain-rates, glacier gradients and simplified mass balances *[McGEE, 1997]*. The movement pattern on both lines is nearly identical, slight differences occur in the marginal zones reflecting topographic peculiarities. A parabolic flow with a

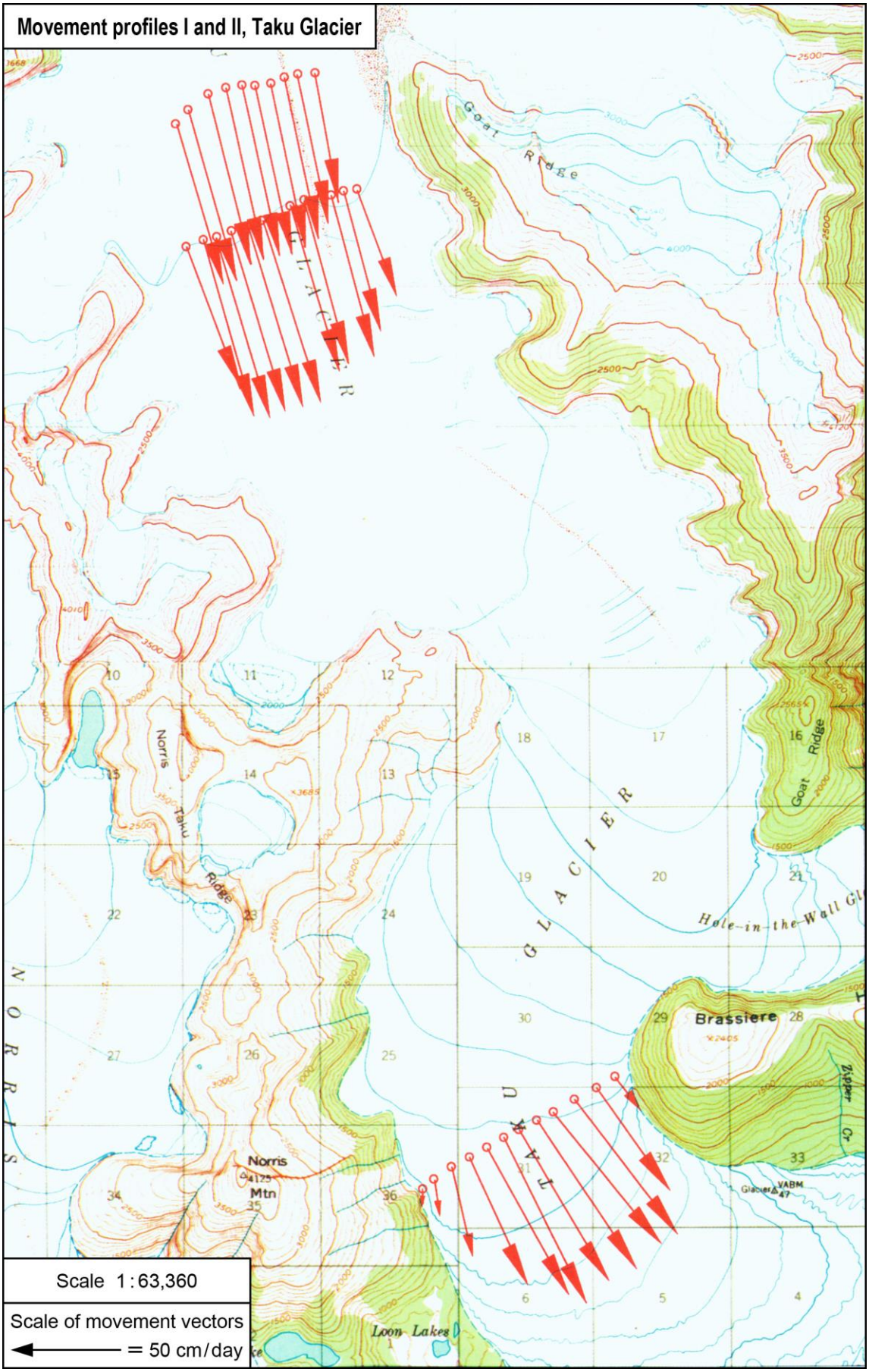
Movement profiles I and II, Taku Glacier
GLACIER
Goat Ridge
Norris Taku Ridge
Norris Mtn
4175
GLACIER
Goat Ridge
Hole-in-the-Wall Gl
Brassiere
Zipper Cr
VABM
Glacier
Loon Lakes
NORRIS
Scale 1:63,360
Scale of movement vectors
= 50 cm/day

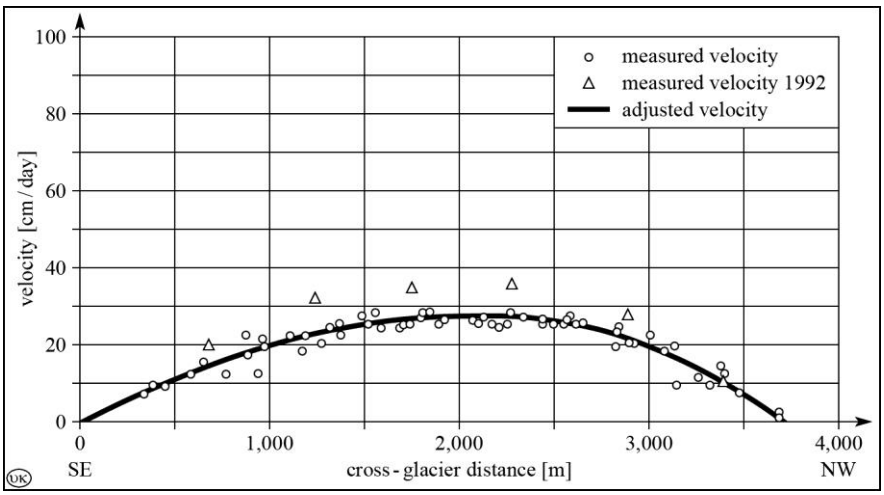

Fig. 4: Profile III: measured and adjusted velocities

broadened central zone spreading more than two kilometers showing a similar high velocity of 50 to 60 cm/day. In 1949, 1950 and 1964 *[MILLER, 1953; HAVAS, 1965]* maximum velocities of 90 cm/day and higher were reported. They may result from a minor accuracy of the surveys in former years. For the timespan from 1986 to 1996 the variations are negligible. A fourth order polynom fits all the data except those from 1987 revealing a mean velocity of 38 cm/day (Fig. 5).

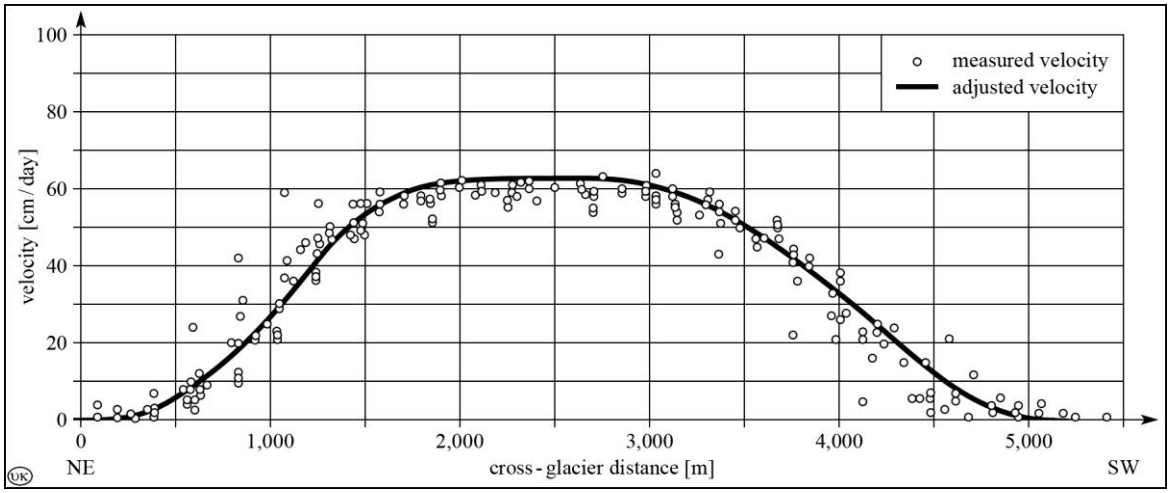

Fig. 5: Profile IV: measured and adjusted velocities

Profile IVa crossing Icy Basin with measurements in 1986-1989, 1992 and 1995 and Profile IVb traversing North Bassin (north of Camp 10) observed in 1989 only are not evaluated here. The majority of the movement vectors is neither significant nor conclusive.

Profile V is located between Juncture Peak and Peak 4066 some 800 m above the confluence of the SW-Branch and the Taku Glacier. It has been observed yearly since 1986. With an area of about 40 km^2 the SW-Branch is the smallest tributary within the Taku Glacier system. The flow pattern is perfectly parabolic (Fig. 6) and stable over the period observed. The apparently higher velocities in 1989 are probably caused by the fact than due to ablation all flags had to be re-established for the resurvey. These data were not taken into account. The mean velocity is 6 cm/day; the maximum velocity 12 cm/day.

Approximately 1.5 km up-glacier Profile Va was established in 1989 only. The flow of the western part of the profile is obviously affected by a rocky ridge stretching from Showhorn Peak south-east. The eastern part of the profile shows a parabolic flow up to 8 cm/day.

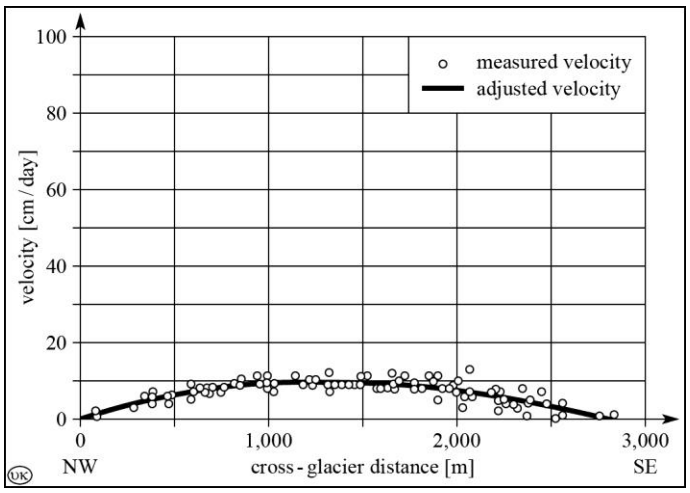

Fig. 6: Profile V: measured and adjusted velocities

2.2.1.3 *Convergence Area of the Matthes and Taku Glaciers*

The NW-Branch of the Taku Glacier and the Matthes Glacier are similar in their areas, both covering about 150 km^2. Although the exact depth profiles of both glaciers are not very well known, the latest results of seismic investigations *[SPRENKE, 1996]* suggest a similarity so that the volumes of both glaciers can be regarded as equal. The NW-Branch of the Taku Glacier represents the maritime side of the Icefield whereas the Matthes Glacier is situated in the transition zone to the drier continental side of the Icefield. Besides topographic peculiarities different movement pattern may reflect this fact.

Profile VI extends from NW Taku Point situated northeast of the Flower Tower to Echo Mountain. After the first measurements in the early fifties the movement vectors were determined in the last decade only rarely (1986, 1989 and 1992). Profile VIa stretches from NW Taku Point to Taku D. In addition to the ice masses passing through Profile VI, the ice developing in the basin formed by Echo Mountain, The Wall, Centurian Peak and Taku D has to pass through Profile VIa. This profile has been measured in 1990 and 1991 and every year since 1993.

Both profiles depict an asymmetric parabolic flow (Fig. 7). This is due to the rocky ridges continuing from Echo Mountain and Taku D. The greater volume passing through the

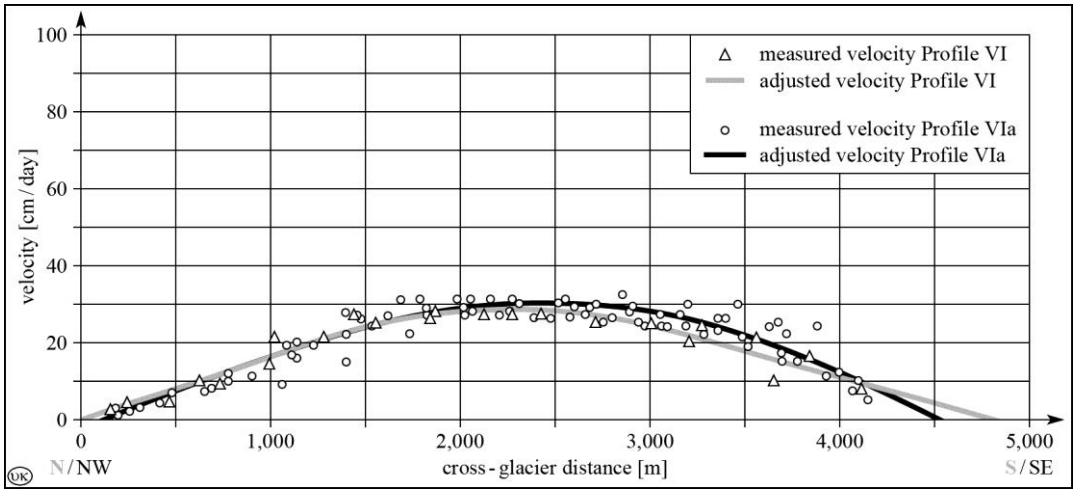

Fig. 7: Profile VI and Profile VIa: measured and adjusted velocities

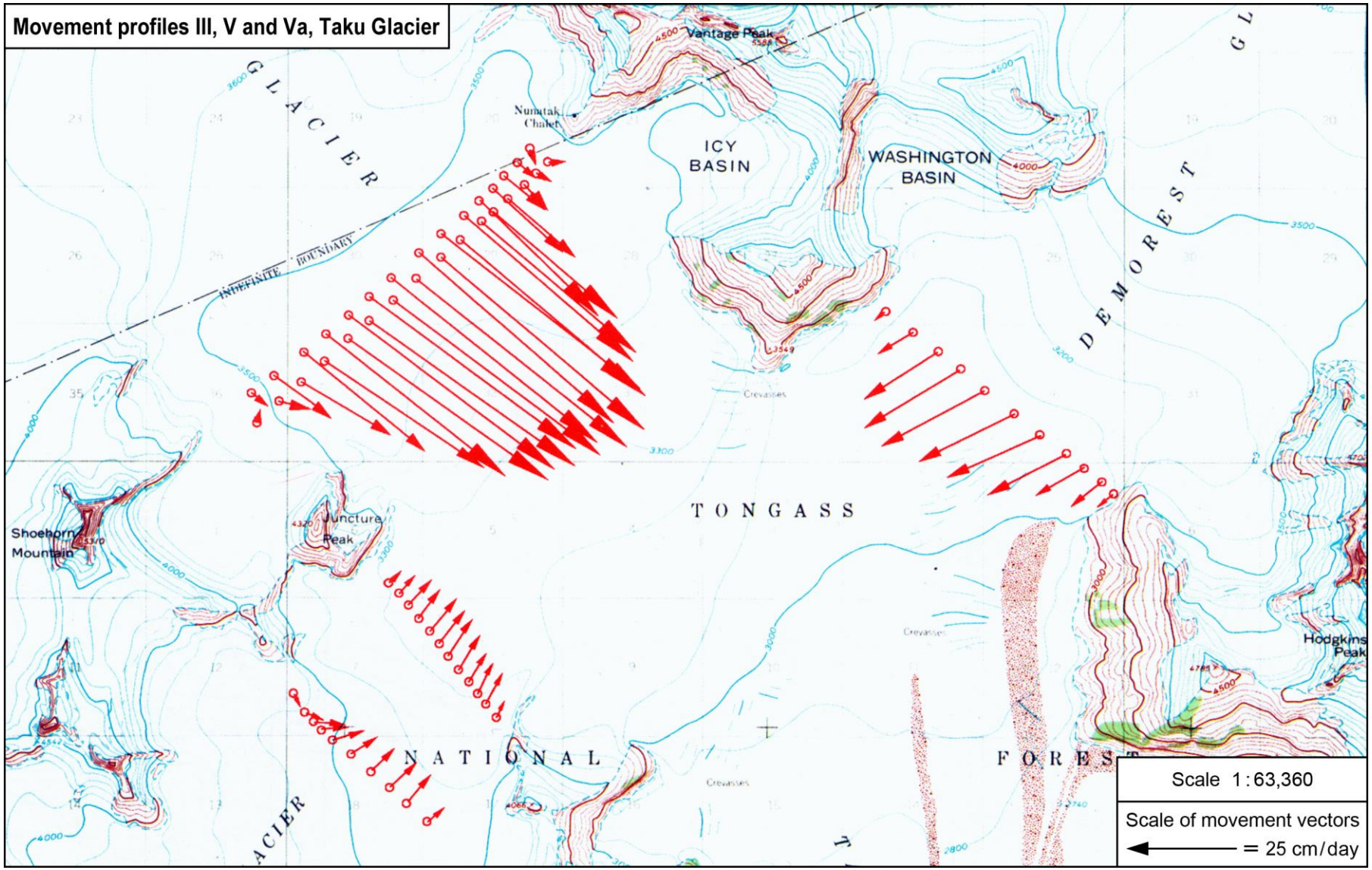
Movement profiles III, V and Va, Taku Glacier
Vantage Peak
Numatak Chalet
ICY BASIN
WASHINGTON BASIN
DEMOREST
INTERNATIONAL BOUNDARY
Crevasses
TONGASS
Shoehorn Mountain
Puncture Peak
Hodgkins Peak
NATIONAL
FOREST
Scale 1:63,360
Scale of movement vectors
= 25 cm/day

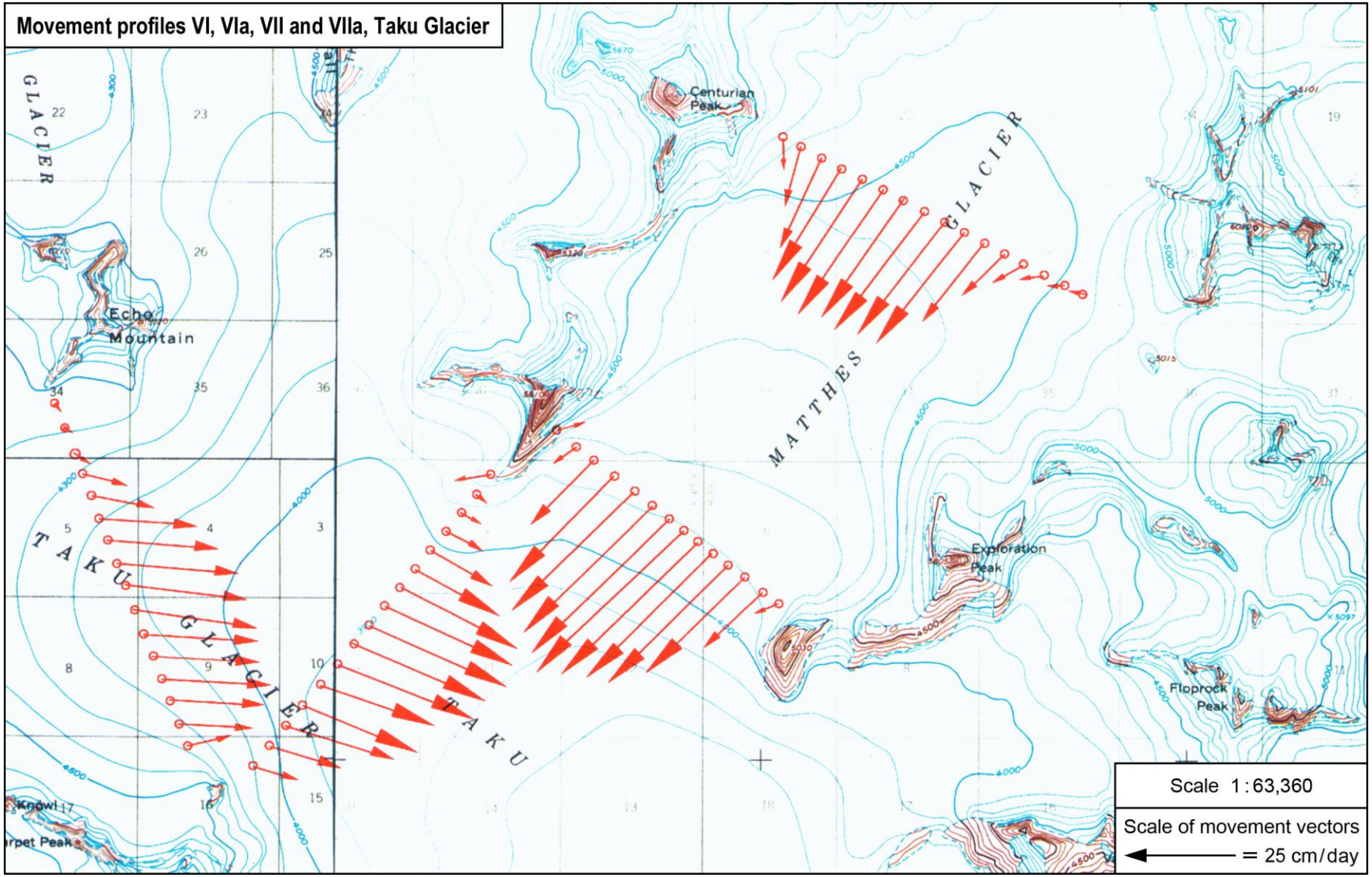
Movement profiles VI, VIa, VII and VIIa, Taku Glacier
Centurian Peak
MATTHES GLACIER
Echo Mountain
TAKU GLACIER
Exploration Peak
Floprock Peak
Scale 1:63,360
Scale of movement vectors
= 25 cm/day

lower Profile VIa is reflected by a 10% increase of the maximum velocity (32 cm/day versus 29 cm/day on Profile VI) and of the mean velocity (18 cm/day versus 16 cm/day). Movement variations over the years were not detected.

Profile VII extends from Camp 9 towards Centurian Peak. It was up to the early nineties the only profile on the lower Matthes Glacier. Data were gathered 1986, 1987, 1989, 1990, 1994 and 1996. Close to the confluence zone of Matthes and Taku Glacier, Profile VIIa between Taku C and Taku D was established in 1993 and yearly monitored.

The flow direction of the easterly part of Profile VII reflects the outflow of the small basin below Camp 9 towards the Matthes Glacier. Apart from this irregularity the flow is perfectly parabolic. Over the last decade the movement pattern has been very stable. The maximum velocity reaches 38 cm/day and the mean velocity 26 cm/day. Compard to the results from earlier JIRP seasons the flow has not changed for the last fifty years. This is in contrast to other profiles.

Towards the confluence zone the Matthes Glacier valley narrows from 4 km at Profile VII to 3 km at Profile VIIa. Since between both profiles no mass is added to the Matthes Glacier, the result is a gain in velocity. Its maximum increases to 45 cm/day and the mean to 29 cm/day. A polynomial fit reveals again a parabolic flow pattern (Fig. 8) which is asymmetric with higher velocities towards Taku C. The movement variations are very small and can be assigned to the small differences of the positions of the profile over the last three years.

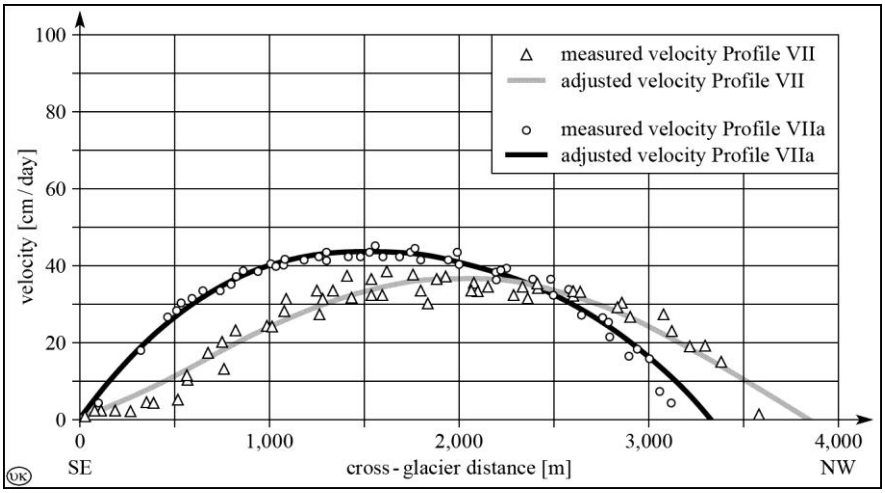

Fig. 8: Profile VII and Profile VIIa: measured and adjusted velocities

Although the distances to the confluence zone are comparable the lower Matthes Glacier (Profile VIIa) moves about 50% faster than the NW-Branch of the Taku Glacier (Profile VIa). This fact should give rise to further investigations of depth profiles in various locations of both glaciers.

2.2.1.4 Nevé Area of the Matthes, Vaughan-Lewis and Llewellyn Glaciers

The so-called High Plateau at an elevation of 1,800-1,900 m is the source or the two main glaciers of the Juneau Icefield: the Llewellyn Glacier representing the continental part of the Icefield flowing north into Canada and being the ultimate headwaters of the Yukon, and the Matthes Glacier flowing south into the Taku Glacier. The Matthes Glacier is one of the main tributaries of the Taku representing 20% of the Taku Glacier system.

The area of the High Plateau is characterized by extensive ice surfaces with only a few nuntaks. Long periods of poor visibility due to haze and fog are a limitations for terrestrial surveying methods. In addition to the classical profiles VIII (Upper Matthes Glacier) and IX (Upper Vaughan-Lewis Glacier) new profiles were established only when GPS became available. The new profiles on the Llewellyn Glacier and in the area of the Divide give a first glance of the movement pattern of the highest part of the Taku-Llewellyn system.

Profile VIII is located between Blizzard Point and Camp 8. The re-observation of the profile shows some unexpected movements over the years. In 1994, for instance, almost double the velocity occurred. This is very unlikely so that an unrecovered error in the terrestrial surveys has to be assumed. Therefore the 1994 data as well as those of 1987 when an approximative method for the velocity determination was applied were omitted in Fig. 9. The orientation of the movement vectors (up to 8 cm/day) at the eastern and western end of the line reflect the influence of the ice movements down from Blizzard Peak and Mount Moore resp.. Nevertheless the flow pattern is parabolic (Fig. 9). The maximum velocity ranges from 16 to 19 cm/day and the mean movement is 9 cm/day. With respect to the location of the profile close to the Divide and an average gradient of 0.5° these values appear very high. The reason could be a substantial depth of the glacier which provides the big masses necessary for the high velocities. Applying the flow law according to *GLEN [1958]* a depth of 300 to 500 m can be estimated. This is somewhat in contrast to *MILLER's et al. [1994]* findings of 500 to 800 m.

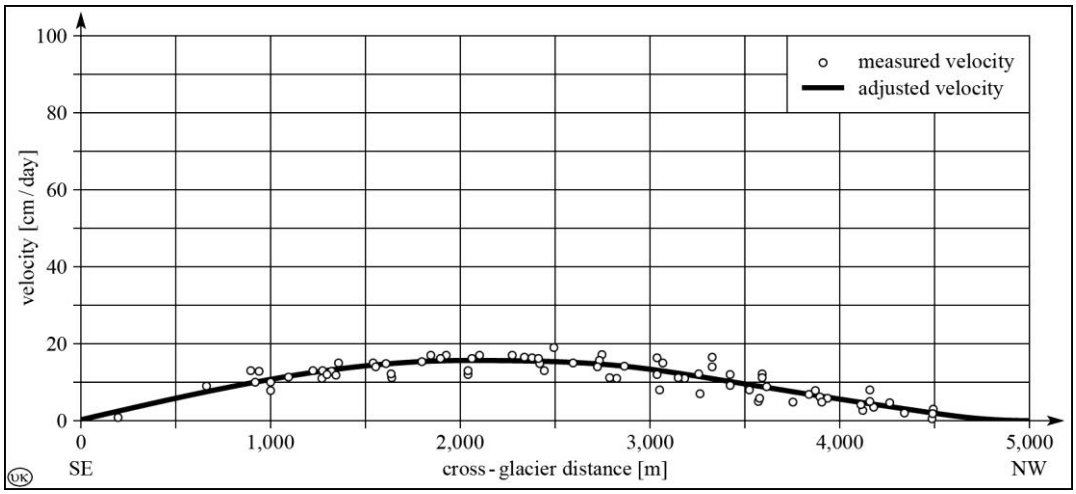

Fig. 9: Profile VIII: measured and adjusted velocities

Profile VIIIa was set in 1995 3 km down-glacier of Profile VIII. The purpose was to demarcate the Matthes from the Vaughan-Lewis Glacier. The results were not satisfying, because the profile was set too far down the Matthes Glacier. The movement pattern is as expected with a maximum velocity of 22 cm/day. It has to be considered that the profile covers only one third of the glacier's width. The survey of Profile VIIIa was not repeated in the following years.

Profile IX is located about 1 km above the top of the Vaughan-Lewis Icefall forming a circle between the ridge of Camp 18 and Mammary Peak. The area is usually heavily crevassed. In some years it has been too dangerous to set the flags or to perform EDM or GPS measurements. Due to this fact and the poor configuration for point determination by intersection, some results (1988 and 1991-1993) are neither plausible nor significant; they are

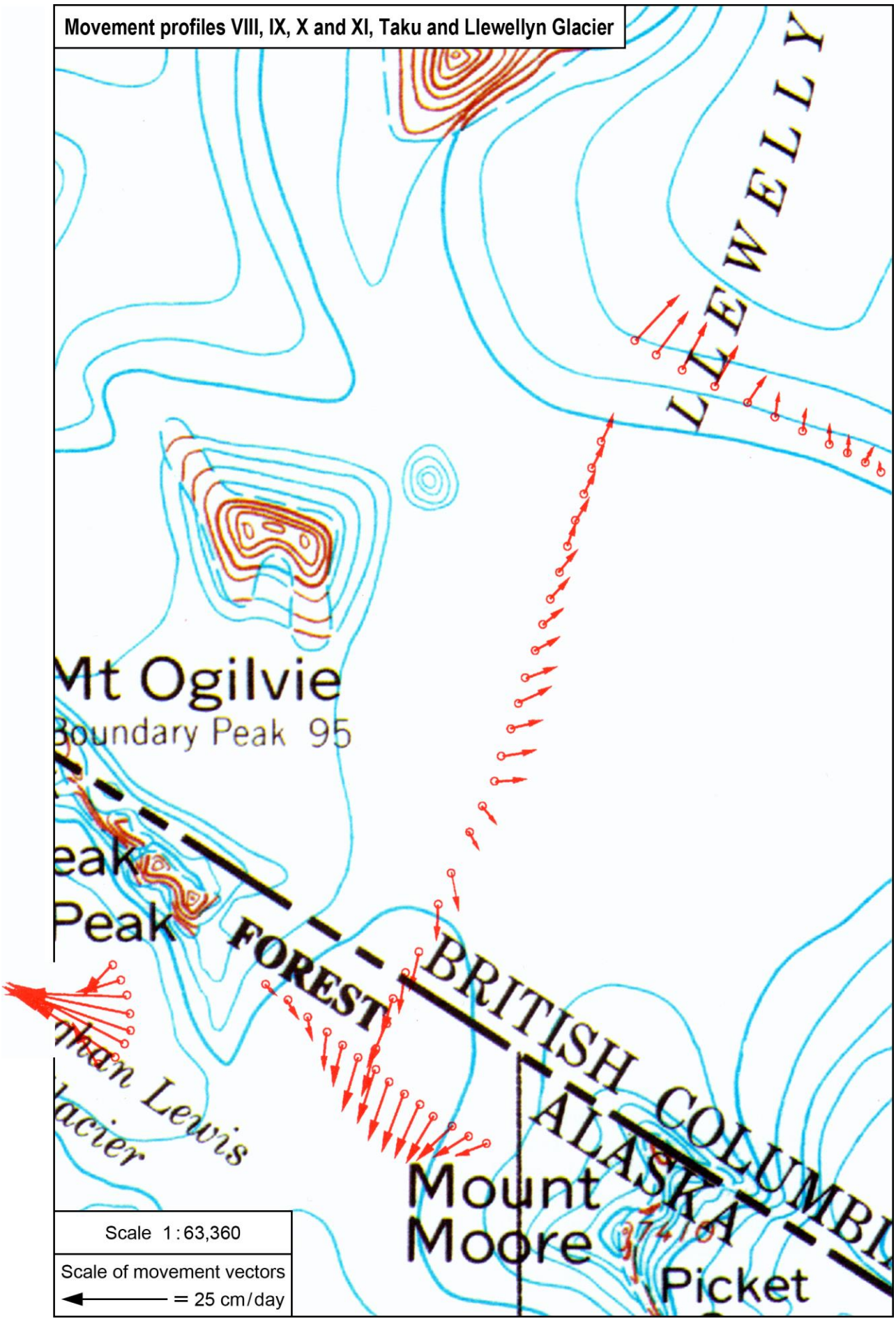
Movement profiles VIII, IX, X and XI, Taku and Llewellyn Glacier
LLEWELLY
Mt Ogilvie
Boundary Peak 95
eak
Peak
FOREST
BRITISH COLUMBI
ALASKA
Mount
Moore
Picket
Scale 1:63,360
Scale of movement vectors
= 25 cm/day

not listed in the appendices. Besides, due to the difficult accessibility the location of the profile varied over the years. Therefore the individual maximum velocities (26 to 35 cm/day) reflect rather the distance to the Icefall than the change of the movement pattern. The orientation of the vectors, however, is consistent throughout the years: radiating towards the icefall and perpendicular to the contour lines.

A dramatic reduction of the maximum velocity from 30 cm/day to some 10 cm/day can be seen in 1996. Using real-time GPS the flag positions were re-established within a meter, so that the location of the profile cannot be responsible for the great change. Even the decrease of the ice thickness from 1995 to 1996 by app. 1 m cannot be causative. Without further investigations it will be difficult to find an explanation.

Profile X was established in 1995 and prolonged a year later to find out where the divide between the Matthes and the Llewellyn Glacier may be located. It extends some 8 km starting in the center of Matthes Glacier at Profile VIII and ends about 5.5 km beyond the Canadian border. The divide is in the area of flag 15 and 16, where the orientation of the movement vectors changes towards the Llewellyn Glacier.

Profile XI is located on the Canadian side of the Icefield 8 km beyond the border and some 3 km before the Llewellyn Glacier enters the narrow channel between F 10 Peak and Sloko Ridge. Extending 4 km, it covers half the width of the glacier. The eastern end shows an erratic but not significant pattern of movement mainly directed towards the center of the Llewellyn Glacier. Further to the west the velocity of the movement increases up to 15 cm/day; the orientation is northwest. The plateau around Mount Nesselrode and Mount Bressler contributes masses to the Llewellyn Glacier which are not monitored. An even higher velocity in continuation of the western end of the profile can be assumed.

It is proposed to relocate Profile XI between F 10 Peak and Sloko Ridge, where all the masses originating from the High Plateau have to pass through. This location could help to elaborate the influence of the cyclic shifts of the Arctic Front on both glaciers over the years.

2.2.1.5 Gilkey Trench

In 1990 six profiles with a total of 45 flags were distributed in the confluence area of the Gilkey Trench (Fig. 10). Here Gilkey Glacier is forced to change the flow direction from south to west within some 1.5 km, Unnamed Glacier changes its flow direction in a similar way from north to west in less than 1 km. The Vaughan-Lewis Glacier is pushing in between after cascading down the icefall and forming wavebulges with amplitudes of about 25 m.

All profiles except for Profile E were set in double lines. Thus slope gradients, movement vectors and strain rates can be derived. Profile A was set on the Unnamed Glacier before its sharp turn, Profile B traverses the Gilkey Trench directly below the confluence of the three glaciers. Profile C consists of two longitudinal lines in the area of the bend of Gilkey Glacier. Profile D was placed on a transect above the Gilkey Glacier turn, Profile E is a single triangle below the icefall of the Little Vaughan-Lewis Glacier, and Profile F was originally placed on the crests of the first and second wavebulges below the Vaughan-Lewis Icefall. A significant number of flags could be found again year after year until 1995, permitting an almost complete and conclusive movement record of the confluence area. Most of the flags of Profile A and the majority of the Profile F flags were lost.

Comparing the short-term „summer“ velocities derived in August 1990 and the long-term yearly velocities (Appendix B), the differences are in general negligible. Therefore a uniform movement throughout the year can be taken as a conclusion.

The central part of Gilkey Glacier (Profil B flags 9-12, Profile C and D) is moving with an average velocity of about 50 cm/day. Since the profiles do not cover the margins of the three glaciers of the trench, definite conclusions about the decrease in velocity on both sides cannot be drawn. However, the numerous crevasses indicate a sudden decrease in velocity supposedly caused by vertical sliding along the steep sidewalls. Thus combined with the ratio of 0.12 of mean annual movement to the glaciers' width (see section 2.2.1.1), a transition from parabolic to Block-Schollen flow ca be assumed.

The Unnamed Glacier moves with an average velocity of about 12 cm/day in the area up-glacier the sharp turn. The equivalents of the points A 1, A 3 and A 5 are the points B 1,

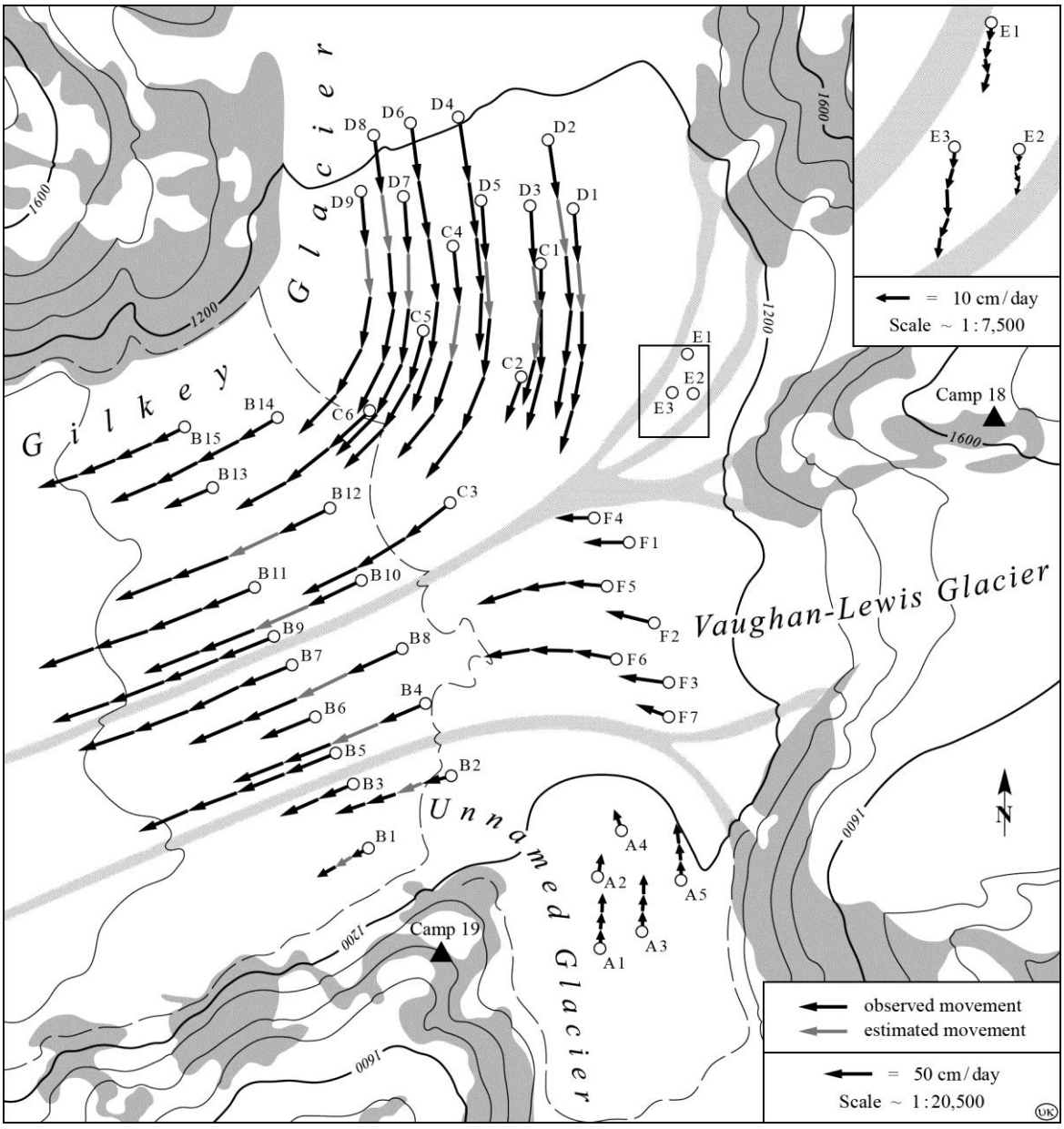

Fig. 10: Movement pattern in the Gilkey Trench

B 2 and B 3 (see Fig. 10). Remarkable is the increase of the velocity of these points: while the increase from A 1 to B 1 is only 4 cm/day, the increase from A 3 to B 2 is 16 cm/day and the acceleration from A 5 to B 3 is even 25 cm/day. At the same time the width of the Unnamed Glacier halves. The reason may be found in the higher velocity of the mighty neighboring glaciers which carry along the small Unnamed Glacier.

The Vaughan-Lewis Glacier shows the greatest velocity variations of all glaciers on the Icefield. Above the icefall maximum velocities of 30 cm/day are reported (see Profile IX in section 2.2.1.4), whereas in the icefall dramatic 5.7 m/day were observed *[RENTSCH et al., 1997]*. In the lower section the icefall slows down to less than 1 m/day *[LANG, 1993]*. Points F 1, F 2 and F 3 located on the first wavebuldge move with 40 cm/day, the points F 4 to F 7 on the second wavebuldge are slower by 15%. Points B 4 and B 8 on wavebuldge No. 8 and points B 5 to B 7 on buldge No. 10 of the Vaughan-Lewis Glacier have an average velocity of 50 cm/day. The width of the Vaughan-Lewis Glacier diminishes from 750 m at the base of the icefall to 500 m at Profile B which may explain the increase in velocity.

All the variations of the velocities do not provide a clue to the bed topography of the three glaciers. They are rather a result of their complex interaction. Further conclusions could be drawn if the bed topography of the Gilkey Trench was reliably investigated by seismic or other means.

2.2.2 Strain rates

Strain rates can by derived according to *WELSCH [1997]* from repeated observations of geometrical figures like triangles. Strain rate measurements are the geodetic contribution to stress and strain relations which are the basis for further glacier studies applying methods of continuum mechanics. Two simple examples are given in *DAELLENBACH and WELSCH [1997]* and *McGEE [1990]*. In the following section the results of strain rate measurements on the main Taku Glacier and in the Gilkey Trench are presented.

2.2.2.1 Main Taku Glacier – Profile IV

In 1994 the western end of Profile IV was extended so that 29 triangles instead of 25 can be used for strain rate analysis. The distribution of the strain rates across the main Taku Glacier is consistent over the years. In Fig. 11 the maximum principle strain rates (e_1) are shown.

The strain rates of the first two triangles at the eastern end are very small, indicating only little stress within the first 500 m. This is an accordance with the small increase of velocity in this area. Within the next 1 km the velocity is increasing with the consequence of maximum principle strain rates which are 10 times higher than before. This is made obvious by numerous shear crevasses. In the central area of Profile IV a more or less homogeneous movement is dominant indicated by strain rates which are as low as at the eastern end. Towards the western end the velocity slows down causing again a peak of maximum principle strain. The velocity and the strain rates at the western end show the disturbing influence if the ice flow from the basin between Shoehorn Mountain and Juncture Peak.

2.2.2.2 Gilkey Trench

The movement of Profile A on the Unnamed Glacier is very consistent. Thus the relatively small strain rates which were observed can be expected.

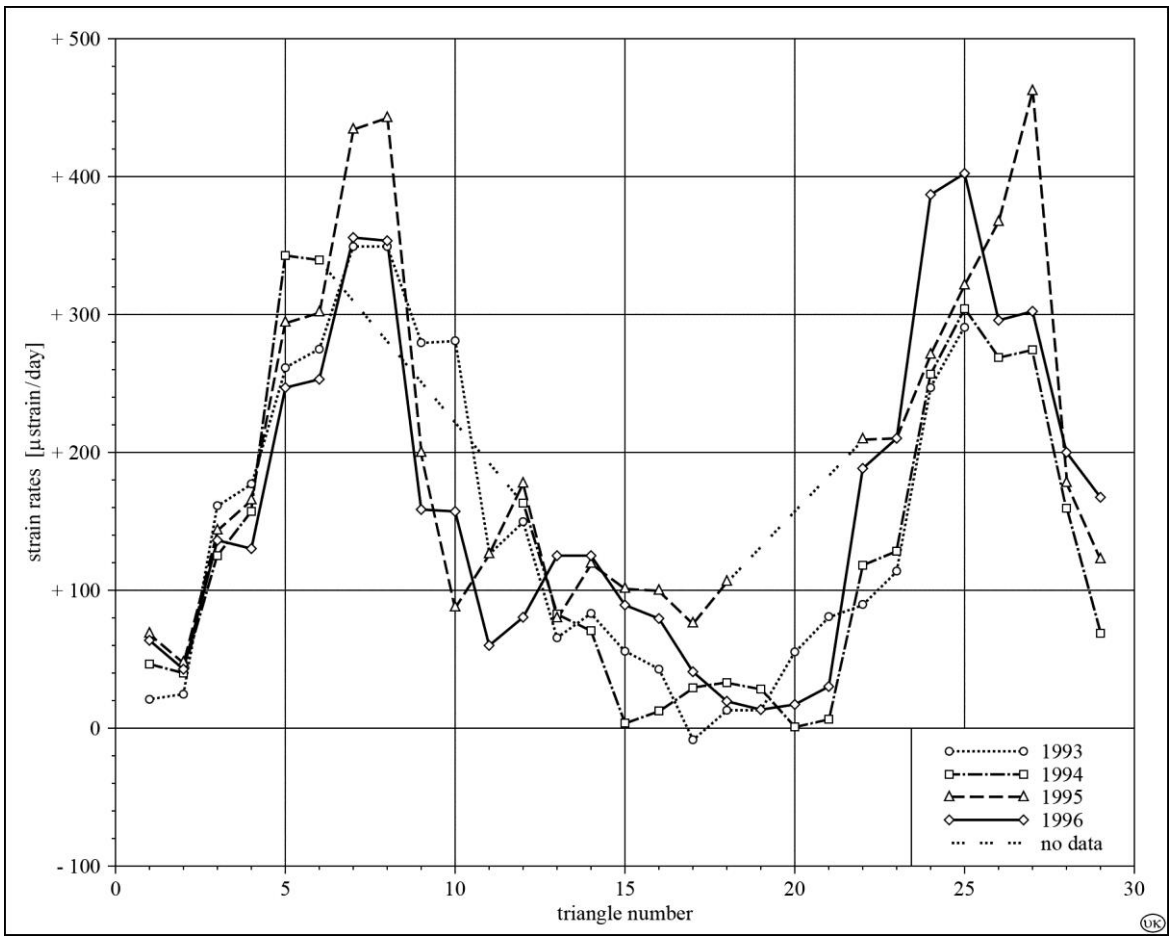

Fig. 11: Profile IV, 1993-1996: maximum principal strain rates (e_1)

The results of Profile B traversing the Gilkey Trench completely, reveal some peculiarities. The strains of the Unnamed and the Vaughan-Lewis Glaciers are rather homogeneous but decreasing towards the Gilkey Glacier. Here compressional flow is dominant extending far across the glacier. The strain of the last triangle of the profile is extensional. The crevasses beyond the profile may indicate that the extensional strain increases towards the bank of the glacier.

The triangles of Profile C cover the area where Gilkey Glacier has its 90° turn. Apart of the triangle which includes point C 6, the strain values and the orientations of the strain ellipses are consistent with the uniform speed in this area.

The strain values of Profile D are astonishingly high and variable. Beginning from the eastern end there is a built-up of extensional flow, a sudden decrease in the center and towards the corner again an increase of extension by more than a magnitude. Finally at the western end compressional flow dominates. So far there is no obvious explanation of this phenomenon.

The results found with Profile E is as expected: point E 2 as the closest to the glacier's margin is the slowest, so that increasing extensional strain towards the faster moving center is regular.

Extensional strain in the flow direction of the Vaughan-Lewis Glacier can be assumed

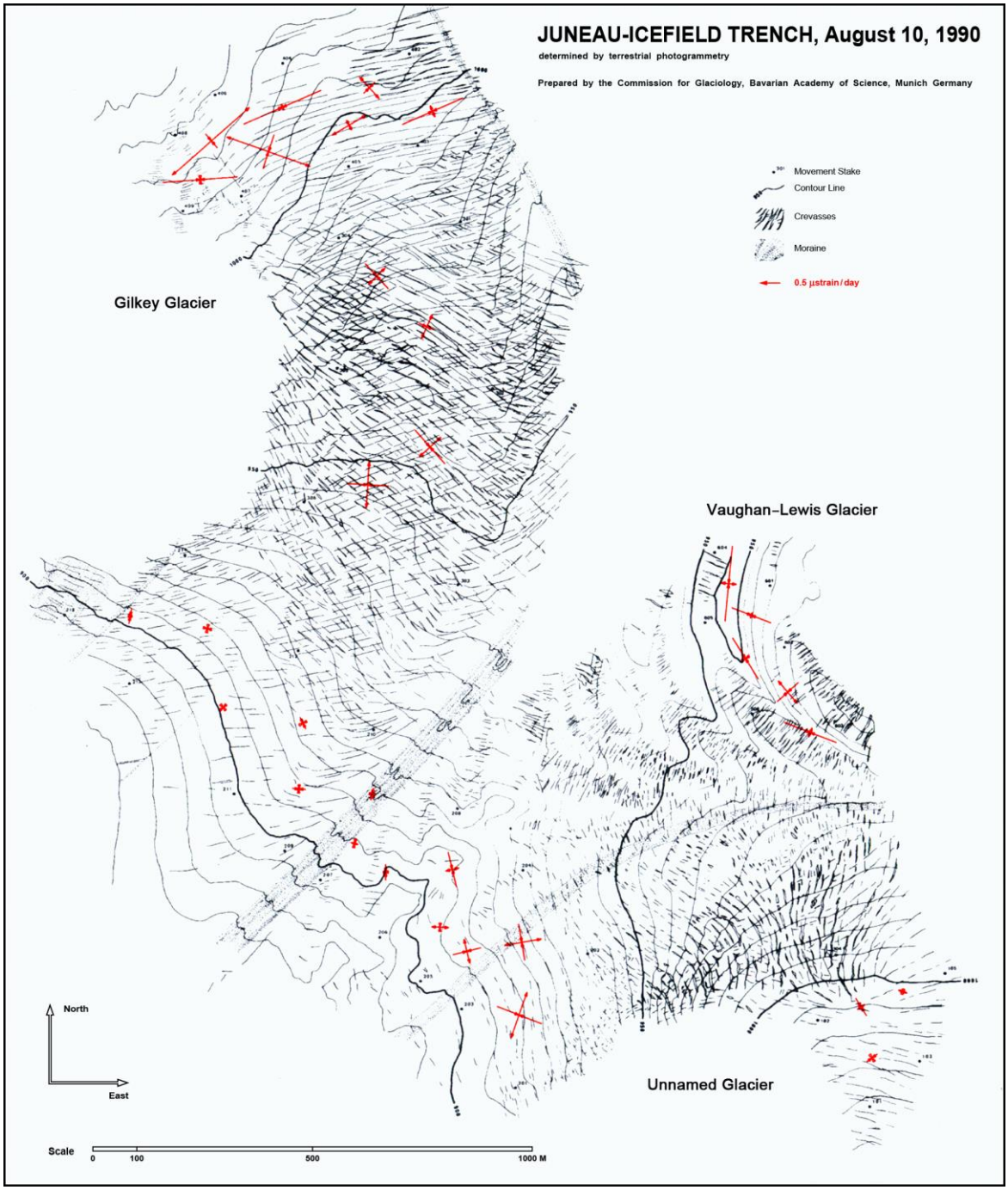
JUNEAU-ICEFIELD TRENCH, August 10, 1990
determined by terrestrial photogrammetry
Prepared by the Commission for Glaciology, Bavarian Academy of Science, Munich Germany
Movement Stake
Contour Line
Crevasses
Moraine
0.5 µstrain / day
Gilkey Glacier
Vaughan-Lewis Glacier
Unnamed Glacier
North
East
Scale
0
100
500
1000 M

for all the triangles formed by the points of Profile F. But it turns out to be true only for some triangles. Especially in the central part, where the curvature of the wavebuldges is minimal, compressional flow is found.

The strain rates (except for Profile E) are plotted on page 113 against the crevasse pattern which occurred at the time of the measurements *[RENTSCH, 1997]*. The strain ellipses correspond reasonably to the crevasse pattern.

References

DAELLENBACH, K. K. and WELSCH, W. M. [1997]: Determination of Surface Velocities, Strain and Mass Flow Rates of the Taku Glacier, Juneau Icefield, Alaska. – In: *WELSCH, W. M., LANG, M. and MILLER, M. M. (eds.):* Geodetic Activities, Juneau Icefield, Alaska, 1981-1996. Schriftenreihe des Studiengangs Vermessungswesen, Heft 50, Universität der Bundeswehr München, Neubiberg; p. 117-126

EDMAIER, B. and JUNG-HÜTTL, A. [1996]: Eisige Welten. Im Kosmos der Minusgrade. BLV Verlagsgeschaft, München; 153 pp.

FINSTERWALDER, R. [1950]: Some Comments on Glacier Flow. Journal of Glaciology, Vol. 1, No. 7, Cambridge; p. 383-388

GLEN, J. W. [1958]: The Flow Law of Ice. A Discussion of the Assumptions Made in Glacier Theory, Their Experimental Foundations and Consequences. International Association of Scientific Hydrology, Publication No. 47, Paris; p. 171-183

HAVAS, T. [1965]: Surface Velocity and Strain-Rate Measurements on Several Alaskan Glaciers, 1964. M. Sc. Thesis, Michigan State University, East Lansing

LANG, M. [1993]: Report on the Geodetic Activities during the 1993 Juneau Icefield Research Program Field Season. JIRP Survey Report, 1993. Juneau Icefield Research Program, Foundation for Glacial and Environmental Research, Juneau; Bundeswehr University Munich, Germany

McGEE, S. R. [1990]: Surface Strain-Rate Measurements on the Gilkey Glacier, Juneau Icefield, Alaska, 1989. JIRP Survey Report, 1990. Juneau Icefield Research Program, Foundation for Glacial and Environmental Research, Juneau

McGEE, S. R. [1997]: Using GPS to Determine Local Surface Mass Balance: A Case Study on the Taku Glacier. – In: *WELSCH, W. M., LANG, M. and MILLER, M. M. (eds.):* Geodetic Activities, Juneau Icefield, Alaska, 1981-1996. Schriftenreihe des Studiengangs Vermessungswesen, Heft 50, Universität der Bundeswehr München, Neubiberg; p. 127–135

MILLER, M. M. [1953]: Juneau Icefield Research Project, Report No. 8. Department of Exploration and Field Research, American Geographical Society, New York

MILLER, M. M., SPRENKE, K., BENEDICT, T., ADEMA, G., AUERBACH, D., PRUIS, M. and VOLKENING, L. [1994]: Preliminary Report of the 1994 Seismicv Surveys on the Juneau Icefield, Alaska. JIRP Geophysical Report, 1994. Juneau Icefield Research Program, Foundation for Glacial and Environmental Research, Juneau

PELTO, M. S. and MILLER, M. M. [1990]: Mass Balance of the Taku Glacier, Alaska from 1946 to 1986. Northwest Science, Vol. 64, No. 3, Washington; p. 121-130

PILLEWITZER, W. [1958]: Neue Erkenntnisse über die Blockbewegung der Gletscher. Zeitschrift für Gletscherkunde und Glaziologie, Band 4, Heft 1-2, Innsbruck; p. 23-33

RENTSCH, H., WELSCH, W. M., HEIPKE, C. and MILLER, M. M. [1997]: Digital Terrain Models as a Tool for Glacier Studies. – In: *WELSCH, W. M., LANG, M. and MILLER, M. M. (eds.):* Geodetic Activities, Juneau Icefield, Alaska, 1981-1996. Schriftenreihe des Studiengangs Vermessungswesen, Heft 50, Universität der Bundeswehr München, Neubiberg; p. 171–184

SPRENKE, K. [1996]: University of Idaho, Department of Geology and Geological Engineering, Moscow, Idaho 83844-3022, USA. Personal communication

WELSCH, W. M. [1997]: Description of Homogeneous Horizontal Strains and some Remarks to their Analysis. – In: *WELSCH, W. M., LANG, M. and MILLER, M. M. (eds.):* Geodetic Activities, Juneau Icefield, Alaska, 1981-1996. Schriftenreihe des Studiengangs Vermessungswesen, Heft 50, Universität der Bundeswehr München, Neubiberg; p. 73–90

Keith K. Daellenbach and Walter M. Welsch

Determination of Surface Velocities, Strain and Mass Flow Rates of the Taku Glacier, Juneau Icefield, Alaska [1)]

1. Surface Velocity

During the 1988 Juneau Icefield Research Program, the movement „Profile IV“ in the vicinity of Camp 10 on the Juneau Icefield was re-established. It is located appr. 26 km above the glacier's terminus and 5 km above the mean neve line. The elevation above sea level is appr. 1,100 m. The length of the profile is some 5 km (Fig. 1).

This profile line has historically been a source of intense study. Results of annual surveys of across-glacier stakes report a velocity profile that varies from parabolic to plug flow *[MILLER, 1958]*. A glacier bore-hole experiment was conducted *[MILLER, 1958]* in order to determine physical properties and flow characteristics of the glacier. Bedrock profiles that record the glacier's depth have been obtained from various seismic techniques and from gravity measurements *[POULTER et al., 1950]*. Also seasonal accumulation and ablation rates have been recorded since forty years.

In 1988 a study of surface flow rates and for the first time also of surface strain rates was conducted on this very Profile IV. Twelve rods and three strain triangles were evenly spaced across the glacier perpendicular to the glacier's flow (Fig. 1). The rods of the movement profile and the strain triangles were initially surveyed and then re-surveyed several days later to determine how the positions of the rods and the shapes of the triangles had changed. For the surveys precise optical theodolites and electronic distance measuring instruments were used. Due to heavy ablation special precautions had to be taken in order to guarantee point identity of the sdurvey stations and targets on snow between the observation epochs *[BYERS et al., 1988]*.

For comparison, Fig. 2a depicts the velocity profiles from the 1949, 1950, and 1952 surveys *[MILLER, 1958]* while Fig. 2b presents the 1986, 1987, and the 1988 surveys of Profile IV *[KERSTING, 1986; BLACHNITZKY, 1987; DAELLENBACH, 1989]*. Surveys of the late 1940s and early 1950s reveal a maximum surface velocity rate ranging between 50 and 90 cm/day. The maximum surface velocities between 1986 and 1988 ranged between 50 and 60 cm/day. In each study, the maximum surface velocity was measured approximately at mid-glacier. The glacier flow patterns of the late 1940s and early 1950s exhibit a Block-Schollen or plug flow while the pattern between 1986 and 1988 show a partial parabolic streaming flow.

[1)] Zeitschrift für Gletscherkunde und Glazialgeologie, Vol. 26, No. 2, Innsbruck *[1990]*; p. 169-177

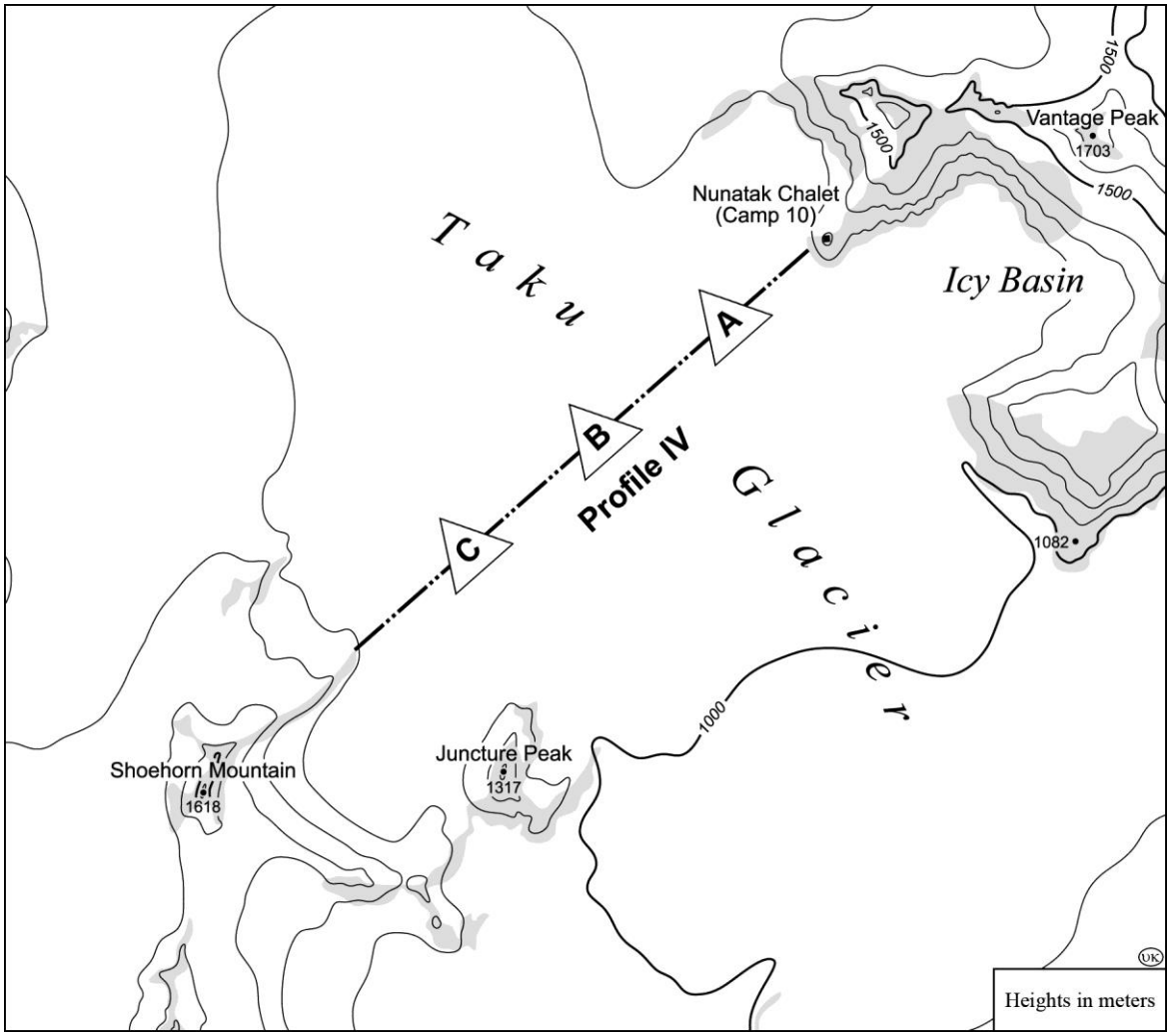

Fig. 1: The main Taku Glacier, the movement Profile IV, and the strain triangles

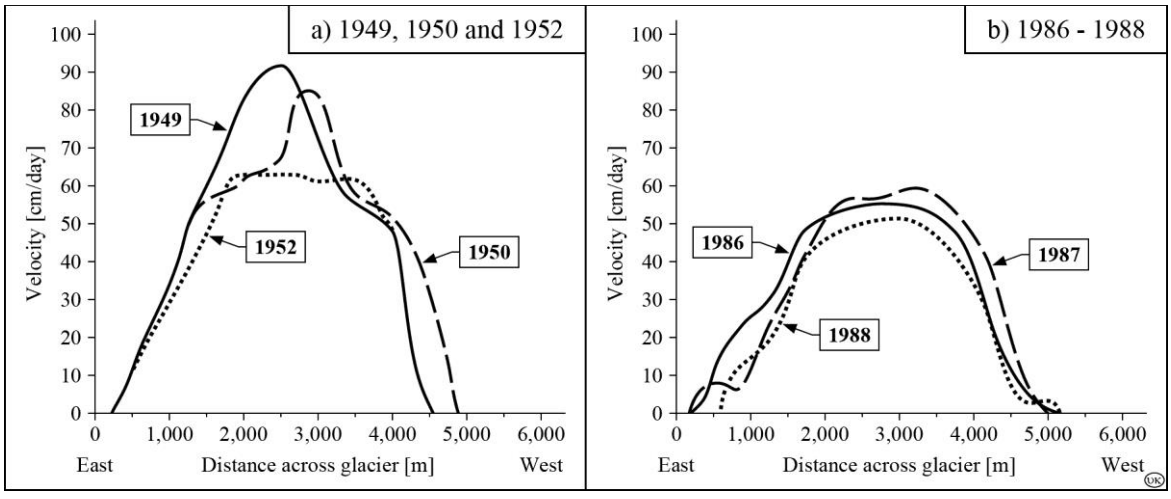

Fig. 2: Surface velocity patterns at Profile IV

2. Surface Strain Rates

As mentioned, three triangles were evenly spaced across the movement profile (triangles A, B, C; Fig. 1). The triangles were equilateral with side lengths of some 500 m. The three side lengths and the three angles of each triangle were precisely observed. Re-observation after a period of time led by comparison to the distortions of the individual elements. The distortions of the six elements of a triangle serve as the basis for the analysis of principal strain rates occurring in the area of that triangle. The least squares estimation of the strain tensor elements and their transformation to the so-called strain ellipse representing the principal strain rates and their orientation is given e.g. by *WELSCH [1997]*. In constrast, *NYE [1959]* applies diamond-shaped quadrilateral figures for strain measurements.

The spacing of the triangles allows to show how the orientation and magnitude of the strain rates vary across the glacier. Fig. 3 depicts the results (see also Table 1). The representation of strain accumulation for each strain triangular study field is given as a two-dimensional, homogeneous strain ellipse; e_1 is extensional (maximum principle strain), e_2 compressional (minimum principle strain). Also mapped are the representative surface crevasses that existed in each area.

Strain triangle Taku A yielded the largest strain rates of the three study areas. The orientation of the maximum principle strain rate e_1 was perpendicular to the observed pattern of crevasses. This field was heavily crevassed by the time the initial survey was made.

Strain triangle Taku B was situated approximately at mid-glacier in an area of high surface velocities. The maximum principle strain rate measurement was approximately $^1/_{16}^{th}$ of that experienced in Taku A. This dramatic decrease in the magnitude of strain rate correlates well with the nearly complete absence of surface crevasses in the Taku B study area. The orientation of e_1 was perpendicular to the few observed surface crevasses only in a general way.

Strain triangle Taku C experienced a maximum principle strain rate of about $^1/_2$ that of Taku A. As in Taku A, the orientation of e_1 was perpendicular to the observed pattern of surface crevasses.

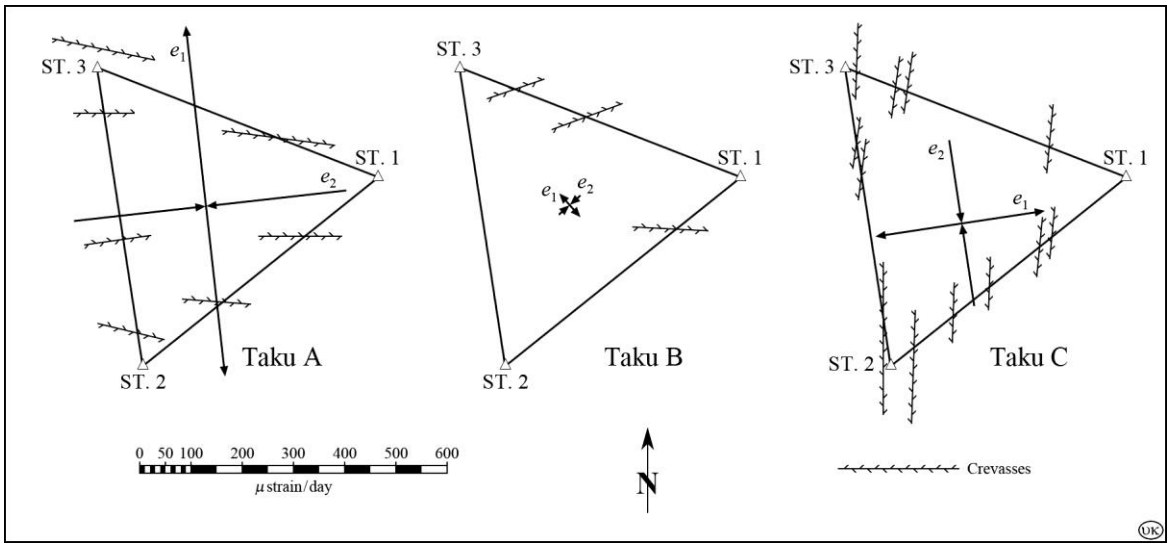

Fig. 3: Results of the strain rate measurements at the strain triangles Taku A, B, and C superimposed by the crevasse patterns

3. Stress Conditions

Based on a series of laboratory tests, *GLENN [1955]* developed a flow law for ice. This flow law describes an exponential relationship between stress and strain rates:

$$e = k \cdot \tau^n .$$

e is the effective shear strain rate

$$2\,e^2 = e_1^2 + e_2^2 + e_3^2 ,$$

where e_1 and e_2 are evaluated from the strain triangles and e_3 is determined through the continuity condition (no volume change)

$$e_1 + e_2 + e_3 = 0 ;$$

k is an empirical constant largely dependent on temperature, n is an empirical constant which is dependent on physical characteristics of the ice, τ represents the effective shear stress. In the vicinity of the present study area, the constants k and n were determined by *MILLER [1958]* to be 0.019 and 3, respectively,

Principle stress deviators σ_i' are found from *[NYE, 1959]*

$$\sigma_i' = \frac{\tau}{e}\, e_i .$$

Since the vertical stress $\sigma_3 = 0$ on the ice surface, the actual horizontal principal stresses σ_i, given by the relationship

$$\sigma_i' = \sigma_i - \frac{1}{3}(\sigma_1 + \sigma_2 + \sigma_3) ,$$

are

$$\sigma_1 = 2\,\sigma_1' + \sigma_2' ,$$
$$\sigma_2 = \sigma_1' + 2\,\sigma_2' .$$

Finally, the hydrostatic stress σ is defined by

$$\sigma = \frac{1}{3}(\sigma_1 + \sigma_2 + \sigma_3) .$$

The results for the areas under investigation are recorded in Table 1.

Table 1: Stress conditions of the Taku Glacier calculated from measured strain-rates

Study Area	$\dot{e}_1$	$\dot{e}_2$	$\dot{e}_3$	$\dot{e}$	τ	σ_1	σ_2	σ
Taku A	395.2	-333.8	-61.4	368.4	26.8	33.3	-19.8	4.5
Taku B	24.5	- 26.5	2.0	25.6	11.0	9.7	-12.3	-0.9
Taku C	177.6	-175.6	- 2.0	176.6	21.0	21.4	-20.6	0.2
(strain rates in μstrain/day ; stresses in bar)								

4. Mass Flow Rate

The total mass flow rate Q across a transverse section of the glacier is a useful calculation when considering the glacier's mass balance. By assuming a steady flow rate, independent of time the conservation of mass equation becomes

$$Q = \rho \cdot A \cdot U_{ave}$$

where ρ is the average density of glacier ice (917 kg/m^3), A ist the cross-sectional area of the transverse section across the glacier, and U_{ave} is the average velocity normal to the transverse section.

The bedrock profile in the vicinity of movement Profile IV has been determined with seismic measurement techniques *[POULTER et al., 1950]* ; Fig. 4 illustrates the transverse section across the glacier. The total across-sectional are was found to be $A = 1.35 \cdot 10^6$ m^2.

The value for U_{ave} is determined by empirical formulas which are based on a simplified laminar flow model *[NYE, 1952; MILLER, 1958]* referring to the velocity profiles U_0 at the glacier's surface and U_d at a given depth d:

$$U_d = U_0 - \frac{2k}{n+1} \cdot d \cdot \tau_d^n$$

where τ_d is the shear stress on a layer at a depth d according to

$$\tau_d = d \cdot \rho \cdot g \cdot \sin\alpha$$

with the constant density ρ; g is the acceleration due to gravity and α is the angle of the slope. Assuming a slope of $\alpha = 1°$, $\tau_d = 1.57 \cdot 10^{-3} \cdot d$ [bar].

U_0 (see Fig. 2b, profile 1988) can be expressed as a function of the width w of the glacier by a best-fitting polynomial curve of 4th order. U_d is then a function of the width w and the depth d of the glacier.

U_{ave} can finally be derived by the following integral

$$U_{ave} = \frac{1}{A} \int_0^d \int_0^w U(w,d)\, \mathrm{d}w\, \mathrm{d}d$$

with the result of U_{ave} = 29 cm/day.

Assuming the velocity

$$U_b = U_0 - U_{d_{\max}}$$

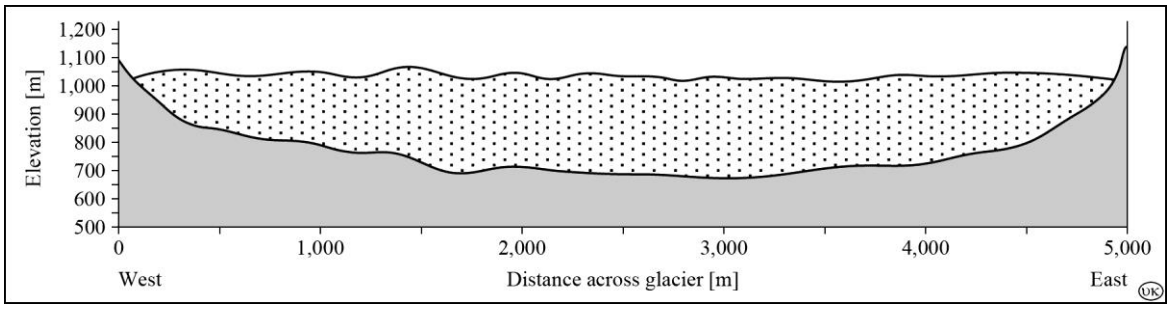

Fig. 4: Transverse section across the main Taku Glacier in the close vicinity of Profile IV

at depth $b = d_{\max}$ (bottom of the glacier) to be basal sliding, and averaging it across the profile with the result $U_{b_{ave}} = 0.57\, U_0$, the statement *[MILLER, 1958]*, that *„two-thirds of the down-glacier movement ... is due to bottom slip“* is verified.

With the average density ρ, the cross-sectional area of the traverse section A, and the average velocity U_{ave} normal to this transverse section, the total mass flow rate Q across Profile IV is eventually calculated to be appr. $360 \cdot 10^6$ kg/day.

Acknowledgement

This paper is dedicated to the memory of Dipl.-Ing. *Klaus Blachnitzky* who died on the Juneau Icefield in 1988 in fulfilment of his work as an academic teacher and researcher.

Addendum

Using radio-echo soundings and seismic reflections, cross-sections of Taku Glacier were recently measured (*BENEDICT et al. [1993, 1994], NOLAN et al. [1995]* as compared

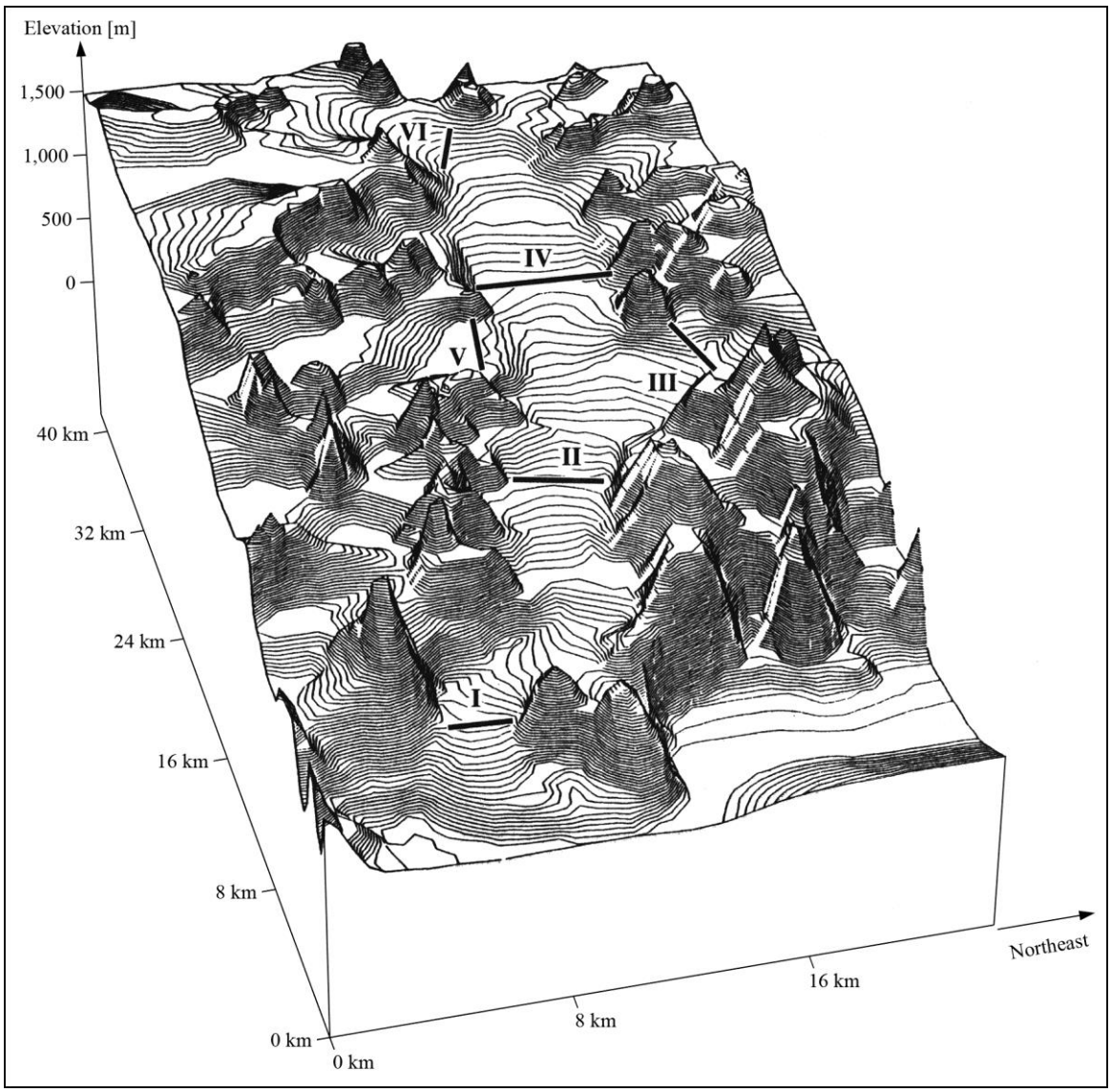

Fig. 5: DTM of the Taku Glacier with the location of the following profiles

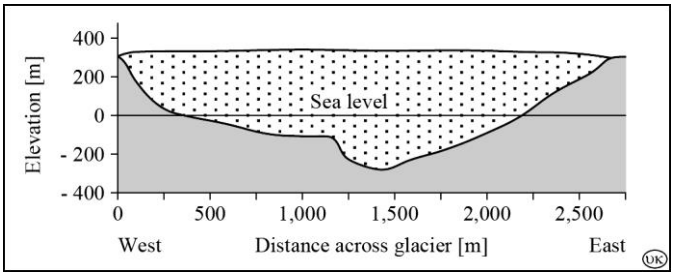

Fig. 6: Profile I

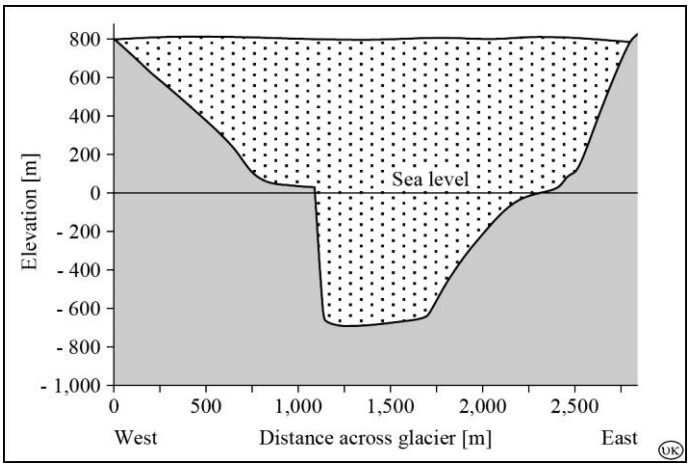

Fig. 7: Profile II

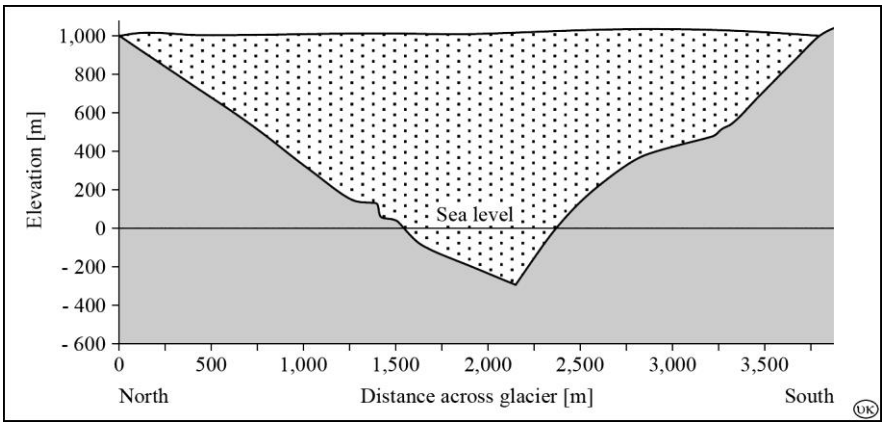

Fig. 8: Profile III

to *POULTER et al. [1950]*) to resolve inconsistencies in previous measurements and to understand better the glacier's dynamics. The maximum thickness found is about 1,480 m and the minimum bed elevation is about 600 m below sea level, which establishes Taku Glacier as the thickest and deepest temperate glacier yet measured. The measurements were repeated and extended *[SPRENKE, 1966]* so that a series of cross-sections reveals the thickness of the glacier body (see the diagrams of Profile I through VI (Fig. 6 to 11) and their locations across Taku Glacier, Fig. 5).

The flow laws described by *NYE [1952]*, *GLENN [1955]*, and *MILLER [1958]* are to be questioned in consideration of such a profoundly different glacier body. New investigations are indispensable to develop a refined and differentiated flow model for this worldwide very unusual situation *[FRIEDMANN, 1997]*.

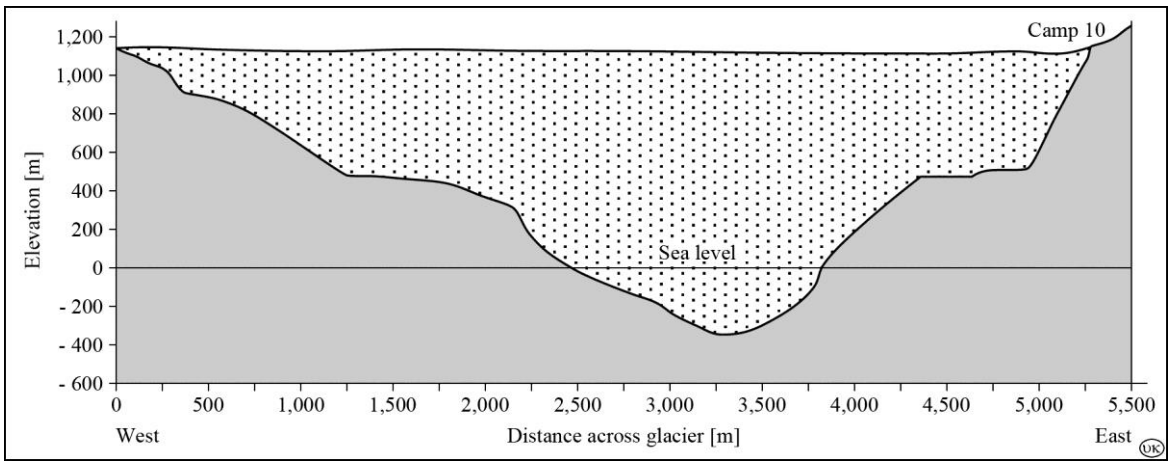

Fig. 9: Profile IV

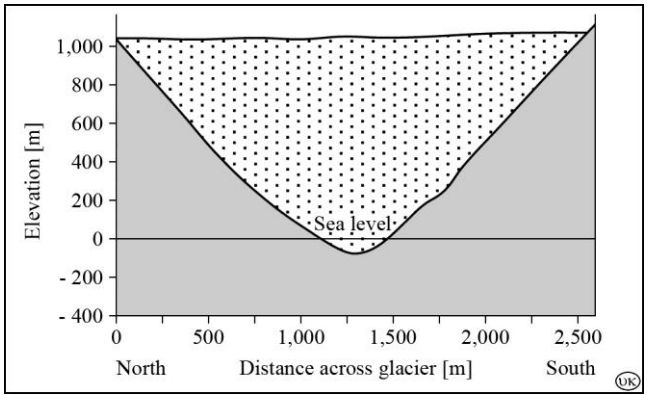

Fig. 10: Profile V

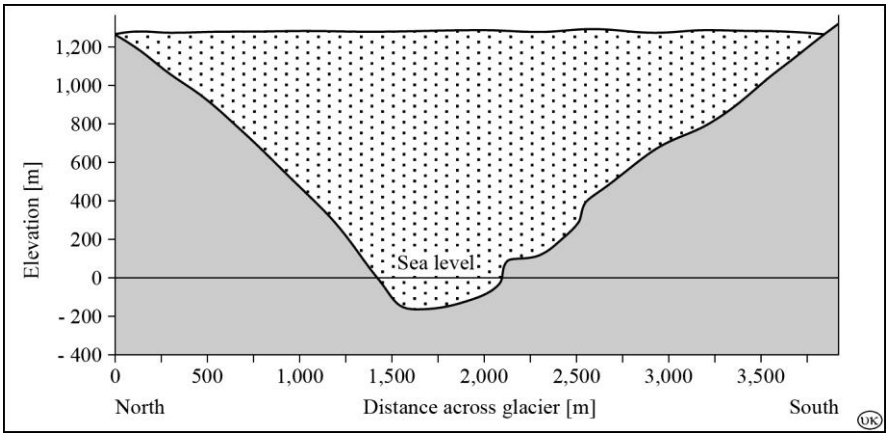

Fig. 11: Profile VI

As a consequence, the mass flow rate as described in the above article may represent only the ice transport within the upper layers of Taku Glacier across Profile IV.

References

Benedict, T., Sprenke, K., Gilbert, G., Stirling, J. and Miller, M. M. [1993]: New Seismic Depth Profiles on Taku Glacier, 1993, Juneau Icefield, Alaska. JIRP Open File Report, 1993. Juneau Icefield Research Program, Foundation for Glacier and Environmental Research, Juneau

BENEDICT, T. and SPRENKE, K. [1994]: Preliminary Results of the Seismic Investigations on the Taku Glacier, Alaska, 1994. JIRP Open File Report, 1994. Juneau Icefield Research Program, Foundation for Glacier and Environmental Research, Juneau

BLACHNITZKY, K. [1987]: Report on the Geodetic Activities During the 1987 Juneau Icefield Research Program Field Season. JIRP Survey Report, 1987. Juneau Icefield Research Program, Foundation for Glacier and Environmental Research, Juneau; Bundeswehr University Munich, Germany

BYERS, C., DAELLENBACH, K. K., MARKLILLIE, J. R., Mc GEE, S. R. and PETERSON, E. [1988]: Results of the Summer 1988 Surveying Program. Conducted under the Auspices of the Juneau Icefield Research Program. JIRP Survey Report, 1988. Juneau Icefield Research Program, Foundation for Glacier and Environmental Research, Juneau

DAELLENBACH, K. K. [1989]: Determination of Surface Velocities and Strain Rates on the Taku Glacier, Alaska. Final Paper ME 406, Oregon State University, Department of Mechanical Engineering, Corvallis, USA

FRIEDMANN, A. [1997]: The Ice Flux and Dynamics of Taku Glacier, Juneau Icefield, Alaska. – In: *WELSCH, W. M, LANG, M. and MILLER, M. M. (eds.):* Geodetic Activities, Juneau Icefield, Alaska, 1981-1996. Schriftenreihe des Studiengangs Vermessungswesen, Heft 50, Universität der Bundeswehr München, Neubiberg; p. 61-72

GLENN, J. W. [1955]: The Creep Polycristalline Ice. Proceedings of the Royal Society of London, Ser. A, Vol. 228, No. 1175, London; p. 519-538

KERSTING, N. [1986]: Determination of the Taku Glacier Movement, Juneau Icefield, Alaska, 1986. JIRP Survey Report, 1986. Juneau Icefield Research Program, Foundation for Glacier and Environmental Research, Juneau; Bundeswehr University Munich, Germany

MILLER, M. M. [1958]: Phenomena Associated with the Deformation of a Glacier Bore-Hole. Extrait des Comptes Rendus et Rapports – Assemblée Générale de Toronto 1957, Tome IV, Gentbrugge; p. 437-452

NOLAN, M., MOTKYA, R. J., ECHELMEYER, K. and TRABANT, D. C. [1995]: Ice-Thickness Measurements of Taku Glacier, Alaska, USA, and their Relevance to its Recent Behaviour. The Journal of Glaciology, Vol. 41, No. 139, Cambridge; p. 541-552

NYE, J. F. [1952]: The Mechanics of Glacier Flow. The Journal of Glaciology, Vol. 2, No. 12, Cambridge; p. 82-93

NYE, J. F. [1959]: A Method of Determining the Strain-Rate Tensor at the Surface of a Glacier. The Journal of Glaciology, Vol. 3, No. 25, Cambridge; p. 409–419

POULTER, T. C., ALLEN, C. F. and MILLER, S. W. [1950]: Seismic Measurements on the Taku Glacier. Sponsored by American Geographical Society, New York, as part of their Juneau Ice Field Research Project, summer of 1949. Stanford Research Institute Special Publication, Stanford; 12 pp.

SPRENKE, K. [1996]: University of Idaho, Department of Geology and Geological Engineering, Moscow, Idaho 83844-3022. Personal communication

WELSCH, W. M. [1997]: Description of Homogeneous Horizontal Strains and some Remarks to their Analysis. – In: *WELSCH, W. M, LANG, M. and MILLER, M. M. (eds.):* Geodetic Activities, Juneau Icefield, Alaska, 1981-1996. Schriftenreihe des Studiengangs Vermessungswesen, Heft 50, Universität der Bundeswehr München, Neubiberg; p. 73-90

Scott R. McGee

Using GPS to Determine Local Surface Mass Balance: A Case Study on the Taku Glacier, Alaska 1993-1995

1. Introduction

Mass balance studies are critically important to the interpretation and prediction of glacier behavior. While surface movement, surface and bed slope, ice temperature, and ice thickness are important factors contributing to the dynamics of a glacier system, a glacier's mass balance is the fundamental motive force affecting all other aspects of glacier advance, stagnation, or retreat. Methods to accurately determine mass balance are, therefore, of great interest to those studying the history of glacial advance and retreat, and to those who hope to predict future glacier behavior.

Traditionally, researchers have determined mass balance by comparing the mass gained by annual accumulation (c_a) against the mass lost to annual ablation (a_a). The result indicates the net volume (b_n) of mass, in water equivalent, remaining at the end of the balance year. Simply put, the glacier's mass is increased if the result is positive, decreased if it is negative, and remains the same if the result is zero. In practice, however, calculating the magnitude of b_n is complicated by various factors. Determining the exact end of the balance year, calculating the amount of winter ablation due to sublimation and drifting, measuring the depth of occasional summer accumulation, the frequent inability to collect winter accumulation data, accounting for internal accumulation, and the typically sparse sampling density, make mass balance calculations a complex process. It is beyond the scope of this paper top present a detailed description and analysis of the traditional methods of mass balance determination. For a discourse on these methods, the reader is referred to *SHARP [1988]* and *HAMBREY [1992]*, who provide an excellent introduction to the concepts of glacier budget and mass balance. For those readers wishing to gain a more complete understanding, *PATERSON [1981]* and *ANDREWS [1975]* delve deeper into the mechanics and mathematics of mass balance studies in general, while *PELTO and MILLER [1990]* focus primarily on the mass balance record of the Taku Glacier, Juneau Icefield, Alaska.

2. Traditional Mass Balance Studies on the Taku Glacier

With a total area of approximately 671 km^2, the Taku Glacier is the largest glacier of the Juneau Icefield. It also has the longest continuous record of mass balance research of any glacier in North America, with annual studies dating from 1946 to the present *[PELTO and MILLER, 1990]*. This research has focused primarily on determining the surface balance for the balance year, rather than investigating the actual winter accumulation and summer ablation balances.

Briefly, the traditional mass balance methods used on the Juneau Icefield, and the Taku Glacier is particular, rely on the examination of snow pit stratigraphy. At each of 19 fixed sites, a pit is dug through the current year's accumulation layer. Snow samples are taken every 15-20 cm from the surface to the bottom of the accumulation layer in order to determine mean density and water equivalent. The stratigraphy of the accumulation layer is also analyzed to determine the contribution of ice lenses and layers to the mean density. The mean water equivalent is then found for each pit; integration of all pit data determines the average accumulation, in water equivalent, for the current balance year. Ablation is measured at a series of stakes to determine the mean daily ablation, and the net balance (b_n) is then found by subtracting the ablation from accumulation.

While this method is conceptually simple, implementation of it in the field is somewhat more complex. Ideally, the net accumulation and ablation should be obtained at the end of the balance year, that point in time during late summer or early fall when accumulation begins to exceed ablation. Determining this exact date however, and carrying out the resultant measurements is often very difficult given the complex logistics involved in field studies. For this reason, measurements are usually obtained during the summer, forcing extrapolation of net accumulation and ablation to the end of the predicted balance year. This necessarily introduces some error into the final mass balance calculations. A more detailed discussion of the methodology used, and a discussion of the inherent errors, can be found in *PELTO and MILLER [1990]*.

3. Why use GPS?

There are many differences between the traditional mass balance methods used on the Taku Glacier and the recently implemented GPS method (Table 1). This is not to say that one method is desirable over or superior to the other, but rather that data gathered via GPS are an important supplement to traditional snow pit data. In other words, the use of GPS to determine mass balance is not meant to replace the need for traditional methods; used in conjunction with snow pit data, a more complete understanding of the dynamics of the Taku Glacier mass balance history is possible.

While the traditional method used on the Juneau Icefield is suitable for monitoring the long-term general mass balance trend of the entire Icefield, it can not identify local, small-scale trends. This is due primarily to the inability to sample a large number of points during the summer research period. The time consuming and labor intensive process of digging snow pits from which to sample dictates that only a few pits, relative to the local area of the glacier, be studied. This necessarily forces the resultant data and interpretations to be of a general nature. If however, we wish to examine mass balance trends in greater detail, for example on a localized cross-glacier transect, more snow pits must be laboriously dug and sampled.

GPS derived data, on the other hand, are ideally suited to localized mass balance studies. This method is significantly less time and labor intensive than the snow pit method – indeed, a great number of points can be surveyed via GPS in the time it takes to dig and sample one snow pit. This efficiency translates into a higher ratio of sample points/area than with the snow pit method. This then makes higher resolution mass balance studies possible. For example, suppose we want to examine the mass contribution of numerous tributary glaciers to the total glacier system. One way to do this is to establish a cross-glacier transect, down-

glacier from the convergence of all the tributaries, from which the surface elevation is measured at numerous points along the transect. Tracking the surface elevation changes along the transect can then provide a better understanding of the mass contributions of the various tributary glaciers. This type of study is not practical using the snow pit method because a large number of points along the transect must be sampled. The GPS method is perfectly suited to this type of research because it is significantly less time and labor intensive.

Table 1: Comparison of snot pit and GPS mass balance methods

Criterium	Snow pit method	GPS method
Basis	Balance year	Measurement year
Additional results	Depth of accumulation layer and detailed stratigraphy	Exact surface elevation and ablation rates
Ratio samples/area	Small	Large
Internal accumulation	Is taken into account	Can't be detected
Spatial distribution of balance data	Very general for entire glacier system	Detailed on a cross-glacier transect
Deficiency of the method	Extrapolation of accumulation/ablation to end of balance year	–
Ratio labor/result	High	Low

The greatest advantage of the GPS method is that it allows the surface elevation to be determined to a high degree. For example, monitoring the surface elevation change from year to year can provide significant insight into the effect of climate on mass balance. GPS obtains this data directly, without having to rely on photogrammetric or remote sensing methods, or extrapolation from other data. With a relative accuracy of about 5 cm, GPS provides very exactly heights which are able to discern annual surface elevation changes. The snow pit method provides a great deal of information about the accumulation layer and its stratigraphy, but it cannot determine the surface elevation, and thus the annual height change.

Allied with surface elevation determination, GPS provides the capability to directly determine the spatial distribution of accumulation and ablation. Accumulation layer depth, density, and stratigraphy are critically important, but many times it is equally important to know *where* the maximum and minimum accumulation and ablation occur. Because of the higher resolution of GPS derived data, small-scale changes in accumulation and ablation patterns can easily be detected, and this in turn can be linked to meteorological changes across various sectors of the Juneau Icefield.

Mass balance measurement methods can be grouped into two broad categories; those based on the balance year, and those based on the measurement year *[PATERSON, 1981]*. The balance year is defined as that point in time, in late summer or early fall, when the glacier surface elevation attains its yearly minimum, and before accumulation begins. It will differ from year to year, and from glacier to glacier. Additionally, higher elevations will usually experience accumulation while lower elevations are still undergoing ablation. These

factors make determining the exact time when accumulation at the higher elevations cancels ablation at the lower elevations very difficult. Past mass balance studies on the Taku Glacier have been based on the balance year, necessitating the need to extrapolate ablation data to the end of the predicted balance year *[PELTO and MILLER, 1990]*. Conversely, the measurement year is simply a time span of one year, beginning and ending on the same date every year. Accumulation and ablation data are then collected on the specified date, allowing direct comparison from year to year. There is no need to extrapolate the data to the end of the predicted balance year. This is the method used to collect mass balance data with GPS. In practice however, it is not possible to survey all movement profiles on the same date every year. Some level of adjustment must be done to normalize the data to the specified measurement year data. However, this usually is not a problem because the movement year date on the Icefield is set at July 25, and this date falls between the first survey and the resurvey of all profiles measured with GPS. The mean daily ablation rate during the survey period for each profile is therefore known, and is used to adjust the surface elevation to July 25. Since the measurement year date is constant from year to year, the adjustment is much more accurate than attempting to adjust to an uncertain, predicted balance year date which varies from year to year.

4. The Taku Profile IV Mass Balance Project

All surveys on the Juneau Icefield had, until 1991, been conducted using traditional terrestrial survey methods. Beginning in 1992, with significant equipment and personnel support from the Institute of Geodesy, Bundeswehr University Munich, Germany, GPS has been utilized in the collection of surface movement, ablation, and strain rates on the Taku Glacier. At about the same time, personal computers and three-dimensional analysis programs became sufficiently powerful to generate sophisticated three-dimensional surface models of geomorphic phenomena. In conjunction with GPS, this ability to visualize and analyze features in three dimensions, such as the glacier surface at Profile IV, has made it possible to gain a detailed view of spatial and temporal mass balance changes.

Given the combined capabilities of GPS, personal computers, and surface modeling software, a new study of Profile IV was initiated in 1993. This profile was chosen due to its close proximity to Camp 10 and ease of access. Profile IV also has the longest record of continuous study of all profiles on the Juneau Icefield. Glacier bore holes, seismic refraction, gravimetric, ice radar, surface movement, strain rate, and snow pit mass balance studies have been conducted here. The aim of this study was to monitor the local surface mass balance regime at this profile. By utilizing GPS to obtain precise surface elevations, and surface modeling to create and analyze three-dimensional models of the glacier surface, small-scale mass balance patterns could be identified and hopefully correlated with the larger scale mass balance data obtained via snow pits. This project was designed to answer the following questions:

- Is the Taku Glacier at Profile IV gaining or losing volume? Or is it in equilibrium?
- What is the magnitude of surface elevation change at each flag from year to year?
- Where is minimal/maximal ablation/accumulation occurring?

The answers of these questions could then be applied to other mass balance and glaciodynamic topics. For example, the flow through Profile IV is composed of the western accumulation area of the Juneau Icefield, and the highest elevation névés in the eastern

accumulation area. The flow of these two areas converge at a point some 6 km up-glacier from Profile IV, so that the western portion of the profile reflects the accumulation regime on the western, more maritime side of the Icefield. Likewise, the eastern third of the profile reflects accumulation on the eastern, more continental side of the Icefield. Monitoring the surface elevation changes across Profile IV may, when correlated with snow pit data, help to detect and quantify changes in maritime versus continental weather patterns.

As another example of the utility of the project, detection of kinematic waves may be possible. The down-glacier propagation of a kinematic wave induces a rise of the surface elevation at the crest of the wave. GPS derived elevation data would quantify the amplitude of the wave, while several cross-glacier profiles would determine the wavelength. The volume of ice within the wave could then be calculated using three-dimensional surface modeling.

In the past, Profile IV was comprised of 14-16 movement flags. Beginning in 1993, this was increased to 27 flags arranged in two parallel cross-glacier transects, separated by approximately 200 meters. Four additional flags were added in 1994, bringing the total to 31. The up-glacier transect is composed of 15 flags and the down-glacier transect contains 16 flags. The two lines are offset so as to form a series of triangles between them. This geometry defines an area of slightly more than 1 km^2. Extending from Camp 10 to the base of Shoehorn Peak, the profile is approximately 4.6 km long.

5. The GPS Mass Balance Method

In 1993 and 1994 the positions of the profile points were derived using rapid static GPS survey techniques with observation times of 10 minutes at least. The very positions were determined in 1995 using real time GPS. A minimum of five independent positions per point were recorded to assure a comparable accuracy. The original positions from 1993 could be reconstructed within 3 meters in 1994 and 1995 respectively.

The methods used to determine local mass balance were the same as those used for conducting standard GPS surface movement surveys. This entailed the establishment of the profile, taking readings at each flag, and performing the post-survey data analysis. The resultant data provided the easting, northing, and height coordinates of the points surveyed.

Determining the annual mass balance of Profile IV was accomplished by constructing yearly surface models which depict the surface morphology of the profile. Briefly, this was accomplished using a commercial computer program called *Surfer*, whereby a regularly spaced grid of easting, northing, and height coordinates was interpolated, using a linear kriging algorithm, from the irregularly spaced easting and northing coordinates of the surveyed flags in the profile. The interpolated surfaces are comprised of a series of rows and columns, the intersections of which are spatially located by X, Y, and Z coordinates (easting, northing, and height). Comparison of the annual surface models allowed the volume between the surfaces to be computed. Given the surface area of Profile IV and the volume between the surfaces, the mean change in surface height was then determined.

It is beyond the scope of this report to document the interpolation and gridding method in detail. Refer to *McGee [1994, 1995]* for a complete discussion of the application of surface modeling to local mass balance determination.

6. The Surface Mass Balance at Profile IV, 1993-1995

The goal of this study was to monitor, on an annual basis, the surface elevation changes across Profile IV to determine the magnitude of thickening of thinning, and to identify the spatial distribution of accumulation and ablation. Although the present study from 1993 to 1995 is too short to quantify long-term local mass balance trends at Profile IV, it does document the spatial and temporal mass changes since 1993. Continued monitoring of the profile will eventually produce a sufficient long-term record from which the prediction of future advance or retreat of the Taku Glacier may be made.

6.1 The measurement year July 25, 1993 to July 25, 1994

During the period of July 25, 1993 to July 25, 1994, the mean surface elevation of Profile IV increased 0.17 meter. This equates to an increase in firn mass throughout the area of the profile of 177,797 m^3, or approximately 97,788 m^3 water equivalent, based on a firn density of 0.55 g/cm^3. Accumulation on the northeast half of the profile (flag 1-15), at 0.21 meter, was greater than the accumulation on the southwest half (flags 16-27) which experienced an increase of 0.15 meter. Accumulation occurred at 23 of the 27 flags in the profile. The greatest accumulation of 0.65 m was seen at flag 26, while the greatest ablation was at flag 23, which was 0.31 m lower than the previous year. Fig. 1 shows a graph of the surface elevation change at each flag from July 25, 1993 to July 25, 1994.

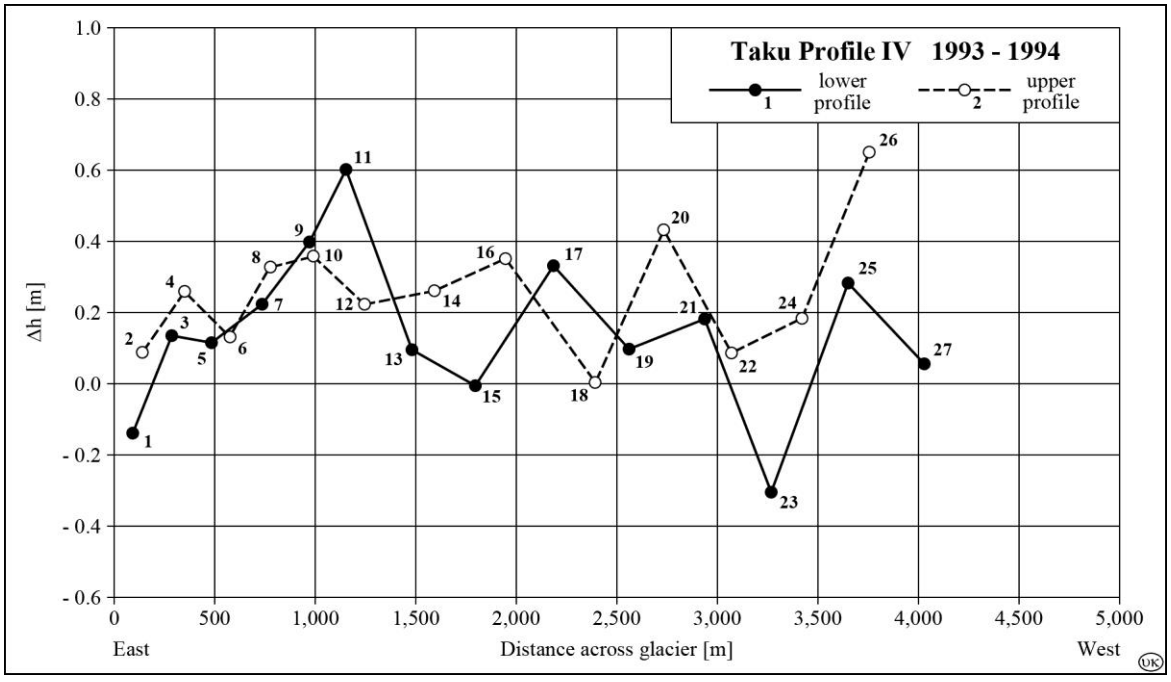

Fig. 1: Annual surface elevation change of Profile IV as measured with GPS at each flag (1993/94)

6.2 The measurement year July 25, 1994 to July 25, 1995

With a mean surface elevation decrease of 1.356 meters since July 25, 1994, the 1995 mass balance conditions at Profile IV mirrored the overall Juneau Icefield mass balance during the summer of 1995. This was a significant departure from the slight surface elevation increase from 1993 to 1994. In terms of mass, approximately 1,701,100 m^3 of firn, or 935,605 m^3 water equivalent was lost across the extent of the profile.

In contrast to the overall gain at all flags in 1994, the 1995 survey reveals a decrease of surface elevation at all flags. The surface at flag 1, on the northeast (flags 1-15) side of the profile nearest Camp 10, decreased 0.45 m, while flag 20 within the southwest (flags 16-31) half decreased 1.83 m. In 1994, the northeast half of the profile experienced more accumulation that the southwest half; interestingly enough, the magnitude of elevation decrease on the northeast half from 1994 to 1995, at 1.15 m, was less than that on the southwest half, which decreased 1.43 m. This suggests increased accumulation, decreased ablation, or some combination of both on the northeast half of the profile relative to the southwest half. Fig. 2 shows a graph of the surface elevation change at each flag from July 25, 1994 to July 25, 1995.

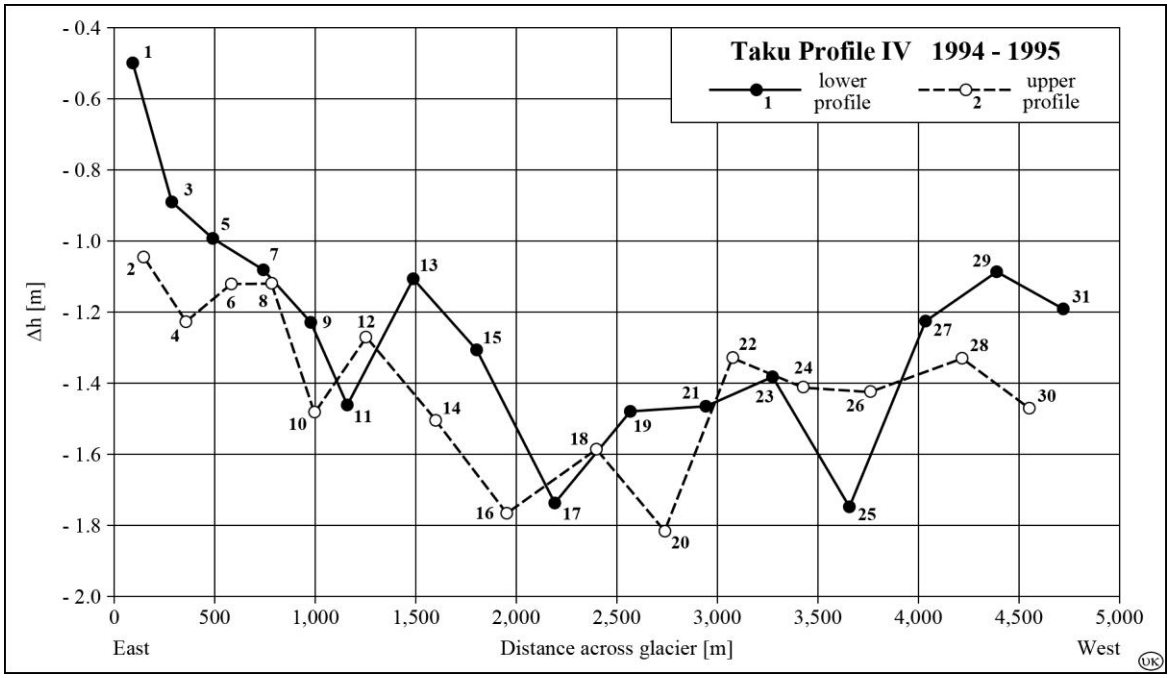

Fig. 2: Annual surface elevation change of Profile IV as measured with GPS at each flag (1994/95)

6.3 Cumulative Change from July 25, 1993 to July 25, 1995

The annual surface balance record reveals a slightly positive balance from 1993 to 1994, and a strongly negative balance from 1994 to 1995. The mean surface elevation increased 0.17 meter from July 25, 1993 to July 25, 1994, with a positive annual balance at 23 of 27 flags, while the surface elevation at flags 1, 15, 16, and 23 decreased. In contrast, all flags experienced a surface elevation decrease from 1994 to 1995 of 1.36 m. The cumulative 2 year balance period shows a net surface elevation decrease of 1.18 m since July 25, 1993. This equates to 1,211,960 m^3 of firn, or 666,780 m^3 water equivalent across the extent of the profile. The annual greater accumulation/least ablation trend seen on the northeast half of the profile is also reflected in the cumulative two year record. Since July 25, 1993, the northeast half of the profile has experienced a surface elevation decrease of 0.9 m, while the southwest half has decreased 1.34 m during the same time period. This interesting observation may give an indication of continental versus maritime atmospheric conditions, particularly if the trend continues into the near future; although if, and why, the trend would be observed across such a small well-defined boundary is unclear.

Fig. 3 shows the cumulative mass balance change of Profile IV from 1993 to 1995 (the exact numbers for the mentioned comparisons can be found in Appendix C).

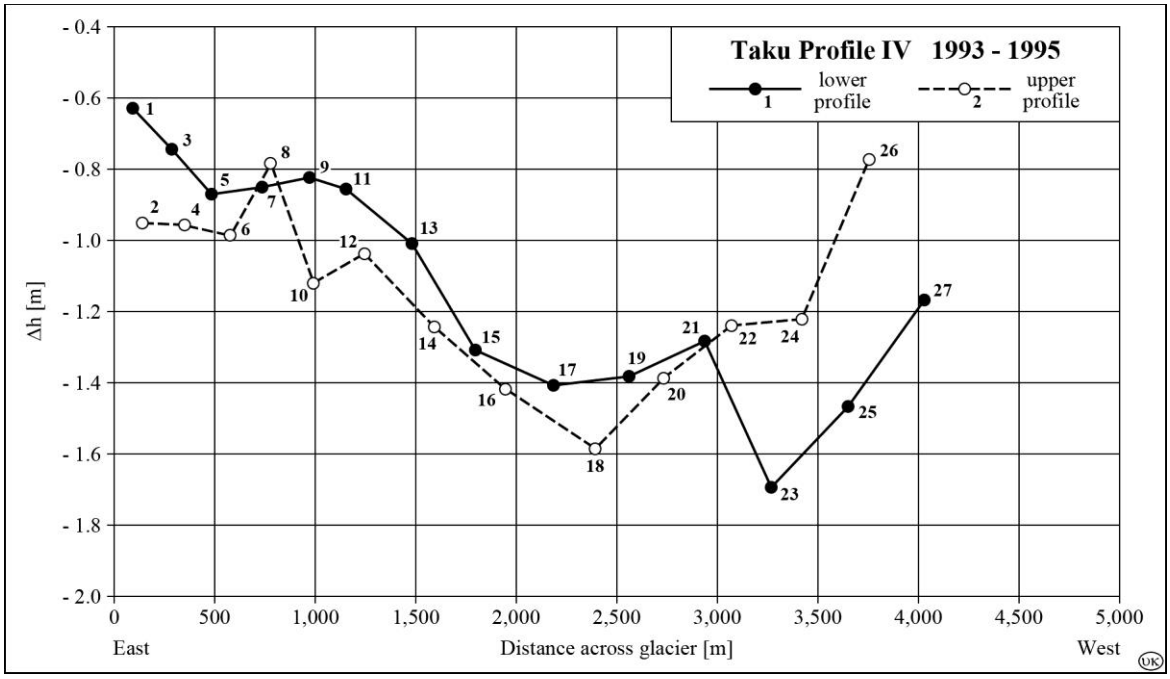

Fig. 3: Mean cumulative surface elevation change for Taku Profile IV from 1993 to 1995

7. Summary

This study has confirmed the utility and validity of a GPS-based approach to local surface mass balance determination. Used in conjunction with three-dimensional surface modeling, GPS-derived data allow a very detailed analysis and quantification of the spatial and temporal mass balance changes to be made. The local surface mass changes observed at Profile IV on the Taku Glacier since 1993 appear to indicate an overall loss of mass. It must be cautioned however, that this apparent loss of mass may be due to factors other than actual mass loss; for example, the movement of a kinematic wave through the profile could produce data with the observed characteristics. The current study of Profile IV is too limited to be able to determine the exact cause of surface elevation changes and mass loss or accumulation. For this kind of determination to be reliably made, a greater number of profiles in the vicinity of Profile IV, both up-glacier and down-glacier, would have to be established and monitored.

The current two year study reported here cannot yet reveal long-term mass balance trends at this profile. Continued annual monitoring of the profile utilizing GPS and surface modeling will prove invaluable in documenting the ever-changing annual mass balance and will eventually provide a long-term examination of the surface mass balance regime of Profile IV.

References

ANDREWS, J. T. [1975]: Glacial Systems: An Approach to Glaciers and their Environments. Environmental Systems Series. Duxbury Press, North Scituate, Mass.; 191 pp.

HAMBREY, M., ALEAN, J. [1992]: Glaciers. Cambridge University Press, Cambridge; 208 pp.

McGEE, S. R. [1994]: A Comparison of Methods for Determining the Mass Balance of a GPS Surveyed Movement Profile. JIRP Survey Rerport, 1994. Juneau Icefield Research Program, Foundation for Glacier and Environmental Research, Juneau

McGEE, S. R. (ed.) [1995]: Geodetic Activities during the 1994 Juneau Icefield Research Program Field Season. JIRP Survey Report, 1995. Juneau Icefield Research Program, Foundation for Glacier and Environmental Research, Juneau

PATERSON, W. S. B. [1981]: The Physics of Glaciers. 2nd Edition. Pergamon Press, Oxford; 380 pp.

PELTO, M. S. and MILLER, M. M. [1990]: Mass Balance of the Taku Glacier, Alaska from 1946 to 1986. Northwest Science, Vol. 64, No. 3, Washington; p. 121-130

SHARP, R. P. [1988]: Living Ice: Understanding Glaciers and Glaciation. Cambridge University Press, Cambridge; 225 pp.

Martin Lang

Geodetic Contributions to Glaciology – A Review of various JIRP Survey Perojects

Within the scope of the Juneau Icefield Research Program (JIRP) geodetic aspects play a crucial role: On the one hand, determination of glacier flow rates, glacial strainrates and changes in elevation of distinct points in connection with glaciological, meteorological and geophysical results contribute to a better understanding of the system „glacier" and its short- and long-term variations due to the changing environment. On the other hand determination of benchmark positions and mapping of different areas create a spatial frame for investigation in various sciences like geobotany, geology and entomology.

1. Networks

Before the use of GPS became a standard surveying technique, three main local networks with different datum definitions were set up on the Icefield: The Lemon network surrounding the Lemon Creek Glacier, the Taku network including the central part of the Taku Glacier around Camp 10 and the Gilkey network covering parts of the high plateau in the Camp 8/18 and the Gilkey Trench area. Whereas no plans existed to connect the Lemon network neither to the other local networks nor to the USGS network, it was an aim for many years to tie the Taku and Gilkey networks together. Despite considerable efforts the interconnection of both networks by means of terrestrial surveying techniques showed only unsatisfactory results *[WELSCH, 1984]*.

In 1994 the International Association of Geodesy (IAG) established the International GPS Service for Geodynamics (IGS) to provide the scientific community with GPS observations from an increasing number of permanently tracking GPS stations around the world, very precise orbits for all GPS satellites and other GPS derived products like earth rotation parameters *[BEUTLER et al., 1994]*. The positions of the IGS-stations are derived using observations of space measurement techniques such as VLBI (Very Long Baseline Interferometry), SLR (Satellite Laser Ranging) and GPS, to obtain a highly accurate representation of a worldwide reference coordinate system. This reference frame is called International Terrestrial Reference Frame (ITRF). The coordinates of the IGS-stations are updated yearly and named after the year, e. g. ITRF93. All IGS products are open to the public and can be downloaded from the data center managed by the IGS.

In order to connect the local Taku and Gilkey networks to the ITRF93 reference frame, in a first step GPS observations at two benchmarks (106 hours of observation on Scott at Camp 10 and 41 hours of observation on N1 at Camp 18) and simultaneous GPS observations of four IGS-stations (Alberthead in British Columbia, Fairbanks in Alaska, Penticton in British Columbia and Yellowknife in Northwest Territories; Fig. 1) were processed applying the Geotracer GPS software (version 2.0).

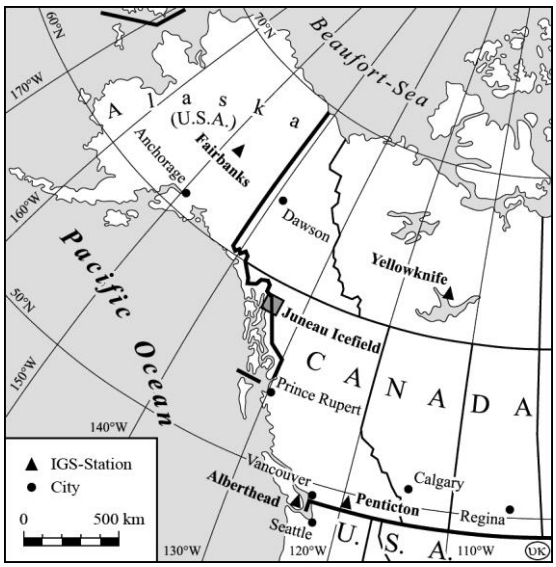

Fig. 1: Spatial distribution of the IGS–stations used

Table 1: Parameters of the projection set „JIRP“

Parameter	Value
Projection type	Transverse Mercator
False Easting	500,000 m
False Northing	0 m
Central meridian	134°00’00” W
Latitude of origin	0°00’00” N
Scale on central meridian	1 : 1
Zone width	3°00’00”

Table 2: Repeatability of the „IGS-baseline“ measurements

Latitude [mm]	Longitude [mm]	Height [mm]
36.5	46.4	68.4

After a preanalysis to exclude outliers, 36 baselines varying from some 970 km to 1,420 km were computed. Due to the baseline lengths precise ephemeres were used: for the elimination of ionospheric and tropospheric effects standard models were applied. The final 3d-coordinates determined by least squares adjustment were transformed to conformal coordinates using the JIRP projection (Table 1).

For the residuals of the adjustment the repeatability for each coordinate component was calculated as a measure of accuracy (Table 2).

In a second step all baselines between benchmarks observed with GPS in the period 1992-1995 were recomputed and connected to the ITRF93 by a 3d-adjustment with the points N1 and Scott as fixed points. Benchmark „Camp 9“ was added in 1996 by computing a single baseline from station Scott (5 hours of observation).

In a third step transformations of the local Taku and Gilkey networks to the ITRF93 reference frame were performed. These transformations were based on identical points, i.e. points which were observed by both terrestrial and satellite aided means.

Points „Taku D Lower“ and „SW Taku Lower“ revealed residuals in position of about 2 m in the local network. Using the old reports describing the set-up, observation and adjustment of that network *[WELSCH, 1984; HEISTER, 1985; BLACHNITZKY, 1987]* no reason could be found for these discrepancies. The final set of Transformation parameters for the Taku network was derived without the two doubtable points. The remaining residuals of the identical points show a mean point error of about 18 cm in position and about 6 cm in height. Compared to the accuracies achieved in the adjustment performed in 1984 *[WELSCH, 1984]*, this is a better result than could be expected. The scale factor of -188 ppm (= 18.8 cm per km) confirms a gross scale error in the local Taku network, but not the order of magnitude (-325 ppm) stated by *BLACHNITZKY [1987]*.

In 1986 part of the local Gilkey network was readjusted using additional measurements made in 1985 and 1986 *[KERSTING, 1986]* resulting in coordinate changes from some cen-

timeters up to some meters. After a first transformation point „FFGR 39“ showed a residual of about 1.5 m in height, and point „FFGR 12“ revealed residuals in position of about 1.5 m in the local network. Again no explanation for these disagreements could be found. The final set of transformation parameters was derived using only the position of point „FFGR 39“ and the height of point „FFGR 12“ in combination with all three components of points „FFGR 24“„FFGR 31“„FFGR 43“ and „N 1“. The remaining residuals of the identical points show a mean point error of about 4 cm in position and about 3 cm in height. That is in combination with the scale factor of -12 ppm (= -1.2 cm per km) an indicator for the very good accordance of both sets of coordinates and the height quality of the local Gilkey network determined in 1986.

All benchmarks on the Icefield determined with GPS are depicted on the map of page 141. A listing of conformal ITRF 93 coordinates of all benchmarks is displayed in appendix F.

All coordinates and the results shown in the appendices were transformed to the ITRF 93 datum. Note that due to the transformation to the ITRF 93 reference frame any results published in internal reports cannot be directly compared with the results contained in this book.

2. Height Comparisons

Ice thickness changes in different areas over larger timespans can be used to predict the glacier's behavior in future. A basic demand comparing heights over time is that they are measured at identical (x,y)-positions. It is time consuming to re-establish former positions by terrestrial survey techniques. Assuming a slope gradient of 1°, a position error of 3 m will lead to an error in height of 5 cm. In addition, trigonometrically determined heights are more or less influenced by great variations of the refractive index of the air over snow-covered surfaces *[ANGUS-LEPPAN, 1968]*. Thus, only rather large height changes can be regarded as significant. In contrast, real-time GPS-techniques show great advantages: The former (x,y)-position of a point can be found in no time, and the height determination is (within the range of some centimeters) hardly influenced by the refractivity of the atmosphere. The dominant factor is rather the roughness of the snow-covered surface (sun-cups!) which is a poor reference for precise height measurements. Using short baselines (< 10 km), the height accuracy can be seen as distance independent. Taking all factors into account, GPS derived heights can be estimated to be as accurate as about 5 cm.

Nevertheless, trigonometrical height determination was used in two cases. In 1989, a traverse across the Lemon Creek Glacier from Camp 17 to the saddle between Observation and Martin Peak was surveyed applying classical surveying methods. A resurvey was carried out four years later to quantify the obvious loss of volume. By mistake the line was re-established some 50 m up-glacier from the original position. Considering a gradient of 0.5°, the wrong position of the traverse creates an error in height of about 0.4 m. Due to the short distances the maximum influence of refraction will not exceed 0.2 m. Summing up these factors, a standard deviation of a height difference can be considered to be 0.5 m. The mean change of height in the central part of the glacier is some 5 m. This number is reduced to 2 m on both banks. These results are significant. A plot of both height profiles is given in Fig. 2.

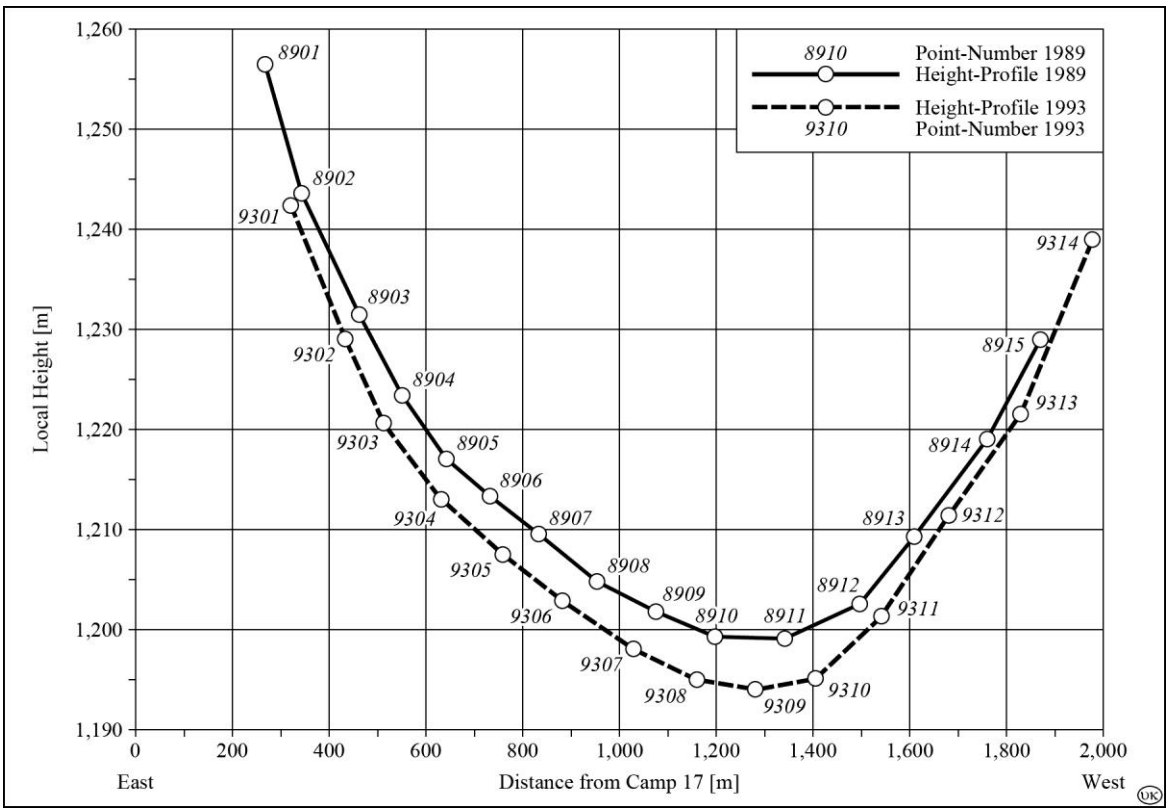

Fig. 2: Height comparison Lemon Creek Glacier 1989/1993

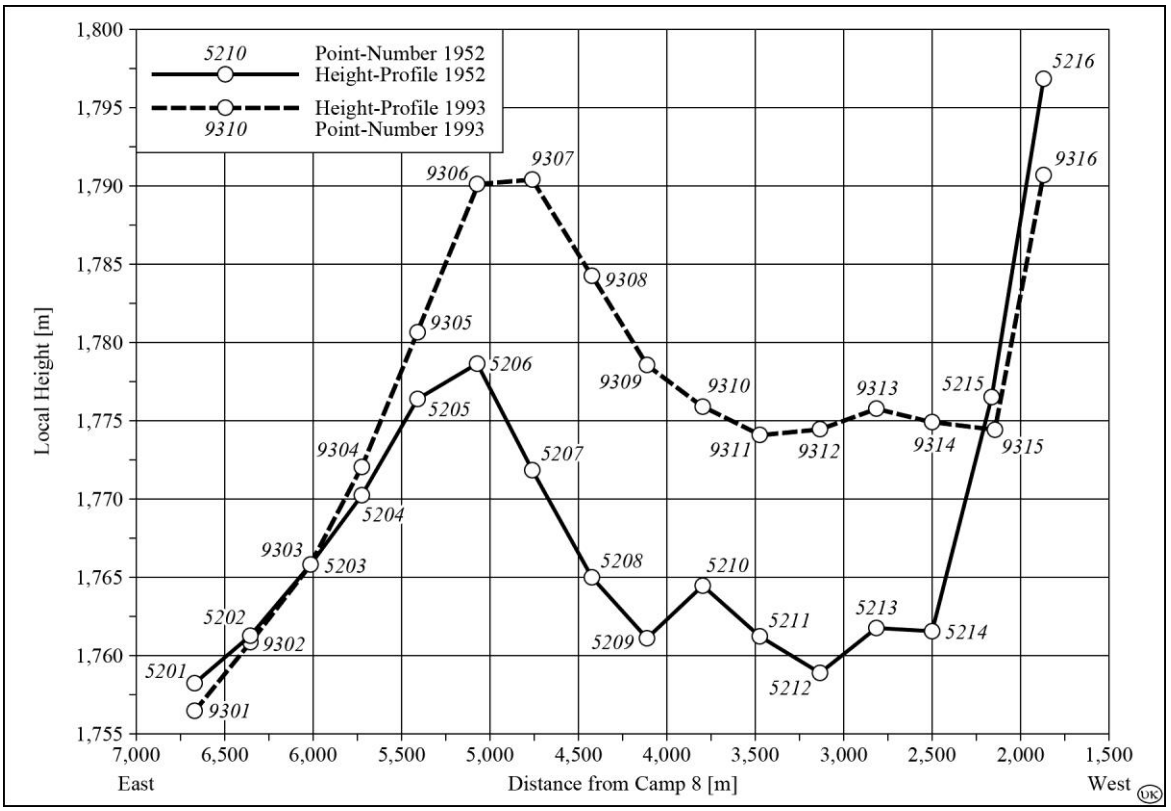

Fig. 3: Height comparison Upper Matthes Glacier 1952/1993

Locations of GPS survey points, Juneau Icefield

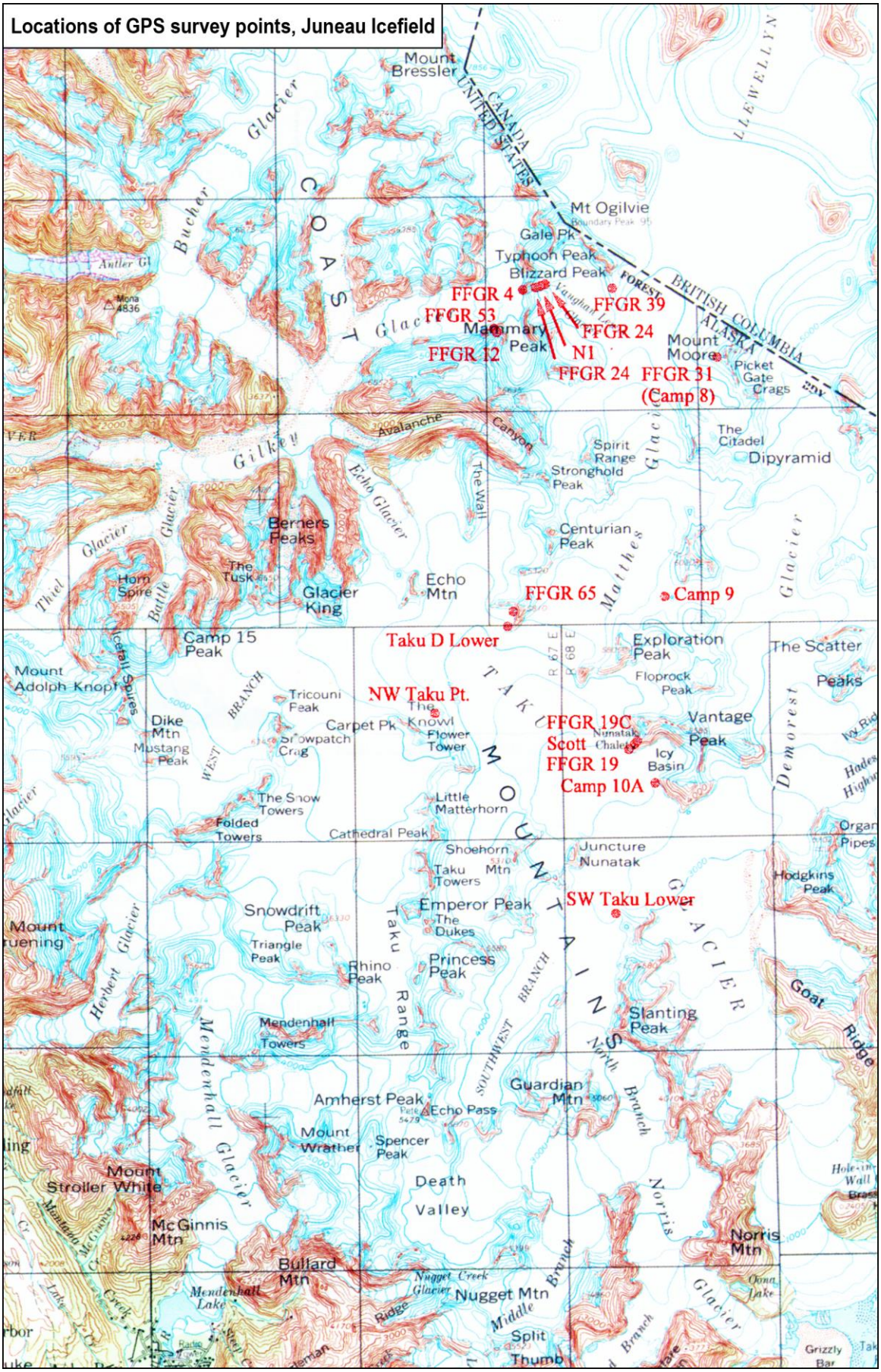

In 1952 , heights were determined on the High Plateau of the Taku Glacier system in distinct points creating a line from Camp 8 towards Camp 18. These heights are listed in *MILLER [1963]*, the positions, however, can be reconstructed only graphically from a map. The re-established positions of 1993 can be estimated to be identical within 50 m. The slope gradient in the area does not exceed 1° resulting in a maximum error in height of about 0.8 m. The influence of refraction for the original survey is estimated to be less than 0.5 m. Summarizing the standard deviation of a height difference is about 1 m. Thus the 10-15 m increase of the height of the glacier surface as determined in 1993 is significant. The result is supported by investigations by *NOLAN et al. [1995]* reporting similar numbers. A table of the results can be found in appendix C, a plot is shown in figure 3.

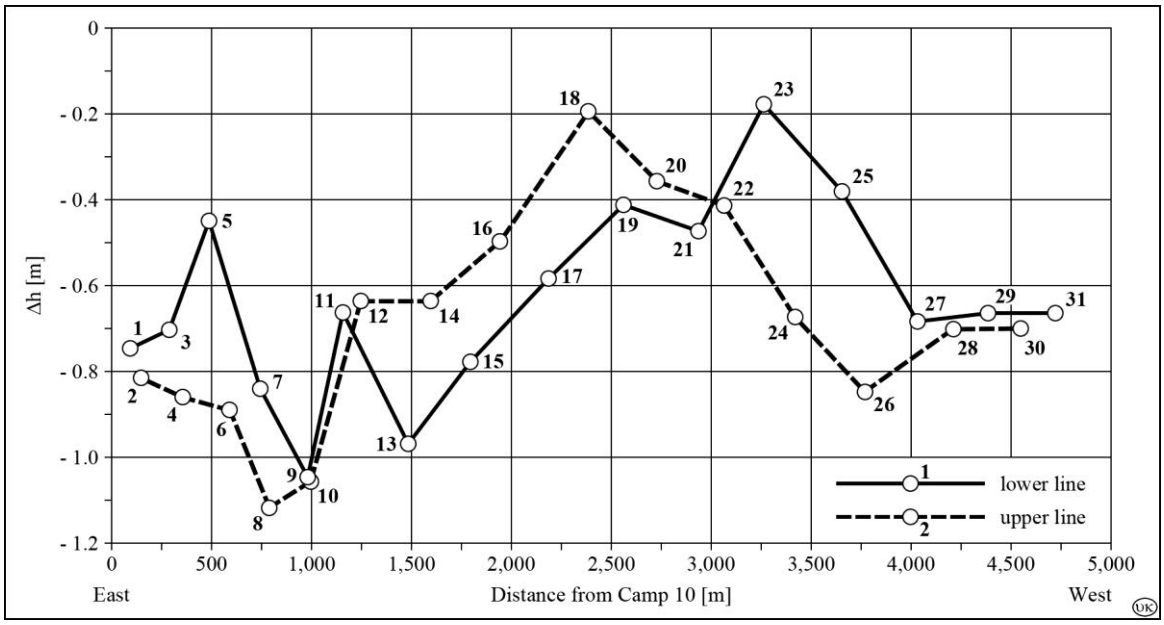

Fig. 4: Height comparison Profile IV 1995/1996

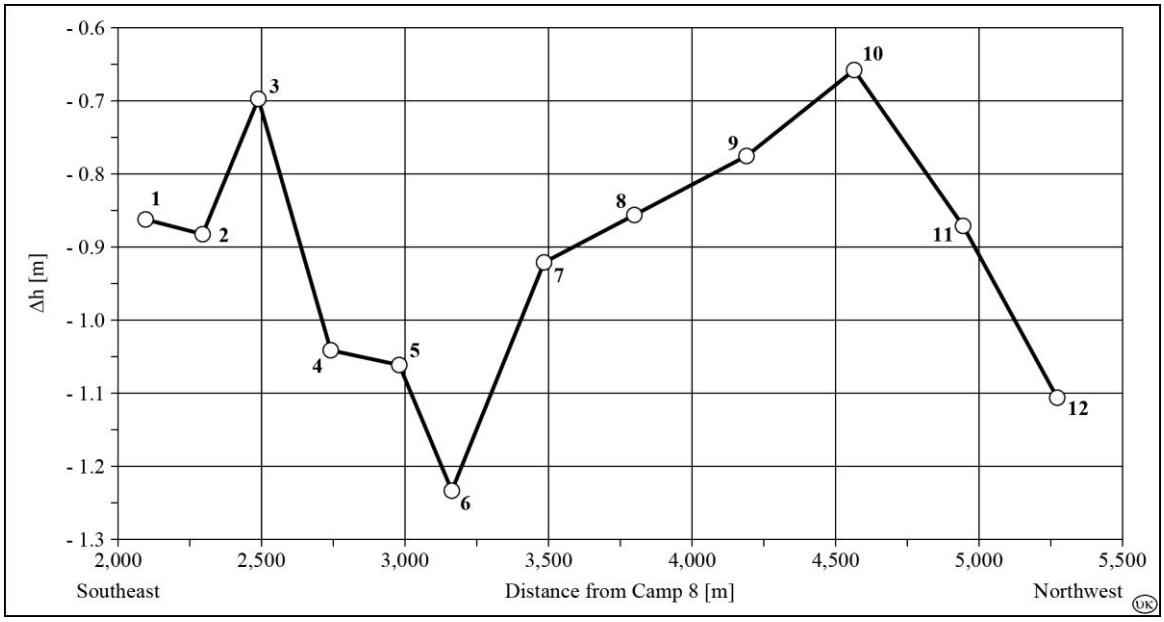

Fig. 5: Height comparison Profile VIII 1995/1996

Beginning in 1995, the former positions of Profiles IV, V, VIII und IX were re-established using real-time GPS. The data base is still insufficient for far-reaching conclusions, and the close vicinity of Profile IV and V, VIII and IX resp. do not allow a detailed discussion of elevation changes over the years. So far, the general trend is that the height changes do not depend on the location of the particular profiles. For example, Profile IV (elevation 1,100 m) depicts a loss of about 0.7 m between 1995 to 1996 (Fig. 4), Profile VIII (elevation 1,750 m) of about 0.9 m (Fig. 5). Although the patterns may be different, the bandwidth of the variations is similar. The long-term variations determined with GPS can be found in detail in appendix D.

Short-term variations of heights during one summer season have been called in previous JIRP-reports „ablation“. The term is misleading because the true ablation (height change due to the melting of snow or ice) was not separated from an apparent change of heights due to the downhill movement of a distinct point. Assuming a gradient of 1°, a daily movement of 0.5 m causes the height to change by 1 cm. Taking the influence of the slope into account the ablation rate at profiles in high elevations (e. g. Profile X – elevation 1,850 m) is about 2 cm/day, in elevations of some 1,100 m (e. g. Profile IV) about 4 cm/day, and in low elevations approximately 8 cm/day (e. g. Profile II – elevation 800 m).

Over the years, those numbers proved to be similar and consistent. It has, however, to be considered, that the high elevation profiles can experience snowfall in individual summers which falsifies the ablation rate measurements. GPS derived short-term height changes are listed in appendix C.

3. Continuous Movement Monitoring

The movement of glaciers is said to be time dependent *[PATERSON, 1981]*. It varies between day and night or summer and winter. The variations in velocity my exceed a factor of two within a few hours. To verify this theory, a 48 hours survey on the Taku Glacier was initiated in 1995. A permanently tracking GPS receiver was established on a platform near flag 15 on Profile IV, another simultaneously observing one on station Scott at Camp 10.

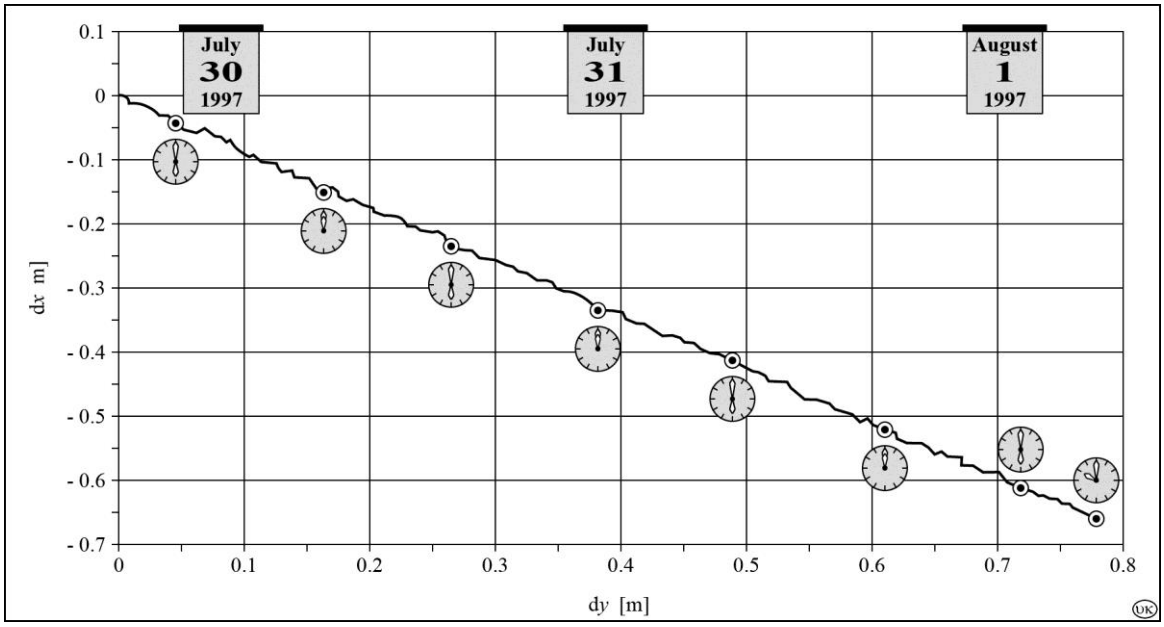

Fig. 6: Movement of Taku Glacier near flag 15 of Profile IV

The baseline length between the two receivers is 1.5 km. In the vicinity of flag 15 the Taku Glacier reaches a depth of about 1.300 m *[SPRENKE et al., 1995, 1996]*. 43 consecutive hours of observation could be used for the analysis. The positions of the moving receiver are depicted in Fig. 6. They show despite Paterson's statement a more or less steady movement.

Consequently, a linear regression analysis was applied. The residuals are shown in Fig. 7. They seem to reveal a cycle length of about 24 hours. This could indicate a day-night variation of the velocity. However, it seems implausible that a glacier as extended as the Taku Glacier (60 km long, 3 to 6 km wide *[MILLER, 1963]* and on average some 900 m

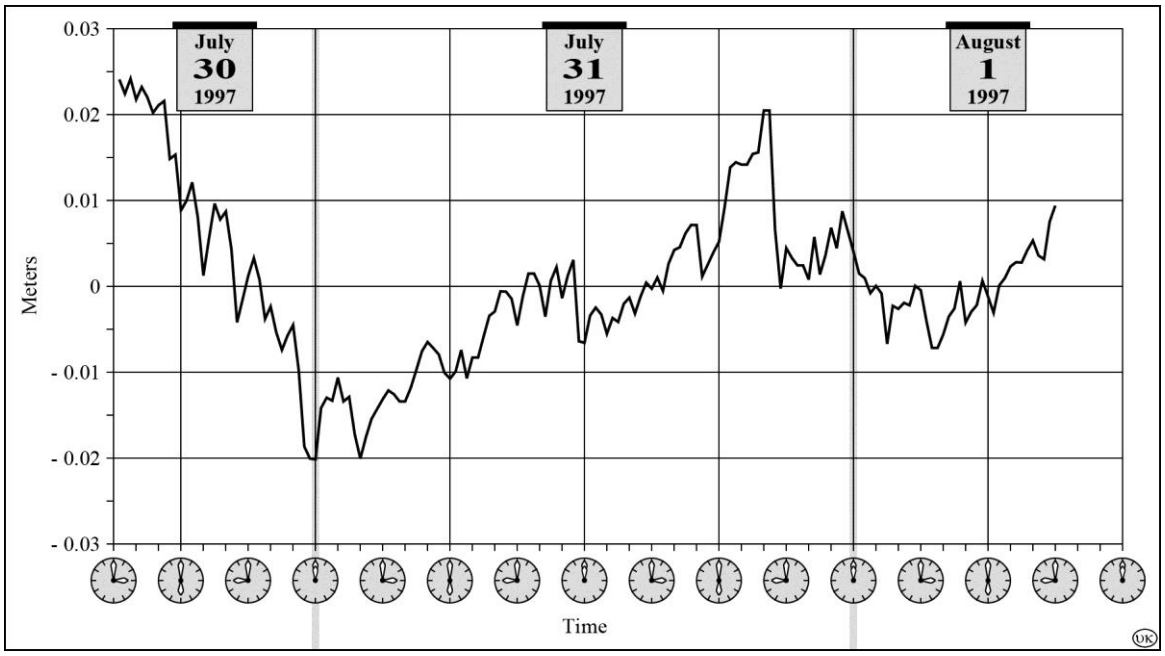

Fig. 7: Residuals of regression analysis

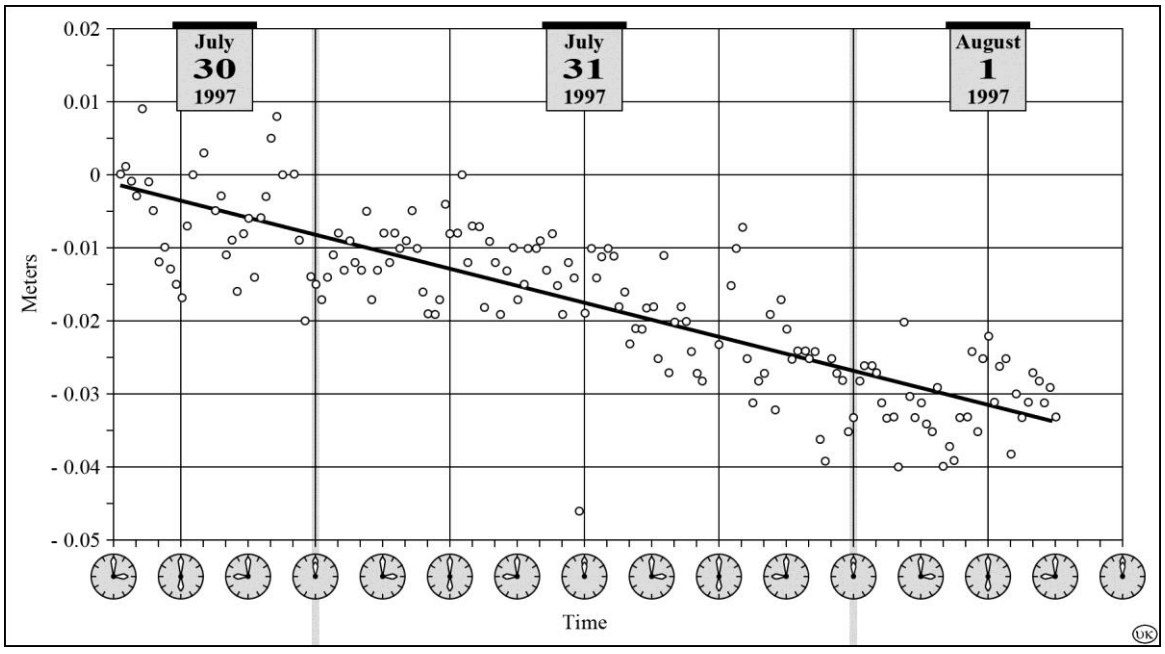

Fig. 8: Height movement of Taku Glacier near flag 15

deep *[NOLAN et al., 1995]* shows short-term responses to the daily variations of e. g. the temperature. A more reliable statement could be given if the length of the time series would be at least three times the length of the anticipated cycle.

A deviation from a linear movement can also not be seen for the height observations. Fig. 8 shows the change of the height due to the downhill movement of the receiver's platform and a best fit line. Referring to a daily horizontal movement of 60 cm/day, the vertical change of -1.8 cm/day can be used as a measure for the glaciers gradient (= 1.7°) in that area.

References

ANGUS-LEPPAN, P. V. [1968]: An Experimental Determination of Refraction over an Icefield. Unisurv Report No. 10, University of New South Wales, Department of Surveying, Kensington, N.S.W.

BEUTLER, G., MUELLER, I. I., NEILAN, R. E. and WEBER, R. [1994]: IGS – Der internationale GPS-Dienst für Geodynamik. Zeitschrift für Vermessungswesen, Vol. 119, No. 5, Stuttgart; p. 221-232

BLACHNITZKY, K. [1987]: Report on the Geodetic Activities during the 1987 Juneau Icefield Research Program Field Season. JIRP Survey Report, 1987. Juneau Icefield Research Program, Foundation for Glacial and Environmental Research, Juneau; Bundeswehr University Munich, Germany

HEISTER, H. [1985]: Adjustment of Network at Camp 10, Juneau Icefield, Alaska. JIRP Survey Report, 1985. Juneau Icefield Research Program, Foundation for Glacial and Environmental Research, Juneau; Bundeswehr University Munich, Germany

KERSTING, N. [1986]: Densification of the Gilkey Network 1985 and 1986. JIRP Survey Report, 1986. Juneau Icefield Research Program, Foundation for Glacial and Environmental Research, Juneau; Bundeswehr University Munich, Germany

MILLER, M. M. [1963]: Taku Glacier Evaluation Study. Conducted for the State of Alaska, Department of Highways, in Cooperation with the U.S. Department of Commerce, Bureau of Public Roads; n. p.

NOLAN, M., MOTYKA, R., ECHELMEYER, K. and TRABANT, D. [1995]: Ice-Thickness Measurements of Taku Glacier, Alaska, USA and their Relevance to its Recent Behavior. The Journal of Glaciology, Vol. 41, No. 139, Cambridge; p. 541-553

PATERSON, W. S. B. [1981]: The Physics of Glaciers. 2nd Edition. Pergamon Press, Oxford; 380 pp.

SPRENKE, K., MILLER, M. M., BENEDICT, T. and ADEMA, G. [1995]: Glacier Depth Profiles on the Juneau Icefield, Alaska, Using Seismic Methods. The Journal of Glaciology, Cambridge *(in review)*

SPRENKE, K., MILLER, M. M., BENEDICT, T., GILBERT, G., ADEMA, G., AURBACH, D. and PRUIS, M. [1996]: Geophysical Depth Surveys on the Juneau Icefield, Alaska-Canada – 1993-1995. Journal of Geophysical Research, Washington, D. C. *(in review)*

WELSCH, W. M. [1984]: Adjustment of Taku and Gilkey Networks, Juneau Icefield, Alaska. JIRP Survey Report, 1984. Juneau Icefield Research Program, Foundation for Glacial and Environmental Research, Juneau; Bundeswehr University Munich, Germany

Photo H. Heister, 1990

Camp 17

Photo H. Heister, 1985

Camp 18

Photo W. Welsch, 1981

Taku Glacier towards terminus from Camp 10

Photo W. Welsch, 1996

Kitchen area, Camp 10

Photo M. Lang, 1989

Opening crevasses, Taku Glacier near Camp 10

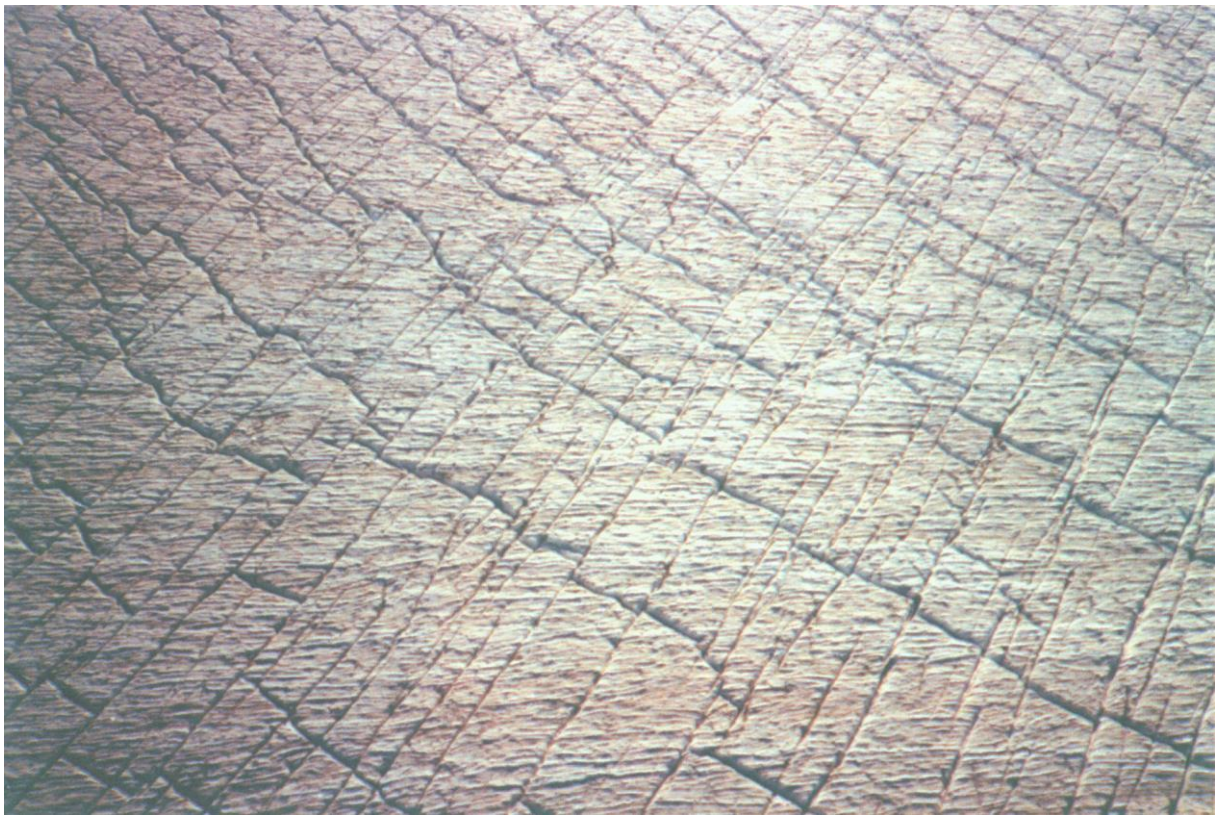

Photo M. Lang, 1989

Crevasse pattern, Taku Glacier near Goat Ridge

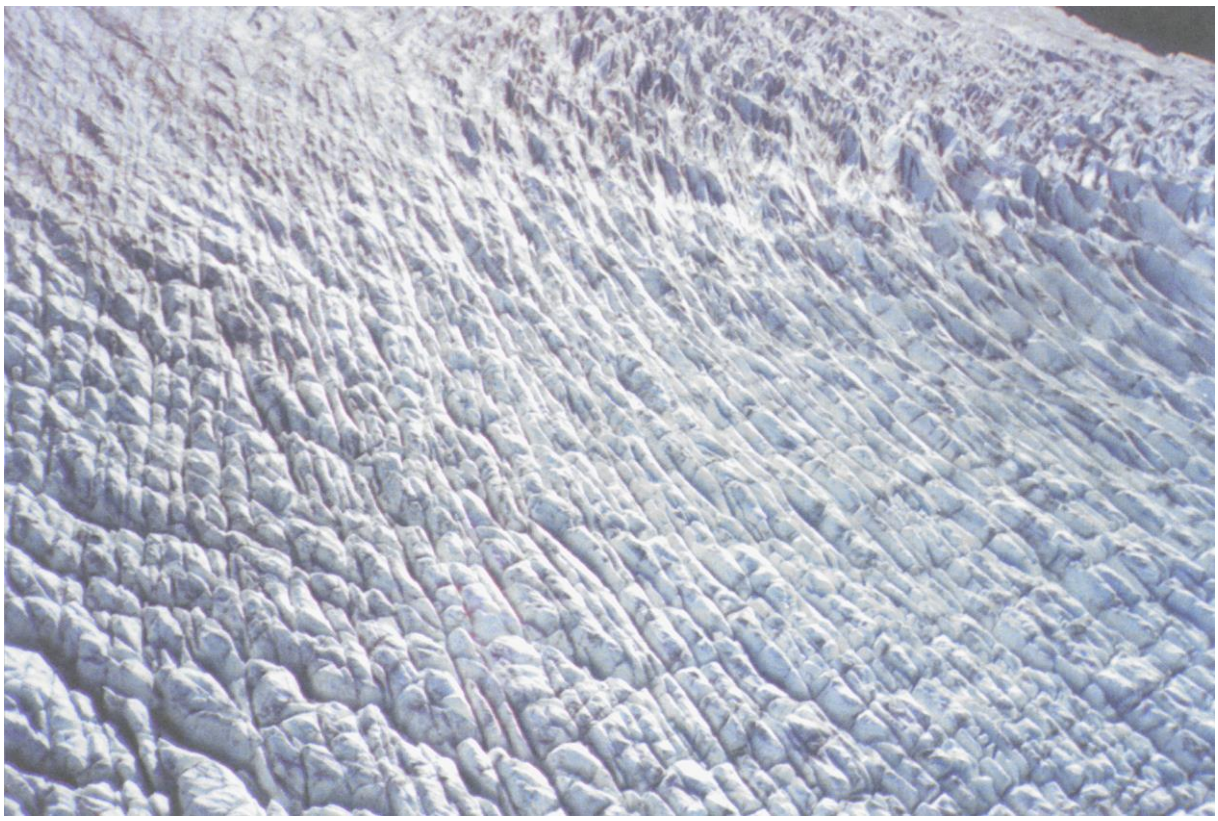

Photo M. Lang, 1989

Taku Glacier moving around Brassiere Hills

Photo M. Lang, 1989

Scattered ice, Taku Glacier near terminus

Photo M. Lang, 1995

Taku Glacier Southwest Branch from Camp 10

Photo H. Heister, 1985

Taku Glacier Northwest Branch from Taku Northwest Point

Photo W. Welsch, 1996

Taku Range with Taku Towers from Camp 10

Photo W. Welsch 1996

Sunset, Taku Glacier towards Glacier King from Camp 10

Photo M. Lang, 1991

Camp 18 and Gilkey Glacier Trench

Photo M. Lang, 1993

Vaughan-Lewis Icefall

Photo M. Lang, 1991

View from Camp 19 across the Gilkey Glacier Trench towards Mt. Bressler

Photo M. Lang, 1993

Unnamed Glacier (left), Vaughan-Lewis Glacier (center)
and Gilkey Glacier (right) moving down the Gilkey Glacier Trench

Photo W. Welsch, 1996

Starting a Thiokol trip to supply Camp 18

Photo M. Lang, 1995

Trailparty on the Llewellyn Glacier

Hermann Rentsch

Terrestrial Photogrammetry on the Juneau Icefield

Terrestrial photogrammetry was applied for some projects on the Juneau Icefield using either stereoscopic images taken with the so-called *„Technical Equipment Finsterwalder“*, i.e. the metric camera TAF, or single-images taken with an automatic non-metric Contax camera.

The activities concentrated on the Upper Lemon Glacier and on the Vaughan-Lewis and Gilkey Glacier area. The photogrammetric measurements aimed at

- recording of glacier surfaces by Digital Terrain Models (DTM) as a basis for manifold applications and investigations,
- derivation of flow velocities of glacier surfaces,
- determination of time dependent variations of glacier surface details,
- plotting of the structure of glacier surfaces.

The following table reports on the activities:

Table 1: Photogrammetric activities 1982-1990

Methodology	Area	Time	Application
Stereoscopic Image Photogrammetry (TAF)	Vaughan-Lewis Icefall	29.07.1982 13.08.1982 15.08.1982 19.08.1982	Surface Flow DTM Velocity
		15.08.1985	DTM
		01.08.1990 08.08.1990 11.08.1990	Surface Flow Velocity and DTM
	Vaughan-Lewis and Gilkey Glacier	11.08.1990	Crevasse Pasttern and DTM
	Lake Linda Upper Lemon	17.07.1985 27.08.1985	DTM DTM
Single-Image Photogrammetry (automatic)	Lake Linda	05.07.1985 through 02.08.1985 daily 2 photos	Variation of the Water Level of Lake Linda

DTMs were generated for the Vaughan-Lewis Icefall in 1982. Perspective views of these DTMs as wire frame models are attractive graphic representations. In the article *„Digital Terrain Models as a Tool for Glacier Studiers“ [RENTSCH et al., 1997]* the generation and the application of DTMs are described with respect to the Vaughan-Lewis Icefall.

Lake Linda and Lake Lynn are water reservoirs in the firn layer of Lemon Creek Glacier. They are interconnected by an underground drainage system. One every year they drain spontaneously. DTMs for the Lake Linda area were constructed in 1985. Repeated obser-

vations at different points of time were used to calculate the loss of water which amounts to 79,300 m^3 for Lake Linda and to 2,400 m^3 for Lake Lynn. The wire frame models and contour maps are presented in the following figures.

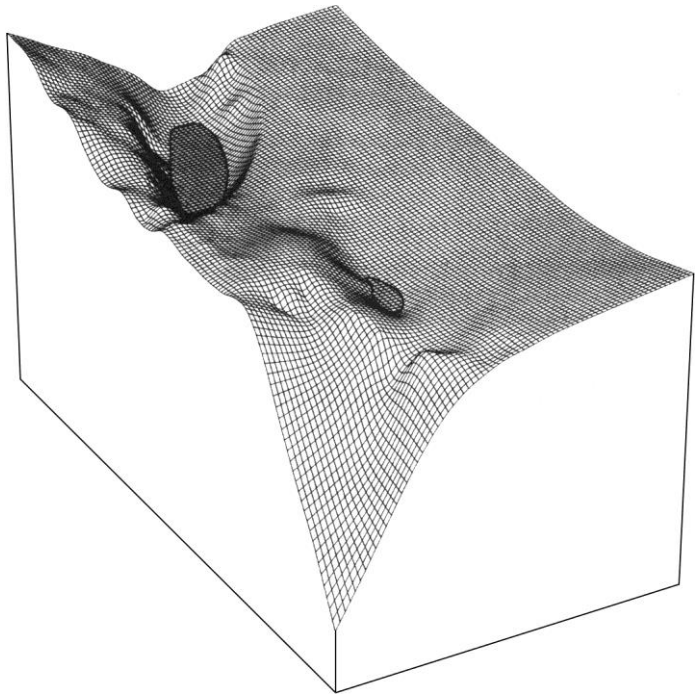

Fig. 1: DTM – Lake Linda and Lake Lynn, July 05, 1985

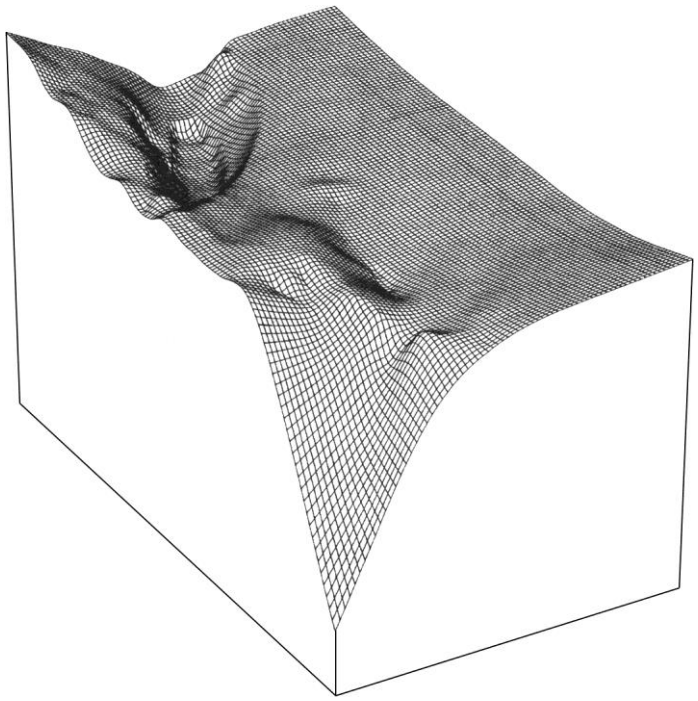

Fig. 2: DTM – Lake Linda and Lake Lynn, August 02, 1985

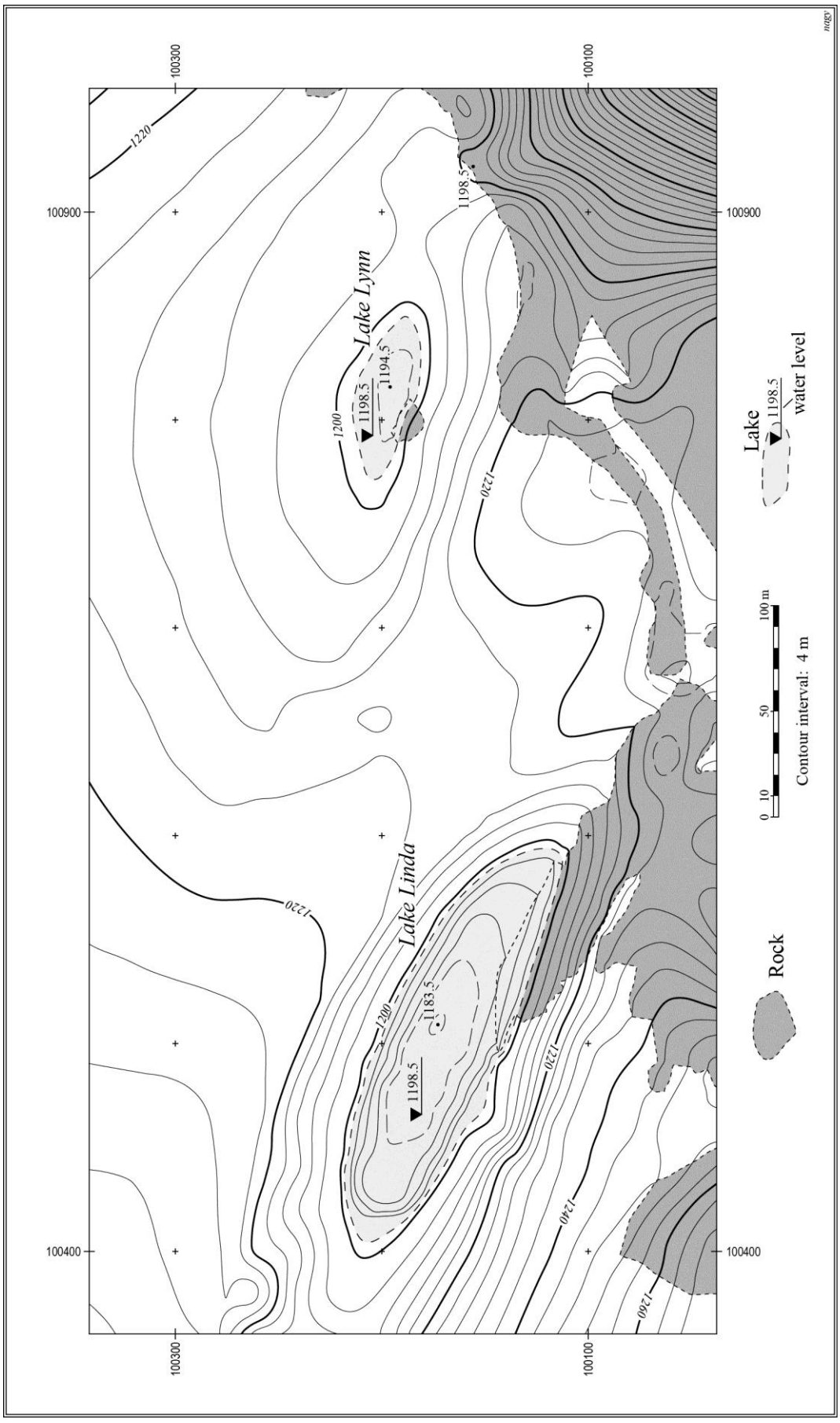

Fig. 3: Linda Linda and Lake Lynn: July 05, 1985 - August 02, 1985

Reference

RENTSCH, H., WELSCH, W. M., HEIPKE, C. and MILLER, M. M. [1997]: Digital Terrain Models as a Tool for Glacier Studies. – In: *WELSCH, W. M., LANG, M. and MILLER, M. M. (eds.):* Geodetic Activities, Juneau Icefield, Alaska, 1981-1996. Schriftenreihe des Studiengangs Vermessungswesen, Heft 50, Universität der Bundeswehr München, Neubiberg; p. 171-184

Hermann Rentsch, Walter M. Welsch
Christian Heipke and Maynard M. Miller

Digital Terrain Models as a Tool for Glacier Studies [1)]

1. Introduction

The generation of digital terrain models (DTM) at subsequent epochs is a way of studying glaciers and time-dependent geometrical properties of glaciers, such as the rate and direction of surface movements, the rate of distortions, or the mass balance *[PEIPE et al., 1978]*. The basic idea of a terrain model is to replace the real glacier surface by a model that can be taken back to an institute's laboratory in order to study the phenomena in question without the obstacles and aggravations that Nature provides to the field worker.

In the following, first the procedure of generating a DTM is reviewed. Next a short description of the investigated region of the Juneau Icefield in Alaska is given. Then the derivation of a DTM of the Vaughan-Lewis Icefall from photogrammetric image data is explained and the glacier-flow velocity at discrete points, distributed over the whole surface, is derived. Finally, some digital image-processing techniques are applied for the visualization of the DTM, and the way of integrating these raster data into a geographical information system (GIS) is pinted out.

The aim is to show the kind of digital products available today as an aid to the interactive interpretation of glacier surfaces. It is, however, not the intention to discuss in detail the glaciological phenomena encountered during the investigation of the icefall.

2. Data Acquisition and Evaluation of a Digital Terrain Model

Digital terrain models (DTM) were introduced about 30 years ago in the realm of road construction *[MILLER and LAFLAMME, 1958]*. Since then, they have become more and more important to many fields of scientific and practical application. A DTM consists of a network in the XY-plane of the object space with Z-values at every node, and also includes rules for the interpolation of Z-values at arbitrary XY-locations. The network data structure may be a raster, a quad tree, a triangular irregular network (TIN), or any combination of the three. Thus, a DTM allows the geometrical description of the entire surface of the object in question by three-dimensional coordinates.

A DTM is generated from height information of the object surface such as

- terrestrial measurements, e. g. tacheametry,
- digitized analogous information like contour maps,
- evaluation of photogrammetric stereo-models.

Photogrammetry is one of the most common procedures for DTM data acquisition. Its main advantage for this application is the possibility of a non-contact measurement,

[1)] Journal of Glaciology, Vol. 36, No. 124, Cambridge *[1990]*; p. 273-278

enabling a survey of inaccessible regions. Photogrammetry has been a tool of Alpine studies for more than 90 years *[FINSTERWALDER, 1897]*.

Photogrammetric data acquisition includes *[EBNER and REINHARDT, 1984]*

- single points,
- points of significant geomorphological features,
- points along contour lines,
- raster points in a grid.

The coordinates of the grid points serve as the basic reference information which is supplemented and completed by non-grid information such as the coordinates of single points and points of geomorphological features relevant to the shaping of the terrain (break lines, skeletal lines, water courses, etc.). If this non-grid information is available, the general grid structure can be combined with local triangulation networks (TIN) within individual overlays.

The number of grid points, which have to be measured, and hence the measurement time, can be considerably reduced following the concept of progressive sampling *[MAKAROVIC, 1973]*.

This method begins with the measurement of a basic grid. The terrain curvature is then analyzed via the second-height differences of adjacent grid points. If they exceed an appropriately chosen threshold, the basic grid is locally densified to half the original mesh size. This procedure is repeated until the predetermined smallest grid is reached. In this way, the final grid density automatically matches the shape of the terrain. Operational software for this measurement procedure is available *[EBNER and REINHARDT, 1984]*. Fig. 1 shows an example of a sub-area with grid meshes of different size, a crossing break line, and the associated local triangulation networks.

For these measurements, also referred to as primary DTM data, a DTM can be generated by constructing an interpolation surface based on finite elements, taking into account the non-grid information. This surface can be stabilized by introducing constraints for its inclination and curvature. This concept has been achieved with bi-linear finite elements in the program package HIFI-88 (height interpolation by finite elements; *[EBNER et al., 1988]*).

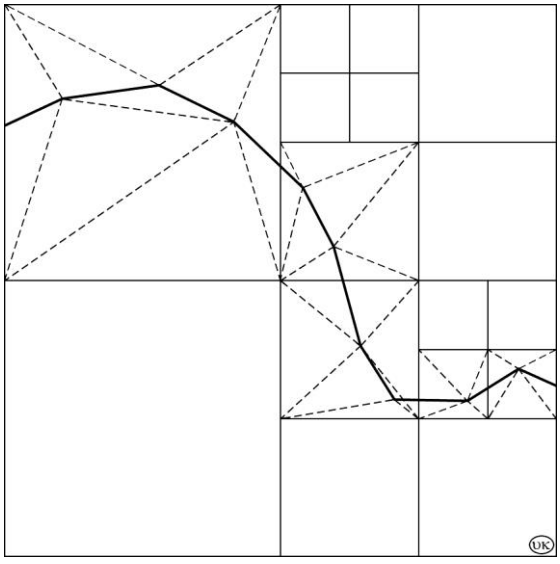

From this DTM, various products can be derived. Typical examples are

- contour-line maps with optional height intervals,
- terrain profiles, e.g. for the production of orthophotos,
- perspective views and visibility maps,
- slope and aspect information,
- changes in elevation (if DTM from at least two epochs are available).

Fig. 1:
General DTM data structure combining a quad tree with local triangular networks where non-grid information is available *[EBNER et al., 1988]*

Further products can be derived from the DTM by use of digital image-processing techniques. However, before these products are shown in greater detail, the generation of DTM for the glacier-velocity study of Vaughan-Lewis Icefall, Juneau Icefield, Alaska, will be demonstrated.

3. Vaughan-Lewis Icefall, Juneau Icefield, Alaska

Vaughan-Lewis Icefall (lat. 58°49'N, long. 134°17'W) is part of the Juneau Icefield in the Alaska-British Columbia Boundary Range north-east of Juneau, Alaska. It is fed from the same névé at 1,600-1,800 m above sea-level as Taku and Llewellyn Glaciers which are the primary drainages of the approximately 4,000 km^2 area of Juneau Icefield.

Vaughan-Lewis Glacier is categorized glaciothermally as being temperate and is considered to be a climatologically controlled, normal discharge-type glacier. Its source area lies at a mean altitude of 1,680 m on the southern flank of Blizzard Range near Mount Ogilvie (Fig. 2). The ice flows westward off the névé plateau into Gilkey Trench, descending about 500 m in a spectacular ice cascade – the famous Vaughan-Lewis Icefall (p. 175) – in a planar distance of only 800 m. At the base of the icefall lies a series of extraordinary wave bulges, which are arcuate and convex down-glacier, and have an amplitude of up to 25 m and a wavelength of about 150 m. These wave bulges (also referred to as wave ogives) have been the subject of extensive studies (e. g. *KITTREDGE [1964], FREERS [1965], MILLER et al. [1968], COYES [1978]*).

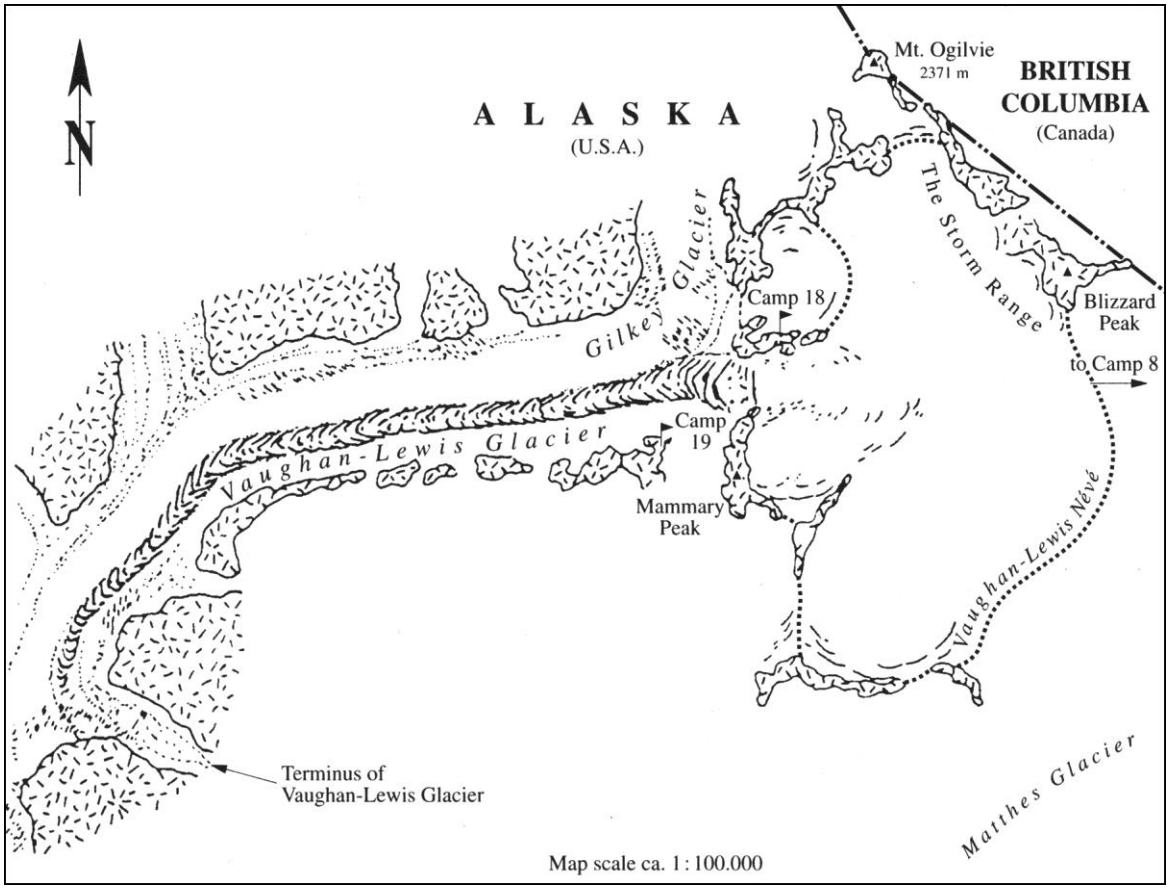

Fig. 2: The Lewis-Gilkey Glacier complex *[COYES, 1978]*

Velocity measurements have only been carried out at the lower part of the icefall which is not too difficult and dangerous for terrestrial measurements. Vaughan-Lewis Icefall is, therefore, a typical example for the application of terrestrial photogrammetry.

4. The DTM of Vaughan-Lewis Icefall

The primary data for the DTM were recorded from terrestrial photogrammetric stereo models *[RENTSCH, 1997]*. All measurements refer to a local coordinate system, defined by geodetic control points and camera positions (Fig. 3). For the photogrammetric evaluation, the analytical plotter ZEISS PLANICOMP C100 at the Institute of Photogrammetry of the Technical University Munich, has been made available.

Along 5 m contour lines, 11,500 points have been recorded. In addition, 280 points along the boundary between the ice-covered surface and the surrounding bedrock were measured and introduced as break-line information. From these data, a regular grid DTM was interpolated using the program package HIFI-88. With regard to the distribution of the primary DTM data, a grid width of 20 m was selected. The generated DTM shows an accuracy of 2.1 m compared to the actual measurements; this is caused by the surface approximation with the grid elements and the smoothing effect of the bilinear interpolation, especially within the areas of fractured ice. Besides the essential advantages concerning data processing and storage, the regular grid DTM was necessary as a basic data structure for the DTM visualization.

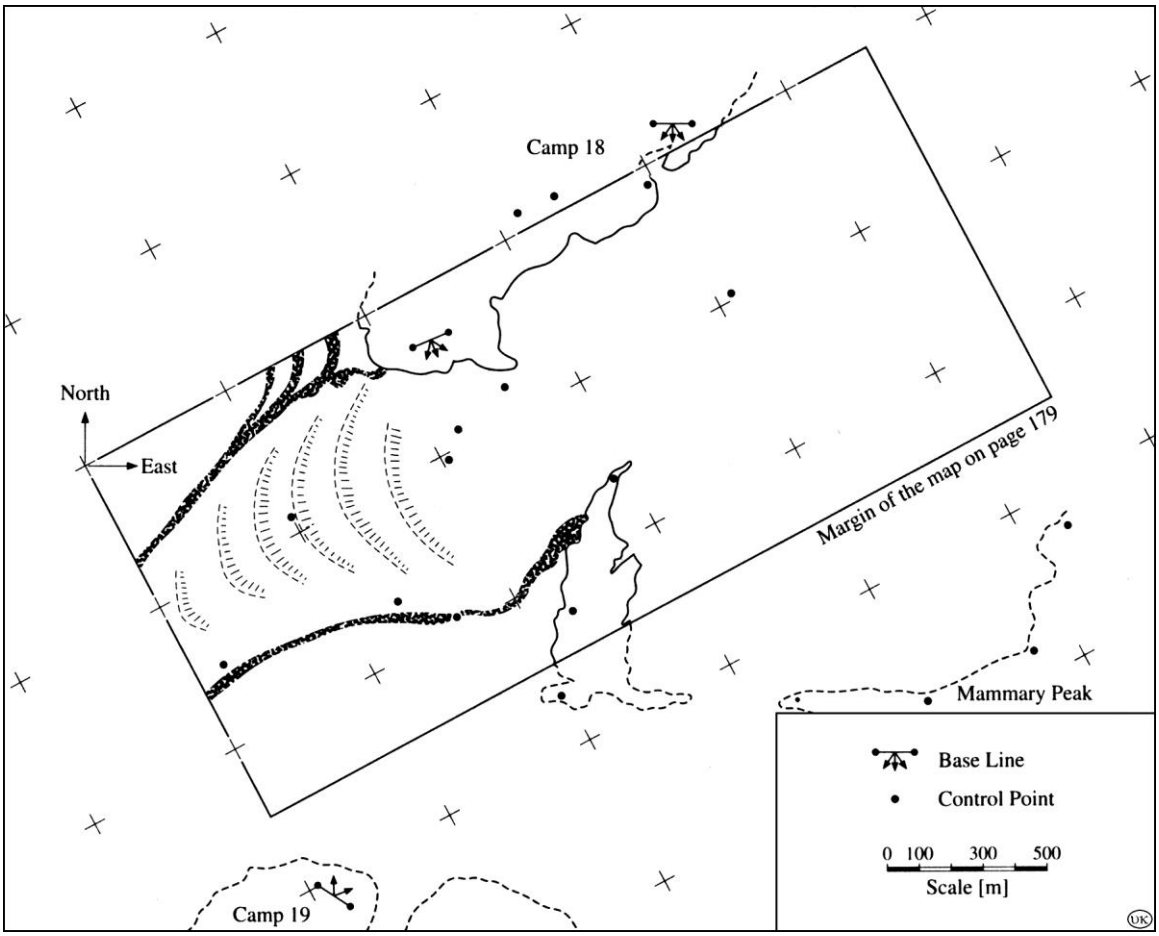

Fig. 3: Set-up of the terrestrial photogrammetric observations

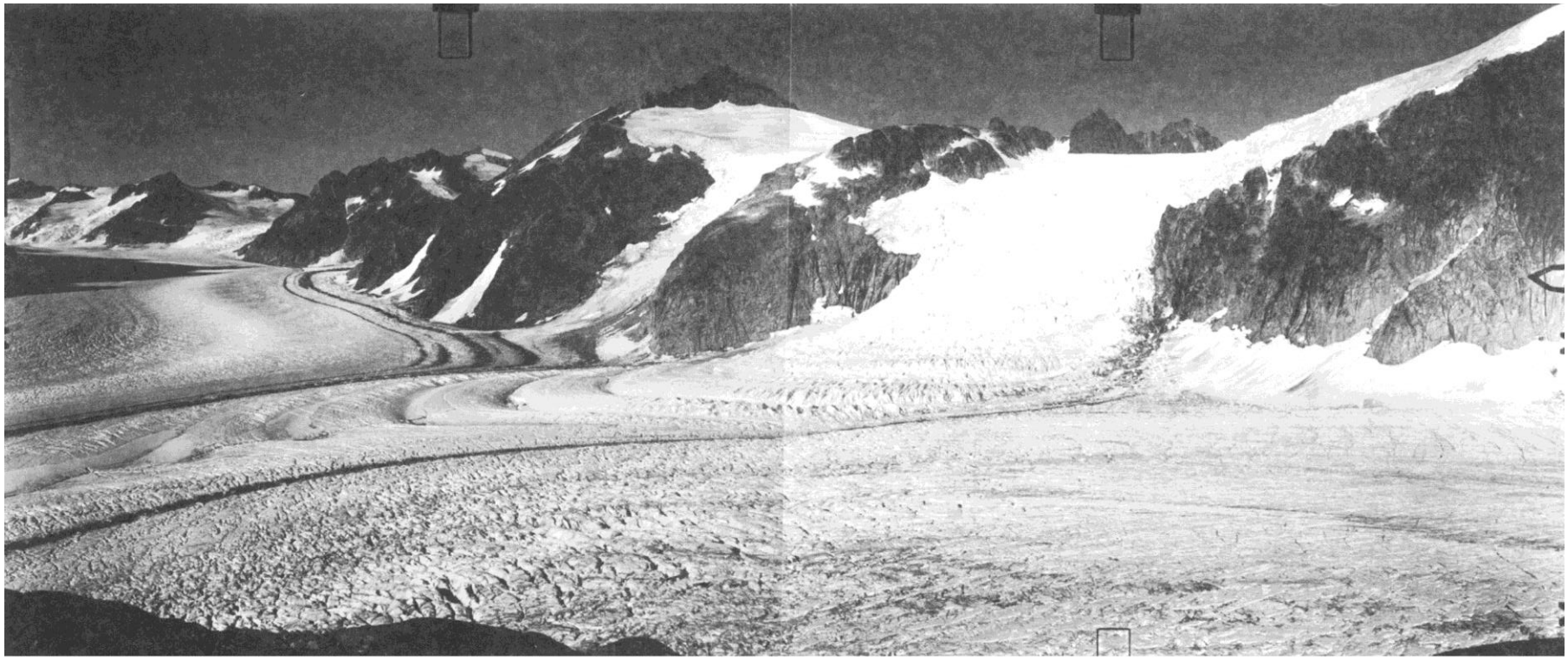

Photo H. Rentsch, 1982

Vaughan-Lewis Icefall from Camp 19

5. Glacier Flow and Flow Velocity of Vaughan-Lewis Icefall

For the measurement of the surface-flow velocity of Vaughan-Lewis Icefall, the glacier was repeatedly surveyed by terrestrial photogrammetry between July 29, 1982 and August 19, 1982. It was decided to measure about 240 single points for the velocity determination. They refer to morphological features of the icefall which could be recognized on the images taken on different days. Their movements in time are a measure of the spatial velocities of these points. The standard deviations of the vectors from double measurements are 0.1 m in length and 4° in azimuth.

Page 179 shows a plan view of the vector field of point velocities superimposed on the contour lines, and a digitally shaded relief model. The velocity of the ice increases to a maximum amount of 5.7 m per day at the narrowest gap between the bedrock banks on both sides. Where the slope flattens, the velocity decreases to 1 m and 0.4 m per day. Thus, the average velocity amounts to about 150 m per year at the foot of the icefall, where the wave ogives occur. Remarkably, this annual surface velocity matches the average wave length of the ogives, a fact, which had been already observed by *HAEFELI [1951]* on other glaciers. Thus, the velocity measurements help to explain some phenomena of the ice surface. The discussion of the glaciological phenomena encountered during the investigation of the icefall is, however, beyond the scope of this paper.

6. Better Visualization by Means of Digital Image Processing

From the DTM, further products can be derived by the use of digital image processing techniques *[EBNER, 1987; HANSON and QUAM, 1988]*

- color-coded representations of height, slope, aspect, and height-difference information,
- shaded relief models in orthoprojection (also superimposed with terrain-cover information or contour lines),
- perspective views,
- stereo perspectives and videos.

In the following, the generation of some of these products is explained and illustrated by examples.

In a shaded relief, each elevation of the DTM is given a grey value (normally with a resolution of 8 bits), which in the simplest case is proportional to the cosine of the angle between the surface normal and the direction towards an artificial illumination source *[STEFANOVIC and SIJMONS, 1984]*. This light source ism placed in the north-west, as it is common practice in cartography. For this purpose, the original 20 m by 20 m basic grid was densified to a 5 m by 5 m grid using the HIFI-88 program package. A shaded relief is very useful for the visual inspection of the DGM, since it is very sensitive to small height changes.

To visualize the shaded relief on a high-resolution monitor with 1,024 x 1,204 pixels (picture elements), a further densification down to a mesh size of 2.5 m by 2.5 m is needed. This is done by using a bilinear interpolation. Then the terrain cover can be superimposed onto the shaded relief to obtain a synthetic terrain representation. The digitized terrain cover borders are vector-raster transformed and registered in a shaded relief. To

color or grey value of each cover type (rock, ice, snow, water, and moraine in the case of Vaughan-Lewis Icefall) can be selected interactively on the monitor or taken from digitized photographs or satellite data (e.g. LANDSAT or SPOT). Thus, for each pixel, three-color values (red, green, and blue) or one grey value are generated. The multiplication of these values with the grey value of the shaded relief yields the desired result (p. 181).

The procedure described here is the one used to merge raster data into a geographical information system (GIS) for the superimposition of vector data *[GÖPFERT, 1987]*. Thus, all the GIS tools are readily available for further terrain analysis.

Another possibility is the derivation of inclination maps from the height data. The different inclinations can be grouped into different classes and displayed, one color per class.

The products described so far can be compiled into cartographic maps. As such, they are scale-independent and can be updated or combined efficiently with thematic information by digital maps.

A perspective representation of the relief offers further help for interpretation. After selecting a suitable viewpoint, the intersection between the ray of sight for each pixel of the new projection plane and the DTM is computed. The color or grey value of the shaded relief at the intersection point is assigned to the corresponding new pixel (method of ray tracing; *[THIEMANN et al., 1989]*; p. 181).

Two perspectives with slightly different perspective centers (5° in azimuth) form a pair of stereo photographs and can thus be viewed in three dimensions.

If the perspective center is moved continuously in space and perspectives are calculated with small time intervals, the frames can be recorded on video tape. Displaying this video, one has the impression of flying across the terrain, and viewing the glacier from all sides.

These perspectives, stereo perspectives, and videos open up new ways of interpreting glacier phenomena, because synthetic views can be generated from arbitrary projection centers. Especially, for the explanation of the topography and the geomorphology, they offer considerable assistance.

7. Conclusions

Digital terrain modeling has become a highly technical and fully operational tool, which can be integrated into glaciology and geoscience for better efficiency. The application of DTM, in combination with digital image processing, aids not only considerably the interpretation of surface phenomena but also opens up the way for new digital cartographic products. Furthermore, it is the first step in the integration of raster products into a GIS, allowing, for example, simulations of ice movement or melting, taking into account different terrain covers.

Acknowledgements

The authors are indebted to Professor Dr. *H. EBNER*, Institute of Photogrammetry, Technical University Munich, for making the facilities of his institute available, and *K. EDER* for his assistance in generating the DTM of Vaughan-Lewis Icefall.

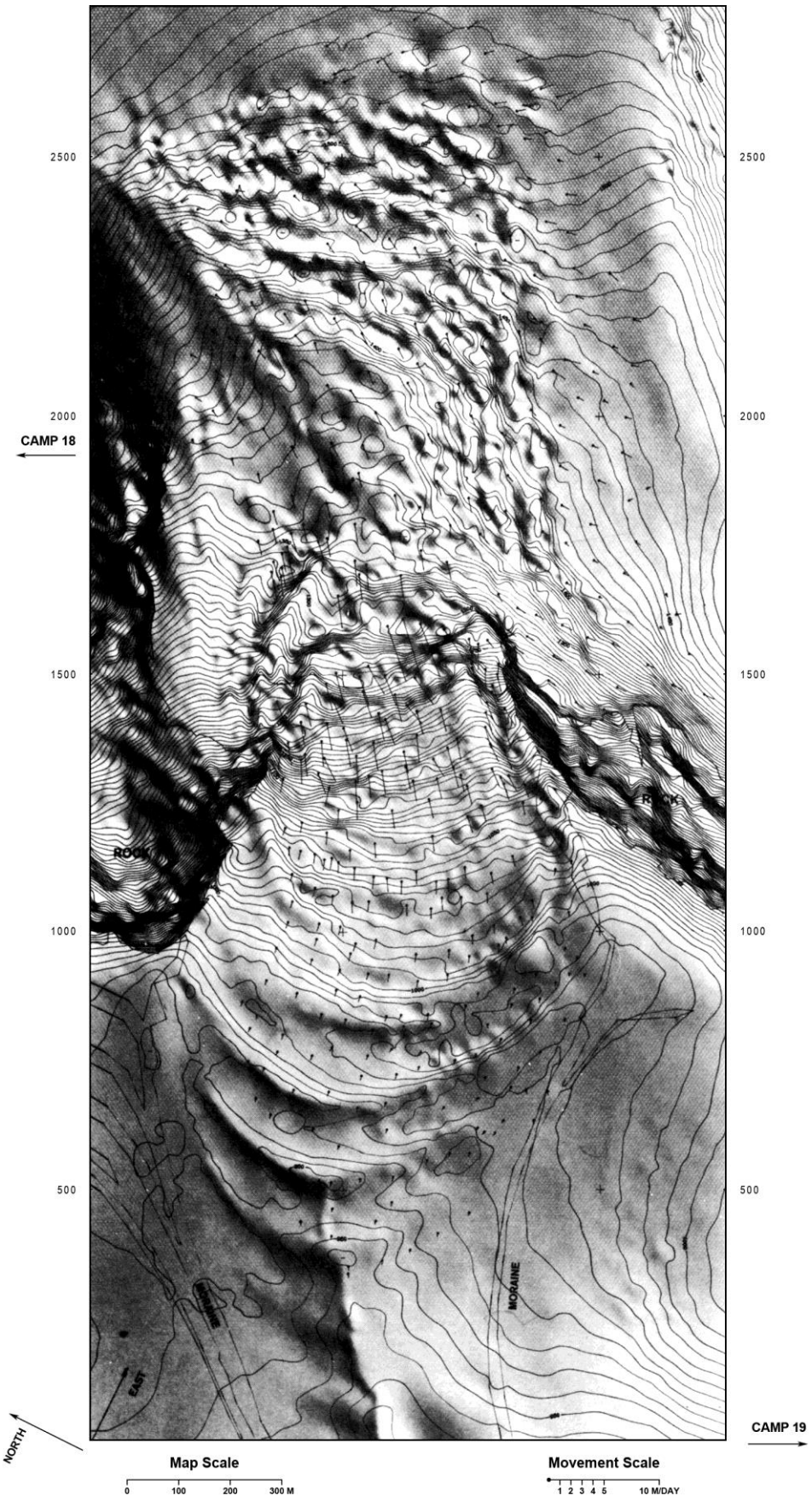

Vaughan-Lewis Icefall, conturlines movement vectors

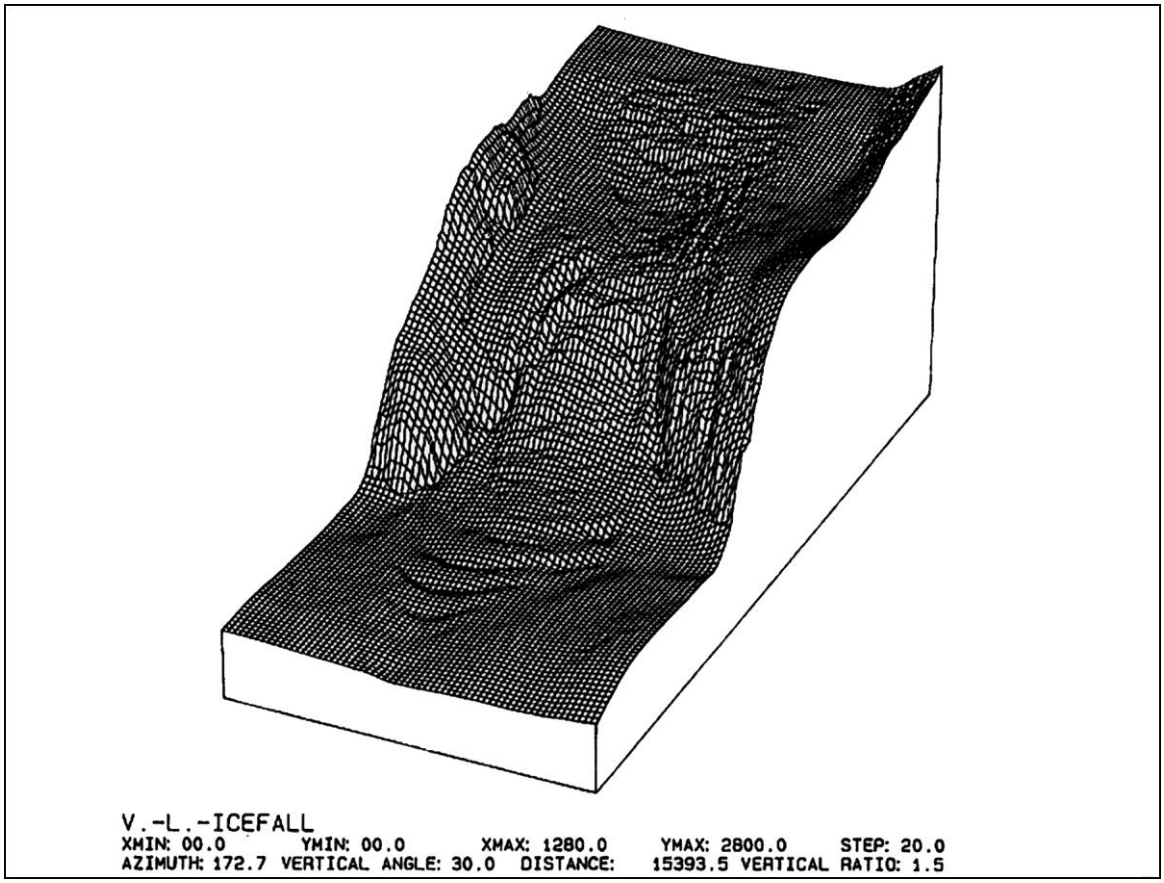

Vaughan-Lewis Icefall, grid model

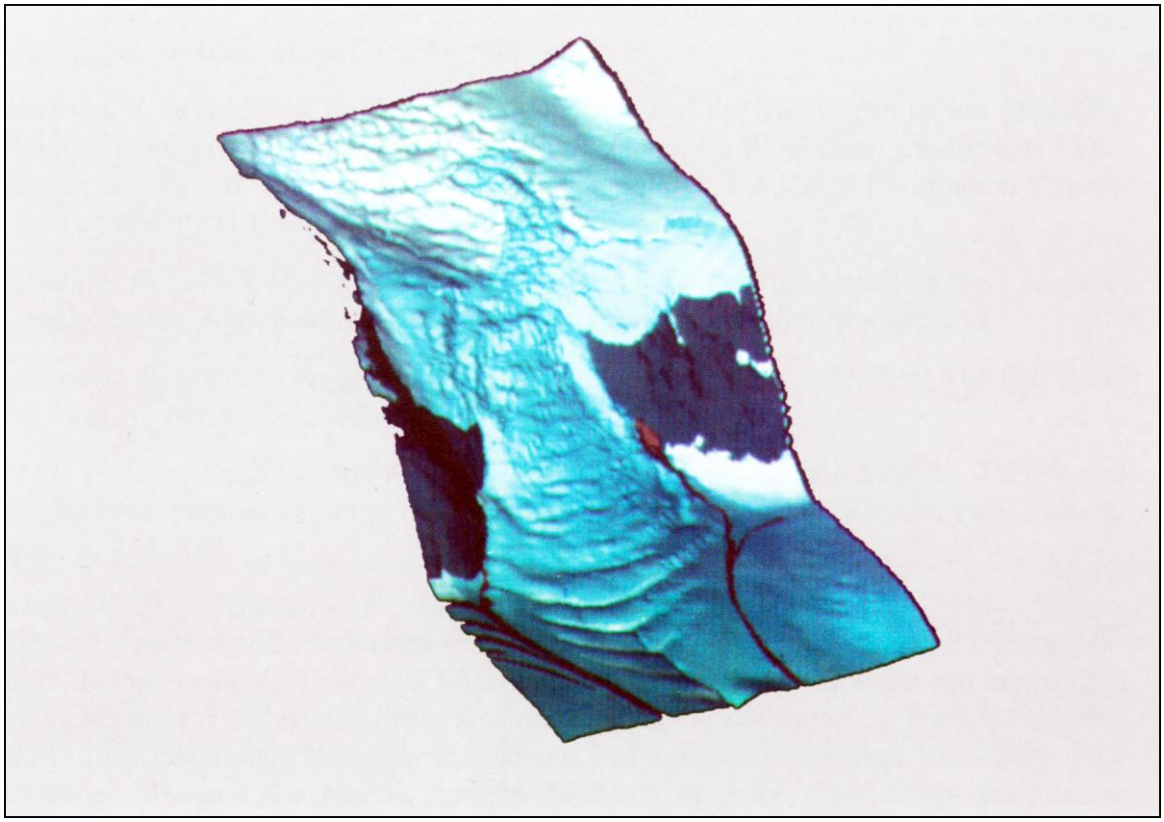

Vaughan-Lewis Icefall, colored digital 3d model

References

COYES, G. M. [1978]: The Development of the Compression Theory and Related Studies on the Vaughan-Lewis Icefall, Juneau Icefield, Alaska. Ph.D. Thesis. Senior Paper Series, Yale University, Department of Geology and Geophysics, New Haven; 52 pp.

EBNER, H. [1987]: Digital Terrain Models for High Mountains. Mountain Research and Development, Vol. 7, No. 4, Boulder, CO.; p. 353-356

EBNER, H. and REINHARDT, W. [1984]: Progressive Sampling and DTM Interpolation by Finite Elements. Bildmessung und Luftbildwesen, Vol. 52, Karlsruhe; p. 172-178

EBNER, H., HÖSSLER, R. and REINHARDT, W. [1988]: Generation Management and Utilization of High Fidelity Digital Terrain Models. Proceedings of the 16th International Congress of the International Society for Photogrammetry and Remote Sensing, Commission III, Kyoto, 1988. International Archives of Photogrammetry and Remote Sensing, Vol. 27, Part B11, Kyoto; p. III-556-III-566

FINSTERWALDER, S. [1897]: Der Vernagtferner, seine Geschichte und seine Vermessung in den Jahren 1888 und 1889. Wissenschaftliche Ergänzungshefte zur Zeitschrift des Deutschen und Österreichischen Alpenvereins, Vol. 1, No. 1, München; 112 pp.

FREERS, T. F. [1965]: Preliminary Structural Glaciological Investigation of Wave-Bands on the Vaughan-Lewis Glacier, Alaska. Michigan Academy of Science, Arts and Letters, Ann Arbor, MI.

GÖPFERT, W. [1987]: Raumbezogene Informationssysteme: Datenerfassung – Verarbeitung – Integration. H. Wichmann Verlag, Karlsruhe; 278 pp.

HAEFELI, R. [1951]: Some Observations on Glacier Flow. The Journal of Glaciology, Vol. 1, No. 9, Cambridge; p. 496-500

HANSON, A. J. and QUAM, L. H. [1988]: Overview of the SRI Cartographic Modeling Environment. Proceedings of the Image Understanding Workshop, Cambridge, MA., April 1988, Vol. II. Defense Advanced Research Projects Agency, Information Science and Technology Office, Cambridge, MA.; p. 576-582

KITTREDGE, R. F. [1964]: Formation of Wave-Ogives Below the Icefall on the Vaughan-Lewis Glacier, Alaska. Master Thesis, University of Colorado, Boulder, CO.

MAKAROVIC, B. [1973]: Progressive Sampling for Digital Terrain Models. The ITC Journal, Vol. 1, No. 4, Enschede; p. 397-416

MILLER, C. L. and LAFLAMME, R. A. [1958]: The Digital Terrain Model – Theory and Application. Photogrammetric Engineering and Remote Sensing, Vol. 24, Falls Church, VA.; p. 433-442

MILLER, M. M., FREERS, T. F., KITTREDGE, R. F. and HAVAS, T. [1968]: Wave-Ogive Formation and Associated Phenomena on the Vaughan-Lewis and Gilkey Glacier, Juneau Icefield, Alaska. 19th Alaska Science Conference „Science and the North", Whitehorse, Y.T., Canada, 1968. Abstracts and papers presented by participants and staff of the Glaciological and Arctic Sciences Institute, Michigan State University, East Lansing, MI., and the Juneau Icefield Research Program, Foundation for Glacier Research, Seattle, WA.; n.p.

PEIPE, J., REISS, P. and RENTSCH, H. [1978]: Zur Anwendung des digitalen Geländemodells in der Gletscherforschung. Zeitschrift für Gletscherkunde und Glazialgeologie, Vol. 14, No. 2, Innsbruck; p. 161-172

RENTSCH, H. [1997]: Terrestrial Photogrammetry on the Juneau Icefield. – In: *WELSCH, W. M., LANG, M. and MILLER, M. M. (eds.):* Geodetic Activities, Juneau Icefield, Alaska, 1981-1996. Schriftenreihe des Studiengangs Vermessungswesen, Heft 50. Universität der Bundeswehr München, Neubiberg; p. 167-170

STEFANOVIC, P. and SIJMONS, K. [1984]: Computer-Assisted Relief Representation. The ITC Journal, Vol. 12, No. 1, Enschede; p. 40-47

THIEMANN, R., FISCHER, J., HASCHEK, G. and KNEIDL, G. [1989]: Visualization of Terrain Data. – In: *HANSMANN, W., HOPGOOD, F. R. A. and STRASSER, W. (eds.):* Eurographics '89, Proceedings of the European Computer Graphics Conference and Exhibition, Hamburg, F.R.G., 4-8 September, 1989. Elsevier, Amsterdam; p. 173-195

Melvin G. Marcus, Fred B. Chambers,
Maynard M. Miller and Martin Lang

Recent Trends in Lemon Creek Glacier, Alaska [1)]

1. Introduction

This paper reports the 1989 re-mapping of the Lemon Creek Glacier, Alaska, and in conjunction with 1948 and 1957 maps of the glacier, determination of 9-year and 32-year changes of glacier mass and terminal position. Lemon Creek Glacier, a relatively small valley about 6 km long located in the southwestern corner of the Juneau Icefield, Alaska (Fig. 1), has been a benchmark for interpretation of glacier behavior and associated climatic influences in the marine Coast Range environment of southeastern Alaska for more than 40 years. From 1953 through 1958, the glacier was the focus for several glaciological and glacio-climatic investigations; field research in 1957 and 1958 was directly associated with the International Geophysical Year (IGY). These activities were under the operational umbrella of William O. Field's Department of Exploration and Field Research at the American Geographical Society.

The 1953-1958 research included:

(1) investigations of glacier dynamics *[NIELSEN, 1955]*,

(2) gravimetric measurements *[THIEL et al., 1957]*, glacier mapping *[AMERICAN GEOGRAPHICAL SOCIETY, 1960]*,

(3) mass balance and glacier flow studies, which included a series of progress reports by *LA CHAPELLE [1955, 1956]* and publications by *WILSON [1959]*, *HEUSSER and MARCUS [1964b]*, *MARCUS [1964]*, and *ZENONE [1962]*; late Holocene history of the glacier *[HEUSSER and MARCUS, 1964a]*; and glacier climatology *[HUBLEY, 1955, 1957]*.

Subsequent studies of Lemon Creek Glacier have included seismic measurements *[PRATHER et al., 1968]*, analyses of geomorphological and fluvioglacial processes *[MARSTON, 1983; MILLER, 1972, 1975]*, and energy balance climatology *[WENDLER and STRETEN, 1969]*.

An important element of the 1950s work was construction of two topographic maps of Lemon Creek Glacier at a scale of 1:10,000 and a 5-m contour interval. The glacier was one of nine American glaciers mapped by the *AMERICAN GEOGRAPHICAL SOCIETY [1960]* in conjunction with the IGY (Fig. 1). These were intended to provide the bases, when compared with future maps, to determine glacier dimensions and mass change. *CASE [1958]* produced the 1957 IGY map of Lemon Creek Glacier (see page 187), *MARCUS [1964]*, using earlier aerial photography, constructed a map for 1948.

The selected IGY glaciers were small alpine systems considered to be representative of various glaciological environments in the western United States. They ranged from Blue

1) Physical Geography, Vol. 16, No. 2, Silver Springs, MD. *[1995]*; p. 150-161

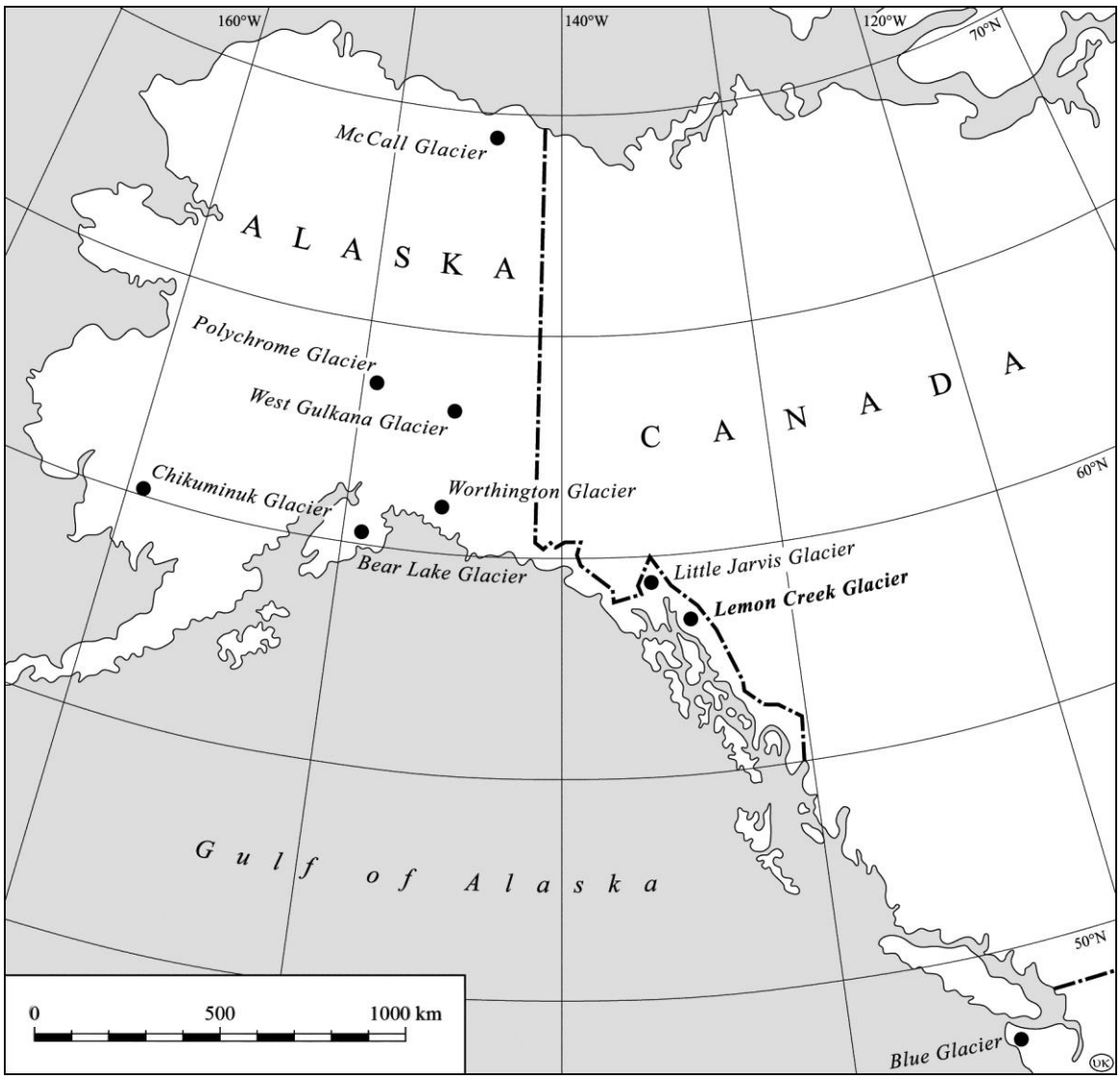

Fig. 1: Location of the nine American glaciers mapped during the International Geophysical Year, 1957-1958 *[AMERICAN GEOGRAPHICAL SOCIETY, 1960]*

Glacier on Washington's Olympic Peninsula, through Lemon Creek and Little Jarvis glaciers in southeastern Alaska, to five others ranging poleward from the Gulf of Alaska to West Gulkana Glacier in the Alaska Range and McCall Glacier in the Brooks Range (Fig. 1). The glaciers were selected because of their geographical distribution, relative accessibility, and the prevailing wisdom at the time – espoused by the distinguished Norwegian glaciologist *Hans Ahlmann* – that small glaciers were the best medium through which to interpret glacier behavior and to understand related climatic interactions. Because accessibility was an issue, the glaciers were situated at relatively low elevations.

Lemon Creek Glacier exemplifies this pattern. It is about 6 km long and its maximum width approaches 2 km. In 1989 its surface area was 11.728 km^2. The glacier flows to the north from 1,500 m, dropping to around 600 m above sea level (maps 1957 and 1989). According to gravimetric and seismic measurements, it attains a maximum thickness of over 200 m some 1,500 m downglacier from its head; ice exceeds 150 m depth from about 400 m below the head to just above the icefall. Further, it is easily reached within one or two days by foot or ten minutes by helicopter.

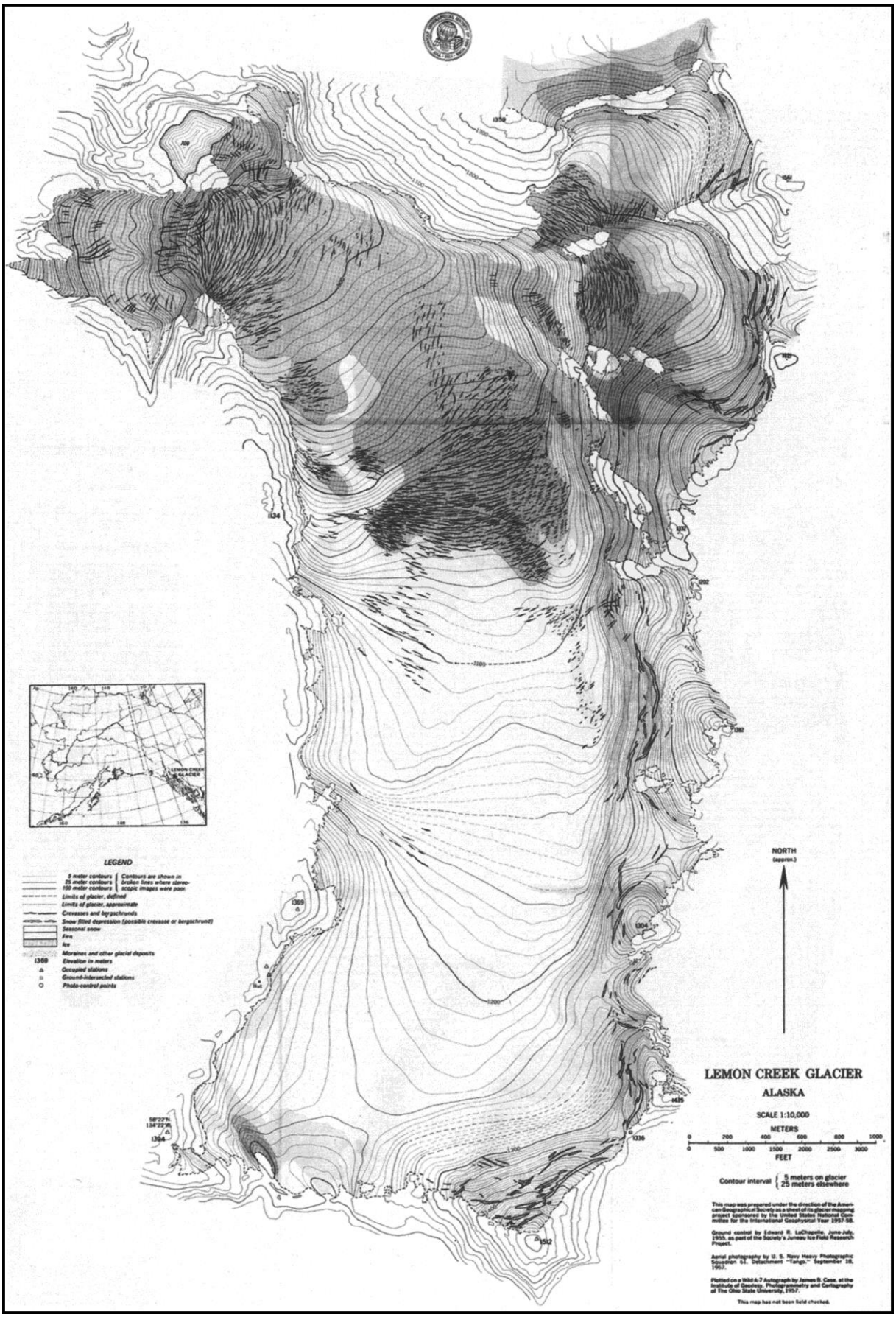

Reduced version of the 1957 Lemon Creek Glacier map
[AMERICAN GEOGRAPHICAL SOCIETY, 1960]

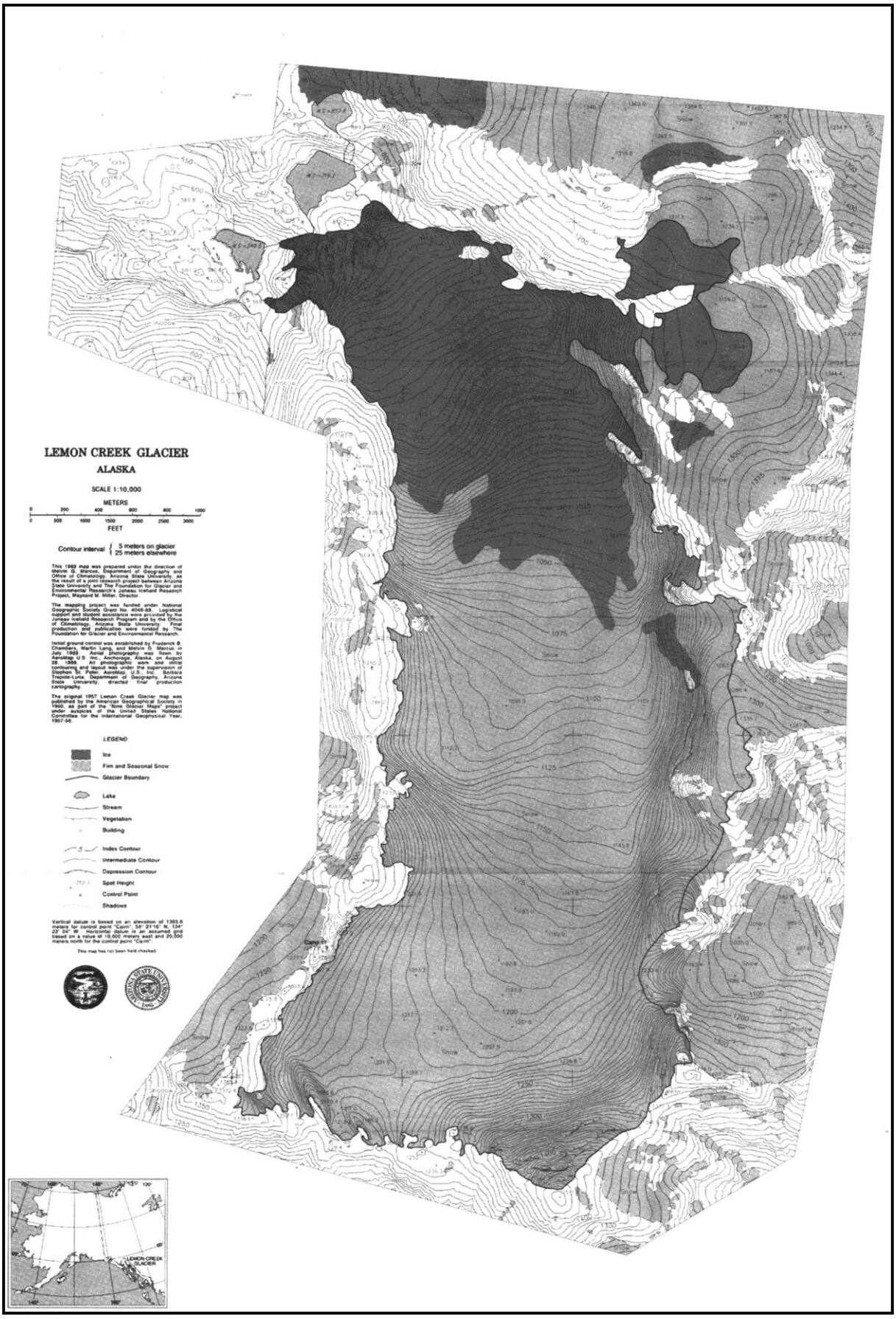

Reduced version of the 1989 Lemon Creek Glacier map
[FOUNDATION FOR GLACIER AND ENVIRONMENTAL RESEARCH, 1994]

2. The 1989 Lemon Creek Glacier Map

None of the IGY glaciers were re-mapped until West Gulkana Glacier in 1987, resulting in a published map and the computation of change in mass balance over three decades *[MARCUS and REYNOLDS, 1988; CHAMBERS et al., 1991]*. Subsequently, it was decided to extend the new mapping net through 7° of latitude south to Lemon Creek Glacier. Original survey photography and data, fields notes, and diapositives of U.S. Navy aerial photography taken on September 18, 1957 were retrieved from storage at the United States Geological Survey and the Byrd Polar Research Center, Ohio State University. In consultation with Aeromap U.S., who flew the aerial photography mission, eight ground control points were selected for the new map. Cairn Peak was the only station reoccupied from the original 1957 survey.

The ground control grid was surveyed in July 1989, during a five-day period of clear weather. Distance and angle measurements were by AGA Geodimeter and Wild T2 theodolite. Survey markers – 1·10 m vinyl strip crosses – were centered over each control point following the ground survey. These remained in place until aerial photography was flown on August 28, 1989; the eight control points were clearly visible in the air photos.

The 1989 control points were calculated in an orthogonal grid with reoccupied (from 1957) Cairn Peak as the point of origin. The net was subsequently linked to a USGS benchmark 25.85 m to the southwest and 7.37 m lower than the point of origin. To enhance error control, x, y and z coordinates were independently calculated at both Arizona State University (by traditional survey geometry) and the Bundeswehr University Munich (by the least squares Program KINAUS). The differences were neglibible; the German figures yielded only a 0.00001 percent greater distance over the length of the glacier.

Black and white aerial photography at a scale of 1:30,000 was flown, utilizing a certified, six-inch focal length cartographic camera. A line of four stereo-pairs was obtained. The final map was photogrammetrically plotted at Aeromap U.S. at a scale of 1:10,000, with a 5-m contour interval over glacier surfaces and a 25-m interval elsewhere (page 189). These replicated the scale and contour intervals for the 1957 IGY map of the Lemon Creek Glacier. Both linked and scribed masters of the map were generated.

3. Mass Balance Measurements

Most direct measures of glacier behavior involve determination of mass balance, which is defined as the net water gain or loss for a glacier during any assigned time period, usually one or more glacier years. There are several ways to determine mass balance. These have been enumerated most recently in the manual *„Glacier Mass Balance Measurements“* by *ØSTREM and BRUGMAN [1991]* and include the geodetic method, which compares two or more topographic maps through time; stratigraphic and fixed-date methods, both of which employ direct field measurement of annual accumulation and ablation; and the method using equilibrium line altitude (ELA)/accumulation aera ratio (AAR).

This paper focuses on the geodetic method, which utilizes the old and new Lemon Creek Glacier maps and identifies mass balance over multi-year periods through superimposition and comparison of maps at the same scale and contour interval. This procedure was refined by *FINSTERWALDER [1952, 1960]* and subsequently used in North America by, among others, *HAUMANN [1960]*, *KONECNY [1966]*, and *CHAMBERS et al. [1991]*. It also was

used to determine the 1948-1957 Lemon Creek Glacier budget *[MARCUS, 1964]*. Advantages of this method are that mass balance can be calculated over several years without annual field observations and that the entire glacier is surveyed and not subject to errors associated with field sampling methods. The obvious drawback is that annual mass changes cannot be determined nor their short-term relationship to climate assessed.

3.1 1957-1989 Mass Balance

The 32-year mass balance for Lemon Creek Glacier was determined by the geodetic method, calculating volume changes from contour line displacement between 1957 and 1989. Fig. 2 illustrates a schematic section of that method. Areas were calculated for both the main trunk glacier and the northeast feeder tributary (note glacier margins in 1957 and 1989 maps). Contour interval areas were measured by both digital and traditional hand planimetry; each area was measured twice. The two methods yield an area difference $< 0.001 \cdot 10^6$ m^2.

Mass balance changes for 1957-1989 are summarized in Table 1. Assuming a traditio nal mean glacier density of 0.90, the system experienced a water-equivalent loss of $-118.71 \cdot 10^6$ m^3. During this period, the terminus retreated around 700 m (Fig. 3) and the surface area diminished by $0.878 \cdot 10^6$ m^2. Excluding the northeast feeder, the glacier lost 3.9% water and 10.3% area between 1957 and 1989.

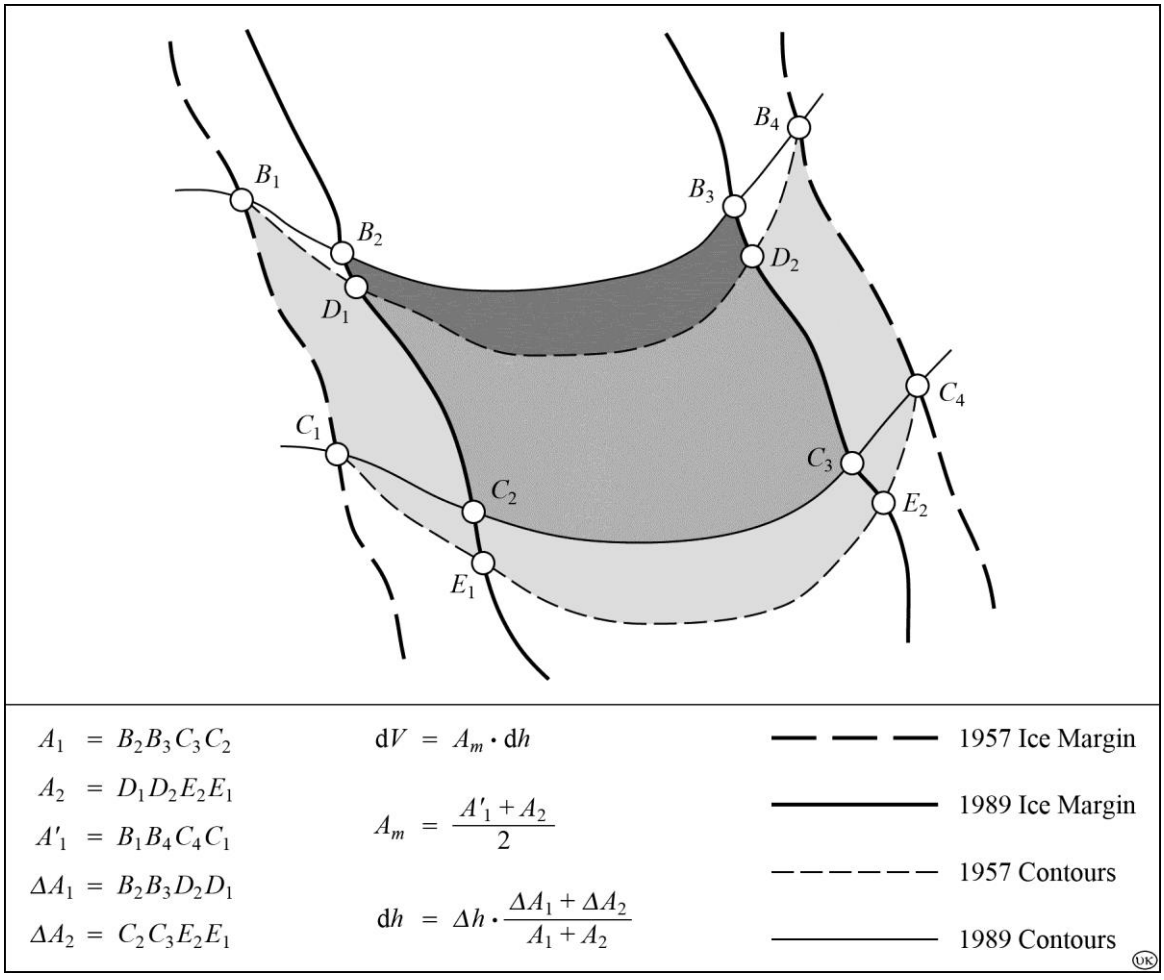

Fig. 2: Schematic representation of volume changes between successive contour line positions per the geodetic method of mass balance measurement

Total change of glacier volume also was estimated. On the basis of respective gravimetric and seismic data from *THIEL et al. [1957]* and *PRATHER [in MILLER, 1975]*, the 1957 ice volume was estimated to be $901.72 \cdot 10^6$ m^3 (Table 2). Subtracting the 32-year ice loss ($131.90 \cdot 10^6$ m^3) yield a glacial loss of roughly 14.6% of its volume between 1957 and 1989.

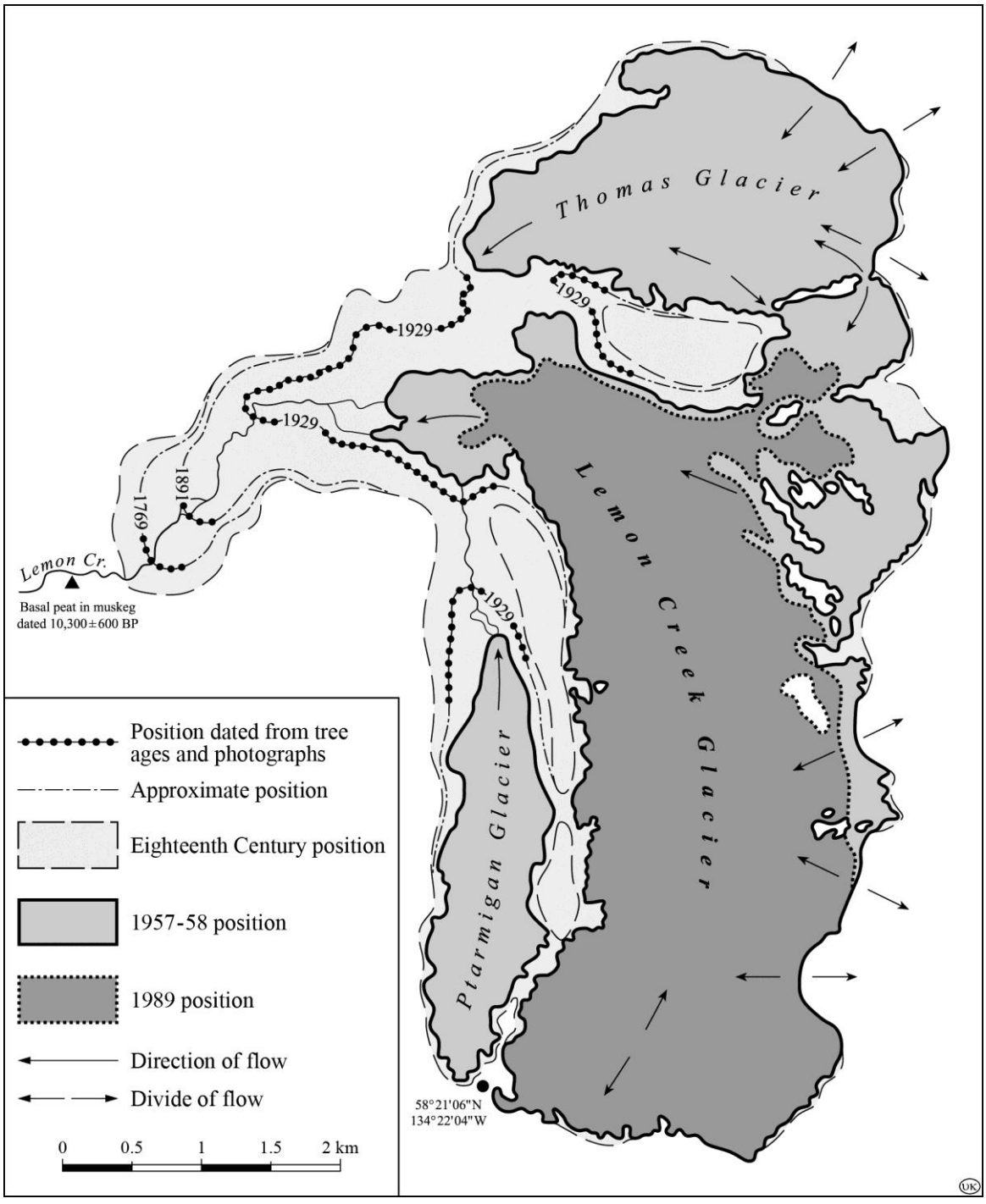

Fig. 3: Historical variations of Lemon Creek Glacier through 1989;
1958 base after *HEUSSER and MARCUS [1964a]*

Table 1: Mass Balance Data Lemon Creek Glacier

Area	Change of surface area [10^6 m^2]	Change of ice volume [10^6 m^3]	Change of water volume [10^6 m^3]	Annual change ice volume [10^6 m^3]	Annual change water volume [10^6 m^3]
Full Glacier	- 0.878	- 131.90	- 118.71	- 4.12	- 3.71
Northeaster feeder	- 0.090	- 5.17	- 4.65	- 0.16	- 0.15
Glacier less northeast feeder	- 0.788	- 126.73	- 114.06	- 3.96	- 3.56

Table 2: Estimated volume change Lemon Creek Glacier 1957-1989

Year	Ice volume [10^6 m^3]	Water volume [10^6 m^3]	Ice volume change [10^6 m^3]	Water volume change [10^6 m^3]	Percentage
1957	901.72	811.54	–	–	–
1989	769.82	692.84	- 131.90	- 118.71	14.6

3.2 Comparison to 1948-1957 Mass Balance

The 1948-1957 mass balance of Lemon Creek Glacier had been determined earlier *[MARCUS, 1964]*. Water equivalent values from that study have been adjusted from an original density multiplier of 0.85 to 0.90. The nine-year water loss was $22.1 \cdot 10^6$ m^3.

Although annual average losses can be calculated, they can be a misleading statistic. For example, between 1948 and 1957 when annual mass balance were determined by either stratigraphic or ELA/AAR methods, actually yearly values ranged between $-9.9 \cdot 10^6$ m^3 and $+13.3 \cdot 10^6$ m^3 – dramatic departures from the annual mean change of $-2.45 \cdot 10^6$ m^3 based on geodetic methods. In comparison, the 1957-1989 mean water loss was $-3.71 \cdot 10^6$ m^3 yr^{-1}, an increase of 51% over 1948-1957. Thus, although these statistics do not reflect actual yearly conditions, they do demonstrate an overall increase in the rate of glacier wastage.

In areal terms, ice loss was almost entirely or below 1,100 m elevation during the period 1940-1957, with the greatest thickness changes occurring immediately above and below the lower glacier icefall. In later years, however, significant height and mass loss also occurred within 100-200 m of the glacier head.

Lastly, during 1948-1957, the terminus retreated an average 240 m along an irregular front. An additional retreat of roughly 700 m occurred during the 1957-1989 (Fig. 3); thus, the decadal rate was roughly just under that of 1948-1957. This exemplifies problems in gauging glacier health by terminal position. Change of terminal position did not reflect the escalated rates of mass wastage.

4. Summary

This paper has described the 1989 re-mapping of Lemon Creek Glacier, Alaska, and in conjunction with 1948 and 1957 maps of the glacier, identified 9-year and 32-year changes

of glacier mass and terminal position. The four-decade period was one of overall glacier wastage, with a loss of about one-seventh of the glacier's total mass. These results correspond to negative mass balance trends for West Gulkana Glacier in the eastern Alaska Range *[CHAMBERS et al., 1991]* and McCall Glacier in the Brooks Range during 1958-1971 *[DORRER and WENDLER, 1976]*.

It is not the intent of this paper to address climate implications of the IGY mass balance data. It should be noted, however, that the relationship of glacier behavior to climate change in northwestern North America cannot be defined solely from selected „representative" IGY glaciers such as Lemon Creek. They provide valuable inputs to interpretation of the glacier-climate equation in lower elevations, but glaciers at higher elevations will have to be included to understand more fully these important interacting processes.

Acknowledgements

Primary support for this study was provided under National Geographic Society Grant #4048-89. Additional funds and services were provided by Arizona State University and the Foundation for Glacier and Environment Research (FGER). Field operations would not have been possible without logistical and personal support from the Juneau Icefield Research Program (JIRP), jointly sponsored by FGER and the Glaciological and Arctic Sciences Institute, University of Idaho. A number of JIRP staff and students assisted the ground survey program, including *L. Hay, J. Merritt, R. Merritt, A. Pinchak,* and *H. Sigmund*, as well as NSF-student participants *K. Nygren* and *B. Pratt*. *S. St. Peter* of Aeromap U.S. was a valued participant in photogrammetric plotting, *K. Cessnock* and *R. Shroder* assisted in data processing at the Office of Climatology, Department of Geography, Arizona State University. *B. Trapido* produced final manuscript cartography. The 1:10.000, 1989 map of Lemon Creek Glacier (*[MILLER et al., 1994]*, p. 187) was produced under a grant from the Foundation for Glacier and Environment Research.

References

AMERICAN GEOGRAPHICAL SOCIETY [1960]: Lemon Creek Glacier, Alaska. Nine Glacier Maps, Northwestern North America, to accompany nine separate map sheets on scale of 1:10,000. Special Publication No. 34, Map 1. American Geographical Society, New York

CASE, J. B. [1958]: Mapping of Glaciers in Alaska. Photogrammetric Engineering, Vol. 24, Falls Church, VA.; p. 815-821

CHAMBERS, F. B., MARCUS, M. G. and THOMPSON, L. T. [1991]: Mass Balance of West Gulkana Glacier, Alaska. The Geographical Review, Vol. 81, New York; p. 70-86

DORRER, E. and WENDLER, G. [1976]: Climatological and Photogrammetric Speculations on Mass-Balance Changes of McCall Glacier, Brooks Range, Alaska. The Journal of Glaciology, Vol. 17, Cambridge; p. 479-490

FINSTERWALDER, R. [1952]: Photogrammetry and Glacier Research with Reference to Glacier Retreat in the Eastern Alps. The Journal of Glaciology, Vol. 2, Cambridge; p. 306-315

FINSTERWALDER, R. [1960]: On the Measurement of Glacier Fluctuations. International Association for Scientific Hydrology Publications, Vol. 54; p. 325-336

HAUMANN, D. [1960]: Photogrammetric and Glaciological Studies of Salmon Glacier. Arctic, Vol. 13, Calgary; p. 75-110

HEUSSER, C. J. and MARCUS, M. G. [1964a]: Historical Variations of Lemon Creek Glacier, Alaska. The Journal of Glaciology, Vol. 5, Cambridge; p. 77-86

HEUSSER, C. J. and MARCUS, M. G. [1964b]: Surface Movement, Hydrological Change and Equilibrium Flow on Lemon Creek Glacier, Alaska. The Journal of Glaciology, Vol. 5, Cambridge; p. 61-76

HUBLEY, R. C. [1955]: Measurements of Diurnal Variations in Snow Albedo on Lemon Creek Glacier, Alaska. The Journal of Glaciology, Vol. 2, Cambridge; p. 560-563

HUBLEY, R. C. [1957]: An Analysis of Surface Energy during the Ablation Season on Lemon Creek Glacier, Alaska. Transactions – American Geophysical Union, Vol. 38, Washington, D.C.; p. 68-84

KONECNY, G. [1966]: Application of Photogrammetry to Surveys of Glaciers in Canada and Alaska. Canadian Journal of Earth Sciences, Vol. 3, No. 6, Ottawa; p. 783-798

LA CHAPELLE, E. R. [1955]: Juneau Icefield Research Program: Progress Report 1954 and 1955. American Geographical Society (Officve of Naval Research Task order N9onr-83001), New York

LA CHAPELLE, E. R. [1956]: Juneau Icefield Research Program: Progress Report 1956. American Geographical Society (Officve of Naval Research Task order N9onr-83001), New York

MARCUS, M. G. [1964]: Climate-Glacier Studies in the Juneau Icefield Region, Alaska. University of Chicago, Department of Geography, Research Paper 88. University of Chicago Press, Chicago; 128 pp

MARCUS, M. G. and REYNOLDS, W. J. (eds.) [1988]: Glacier and Climate Studies of West Gulkana Glacier and Environs, Alaska Range. Geography Research Paper No. 4, U.S. Military Academy and Arizona State University, and Geography Research Paper No. 1, U.S. Military Academy, West Point, N.Y.

MARSTON, R. A. [1983]: Supraglacial Stream Dynamics on the Juneau Icefield. Annals of the Association of American Geographers, Vol. 73, Washington, D.C.; p. 597-608

MILLER, M. M. [1972]: A Principles Study of Factors Affecting the Hydrological Balance of the Lemon Glacier System and Adjacent Sectors of the Juneau Icefield, Southeastern Alaska, 1965-69. Michigan State University Technical Report 33. In Cooperation with: Foundation for Glacier and Environmental Research Pacific Center, Seattle, WA., with several sections contributed by staff affiliates, Glaciological and Arctic Sciences Institute, Michigan State University. Michigan State University, Institute of Water Research, East Lansing, MI.; v.p.

MILLER, M. M. [1975]: Mountain and Glacier Terrain Study and Related Investigations in the Juneau Icefield Region, Alaska/Canada. U.S. Army Research Office and Foundation for Glacier and Environmental Research, Seattle, WA.

MILLER, M. M., MARCUS, M. G., LANG, M. and CHAMBERS, F. B. [1994]: Lemon Creek Glacier, Alaska, Map, Scale 1:10,000. Foundation for Glacial Environmental Research and Arizona State University in cooperation with the National Geographic Society

NIELSEN, L. E. [1955]: Regimen and Flow of Ice in Equilibrium Glaciers. Bulletin of the Geological Society of America, Vol. 66, Boulder, CO.; p. 1-8

ØSTREM, G. and BRUGMAN, M. [1991]: Glacier Mass Balance Measurements. Science Report 4. Minister of Supply and Services Canada, National Hydrology Research Institute, Saskatoon

PRATHER, B. W., SCHOEN, L., CLASSEN, D. and MILLER, H. [1968]: Seismic Depth Measurements on the Taku, Vaughan-Lewis and Lemon Glaciers, Alaska. 19th Alaska Science Conference „Science and the North", Whitehorse, Y.T., Canada, 1968. Abstracts of papers presented by participants and staff of the Glaciological and Arctic Sciences Institute, Michigan State University, East Lansing, MI, and the Juneau Icefield Research Program, Foundation for Glacier Research, Seattle, Wash.; n.p.

THIEL, E., LA CHAPELLE, E. and BEHRENDTS, J. [1957]: The Thickness of Lemon Creek Glacier, Alaska, as Determined by Gravity Methods. Transactions – American Geophysical Union, Vol. 38, Washington, D.C.; p. 745-749

WENDLER, G. and STRETEN, N. A. [1969]: A Short-Term Heat Balance Study on a Coast Range Glacier, Juneau Icefield, Alaska. Pure and Applied Geophysics, Vol. 77, Basel; p. 68-77

WILSON, C. R. [1959]: Surface Movement and its Relationship to the Average Annual Hydrological Budget of Lemon Creek Glacier, Alaska. The Journal of Glaciology, Vol. 3, Cambridge; p. 355-361

ZENONE, C. B. [1962]: Glacio-Hydrological Parameters of the Mass Balance of Lemon Creek Glacier, Alaska – 1965-1967. M.S. Thesis, Michigan State University, East Lansing, MI.

Appendices

Appendix A

Observation Timetables

Abbreviations:

T2	=	Intersection (Theodolite observations only)
T2/EDM	=	Theodolite and Electronic Distance Meausrement Device (EDM) observations in both epochs
T2/(EDM)	=	Theodolite observations in both epochs, Electronic Distance Measurement Device (EDM) observations in one epoch only
GPS	=	Rapid Static GPS
RT-GPS	=	Real-Time GPS
(12)	=	Number of the points observed

Profile		1986	1987	1988	1989	1990
No.	**Location**					
I	Taku Glacier (Terminus)	–	–	–	–	–
II	Taku Glacier (Goat Ridge)	–	–	–	–	–
III	Demorest Glacier	–	T2 / (EDM) (9)	–	–	–
IV	Taku Glacier (Camp 10)	T2 / EDM (18)	T2 / (EDM) (18)	T2 / EDM (12)	T2 / EDM (14)	T2 / EDM (12
IV a	Taku Glacier (Icy Basin)	T2 / EDM (8)	T2 / (EDM) (8)	T2 / (EDM) (6)	T2 / EDM (8)	–
IV b	Taku Glacier (North Basin)	–	–	–	T2 / EDM (7)	–
V	SW-Branch Taku Glacier	T2 / EDM (13)	T2 / EDM (9)	T2 / EDM (10)	T2 / EDM (14)	T2 / EDM (12)
V a	Upper SW-Branch Taku Glacier	–	–	–	T2 / EDM (10)	–
VI	NW-Branch Taku Glacier (Echo Mountain)	T2 / (EDM) (15)	–	–	T2 / EDM (16)	–
VI a	NW-Branch Taku Glacier (Taku D)	–	–	–	–	T2 / (EDM) (16)
VII	Lower Matthes Glacier (Camp 9)	T2 / (EDM) (13)	T2 / (EDM) (18)	–	T2 / EDM (14)	T2 / (EDM) (10)
VII a	Lower Matthes Glacier (Taku C)	–	–	–	–	–
VIII	Upper Matthes Glacier	–	T2 / (EDM) (14)	T2 / EDM (11) + (8)	T2 / EDM (14)	T2 / (EDM) (7)
VIII a	Matthes / Vaughan-Lewis Glacier Divide	–	–	–	–	–
IX	Upper Vaughan-Lewis Glacier	–	T2 (7)	–	T2 / EDM (9)	T2 / EDM (9)
X	Matthes / Llewellyn Glacier Divide	–	–	–	–	–
XI	Llewellyn Glacier	–	–	–	–	–
A	Gilkey Trench (Unnamed Glacier)	–	–	–	–	T2 / EDM (5)
B	Gilkey Trench (Trench Traverse)	–	–	–	–	T2 / EDM (15)
C	Gilkey Trench (Gilkey Glacier Curve)	–	–	–	–	T2 / EDM (6)
D	Gilkey Trench (Upper Gilkey Glacier)	–	–	–	–	T2 / EDM (9)
E	Gilkey Trench (Little Vaughan-Lewis Glacier)	–	–	–	–	T2 / EDM (3)
F	Gilkey Trench (Vaughan-Lewis Glacier)	–	–	–	–	T2 / EDM (7)

Profile		1991	1992	1993	1994	1995	1996
No.	Location						
I	Taku Glacier (Terminus)	–	–	–	GPS (15)	–	–
II	Taku Glacier (Goat Ridge)	–	–	GPS (10)	GPS (11)	–	–
III	Demorest Glacier	T2 / EDM (14)	GPS (96)	GPS (12)	GPS (12)	GPS (10)	RT-GPS (11)
IV	Taku Glacier (Camp 10)	T2 / EDM (16)	GPS (19)	GPS (27)	GPS (31)	RT-GPS (31)	RT-GPS (31)
IV a	Taku Glacier (Icy Basin)	–	GPS (6)	–	–	GPS (8)	–
IV b	Taku Glacier (North Basin)	–	–	–	–	–	–
V	SW-Branch Taku Glacier	T2 / EDM (12)	GPS (8)	GPS (12)	GPS (12)	RT-GPS (12)	RT-GPS (12)
V a	Upper SW-Branch Taku Glacier	–	–	–	–	–	–
VI	NW-Branch Taku Glacier (Echo Mountain)	–	GPS (9)	–	–	–	–
VI a	NW-Branch Taku Glacier (Taku D)	T2 / EDM (12)	–	GPS (16)	GPS (16)	GPS (10)	RT-GPS (14)
VII	Lower Matthes Glacier (Camp 9)	–	–	–	T2 / EDM (9)	–	GPS (14)
VII a	Lower Matthes Glacier (Taku C)	–	–	GPS (14)	GPS (14)	GPS (13)	RT-GPS 16)
VIII	Upper Matthes Glacier	–	–	GPS (13)	T2 / EDM (14)	GPS (12)	RT-GPS (12)
VIII a	Matthes / Vaughan-Lewis Glacier Divide	–	–	–	–	GPS (8)	–
IX	Upper Vaughan-Lewis Glacier	–	–	–	T2 / EDM (10)	GPS (7)	RT-GPS (8)
X	Matthes / Llewellyn Glacier Divide	–	–	–	–	GPS (16)	RT-GPS (14)
XI	Llewellyn Glacier	–	–	–	–	GPS (11)	–
A	Gilkey Trench (Unnamed Glacier)	T2 / EDM (3)	–	T2 / EDM (3)	–	–	–
B	Gilkey Trench (Trench Traverse)	T2 / EDM (6)	T2 / EDM (11)	T2 / EDM (13)	T2 / EDM (12)	–	–
C	Gilkey Trench (Gilkey Glacier Curve)	T2 / EDM (1)	T2 / EDM (3)	T2 / EDM (5)	T2 / EDM (1)	–	–
D	Gilkey Trench (Upper Gilkey Glacier)	–	T2 / EDM (9)	T2 / EDM (9)	T2 / EDM (9)	GPS (6)	–
E	Gilkey Trench (Little Vaughan-Lewis Gl.)	T2 / EDM (3)	T2 / EDM (3)	T2 / EDM (3)	T2 / EDM (2)	GPS (7)	–
F	Gilkey Trench (Vaughan-Lewis Glacier)	T2 / EDM (4)	T2 / EDM (2)	T2 / EDM (4)	–	–	–

Appendix B

Movement Vectors

Abbreviations:

Pt	=	Point-Number
East.	=	Easting
North.	=	Northing
Veloc.	=	Velocity
Bear.	=	Bearing

Profile I

Taku Glacier – Terminus

Epoch 0: 01.08.1994
Epoch 1: 02.08.1994

Pt	East. y [m]	North. x [m]	Veloc. [m/day]	Bear. [gon]
1	494202.59	6480523.85	0.30	204.86
2	494428.60	6480622.76	0.44	185.97
3	494593.53	6480714.81	0.66	171.96
4	494864.59	6480865.87	0.81	168.17
5	495068.47	6480979.69	0.91	171.17
6	495243.33	6481055.13	0.82	165.06
7	495481.14	6481184.55	0.86	161.51
8	495690.54	6481274.55	0.80	156.13

Pt	East. y [m]	North. x [m]	Veloc. [m/day]	Bear. [gon]
9	495960.18	6481439.30	0.80	158.12
10	496285.80	6481626.19	0.60	161.63
11	496508.09	6481697.42	0.19	157.80
21	494145.13	6480455.64	0.34	185.88
22	494103.29	6480417.76	0.11	171.22
23	494076.20	6480386.36	0.04	228.06
24	494052.50	6480460.04	0.07	201.06

Profile II

Taku Glacier – Goat Ridge

Epoch 0: 23.07.1993
Epoch 1: 27.07.1993

Pt	East. y [m]	North. x [m]	Veloc. [m/day]	Bear. [gon]
1	492680.84	6494031.31	0.65	188.35
2	492463.66	6494020.18	0.74	186.56
3	492265.98	6493951.42	0.80	186.55
4	492127.35	6493904.85	0.82	186.55
5	491991.67	6493859.91	0.84	185.91

Pt	East. y [m]	North. x [m]	Veloc. [m/day]	Bear. [gon]
6	491768.15	6493871.41	0.84	185.92
7	491555.07	6493837.98	0.85	186.11
8	491337.85	6493763.77	0.85	184.16
9	491088.04	6493569.14	0.84	182.34
10	490931.13	6493395.17	0.80	181.21

Epoch 0: 03.08.1994
Epoch 1: 07.08.1994

Pt	East. y [m]	North. x [m]	Veloc. [m/day]	Bear. [gon]
1	493221.51	6492499.94	0.57	177.12
2	493039.31	6492605.95	0.69	182.78
3	492814.38	6492500.29	0.83	183.04
4	492592.09	6492441.78	0.83	182.59
5	492404.72	6492385.76	0.90	173.03
6	492153.15	6492273.13	0.92	180.66

Pt	East. y [m]	North. x [m]	Veloc. [m/day]	Bear. [gon]
7	491825.55	6492148.04	0.93	181.10
8	491579.25	6492064.46	0.91	179.51
9	491446.40	6492025.04	0.91	181.31
10	491291.10	6491990.37	0.87	181.89
11	491071.25	6491905.28	0.74	176.43

Profile III

Demorest Glacier

Epoch 0: 19.07.1987
Epoch 1: 10.08.1987

Pt	East. y [m]	North. x [m]	Veloc. [m/day]	Bear. [gon]
1	494202.59	6480523.85	0.30	204.86
2	494428.60	6480622.76	0.44	185.97
3	494593.53	6480714.81	0.66	171.96
4	494864.59	6480865.87	0.81	168.17
5	495068.47	6480979.69	0.91	171.17

Pt	East. y [m]	North. x [m]	Veloc. [m/day]	Bear. [gon]
6	492906.74	6500222.01	0.28	252.86
7	493139.43	6499989.45	0.25	252.93
8	493371.38	6499757.59	0.22	252.97
9	493604.81	6499524.33	0.22	252.90

Epoch 0: 31.07.1991
Epoch 1: 06.08.1991

Pt	East. y [m]	North. x [m]	Veloc. [m/day]	Bear. [gon]
1	491757.37	6501145.98	0.02	178.24
2	491991.64	6500950.05	0.14	265.49
3	492269.81	6500717.49	0.22	266.38
4	492549.65	6500483.86	0.25	263.77
5	492713.13	6500346.43	0.26	264.00
6	492852.54	6500229.86	0.25	271.50
7	492976.12	6500126.21	0.26	268.74

Pt	East. y [m]	North. x [m]	Veloc. [m/day]	Bear. [gon]
8	493127.92	6499999.76	0.25	271.51
9	493269.20	6499880.18	0.25	270.11
10	493363.14	6499800.82	0.24	270.27
11	493524.30	6499666.08	0.22	270.67
12	493683.80	6499534.86	0.18	262.65
13	493860.99	6499376.70	0.13	264.74
14	493995.65	6499273.76	0.12	256.97

Epoch 0: 27.07.1992
Epoch 1: 30.07.1992

Pt	East. y [m]	North. x [m]	Veloc. [m/day]	Bear. [gon]
1	493950.63	6499477.90	0.20	260.42
2	493489.86	6499812.68	0.31	269.71
3	493070.35	6500111.39	0.34	268.17

Pt	East. y [m]	North. x [m]	Veloc. [m/day]	Bear. [gon]
4	492649.45	6500411.33	0.35	263.22
5	492169.66	6500752.00	0.27	260.68
6	491753.38	6501047.92	0.10	263.43

Epoch 0: 18.07.1993
Epoch 1: 24.07.1993

Pt	East. y [m]	North. x [m]	Veloc. [m/day]	Bear. [gon]
1	491627.15	6501358.29	0.01	245.76
2	491892.37	6501124.84	0.09	261.49
3	492200.78	6500861.40	0.20	263.19
4	492485.33	6500614.48	0.25	264.90
5	492804.26	6500336.75	0.27	268.21
6	493086.37	6500092.50	0.25	273.38

Pt	East. y [m]	North. x [m]	Veloc. [m/day]	Bear. [gon]
7	493375.02	6499845.31	0.25	271.84
8	493683.73	6499583.38	0.21	268.33
9	493970.14	6499333.30	0.12	256.15
10	494079.79	6499236.90	0.09	255.70
11	494158.65	6499169.22	0.07	246.22

Epoch 0: 29.07.1994
Epoch 1: 04.08.1994

Pt	East. y [m]	North. x [m]	Veloc. [m/day]	Bear. [gon]
1	492008.53	6500844.14	0.18	259.65
2	492188.58	6500680.10	0.23	267.20
3	492352.07	6500526.13	0.25	259.46
4	492481.11	6500404.39	0.25	260.79
5	492602.00	6500291.38	0.28	266.40
6	492727.71	6500172.99	0.25	265.91

Pt	East. y [m]	North. x [m]	Veloc. [m/day]	Bear. [gon]
7	492856.33	6500051.56	0.26	263.66
8	493009.34	6499907.19	0.28	263.26
9	493174.86	6499752.12	0.27	258.57
10	493327.23	6499608.75	0.20	262.95
11	493448.16	6499495.37	0.22	259.42
12	493616.33	6499336.19	0.17	256.40

Epoch 0: 17.07.1995
Epoch 1: 25.07.1995

Pt	East. y [m]	North. x [m]	Veloc. [m/day]	Bear. [gon]
1	491649.71	6501295.79	0.02	303.22
2	491985.89	6501039.63	0.11	266.84
3	492269.85	6500824.96	0.20	266.33
4	492528.26	6500632.69	0.26	268.17
5	492817.76	6500395.91	0.24	270.74

Pt	East. y [m]	North. x [m]	Veloc. [m/day]	Bear. [gon]
6	493236.35	6500095.00	0.24	273.63
7	493541.45	6499876.64	0.24	274.52
8	493800.02	6499652.18	0.19	270.21
9	494056.86	6499454.33	0.15	267.09
10	494291.46	6499316.24	0.09	268.02

Epoch 0: 27.07.1996
Epoch 1: 05.08.1996

Pt	East. y [m]	North. x [m]	Veloc. [m/day]	Bear. [gon]
2	491622.28	6500706.58	0.12	255.48
3	491838.29	6500570.26	0.19	257.21
4	492084.71	6500413.64	0.24	256.91
5	492303.59	6500277.52	0.27	258.57

Pt	East. y [m]	North. x [m]	Veloc. [m/day]	Bear. [gon]
6	492521.82	6500139.11	0.27	259.62
7	492744.87	6500000.97	0.26	261.38
8	492974.77	6499866.20	0.27	264.49
9	493183.57	6499745.08	0.28	248.78

Profile IV

Taku Glacier – Camp 10

Epoch 0: 16.07.1986
Epoch 1: 25.07.1986

Pt	East. y [m]	North. x [m]	Veloc. [m/day]	Bear. [gon]
1	487694.87	6503132.31	0.01	189.36
2	487533.84	6503047.81	0.02	179.66
3	487284.63	6502916.26	0.08	156.79
4	487028.03	6502779.25	0.27	145.39
5	486756.03	6502632.47	0.44	147.72
6	486476.69	6502480.16	0.56	144.14
7	486254.31	6502356.25	0.57	146.34
8	486008.41	6502218.54	0.62	142.44
9	485723.24	6502057.91	0.61	141.71

Pt	East. y [m]	North. x [m]	Veloc. [m/day]	Bear. [gon]
10	185454.83	6501904.55	0.60	141.46
11	485171.22	6501741.13	0.58	140.40
12	484896.35	6501580.69	0.57	140.15
13	484566.56	6501388.14	0.47	141.18
14	484261.75	6501206.82	0.28	141.43
15	484036.82	6501068.96	0.24	120.51
16	483788.91	6500916.33	0.21	116.48
17	483573.37	6500780.43	0.06	111.75
18	483382.17	6500656.95	0.04	91.61

Epoch 0: 21.07.1987
Epoch 1: 16.08.1987

Pt	East. y [m]	North. x [m]	Veloc. [m/day]	Bear. [gon]
1	487772.42	6502917.86	0.01	135.11
2	487680.19	6502768.05	0.02	135.09
3	487566.33	6502578.97	0.10	134.86
4	487424.21	6502348.40	0.31	134.78
5	487257.32	6502072.90	0.46	134.67
6	487124.53	6501855.59	0.56	134.66
7	486934.99	6501550.63	0.58	134.78
8	486779.36	6501299.57	0.58	134.85
9	486610.72	6501028.71	0.57	134.93

Pt	East. y [m]	North. x [m]	Veloc. [m/day]	Bear. [gon]
10	486467.03	6500784.63	0.58	134.82
11	486292.51	6500501.38	0.56	134.86
12	486108.75	6500202.09	0.51	134.89
13	485899.00	6499860.94	0.36	134.94
14	485692.40	6499521.20	0.16	134.96
15	485577.38	6499322.52	0.06	134.91
16	485431.11	6499096.44	0.01	135.00
17	485287.44	6498863.50	0.01	135.01
18	485137.35	6498617.32	0.01	135.01

Epoch 0: 19.07.1988
Epoch 1: 31.07.1988

Pt	East. y [m]	North. x [m]	Veloc. [m/day]	Bear. [gon]
1	487888.06	6503109.59	0.04	123.19
2	487635.74	6502707.99	0.05	113.34
3	487378.02	6502298.01	0.30	101.86
4	487172.72	6501971.08	0.51	115.81
5	486947.70	6501613.07	0.52	111.08
6	486735.03	6501275.42	0.57	106.47

Pt	East. y [m]	North. x [m]	Veloc. [m/day]	Bear. [gon]
7	486500.60	6500902.53	0.55	105.79
8	486266.43	6500528.78	0.54	105.45
9	486030.63	6500152.61	0.47	108.13
10	485821.63	6499821.23	0.33	101.99
11	485630.86	6499517.80	0.15	122.93
12	485434.03	6499205.63	0.12	72.30

Epoch 0: 23.07.1989
Epoch 1: 12.08.1989

Pt	East. y [m]	North. x [m]	Veloc. [m/day]	Bear. [gon]
1	487776.56	6503090.50	0.00	211.15
2	487568.66	6502912.93	0.03	149.24
3	487250.94	6502634.63	0.20	146.63
4	486852.54	6502288.60	0.49	146.48
5	486556.34	6502033.72	0.58	145.19
6	486227.10	6501751.02	0.59	143.01
7	485800.43	6501386.46	0.58	141.20

Pt	East. y [m]	North. x [m]	Veloc. [m/day]	Bear. [gon]
8	485473.22	6501105.82	0.55	140.89
9	485149.18	6500823.81	0.45	139.34
10	484809.52	6500528.92	0.26	136.98
11	484406.28	6500177.97	0.03	94.95
12	484051.02	6499867.31	0.02	391.04
13	483862.10	6499700.40	0.02	398.10
14	483690.55	6499550.30	0.01	389.49

Epoch 0: 20.07.1990
Epoch 1: 24.07.1990

Pt	East. y [m]	North. x [m]	Veloc. [m/day]	Bear. [gon]
1	487772.27	6503110.47	0.03	231.49
2	487633.09	6502996.43	0.03	216.15
3	487403.41	6502809.20	0.09	153.25
4	487161.27	6502609.10	0.25	156.60
5	486831.82	6502334.68	0.48	148.40
6	486512.43	6502068.69	0.57	146.98

Pt	East. y [m]	North. x [m]	Veloc. [m/day]	Bear. [gon]
7	486149.83	6501766.15	0.58	144.89
8	485806.27	6501479.51	0.62	142.45
9	485418.12	6501155.41	0.53	141.76
10	485022.21	6500816.37	0.41	141.56
11	484668.53	6500516.11	0.20	139.48
12	484139.54	6500066.18	0.04	328.98

Epoch 0: 20.07.1991
Epoch 1: 30.07.1991

Pt	East. y [m]	North. x [m]	Veloc. [m/day]	Bear. [gon]
1	487859.94	6503172.40	0.00	162.21
2	487709.91	6503042.58	0.01	162.74
3	487449.15	6502820.48	0.06	149.65
4	487235.39	6502635.32	0.21	149.07
5	487075.81	6502496.85	0.36	147.85
6	486924.05	6502368.26	0.47	146.58
7	486563.16	6502065.78	0.57	144.93
8	486323.56	6501864.15	0.60	143.89

Pt	East. y [m]	North. x [m]	Veloc. [m/day]	Bear. [gon]
9	486126.13	6501698.30	0.60	142.49
10	485754.89	6501382.59	0.59	140.91
11	485554.82	6501214.73	0.58	140.25
12	485296.71	6500999.00	0.52	139.41
13	484999.43	6500752.18	0.40	137.31
14	484727.17	6500520.31	0.23	135.26
15	484406.06	6500246.19	0.05	118.65
16	484076.14	6499965.09	0.02	28.07

Epoch 0: 20.07.1992
Epoch 1: 30.07.1992

Pt	East. y [m]	North. x [m]	Veloc. [m/day]	Bear. [gon]
1	487675.94	6502887.32	0.01	132.46
2	487421.20	6502665.15	0.12	150.10
3	487078.70	6502365.78	0.41	146.84
4	486765.63	6502091.87	0.56	144.60
5	486386.42	6501760.17	0.60	144.16
6	486020.24	6501439.55	0.60	142.47
7	485667.04	6501129.73	0.58	140.53
8	485286.03	6500796.01	0.50	139.81
9	484916.65	6500473.00	0.27	135.34
10	484561.87	6500161.54	0.06	103.49

Pt	East. y [m]	North. x [m]	Veloc. [m/day]	Bear. [gon]
21	487421.40	6502664.98	0.12	144.36
22	487992.26	6502479.63	0.05	148.38
23	487511.64	6502068.72	0.38	147.59
51	486387.72	6501759.11	0.59	144.42
52	486905.26	6501583.14	0.60	146.72
53	486498.41	6501253.50	0.61	144.85
81	485287.25	6500795.15	0.50	140.32
82	485739.96	6500659.05	0.55	142.39
83	485381.37	6500402.51	0.44	140.29

Epoch 0: 20.07.1993
Epoch 1: 25.07.1993

Pt	East. y [m]	North. x [m]	Veloc. [m/day]	Bear. [gon]
1	487744.56	6503055.27	0.01	118.93
2	487527.41	6503206.82	0.01	183.92
3	487601.28	6502925.74	0.03	131.60
4	487380.24	6503056.89	0.03	146.80
5	487454.30	6502792.82	0.08	146.57
6	487219.22	6502892.96	0.11	147.18
7	487266.74	6502623.41	0.20	145.92
8	487079.49	6502750.06	0.23	147.14
9	487088.98	6502462.43	0.37	146.92
10	486936.25	6502604.40	0.37	145.80
11	486955.35	6502341.58	0.47	146.60
12	486755.08	6502418.96	0.49	146.67
13	486716.64	6502125.00	0.56	145.93
14	486483.75	6502199.05	0.56	144.92

Pt	East. y [m]	North. x [m]	Veloc. [m/day]	Bear. [gon]
15	486484.70	6501915.58	0.59	144.83
16	486222.78	6501971.82	0.59	143.71
17	486193.39	65011651.59	0.61	142.69
18	485891.84	6501670.77	0.61	141.35
19	485916.03	6501399.69	0.60	141.77
20	485639.95	6501442.83	0.60	141.25
21	485636.64	6501145.95	0.58	140.68
22	485391.51	6501220.81	0.57	140.69
23	485397.77	6500929.20	0.54	141.81
24	485121.57	6500992.81	0.51	140.23
25	485110.39	6500667.97	0.43	139.35
26	484859.27	6500778.01	0.37	138.46
27	484829.92	6500413.74	0.23	134.23

Epoch 0: 25.07.1994
Epoch 1: 05.08.1994

Pt	East. y [m]	North. x [m]	Veloc. [m/day]	Bear. [gon]
1	487748.99	6503059.37	0.01	100.45
2	487530.75	6503207.33	0.01	160.66
3	487602.77	6502928.86	0.03	139.46
4	487382.45	6503057.31	0.03	148.63
5	487456.53	6502794.94	0.07	148.31
6	487221.13	6502893.38	0.11	146.69
7	487269.14	6502623.88	0.24	144.38
8	487081.49	6502750.09	0.22	147.31
9	487091.15	6502462.93	0.42	122.76
10	486938.67	6502604.11	0.37	145.90
11	486957.84	6502341.30	0.59	151.03
12	486757.36	6502418.18	0.50	146.83
13	486719.01	6502124.47	0.56	146.34
14	486486.48	6502198.37	0.56	144.68
15	486487.11	6501914.71	0.59	144.47
16	486225.43	6501970.73	0.59	143.32

Pt	East. y [m]	North. x [m]	Veloc. [m/day]	Bear. [gon]
17	486195.69	6501650.87	0.60	143.03
18	485894.03	6501669.24	0.60	140.74
19	485918.48	6501398.57	0.60	141.89
20	485641.70	6501440.83	0.59	141.72
21	485639.31	6501144.52	0.58	141.40
22	485394.29	6501219.53	0.57	140.32
23	485474.50	6500995.26	0.56	139.70
24	485123.63	6500991.16	0.51	139.99
25	485112.70	6500666.67	0.43	139.35
26	484861.29	6500777.08	0.37	139.29
27	484831.97	6500413.09	0.22	132.95
28	484511.97	6500493.92	0.15	134.47
29	484572.81	6500179.08	0.05	117.60
30	484251.47	6500282.03	0.04	117.85
31	484323.80	6499953.17	0.02	54.07

Epoch 0: 20.07.1995
Epoch 1: 28.07.1995

Pt	East. y [m]	North. x [m]	Veloc. [m/day]	Bear. [gon]
1	487743.55	6503056.14	0.03	97.82
2	487528.41	6503206.26	0.01	184.40
3	487602.07	6502925.20	0.03	130.68
4	487379.73	6503057.23	0.05	146.97
5	487453.69	6502792.80	0.08	152.36
6	487222.00	6502890.74	0.12	143.71
7	487267.13	6502623.70	0.20	145.75
8	487085.97	6502746.55	0.21	147.55
9	487091.30	6502466.82	0.37	145.37
10	486936.64	6502602.23	0.38	149.61
11	486957.20	6502341.18	0.46	145.12
12	486756.73	6502417.72	0.51	145.80
13	486716.33	6502123.84	0.55	145.15
14	486484.48	6502197.61	0.58	142.66
15	486483.74	6501913.90	0.61	145.15
16	486223.46	6501970.00	0.59	146.04
17	486195.81	6501649.16	0.61	143.13
18	485892.97	6501668.95	0.60	143.28
19	485918.79	6501396.57	0.59	141.22
20	485641.42	6501439.73	0.58	140.82
21	485640.91	6501145.93	0.57	139.46
22	485392.60	6501217.95	0.59	141.36
23	485397.04	6500926.53	0.56	139.60
24	485125.78	6500988.69	0.52	142.83
25	485111.78	6500666.61	0.44	137.92
26	484860.76	6500776.90	0.36	143.93
27	484836.50	6500415.01	0.23	134.28
28	484511.80	6500494.14	0.15	140.31
29	484572.95	6500178.02	0.07	114.73
30	484251.32	6500281.15	0.04	141.80
31	484324.05	6499953.28	0.02	18.78

Epoch 0: 28.07.1996
Epoch 1: 06.08.1996

Pt	East. y [m]	North. x [m]	Veloc. [m/day]	Bear. [gon]
1	487743.29	6503056.32	0.01	84.95
2	487528.44	6503206.25	0.02	172.54
3	487602.16	6502925.23	0.03	150.62
4	487379.73	6503057.16	0.03	143.14
5	487453.57	6502792.80	0.08	141.64
6	487221.96	6502890.76	0.10	156.12
7	487266.97	6502623.64	0.20	147.62
8	487085.98	6502746.55	0.21	147.34
9	487091.22	6502466.75	0.37	146.43
10	486936.67	6502602.24	0.36	149.08
11	486956.99	6502341.32	0.43	139.58
12	486756.74	6502417.69	0.48	147.17
13	486716.26	6502123.81	0.54	145.56
14	486484.47	6502197.63	0.57	145.32
15	486483.71	6501913.88	0.58	145.10
16	486223.44	6501969.96	0.59	143.31
17	486195.71	6501649.16	0.59	143.57
18	485892.99	6501668.96	0.60	141.76
19	485918.79	6501396.58	0.59	142.23
20	485641.48	6501439.75	0.59	141.10
21	485640.79	6501145.93	0.64	137.89
22	485392.65	6501217.98	0.56	140.98
23	485397.00	6500926.43	0.55	140.64
24	485125.73	6500988.64	0.50	140.03
25	485111.80	6500666.46	0.41	132.95
26	484860.73	6500776.84	0.38	138.76
27	484836.39	6500414.97	0.21	94.19
28	484511.96	6500494.12	0.15	134.53
29	484572.82	6500178.54	0.06	118.04
30	484251.43	6500281.25	0.04	117.91
31	484324.15	6499953.24	0.02	48.20

Profile V

SW-Branch Taku Glacier

Epoch 0: 20.07.1986
Epoch 1: 27.07.1986

Pt	East. y [m]	North. x [m]	Veloc. [m/day]	Bear. [gon]
1	486991.18	6496351.60	0.08	36.80
2	486901.43	6496466.04	0.08	36.65
3	486777.77	6496623.21	0.10	36.19
4	486681.20	6496743.88	0.11	37.82
5	486556.07	6496899.91	0.12	42.25
6	486452.62	6497026.70	0.11	40.87
7	486348.52	6497153.00	0.12	41.24

Pt	East. y [m]	North. x [m]	Veloc. [m/day]	Bear. [gon]
8	486232.51	6497293.04	0.11	46.29
9	486121.46	6497425.39	0.09	41.54
10	486026.79	6497535.91	0.09	56.84
11	485908.79	6497674.32	0.08	52.72
12	485795.80	6497805.07	0.04	30.96
13	485676.42	6497942.33	0.,03	91.36

Epoch 0: 20.07.1987
Epoch 1: 18.08.1987

Pt	East. y [m]	North. x [m]	Veloc. [m/day]	Bear. [gon]
1	487159.44	6495979.95	0.01	56.58
2	486872.94	6496100.96	0.05	47.32
3	486588.56	6496219.24	0.08	48.01
4	486303.40	6496338.30	0.08	48.47
5	486012.37	6496453.65	0.08	48.34

Pt	East. y [m]	North. x [m]	Veloc. [m/day]	Bear. [gon]
6	485701.68	6496573.73	0.09	46.98
7	485420.70	6496681.86	0.08	48.97
8	485135.31	6496787.01	0.06	47.23
9	484857.38	6496872.81	0.01	259.14

Epoch 0: 20.07.1988
Epoch 1: 28.07.1988

Pt	East. y [m]	North. x [m]	Veloc. [m/day]	Bear. [gon]
1	487043.06	6495813.98	0.01	366.71
2	486680.54	6495699.47	0.07	22.84
3	486234.20	6495555.90	0.09	17.03
4	485776.67	6495405.69	0.11	32.67
5	485289.94	6495242.84	0.08	41.18

Pt	East. y [m]	North. x [m]	Veloc. [m/day]	Bear. [gon]
6	484912.62	6495112.37	0.09	48.95
7	484463.92	6494955.67	0.09	50.02
8	484118.36	6494830.26	0.01	23.83
9	483641.46	6494658.10	0.01	19.64
10	483369.53	6494552.47	0.01	185.22

Epoch 0: 24.07.1989
Epoch 1: 11.08.1989

Pt	East. y [m]	North. x [m]	Veloc. [m/day]	Bear. [gon]
1	485367.94	6497294.40	0.09	7.02
2	485527.01	6497174.30	0.13	8.54
3	485684.50	6497056.03	0.15	18.83
4	485843.82	6496936.52	0.15	19.48
5	485988.27	6496828.15	0.15	14.51
6	486103.82	6496740.96	0.15	11.96
7	486214.48	6496657.16	0.15	11.84

Pt	East. y [m]	North. x [m]	Veloc. [m/day]	Bear. [gon]
8	486333.49	6496567.43	0.15	14.24
9	486432.08	6496492.86	0.14	14.50
10	486549.38	6496404.04	0.14	13.68
11	486669.20	6496313.05	0.13	15.64
12	486779.70	6496229.30	0.12	9.86
13	486897.22	6496140.23	0.11	10.21
14	487021.47	6496045.96	0.10	10.99

Epoch 0: 20.07.1990
Epoch 1: 30.07.1990

Pt	East. y [m]	North. x [m]	Veloc. [m/day]	Bear. [gon]
1	487094.56	6495897.41	0.01	57.48
2	486962.67	6495895.27	0.02	236.69
3	486767.01	6495889.21	0.03	55.50
4	486506.86	6495880.63	0.09	60.54
5	486337.03	6495876.05	0.07	41.44
6	486138.45	6495869.66	0.09	36.46

Pt	East. y [m]	North. x [m]	Veloc. [m/day]	Bear. [gon]
7	485919.29	6495861.37	0.08	66.35
8	485663.44	6495852.21	0.07	55.32
9	485382.14	6495843.07	0.07	94.35
10	485108.52	6495831.77	0.07	93.63
11	484748.56	6495820.54	0.07	118.21
12	484276.21	6495807.22	0.07	97.99

Epoch 0: 21.07.1991
Epoch 1: 30.07.1991

Pt	East. y [m]	North. x [m]	Veloc. [m/day]	Bear. [gon]
1	485652.46	649737.56	0.02	104.32
2	485827.12	6497746.92	0.06	75.38
3	486020.82	6497524.85	0.08	53.19
4	486234.57	6497272.01	0.10	55.56
5	486394.65	6497082.58	0.10	52.32
6	486562.34	6496884.17	0.10	45.66

Pt	East. y [m]	North. x [m]	Veloc. [m/day]	Bear. [gon]
7	486700.30	6496720.83	0.10	51.54
9	486943.39	6496432.70	0.08	50.00
10	487044.27	6496313.45	0.07	69.80
11	487142.66	6496197.43	0.04	72.32
12	487204.97	6496119.15	0.04	135.52

Epoch 0: 21.07.1992
Epoch 1: 28.07.1992

Pt	East. y [m]	North. x [m]	Veloc. [m/day]	Bear. [gon]
1	487241.85	6496138.37	0.00	6.14
2	487102.27	6496297.04	0.04	32.71
3	486894.98	6496532.54	0.07	36.62
4	486674.03	6496783.50	0.09	38.16

Pt	East. y [m]	North. x [m]	Veloc. [m/day]	Bear. [gon]
5	486444.46	6497044.04	0.09	38.91
6	486200.62	6497321.12	0.09	41.84
7	485973.30	6497579.49	0.07	37.85
8	485766.12	6497814.73	0.03	35.50

Epoch 0: 18.07.1993
Epoch 1: 27.07.1993

Pt	East. y [m]	North. x [m]	Veloc. [m/day]	Bear. [gon]
1	485904.84	6497939.63	0.03	50.64
2	486018.54	6497780.71	0.06	43.69
3	486129.71	6497624.84	0.07	40.27
4	486232.88	6497479.82	0.09	43.99
5	486334.68	6497337.13	0.09	45.04
6	486440.62	6497188.25	0.09	39.54

Pt	East. y [m]	North. x [m]	Veloc. [m/day]	Bear. [gon]
7	486527.47	6497066.15	0.09	40.52
8	486600.77	6496963.14	0.09	38.95
9	486688.38	6496839.95	0.08	40.04
10	486791.68	6496695.35	0.08	36.70
11	486890.18	6496568.88	0.08	39.02
12	487019.02	6496378.49	0.06	27.35

Epoch 0: 27.07.1994
Epoch 1: 04.08.1994

Pt	East. y [m]	North. x [m]	Veloc. [m/day]	Bear. [gon]
1	485737.86	6498029.87	0.01	77.53
2	485856.69	6497873.81	0.03	68.72
3	485965.47	6497730.93	0.06	54.11
4	486107.25	6497545.01	0.08	41.55
5	486272.26	6497352.22	0.09	40.28
6	486448.91	6497147.68	0.09	42.50

Pt	East. y [m]	North. x [m]	Veloc. [m/day]	Bear. [gon]
7	486583.24	6496990.88	0.09	35.94
8	486691.20	6496865.61	0.08	32.45
9	486806.21	6496732.04	0.08	33.34
10	486901.96	6496619.54	0.08	37.90
11	487008.34	6496491.02	0.06	34.09
12	487117.33	6496357.61	0.04	35.08

Epoch 0: 23.07.1995
Epoch 1: 29.07.1995

Pt	East. y [m]	North. x [m]	Veloc. [m/day]	Bear. [gon]
1	485734.86	6498030.01	0.04	43.74
2	485859.28	6497874.66	0.05	49.54
3	485960.97	6497734.65	0.10	43.65
4	486104.91	6497545.45	0.08	53.87
5	486272.93	6497352.04	0.10	42.25
6	486450.13	6497147.01	0.11	28.32

Pt	East. y [m]	North. x [m]	Veloc. [m/day]	Bear. [gon]
7	486577.60	6496992.74	0.11	43.36
8	486689.74	6496863.60	0.11	55.07
9	486805.65	6496732.15	0.13	55.26
10	486904.41	6496621.48	0.05	67.81
11	487011.86	6496489.18	0.05	42.66
12	487116.98	6496357.22	0.04	74.35

Epoch 0: 30.07.1996
Epoch 1: 05.08.1996

Pt	East. y [m]	North. x [m]	Veloc. [m/day]	Bear. [gon]
1	485618.93	6497859.22	0.01	55.63
4	486082.02	6497366.49	0.08	42.67
5	486235.98	6497193.25	0.11	31.59
6	486386.19	6497026.00	0.10	29.61
7	486534.09	6496857.61	0.09	41.78

Pt	East. y [m]	North. x [m]	Veloc. [m/day]	Bear. [gon]
8	486681.37	6496687.03	0.08	35.03
9	486827.60	6496515.08	0.05	24.54
10	486922.86	6496403.60	0.06	20.36
11	487014.75	6496295.53	0.07	43.49
12	487103.90	6496195.40	0.03	34.99

Profile Va

Upper SW-Branch Taku Glacier

Epoch 0: 26.07.1989
Epoch 1: 11.08.1989

Pt	East. y [m]	North. x [m]	Veloc. [m/day]	Bear. [gon]
1	484655.76	6496683.60	0.01	159.02
2	484780.26	6496472.73	0.03	147.74
3	484886.66	6496345.44	0.06	104.82
4	484971.40	6496272.63	0.05	74.56
5	485108.45	6496149.10	0.06	78.34

Pt	East. y [m]	North. x [m]	Veloc. [m/day]	Bear. [gon]
6	485329.27	6495968.03	0.07	50.71
7	485562.92	6495772.79	0.07	47.03
8	485782.11	6495570.24	0.08	50.19
9	485979.17	6495386.86	0.07	42.06
10	486222.84	6495161.20	0.04	55.79

Profile VI

NW-Branch Taku Glacier – Echo Mountain

Epoch 0: 23.07.1986
Epoch 1: 19.08.1986

Pt	East. y [m]	North. x [m]	Veloc. [m/day]	Bear. [gon]
1	479282.25	6505451.20	0.05	119.53
2	479359.99	6505703.09	0.04	119.31
3	479444.55	6505981.41	0.06	119.16
4	479530.39	6506268.85	0.11	119.01
5	479641.24	6506643.68	0.14	118.85
6	479750.24	6507019.07	0.14	118.68
8	479960.09	6507762.76	0.19	118.36

Pt	East. y [m]	North. x [m]	Veloc. [m/day]	Bear. [gon]
9	480094.22	6508244.44	0.22	118.21
10	480187.96	6508595.85	0.20	118.04
11	480297.55	6509008.89	0.17	117.87
12	480380.19	6509335.09	0.14	117.70
13	480446.41	6509609.21	0.09	117.53
14	480562.68	6510067.52	0.03	117.37
15	480681.57	6510543.94	0.02	317.20

Epoch 0: 27.07.1989
Epoch 1: 10.08.1989

Pt	East. y [m]	North. x [m]	Veloc. [m/day]	Bear. [gon]
1	477326.76	6509653.92	0.01	260.02
2	477436.05	6509365.69	0.02	161.15
3	477546.44	6509076.15	0.04	137.18
4	477642.83	6508822.99	0.09	114.92
5	477739.07	6508570.04	0.14	111.03
6	477839.86	6508305.04	0.21	103.64
7	477938.87	6508045.44	0.25	104.88
8	478041.70	6507776.24	0.26	106.23

Pt	East. y [m]	North. x [m]	Veloc. [m/day]	Bear. [gon]
9	478141.35	6507515.61	0.27	107.50
10	478246.66	6507239.48	0.27	108.64
11	478349.21	6506969.73	0.25	104.72
12	478453.22	6506696.63	0.25	104.30
13	478549.17	6506444.82	0.24	102.97
14	478648.52	6506183.68	0.21	103.82
15	478748.62	6505921.03	0.16	102.91
16	478846.76	6505662.76	0.08	85.07

Epoch 0: 22.07.1992
Epoch 1: 30.07.1992

Pt	East. y [m]	North. x [m]	Veloc. [m/day]	Bear. [gon]
1	477913.57	6509143.99	0.04	124.16
2	477908.95	6508763.05	0.10	106.94
3	477904.63	6508366.78	0.21	104.64
4	477899.54	6507941.45	0.27	104.70
5	477889.70	6507509.70	0.28	104.07

Pt	East. y [m]	North. x [m]	Veloc. [m/day]	Bear. [gon]
6	477880.79	6507097.98	0.27	105.29
7	477871.24	6506676.41	0.25	102.34
8	477859.34	6506176.01	0.20	97.52
9	477850.79	6505728.10	0.10	92.82

Profile VIa

NW-Branch Taku Glacier – Taku D

Epoch 0: 21.07.1990
Epoch 1: 10.08.1990

Pt	East. y [m]	North. x [m]	Veloc. [m/day]	Bear. [gon]
2	482016.53	6508320.36	0.03	346.36
3	481704.57	6507954.80	0.10	146.56
4	481472.16	6507683.78	0.20	146.73
5	481265.03	6507441.97	0.27	146.91
6	481006.57	6507138.62	0.29	147.21
7	480896.52	6507009.82	0.29	147.36
8	480736.48	6506822.68	0.28	147.61
9	480604.80	6506668.11	0.27	147.86

Pt	East. y [m]	North. x [m]	Veloc. [m/day]	Bear. [gon]
10	480481.13	6506523.10	0.27	148.16
11	480393.87	6506420.98	0.26	148.40
12	480284.28	6506291.84	0.24	148.77
13	480205.97	6506199.42	0.24	149.10
14	480034.76	6505998.39	0.23	150.02
15	479813.28	6505736.84	0.17	152.08
16	479572.65	6505455.15	0.07	157.72

Epoch 0: 23.07.1991
Epoch 1: 06.08.1991

Pt	East. y [m]	North. x [m]	Veloc. [m/day]	Bear. [gon]
1	479554.60	6504940.10	0.04	182.41
2	479757.09	6504864.21	0.11	171.54
3	479988.45	6504808.00	0.15	189.88
4	480185.14	6504762.22	0.21	176.43
5	480382.19	6504716.56	0.22	177.69
6	480586.86	6504668.73	0.24	175.34
7	480721.68	6504637.44	0.25	174.95
8	480905.54	6504594.93	0.25	175.66

Pt	East. y [m]	North. x [m]	Veloc. [m/day]	Bear. [gon]
9	481072.79	6504555.98	0.26	175.66
10	481249.89	6504513.62	0.26	175.20
11	481432.93	6504470.54	0.27	176.65
12	481609.61	6504429.16	0.27	176.86
13	481799.19	6504384.60	0.27	176.98
14	482085.26	6504316.56	0.24	173.95
15	482383.46	6504246.04	0.19	166.93
16	482712.56	6504168.19	0.11	127.67

Epoch 0: 21.07.1993
Epoch 1: 28.07.1993

Pt	East. y [m]	North. x [m]	Veloc. [m/day]	Bear. [gon]
1	482089.89	6508682.79	0.01	162.91
2	481956.62	6508510.90	0.04	141.32
3	481811.30	6508322.89	0.07	143.71
4	481659.40	6508126.45	0.11	139.44
5	481516.50	16507938.05	0.16	134.38
6	481355.52	6507725.36	0.22	131.01
7	481219.26	6507545.25	0.27	130.26
8	481097.69	6507384.86	0.29	129.23

Pt	East. y [m]	North. x [m]	Veloc. [m/day]	Bear. [gon]
9	480952.34	6507193.00	0.31	127.79
10	480824.80	6507023.91	0.31	126.30
11	480675.41	6506825.54	0.31	125.41
12	480558.39	6506670.62	0.30	124.13
13	480442.99	6506517.94	0.29	122.92
14	480295.13	6506321.29	0.27	122.23
15	480174.41	6506160.51	0.26	122.53
16	480011.56	6505943.39	0.24	122.52

Epoch 0: 26.07.1994
Epoch 1: 06.08.1994

Pt	East. y [m]	North. x [m]	Veloc. [m/day]	Bear. [gon]
1	479586.89	6505441.31	0.10	120.52
3	479954.56	6505905.40	0.24	120.52
4	480144.84	6506140.40	0.25	123.75
5	480335.45	6506376.78	0.18	127.29
6	480526.90	6506612.95	0.30	123.56
7	480717.26	6506850.21	0.30	125.96
8	480893.77	6507070.43	0.32	126.90
9	481070.87	6507290.20	0.30	127.61

Pt	East. y [m]	North. x [m]	Veloc. [m/day]	Bear. [gon]
10	481244.91	6507506.30	0.28	128.28
11	481420.57	6507722.68	0.22	132.18
12	481597.02	6507940.19	0.15	132.72
13	481773.62	6508156.38	0.09	132.29
14	481951.75	6508374.41	0.04	135.96
15	482130.83	6508591.08	0.02	159.95
16	482197.48	6508673.09	0.01	101.89

Epoch 0: 18.07.1995
Epoch 1: 28.07.1995

Pt	East. y [m]	North. x [m]	Veloc. [m/day]	Bear. [gon]
1	481867.89	6508186.27	0.08	147.48
2	481627.51	6507877.25	0.17	134.58
3	481351.53	6507507.06	0.26	133.11
4	481133.17	6507214.25	0.31	129.56
5	480924.50	6506937.04	0.31	127.44

Pt	East. y [m]	North. x [m]	Veloc. [m/day]	Bear. [gon]
6	480669.84	6506599.50	0.29	126.60
7	480468.75	6506336.55	0.27	124.70
8	480252.52	6506055.15	0.26	123.43
9	480047.17	6505785.21	0.22	121.92
10	479852.39	6505506.44	0.12	120.62

Epoch 0: 29.07.1996
Epoch 1: 07.08.1996

Pt	East. y [m]	North. x [m]	Veloc. [m/day]	Bear. [gon]
1	482127.34	6508768.43	0.11	294.21
2	481950.50	6508541.22	0.03	143.52
3	481761.20	6508302.15	0.07	139.38
4	481575.85	6508070.17	0.12	133.39
5	481381.92	6507826.93	0.19	129.07
6	481185.85	6507582.16	0.28	134.61
7	481005.85	6507353.61	0.31	132.30

Pt	East. y [m]	North. x [m]	Veloc. [m/day]	Bear. [gon]
8	480819.78	6507117.22	0.31	126.11
9	480623.31	6506868.08	0.30	124.53
10	480438.27	6506638.98	0.29	122.36
11	480264.79	6506421.62	0.28	120.49
12	480075.30	6506177.62	0.24	126.93
13	479882.14	6505925.12	0.22	122.19
14	479715.38	6505720.95	0.19	119.73

Profile VII

Lower Matthes Glacier – Camp 9

Epoch 0: 28.07.1986
Epoch 1: 18.08.1986

Pt	East. y [m]	North. x [m]	Veloc. [m/day]	Bear. [gon]
1	488940.60	6510878.80	0.02	225.61
2	488647.72	6511003.01	0.02	225.58
3	488287.75	6511155.32	0.13	225.49
4	487944.35	6511300.12	0.31	225.40
5	487726.32	6511391.38	0.37	225.36
6	487600.32	6511443.48	0.38	225.33
7	487223.00	6511601.45	0.40	225.30

Pt	East. y [m]	North. x [m]	Veloc. [m/day]	Bear. [gon]
8	486971.16	6511706.05	0.41	225.28
9	486610.26	6511856.18	0.40	225.26
10	486391.68	6511946.07	0.37	225.23
11	486131.07	6512053.29	0.27	225.22
12	485761.34	6512205.83	0.15	225.21
13	485542.41	6512294.88	0.03	225.20

Epoch 0: 01.08.1987
Epoch 1: 10.08.1987

Pt	East. y [m]	North. x [m]	Veloc. [m/day]	Bear. [gon]
1	488939.57	6510946.10	0.01	232.44
2	488809.53	6511016.70	0.01	232.28
3	488671.23	6511091.11	0.02	232.12
4	488504.52	6511180.17	0.04	231.96
5	488338.24	6511267.96	0.11	231.79
6	488175.03	6511352.94	0.20	231.62
7	488019.32	6511432.88	0.30	231.45
8	487865.87	6511510.77	0.31	231.30
9	487717.29	6511584.92	0.33	231.14

Pt	East. y [m]	North. x [m]	Veloc. [m/day]	Bear. [gon]
10	487576.30	6511654.15	0.37	230.98
11	487382.77	6511750.24	0.38	230.82
12	487116.99	6511882.99	0.37	230.67
13	486917.07	6511979.65	0.34	230.52
14	486678.47	6512095.23	0.36	230.37
15	486473.09	6512192.25	0.33	230.21
16	486228.90	6512307.75	0.26	230.06
17	485944.00	6512442.49	0.19	229.91
18	485624.52	6512592.90	0.01	229.77

Epoch 0: 28.07.1989
Epoch 1: 05.08.1989

Pt	East. y [m]	North. x [m]	Veloc. [m/day]	Bear. [gon]
1	488718.56	6510926.35	0.02	324.57
2	488493.41	6511056.21	0.05	278.10
3	488294.75	6511170.57	0.10	259.40
4	488075.50	6511296.75	0.23	246.86
5	487852.54	6511424.66	0.28	247.95
6	487627.85	6511554.02	0.33	244.10
7	487395.67	6511678.32	0.32	245.43

Pt	East. y [m]	North. x [m]	Veloc. [m/day]	Bear. [gon]
8	487148.07	6511822.66	0.37	242.92
9	486958.09	6511932.22	0.33	243.32
10	486696.16	6512088.11	0.34	236.41
11	486528.62	6512185.18	0.33	238.44
12	486317.84	6512308.48	0.29	233.66
13	486113.26	6512427.04	0.27	228.12
14	485918.67	6512539.15	0.19	221.02

Epoch 0: 15.08.1990
Epoch 1: 18.08.1990

Pt	East. y [m]	North. x [m]	Veloc. [m/day]	Bear. [gon]
1	488881.85	6510623.99	0.02	195.34
2	488610.06	6510770.91	0.04	208.05
3	488348.52	6510896.04	0.17	213.23
5	487811.80	6511137.83	0.27	217.95
6	487550.13	6511240.69	0.36	218.78

Pt	East. y [m]	North. x [m]	Veloc. [m/day]	Bear. [gon]
7	487288.92	6511366.04	0.30	220.02
8	487075.60	6511485.82	0.35	221.24
9	486893.57	6511592.46	0.32	222.20
10	486827.34	6511629.85	0.31	222.49

Epoch 0: 10.08.1994
Epoch 1: 13.08.1994

Pt	East. y [m]	North. x [m]	Veloc. [m/day]	Bear. [gon]
1	488866.47	6510996.97	0.02	347.72
2	488573.87	6511156.24	0.04	263.80
3	488245.04	6511336.16	0.17	263.13
4	487873.47	6511539.38	0.33	240.94
5	487552.62	6511714.24	0.23	249.57

Pt	East. y [m]	North. x [m]	Veloc. [m/day]	Bear. [gon]
6	487257.66	6511875.91	0.34	240.51
7	486980.92	6512026.70	0.32	239.56
8	486682.95	6512188.69	0.31	235.37
9	486488.68	6512294.89	0.15	242.62

Epoch 0: 29.07.1996
Epoch 1: 06.08.1996

Pt	East. y [m]	North. x [m]	Veloc. [m/day]	Bear. [gon]
1	489081.76	6510948.61	0.01	320.22
2	489007.10	6510989.09	0.02	315.49
3	488875.59	6511059.34	0.02	302.87
4	488742.07	6511131.09	0.02	287.17
5	488520.95	6511249.39	0.05	263.23
6	488305.85	6511364.04	0.13	244.82
7	488075.24	6511486.36	0.24	242.30
8	487839.93	6511611.35	0.31	241.49

Pt	East. y [m]	North. x [m]	Veloc. [m/day]	Bear. [gon]
9	487614.25	6511731.63	0.32	241.89
10	487386.39	6511854.29	0.33	239.42
11	487147.45	6511982.43	0.33	237.65
12	486912.73	6512107.86	0.34	236.27
13	486677.87	6512231.64	0.32	235.70
14	486445.85	6512251.11	0.30	233.60
15	486214.45	6512478.15	0.23	226.48
16	485980.54	6512606.29	0.15	216.63

Profile VIIa

Lower Matthes Glacier – Taku C

Epoch 0: 22.07.1993
Epoch 1: 29.07.1993

Pt	East. y [m]	North. x [m]	Veloc. [m/day]	Bear. [gon]
1	483189.45	6509304.89	0.09	41.07
2	483415.72	6509124.21	0.07	255.79
3	483619.83	6508963.84	0.21	248.66
4	483849.69	6508782.31	0.32	248.60
5	484075.37	6508603.49	0.38	249.77
6	484285.97	6508435.08	0.41	249.52
7	484480.04	6508280.78	0.42	249.64

Pt	East. y [m]	North. x [m]	Veloc. [m/day]	Bear. [gon]
8	484648.10	6508146.76	0.42	250.75
9	484809.91	6508017.43	0.42	250.57
10	484980.44	6507882.00	0.40	250.31
11	485156.76	6507742.34	0.37	250.42
12	485340.14	6507597.57	0.31	249.50
13	485555.24	6507428.08	0.18	248.05
14	485728.50	6507289.35	0.04	279.21

Epoch 0: 26.07.1994
Epoch 1: 06.08.1994

Pt	East. y [m]	North. x [m]	Veloc. [m/day]	Bear. [gon]
1	483084.21	6509157.48	0.01	109.20
2	483262.56	6509025.79	0.04	251.91
3	483442.96	6508892.97	0.16	244.02
4	483640.69	6508745.60	0.27	247.22
5	483825.11	6508609.38	0.34	247.68
6	484006.00	6508474.98	0.36	249.18
7	484185.51	6508342.99	0.41	246.42

Pt	East. y [m]	North. x [m]	Veloc. [m/day]	Bear. [gon]
8	484362.25	6508212.15	0.43	247.71
9	484540.75	6508081.32	0.43	249.77
10	484722.18	6507949.72	0.43	248.08
11	484902.15	6507816.27	0.41	247.49
12	485081.46	6507683.26	0.38	250.39
13	485252.48	6507557.77	0.33	247.43
14	485362.80	6507472.39	0.28	247.31

Epoch 0: 19.07.1995
Epoch 1: 26.07.1995

Pt	East. y [m]	North. x [m]	Veloc. [m/day]	Bear. [gon]
1	483287.38	6509301.19	0.02	157.97
2	483509.54	6509054.26	0.15	237.90
3	483671.87	6508864.70	0.26	241.39
4	483850.60	6508649.31	0.36	243.71
5	484002.01	6508474.94	0.39	246.14
6	484175.74	6508279.47	0.43	248.91

Pt	East. y [m]	North. x [m]	Veloc. [m/day]	Bear. [gon]
7	484325.78	6508226.19	0.44	247.41
8	484469.25	6507972.90	0.45	249.25
9	484657.46	6507803.60	0.41	252.02
10	484906.83	6507637.56	0.40	247.53
11	485130.86	6507500.17	0.33	245.44
12	485324.44	6507300.28	0.26	237.33

Epoch 0: 31.07.1996
Epoch 1: 07.08.1996

Pt	East. y [m]	North. x [m]	Veloc. [m/day]	Bear. [gon]
1	483727.04	6509199.38	0.18	243.40
2	483850.03	6509107.96	0.25	244.79
3	484016.98	6508983.97	0.33	245.76
4	484171.49	6508870.35	0.36	247.35
5	484330.13	6508753.32	0.38	249.00
6	484487.93	6508636.99	0.40	248.96
7	484646.11	6508520.77	0.41	249.17

Pt	East. y [m]	North. x [m]	Veloc. [m/day]	Bear. [gon]
8	484802.06	6508406.69	0.42	250.22
9	484954.87	6508294.65	0.42	250.37
10	485116.20	6508176.45	0.41	250.32
11	485229.88	6508093.21	0.40	250.73
12	485343.47	6508009.81	0.38	250.31
13	485455.58	6507927.80	0.35	250.47
14	485584.78	6507833.63	0.30	251.20

Profile VIII

Upper Matthes Glacier

Epoch 0: 02.08.1987
Epoch 1: 09.08.1987

Pt	East. y [m]	North. x [m]	Veloc. [m/day]	Bear. [gon]
1	488007.16	6523951.47	0.02	254.39
2	488269.20	6523764.33	0.04	255.85
3	488497.24	6523603.56	0.06	255.97
4	488722.84	6523446.26	0.09	256.10
5	488882.39	6523337.58	0.12	255.66
6	489172.28	6523137.86	0.15	255.52
7	489437.00	6522957.98	0.16	255.47

Pt	East. y [m]	North. x [m]	Veloc. [m/day]	Bear. [gon]
8	489651.01	6522815.55	0.19	255.69
9	489978.17	6522595.87	0.17	255.38
10	490185.57	6522461.50	0.17	255.87
11	490424.94	6522306.58	0.14	255.52
12	490651.90	6522161.89	0.12	255.87
13	490887.86	6522012.66	0.10	255.49
14	491182.50	6521825.31	0.09	256.09

Epoch 0: 14.08.1988
Epoch 1: 17.08.1988

Pt	East. y [m]	North. x [m]	Veloc. [m/day]	Bear. [gon]
1	488024.64	6524002.41	0.03	289.91
2	488209.37	6523876.60	0.05	317.08
3	488484.29	6523701.06	0.06	254.83
4	488797.18	6523495.40	0.05	229.04
5	489052.19	6523330.25	0.12	241.17
6	489424.41	6523083.81	0.11	232.79

Pt	East. y [m]	North. x [m]	Veloc. [m/day]	Bear. [gon]
7	489770.10	6522859.15	0.16	262.57
8	490166.94	6522595.30	0.17	237.48
9	490641.88	6522280.01	0.12	330.52
10	491024.67	6522027.87	0.13	305.81
11	491606.72	6521658.84	0.05	203.87

Epoch 0: 14.08.1988
Epoch 1: 17.08.1988
Profile location appr. 550 m down-glacier from Profile VIII

Pt	East. y [m]	North. x [m]	Veloc. [m/day]	Bear. [gon]
1	491604.03	6521654.24	0.05	251.49
2	490601.32	6521873.88	0.16	263.54
3	490174.07	6522070.43	0.19	237.86
4	489394.07	6522434.02	0.23	225.13

Pt	East. y [m]	North. x [m]	Veloc. [m/day]	Bear. [gon]
5	488780.44	6522660.45	0.23	226.00
6	488315.45	6522816.23	0.17	240.35
7	487994.74	6522917.82	0.13	254.68
8	487722.73	6523020.63	0.12	246.17

Epoch 0: 01.08.1989
Epoch 1: 04.08.1989

Pt	East. y [m]	North. x [m]	Veloc. [m/day]	Bear. [gon]
1	490654.54	6522183.96	0.10	223.05
2	490367.89	6522375.58	0.11	239.69
3	490102.45	6522553.02	0.15	216.01
4	489832.13	6522732.84	0.17	205.47
5	489570.29	6522906.66	0.15	200.17
6	489300.51	6523086.02	0.16	206.66
7	489119.19	6523206.39	0.08	218.67

Pt	East. y [m]	North. x [m]	Veloc. [m/day]	Bear. [gon]
8	488912.24	6523344.01	0.11	197.03
9	488708.68	6523479.47	0.08	190.32
10	488509.12	6523611.87	0.05	200.84
11	488269.08	6523772.41	0.02	149.56
12	488049.31	6523919.18	0.05	267.76
13	487833.58	6524065.71	0.02	366.72
14	487689.99	6524162.60	0.01	361.30

Epoch 0: 13.08.1990
Epoch 1: 22.08.1990

Pt	East. y [m]	North. x [m]	Veloc. [m/day]	Bear. [gon]
1	492836.43	6521011.95	0.01	12.38
2	493167.37	6520975.52	0.08	10.64
3	493486.60	6520938.02	0.07	9.89
4	493796.65	6520903.45	0.08	9.36

Pt	East. y [m]	North. x [m]	Veloc. [m/day]	Bear. [gon]
5	494139.09	6520864.04	0.11	9.00
6	494569.70	6520814.81	0.17	8.69
7	495040.42	6520762.73	0.17	8.42

Epoch 0: 01.08.1993
Epoch 1: 05.08.1993

Pt	East. y [m]	North. x [m]	Veloc. [m/day]	Bear. [gon]
1	487748.29	6524121.50	0.03	142.77
2	488048.94	6523890.69	0.04	168.83
3	488335.97	6523671.42	0.05	188.85
4	488595.79	6523473.05	0.09	207.01
5	488811.61	6523307.40	0.11	213.19
6	489035.77	6523137.14	0.14	217.75
7	489247.15	6522976.98	0.15	223.11

Pt	East. y [m]	North. x [m]	Veloc. [m/day]	Bear. [gon]
8	489455.52	6522818.04	0.16	221.13
9	489676.01	6522649.71	0.16	224.68
10	489881.50	6522493.23	0.15	231.76
11	490082.16	6522340.62	0.15	230.36
12	490338.95	6522144.34	0.13	252.92
13	490565.45	6521971.76	0.13	265.30

Epoch 0: 11.08.1994
Epoch 1: 14.08.1994

Pt	East. y [m]	North. x [m]	Veloc. [m/day]	Bear. [gon]
1	487627.20	6524198.37	0.03	98.57
2	487814.45	6524088.77	0.04	130.49
3	487975.69	6523991.68	0.05	142.92
4	488197.20	6523853.80	0.11	204.12
5	488373.59	6523740.73	0.11	198.20
6	488544.24	6523632.72	0.123	222.39
7	488730.42	6523510.52	0.22	225.21

Pt	East. y [m]	North. x [m]	Veloc. [m/day]	Bear. [gon]
8	488887.13	6523404.79	0.31	223.85
9	489070.01	6523285.52	0.21	220.16
10	489230.86	6523180.16	0.23	220.66
11	489420.69	6523056.90	0.22	223.24
12	489588.71	6522947.05	0.18	221.60
13	489799.47	6522809.79	0.13	217.08
14	490038.10	6522652.16	0.02	274.99

Epoch 0: 06.08.1995
Epoch 1: 10.08.1995

Pt	East. y [m]	North. x [m]	Veloc. [m/day]	Bear. [gon]
1	490903.02	6522004.87	0.08	264.42
2	490613.42	6522169.27	0.13	255.87
3	490366.20	6522305.92	0.11	266.52
4	490119.22	6522443.51	0.12	239.13
5	489885.04	6522574.35	0.16	231.47
6	489636.88	6522711.68	0.14	225.10

Pt	East. y [m]	North. x [m]	Veloc. [m/day]	Bear. [gon]
7	489366.45	6522858.94	0.12	198.50
8	489089.15	6523015.44	0.16	223.48
9	488765.92	6523197.62	0.12	219.92
10	488415.47	6523396.53	0.08	175.30
11	488105.72	6523570.89	0.05	219.22
12	487864.18	6523706.81	0.04	167.80

Epoch 0: 02.08.1996
Epoch 1: 10.08.1996

Pt	East. y [m]	North. x [m]	Veloc. [m/day]	Bear. [gon]
1	490903.01	6522004.83	0.10	277.01
2	490613.40	6522169.25	0.11	269.13
3	490366.27	6522305.85	0.12	249.44
4	490119.21	6522443.51	0.13	227.79
5	489884.94	6522574.35	0.15	221.69
6	489636.91	6522711.65	0.16	217.91

Pt	East. y [m]	North. x [m]	Veloc. [m/day]	Bear. [gon]
7	489366.50	6522858.88	0.16	218.58
8	489089.16	6523015.40	0.14	216.79
9	488765.90	6523197.60	0.11	210.84
10	488415.37	6523396.532	0.07	192.62
11	488105.79	6523570.86	0.04	141.55
12	487864.22	6523706.86	0.08	328.22

Profile VIIIa

Matthes/Vaughan-Lewis Glacier Divide

Epoch 0: 05.08.1995
Epoch 1: 11.08.1995

Pt	East. y [m]	North. x [m]	Veloc. [m/day]	Bear. [gon]
1	488065.53	6521713.61	0.09	200.36
3	487630.59	6521359.72	0.05	172.35
4	487441.50	6521227.07	0.04	116.59
5	487782.61	6521108.74	0.10	187.67

Pt	East. y [m]	North. x [m]	Veloc. [m/day]	Bear. [gon]
6	488016.93	6521018.13	0.17	190.71
7	488205.10	6520935.51	0.22	206.47
8	488149.09	6521193.01	0.18	212.29
9	488106.88	6521466.95	0.14	204.83

Profile IX

Upper Vaughan-Lewis Glacier

Epoch 0: 09.08.1986
Epoch 1: 19.08.1986

Pt	East. y [m]	North. x [m]	Veloc. [m/day]	Bear. [gon]
1	485006.37	6523229.95	0.09	361.85
2	4850034.86	6523384.36	0.17	330.25
3	485082.87	6523644.97	0.27	316.29
4	485128.86	6523901.90	0.26	308.51

Pt	East. y [m]	North. x [m]	Veloc. [m/day]	Bear. [gon]
5	485160.58	6524089.26	0.17	297.82
6	485183.25	6524232.53	0.16	276.90
7	485208.43	6524393.63	0.10	286.70

Epoch 0: 03.08.1987
Epoch 1: 09.08.1987

Pt	East. y [m]	North. x [m]	Veloc. [m/day]	Bear. [gon]
1	486800.32	6523955.53	0.10	176.96
2	486544.20	6523.789.90	0.01	355.24
3	486282.67	6523619.73	0.03	353.30
4	486117.07	6523509.33	0.04	353.34
5	485952.84	6523398.64	0.03	353.21

Pt	East. y [m]	North. x [m]	Veloc. [m/day]	Bear. [gon]
6	485794.19	6523290.41	0.05	350.69
7	485626.02	6523174.83	0.03	352.90
8	485443.35	6523048.55	0.03	351.12
9	485276.30	6522931.29	0.01	171.33
10	485157.37	6522844.64	0.01	170.73

Epoch 0: 29.07.1989
Epoch 1: 03.08.1989

Pt	East. y [m]	North. x [m]	Veloc. [m/day]	Bear. [gon]
1	484318.71	6522629.28	0.12	395.08
2	484393.17	6522724.72	0.16	367.29
3	484466.29	6522817.95	0.21	351.76
4	484538.26	6522909.72	0.27	354.01
5	484614.60	6523010.91	0.28	345.08

Pt	East. y [m]	North. x [m]	Veloc. [m/day]	Bear. [gon]
6	484685.06	6523099.58	0.28	341.43
7	484750.35	6523182.35	0.27	336.04
8	484836.82	6523291.76	0.22	326.62
9	484925.87	6523404.75	0.14	313.98

Epoch 0: 05.08.1990
Epoch 1: 14.08.1990

Pt	East. y [m]	North. x [m]	Veloc. [m/day]	Bear. [gon]
1	484960.83	6524284.04	0.15	249.23
2	485071.87	6524203.68	0.18	257.43
3	485164.92	6524048.11	0.25	279.63
4	485200.61	6523953.99	0.29	285.81
5	485236.28	6523806.24	0.30	288.63

Pt	East. y [m]	North. x [m]	Veloc. [m/day]	Bear. [gon]
6	485231.22	6523662.73	0.30	295.63
7	485230.12	6523543.92	0.29	299.24
8	485185.56	6523396.72	0.21	298.93
9	485111.90	6523231.90	0.09	315.86

Epoch 0: 10.08.1994
Epoch 1: 12.08.1994

Pt	East. y [m]	North. x [m]	Veloc. [m/day]	Bear. [gon]
1	484978.50	6524331.53	0.20	222.02
2	485012.10	6524271.67	0.17	188.28
3	485115.61	6524094.03	0.31	255.18
4	485177.92	6523947.00	0.34	269.91
5	485214.37	6523757.46	0.35	284.23

Pt	East. y [m]	North. x [m]	Veloc. [m/day]	Bear. [gon]
6	485247.27	6523567.60	0.30	292.81
7	485238.75	6523395.65	0.20	309.22
8	485201.24	6523262.74	0.13	313.10
9	485122.84	6523180.19	0.22	350.78
10	485078.35	6523090.36	0.29	43.22

Epoch 0: 07.08.1995
Epoch 1: 12.08.1995

Pt	East. y [m]	North. x [m]	Veloc. [m/day]	Bear. [gon]
1	485620.48	6524358.07	0.10	237.10
2	485747.18	6524153.87	0.11	261.12
3	485830.16	6523948.11	0.23	300.11
4	485874.31	6523693.87	0.24	310.56

Pt	East. y [m]	North. x [m]	Veloc. [m/day]	Bear. [gon]
5	485877.33	6523472.57	0.30	318.76
6	485794.83	6523293.13	0.30	328.51
7	485670.26	6523112.67	0.26	335.19

Epoch 0: 03.08.1996
Epoch 1: 09.08.1996

Pt	East. y [m]	North. x [m]	Veloc. [m/day]	Bear. [gon]
1	485620.50	6524358.05	0.08	256.94
2	485747.25	6524154.68	0.09	294.83
3	485831.28	6523946.30	0.13	315.49
4	485874.02	6523692.93	0.11	335.14

Pt	East. y [m]	North. x [m]	Veloc. [m/day]	Bear. [gon]
5	485876.77	6523471.83	0.11	351.09
6	485795.34	6523393.59	0.12	358.94
7	485669.20	6523112.76	0.10	374.73
8	485441.36	6523027.46	0.06	394.09

Profile X

Matthes/Llewellyn Glacier Divide

Epoch 0: 05.08.1995
Epoch 1: 14.08.1995

Pt	East. y [m]	North. x [m]	Veloc. [m/day]	Bear. [gon]
1	488866.77	6522402.66	0.08	350.75
2	489015.80	6522671.64	0.14	216.69
3	489156.40	6522957.11	0.15	218.81
4	489275.23	6523242.86	0.13	216.87
5	489424.42	6523573.55	0.12	226.33
6	489520.21	6523919.66	0.10	218.34
7	489699.30	6524260.17	0.08	209.17
8	489879.63	6524544.85	0.09	214.91

Pt	East. y [m]	North. x [m]	Veloc. [m/day]	Bear. [gon]
10	490138.88	6525189.66	0.08	202.60
11	490324.06	6525607.58	0.06	186.18
12	490588.40	6526177.43	0.04	167.20
13	489448.08	6523134.84	0.13	211.18
14	489107.76	6523347.30	0.10	213.56
15	490746.22	6526519.92	0.05	148.91
16	490913.45	6526854.31	0.07	82.55

Epoch 0: 04.08.1996
Epoch 1: 10.08.1996

Pt	East. y [m]	North. x [m]	Veloc. [m/day]	Bear. [gon]
16	490913.52	6526854.32	0.06	98.67
17	491022.77	6527209.11	0.07	90.27
18	491139.60	6527561.94	0.07	83.83
19	491251.41	6527917.40	0.07	73.00
20	491363.04	6528270.71	0.06	77.20
21	491477.38	6528633.06	0.06	70.90
22	491588.60	6528985.07	0.06	63.82

Pt	East. y [m]	North. x [m]	Veloc. [m/day]	Bear. [gon]
23	491701.99	6529342.78	0.06	50.13
24	491815.63	6529701.11	0.05	46.39
25	491929.39	6530058.16	0.05	27.70
26	492043.91	6530415.67	0.06	34.22
27	492158.40	6530773.04	0.06	32.94
28	492271.43	6531125.26	0.07	29.73
29	492386.02	6531482.15	0.07	31.94

Profile XI

Llewellyn Glacier

Epoch 0: 07.08.1995
Epoch 1: 13.08.1995

Pt	East. y [m]	North. x [m]	Veloc. [m/day]	Bear. [gon]
1	496272.23	6531070.17	0.02	368.13
2	496044.06	6531210.16	0.02	18.42
3	495796.07	6531324.58	0.03	41.62
4	495545.09	6531448.14	0.03	399.05
5	495172.31	6531627.66	0.03	12.74
6	494800.41	6531824.01	0.05	9.92

Pt	East. y [m]	North. x [m]	Veloc. [m/day]	Bear. [gon]
7	494414.40	6532013.27	0.07	36.41
8	493959.90	6532233.94	0.12	32.92
9	493507.57	6532456.89	0.14	31.26
10	493150.83	6532663.34	0.13	40.95
11	492856.11	6532855.98	0.15	49.70

Profile A

Gilkey Trench – Unnamed Glacier

Epoch 0: 10.08.1990
Epoch 1: 16.08.1990

Pt	East. y [m]	North. x [m]	Veloc. [m/day]	Bear. [gon]
1	482655.19	6522600.13	0.11	8.02
2	482551.45	6522776.03	0.11	6.96
3	482799.50	6522650.16	0.11	396.22

Pt	East. y [m]	North. x [m]	Veloc. [m/day]	Bear. [gon]
4	482594.15	6522974.61	0.13	388.06
5	482930.09	6522811.42	0.11	397.20

Epoch 0: 14.08.1990
Epoch 1: 15.08.1991

Pt	East. y [m]	North. x [m]	Veloc. [m/day]	Bear. [gon]
1	482655.25	6522600.55	0.13	0.22
3	482799.48	6522650.58	0.11	0.58

Pt	East. y [m]	North. x [m]	Veloc. [m/day]	Bear. [gon]
5	482930.07	6522811.48	0.11	397.52

Epoch 0: 15.08.1991
Epoch 1: 13.08.1993

Pt	East. y [m]	North. x [m]	Veloc. [m/day]	Bear. [gon]
1	482655.36	6522649.14	0.13	0.06
3	482799.88	6522690.94	0.11	1.72

Pt	East. y [m]	North. x [m]	Veloc. [m/day]	Bear. [gon]
5	482928.48	6522852.78	0.11	397.99

Profile B

Gilkey Trench – Cross Trench Profile (Trench Traverse)

Epoch 0: 11.08.1990
Epoch 1: 16.08.1990

Pt	East. y [m]	North. x [m]	Veloc. [m/day]	Bear. [gon]
1	481926.71	6522952.83	0.15	286.23
2	482196.24	6523168.66	0.28	292.08
3	481882.74	6523165.58	0.40	280.76
4	482133.17	6523400.72	0.46	280.30
5	481821.26	6523259.85	0.47	278.15
6	481901.45	6523157.45	0.52	279.19
7	481699.85	6523560.40	0.54	279.32
8	482049.74	6523588.57	0.55	273.42

Pt	East. y [m]	North. x [m]	Veloc. [m/day]	Bear. [gon]
9	481649.87	6523653.04	0.52	278.40
10	481942.64	6523827.21	0.56	272.90
11	481593.69	6523816.90	0.52	276.42
12	481854.51	6524059.68	0.53	268.70
13	481471.29	6524140.39	0.46	276.61
14	481700.10	6524360.29	0.43	265.55
15	481395.38	6524341.02	0.36	275.86

Epoch 0: 11.08.1990
Epoch 1: 15.08.1991

Pt	East. y [m]	North. x [m]	Veloc. [m/day]	Bear. [gon]
3	481882.74	6523165.58	0.35	279.14
7	481699.85	6523560.40	0.51	276.28
9	481649.87	6523653.04	0.52	277.53

Pt	East. y [m]	North. x [m]	Veloc. [m/day]	Bear. [gon]
11	481593.69	6523816.90	0.50	276.73
13	481471.29	6524140.39	0.44	277.49
15	481395.38	6524341.02	0.34	275.93

Epoch 0: 11.08.1990
Epoch 1: 08.08.1992

Pt	East. y [m]	North. x [m]	Veloc. [m/day]	Bear. [gon]
2	482196.24	6523168.66	0.27	284.82
4	482133.17	6523400.72	0.45	277.84
8	482049.74	6523588.57	0.50	276.45

Pt	East. y [m]	North. x [m]	Veloc. [m/day]	Bear. [gon]
10	481942.64	6523827.21	0.54	274.79
12	481854.51	6524059.68	0.52	273.42
14	481700.10	6524360.29	0.42	270.34

Epoch 0: 15.08.1991
Epoch 1: 08.08.1992

Pt	East. y [m]	North. x [m]	Veloc. [m/day]	Bear. [gon]
3	481762.06	6523124.56	0.36	278.48
7	481507.59	6523450.49	0.50	277.87
9	481555.09	6523584.44	0.52	278.63

Pt	East. y [m]	North. x [m]	Veloc. [m/day]	Bear. [gon]
11	481421.43	6523750.98	0.52	277.98
15	481277.64	6524294.26	0.35	275.46

Epoch 0: 08.08.1992
Epoch 1: 10.08.1993

Pt	East. y [m]	North. x [m]	Veloc. [m/day]	Bear. [gon]
2	482005.26	6523122.26	0.27	281.81
3	481640.37	6523081.78	0.36	278.61
4	481825.83	6523289.16	0.45	277.84
7	481352.57	6523427.06	0.48	281.92
8	481712.51	6523445.44	0.48	277.55
9	481379.39	6523516.88	0.49	280.52

Pt	East. y [m]	North. x [m]	Veloc. [m/day]	Bear. [gon]
10	481582.26	6523676.57	0.51	277.41
11	481246.06	6523687.78	0.47	282.40
12	481507.56	6523905.76	0.48	278.89
14	481425.93	6524222.44	0.41	277.59
15	481160.12	6524246.57	0.34	280.11

Epoch 0: 10.08.1993
Epoch 1: 15.08.1994

Pt	East. y [m]	North. x [m]	Veloc. [m/day]	Bear. [gon]
2	481911.83	6523094.81	0.27	280.50
4	481671.35	6523233.11	0.46	278.23
5	481363.43	6523097.64	0.44	278.45
7	481186.78	6523372.96	0.48	279.90
8	481547.62	6523384.76	0.50	277.96
9	481208.13	6523462.78	0.50	280.24

Pt	East. y [m]	North. x [m]	Veloc. [m/day]	Bear. [gon]
10	481406.74	6523611.53	0.50	278.73
11	481078.50	6523640.23	0.49	281.61
12	481340.51	6523848.24	0.50	280.06
14	481283.18	6524170.02	0.43	277.22
15	481042.30	6524208.51	0.35	282.06

Profile C

Gilkey Trench – Gilkey Glacier Curve

Epoch 0: 11.08.1990
Epoch 1: 16.08.1990

Pt	East. y [m]	North. x [m]	Veloc. [m/day]	Bear. [gon]
1	482571.57	6524814.85	0.53	192.38
2	482403.56	6524453.56	0.55	212.92
3	482247.37	6524056.64	0.55	260.15

Pt	East. y [m]	North. x [m]	Veloc. [m/day]	Bear. [gon]
4	482301.57	6524888.65	0.59	191.71
5	482184.36	6524617.30	0.55	205.84
6	481997.53	6524366.21	0.51	245.06

Epoch 0: 11.08.1990
Epoch 1: 13.08.1991

Pt	East. y [m]	North. x [m]	Veloc. [m/day]	Bear. [gon]
3	482247.37	6524056.64	0.52	261.29

Epoch 0: 13.08.1991
Epoch 1: 08.08.1992

Pt	East. y [m]	North. x [m]	Veloc. [m/day]	Bear. [gon]
3	482090.94	6523947.75	0.55	269.15

Epoch 0: 08.08.1992
Epoch 1: 09.08.1993

Pt	East. y [m]	North. x [m]	Veloc. [m/day]	Bear. [gon]
3	481916.27	6523855.60	0.53	272.92
5	482024.85	6524290.55	0.49	255.87
6	481719.43	6524144.22	0.47	272.57

Epoch 0: 09.08.1993
Epoch 1: 13.08.1994

Pt	East. y [m]	North. x [m]	Veloc. [m/day]	Bear. [gon]
4	482219.01	6524343.46	0.50	245.70

Profile D

Gilkey Trench – Upper Gilkey Glacier

Epoch 0: 11.08.1990
Epoch 1: 16.08.1990

Pt	East. y [m]	North. x [m]	Veloc. [m/day]	Bear. [gon]
1	482681.91	6524986.19	0.51	190.53
2	482610.51	6525209.72	0.55	190.43
3	482549.22	6525006.72	0.62	183.05
4	482336.27	6525301.75	0.53	190.01
5	482384.55	6525029.54	0.54	187.80

Pt	East. y [m]	North. x [m]	Veloc. [m/day]	Bear. [gon]
6	482166.27	6525296.13	0.61	173.31
7	482133.27	6525061.78	0.53	205.54
8	482046.78	6525247.52	0.52	191.01
9	481997.13	6525082.59	0.50	190.33

Epoch 0: 17.08.1992
Epoch 1: 09.08.1993

Pt	East. y [m]	North. x [m]	Veloc. [m/day]	Bear. [gon]
1	482697.90	6524642.08	0.43	206.14
2	482653.76	6524830.90	0.49	208.17
3	482555.41	6524619.93	0.52	206.85
4	482385.14	6524913.05	0.53	195.32
5	482400.04	6524641.11	0.51	211.23

Pt	East. y [m]	North. x [m]	Veloc. [m/day]	Bear. [gon]
6	482205.19	6524908.81	0.53	192.61
7	482135.41	6524680.06	0.50	209.95
8	482083.98	6524871.37	0.50	196.42
9	482011.32	6524728.56	0.46	211.14

Epoch 0: 09.08.1993
Epoch 1: 13.08.1994

Pt	East. y [m]	North. x [m]	Veloc. [m/day]	Bear. [gon]
1	482687.95	6524489.34	0.41	213.86
2	482658.82	6524655.23	0.48	207.90
3	482535.64	6524436.98	0.50	221.57
4	482398.95	6524725.59	0.52	206.68
5	482368.07	6524461.72	0.50	226.28

Pt	East. y [m]	North. x [m]	Veloc. [m/day]	Bear. [gon]
6	482227.04	6524721.58	0.52	210.30
7	482107.65	6524503.84	0.50	235.40
8	482094.09	6524691.99	0.49	216.63
9	481982.56	6524565.91	0.46	235.46

Epoch 0: 13.08.1994
Epoch 1: 12.08.1995

Pt	East. y [m]	North. x [m]	Veloc. [m/day]	Bear. [gon]
1	482655.51	6524342.66	0.37	221.82
2	482636.99	6524480.17	0.46	214.78
5	482293.86	6524292.25	0.48	244.44
6	482196.36	6524533.51	0.47	223.38

Pt	East. y [m]	North. x [m]	Veloc. [m/day]	Bear. [gon]
7	482010.52	6524347.53	0.49	252.00
8	482047.17	6524516.47	0.47	235.78
9	481892.99	6524422.06	0.44	253.73

Profile E

Gilkey Trench – Little Vaughan-Lewis Glacier

Epoch 0: 11.08.1990
Epoch 1: 16.08.1990

Pt	East. y [m]	North. x [m]	Veloc. [m/day]	Bear. [gon]
1	482984.28	6524507.52	0.06	237.84
2	483006.16	6524372.29	0.05	152.33
3	482939.81	6524379.27	0.06	213.28

Epoch 0: 10.08.1990
Epoch 1: 13.08.1991

Pt	East. y [m]	North. x [m]	Veloc. [m/day]	Bear. [gon]
1	482984.28	6524507.52	0.05	216.22
2	483006.16	6524372.29	0.03	209.84
3	482939.81	6524379.27	0.06	206.37

Epoch 0: 13.08.1991
Epoch 1: 17.08.1992

Pt	East. y [m]	North. x [m]	Veloc. [m/day]	Bear. [gon]
1	482980.09	6524491.42	0.05	198.87
2	483004.71	6524363.01	0.03	211.65
3	482937.67	6524357.94	0.07	213.66

Epoch 0: 17.08.1992
Epoch 1: 09.08.1993

Pt	East. y [m]	North. x [m]	Veloc. [m/day]	Bear. [gon]
1	482976.70	6524473.44	0.05	195.76
2	482999.53	6524354.02	0.03	194.82
3	482926.09	6524335.85	0.07	196.17

Epoch 0: 09.08.1993
Epoch 1: 13.08.1994

Pt	East. y [m]	North. x [m]	Veloc. [m/day]	Bear. [gon]
1	482977.81	6524456.76	0.05	214.10
3	482927.55	6524311.60	0.06	220.11

Epoch 0: 13.08.1994
Epoch 1: 12.08.1995

Pt	East. y [m]	North. x [m]	Veloc. [m/day]	Bear. [gon]
3	482920.28	6524289.37	0.06	215.44

Profile F

Gilkey Trench – Vaughan-Lewis Glacier

Epoch 0: 11.08.1990
Epoch 1: 16.08.1990

Pt	East. y [m]	North. x [m]	Veloc. [m/day]	Bear. [gon]
1	482880.08	6523636.66	0.43	320.05
2	482880.76	6523636.49	0.46	321.23
3	482919.80	6523436.62	0.38	316.00
4	482816.86	6523897.34	0.30	311.63

Pt	East. y [m]	North. x [m]	Veloc. [m/day]	Bear. [gon]
5	482734.67	6523758.39	0.38	314.20
6	482753.59	6523524.71	0.38	321.19
7	482918.64	6523324.28	0.34	322.90

Epoch 0: 10.08.1990
Epoch 1: 13.08.1991

Pt	East. y [m]	North. x [m]	Veloc. [m/day]	Bear. [gon]
2	482880.76	6523636.49	0.41	315.09
5	482734.67	6523758.39	0.35	308.01

Pt	East. y [m]	North. x [m]	Veloc. [m/day]	Bear. [gon]
6	482753.59	6523524.71	0.36	312.98
7	482918.64	6523324.28	0.31	322.87

Epoch 0: 13.08.1991
Epoch 1: 13.08.1992

Pt	East. y [m]	North. x [m]	Veloc. [m/day]	Bear. [gon]
6	482624.02	6523551.51	0.38	304.74

Epoch 0: 13.08.1992
Epoch 1: 13.08.1993

Pt	East. y [m]	North. x [m]	Veloc. [m/day]	Bear. [gon]
5	482398.65	6523665.07	0.34	318.67
6	482485.60	6523561.84	0.40	294.50

Appendix C

Short-Term Height Changes

The following tables show the short-term height changes of various profiles for the years 1992 to 1996:

- Profile I
  Taku Glacier (Terminus)
  - 1994
- Profile II
  Taku Glacier (Goat Ridge)
  - 1993
  - 1994
- Profile III
  Demorest Glacier
  - 1992
  - 1993
  - 1994
  - 1995
  - 1996
- Profile IV
  Taku Glacier (Camp 10)
  - 1992
  - 1993
  - 1994
  - 1995
  - 1996
- Profile V
  SW-Branch Taku Glacier
  - 1992
  - 1993
  - 1994
  - 1995
  - 1996
- Profile VI
  NW-Branch Taku Glacier (Echo Mountain)
  - 1992
- Profile VIa
  NW-Branch Taku Glacier (Taku D)
  - 1993
  - 1994
  - 1995
  - 1996
- Profile VII
  Lower Matthes Glacier (Camp 9)
  - 1996
- Profile VIIa
  Lower Matthes Glacier (Taku C)
  - 1993
  - 1994
  - 1995
  - 1996
- Profile VIII
  Upper Matthes Glacier
  - 1993
  - 1995
  - 1996
- Profile VIIIa
  Matthes/Vaughan-Lewis Glacier Divide
  - 1995
- Profile IX
  Upper Vaughan-Lewis Glacier
  - 1996
- Profile X
  Matthes/Llewellyn Glacier Divide
  - 1995
  - 1996
- Profile XI
  Llewellyn Glacier
  - 1995

Abbreviations:

* = outlier

Profile I

Taku Glacier – Terminus

Epoch 0: 01.08.1994
Epoch 1: 02.08.1994

Point-Number	Height change [cm/day]	Time-span [days]
1	9.0	0.70
2	*	0.74
3	4.1	0.78
4	7.7	0.83
5	15.3	0.91

Point-Number	Height change [cm/day]	Time-span [days]
6	8.1	1.96
7	11.7	1.91
8	11.4	1.87
9	12.0	1.82
10	12.7	1.77

Point-Number	Height change [cm/day]	Time-span [days]
11	12.5	1.73
21	2.5	0.83
22	9.5	1.69
23	*	1.66
24	5.5	1.62

Profile II

Taku Glacier – Goat Ridge

Epoch 0: 23.07.1993
Epoch 1: 27.07.1993

Point-Number	Height change [cm/day]	Time-span [days]
1	8.3	3.94
2	7.0	3.94
3	8.3	3.94
4	10.1	3.95

Point-Number	Height change [cm/day]	Time-span [days]
5	*	3.93
6	9.4	3.93
7	9.7	3.93

Point-Number	Height change [cm/day]	Time-span [days]
8	8.4	3.93
9	9.2	3.93
10	7.9	3.93

Epoch 0: 03.08.1994
Epoch 1: 07.08.1994

Point-Number	Height change [cm/day]	Time-span [days]
1	8.9	4.00
2	9.7	4.01
3	7.9	4.02
4	11.5	4.04

Point-Number	Height change [cm/day]	Time-span [days]
5	13.6	4.03
6	15.1	3.96
7	11.6	3.93
8	12.2	3.93

Point-Number	Height change [cm/day]	Time-span [days]
9	14.4	3.92
10	13.8	3.92
11	12.3	3.93

Profile III

Demorest Glacier

Epoch 0: 27.07.1992
Epoch 1: 30.07.1992

Point-Number	Height change [cm/day]	Time-span [days]
1	6.1	2.80
2	7.2	2.80

Point-Number	Height change [cm/day]	Time-span [days]
3	5.6	2.80
4	6.5	2.80

Point-Number	Height change [cm/day]	Time-span [days]
5	7.9	2.80
6	4.7	2.80

Epoch 0: 18.07.1993
Epoch 1: 24.07.1993

Point-Number	Height change [cm/day]	Time-span [days]
1	4.4	5.05
2	3.2	5.05
3	3.1	5.04
4	4.1	5.04

Point-Number	Height change [cm/day]	Time-span [days]
5	4.2	5.04
6	5.5	5.05
7	3.6	5.06
8	4.7	5.04

Point-Number	Height change [cm/day]	Time-span [days]
9	4.4	5.02
10	4.6	5.02
11	3.8	5.02

Epoch 0: 29.07.1994
Epoch 1: 04.08.1994

Point-Number	Height change [cm/day]	Time-span [days]
1	5.8	6.28
2	5.2	6.25
3	6.1	6.21
4	5.7	6.16

Point-Number	Height change [cm/day]	Time-span [days]
5	4.9	6.10
6	6.1	6.06
7	6.5	6.02
8	6.8	5.99

Point-Number	Height change [cm/day]	Time-span [days]
9	5.5	5.95
10	7.8	5.91
11	6.9	5.87
12	7.6	5.83

Epoch 0: 17.07.1995
Epoch 1: 25.07.1995

Point-Number	Height change [cm/day]	Time-span [days]
1	3.0	8.11
2	4.1	8.10
3	4.7	8.10
4	4.8	8.14

Point-Number	Height change [cm/day]	Time-span [days]
5	5.5	8.12
6	6.5	8.12
7	6.1	8.06

Point-Number	Height change [cm/day]	Time-span [days]
8	5.8	8.07
9	5.4	8.06
10	5.0	12.21

Epoch 0: 27.07.1996
Epoch 1: 05.08.1996

Point-Number	Height change [cm/day]	Time-span [days]
2	2.4	8.95
3	3.6	8.94
4	3.0	8.94

Point-Number	Height change [cm/day]	Time-span [days]
5	3.5	8.94
6	3.3	8.94
7	5.1	8.93

Point-Number	Height change [cm/day]	Time-span [days]
8	2.3	8.94
9	*	8.94

Profile IV

Taku Glacier – Camp 10

Epoch 0: 20.07.1992
Epoch 1: 30.07.1992

Point-Number	Height change [cm/day]	Time-span [days]
1	4.3	7.81
2	4.4	7.81
3	4.3	7.81
4	4.8	6.94
5	6.4	6.94
6	6.7	6.94
7	5.6	6.94

Point-Number	Height change [cm/day]	Time-span [days]
8	5.8	6.94
9	5.5	6.94
10	4.7	6.94
21	4.0	5.98
22	4.2	5.98
23	4.1	5.98

Point-Number	Height change [cm/day]	Time-span [days]
51	5.2	6.11
52	6.1	6.11
53	6.8	6.11
81	4.4	5.92
82	6.0	5.92
83	5.4	5.92

Epoch 0: 20.07.1993
Epoch 1: 25.07.1993

Point-Number	Height change [cm/day]	Time-span [days]
1	3.2	5.01
2	5.0	5.01
3	3.4	5.00
4	4.8	4.99
5	3.6	5.00
6	2.5	4.98
7	3.9	5.00
8	4.8	4.98
9	4.9	5.00

Point-Number	Height change [cm/day]	Time-span [days]
10	4.6	4.99
11	4.2	5.00
12	4.7	4.99
13	4.4	5.00
14	5.8	5.00
15	5.6	5.00
16	7.3	5.00
17	8.2	5.00
18	7.3	5.00

Point-Number	Height change [cm/day]	Time-span [days]
19	5.9	5.00
20	7.3	5.00
21	5.9	5.00
22	6.6	5.00
23	5.9	5.00
24	4.8	5.00
25	5.2	5.00
26	5.2	5.01
27	4.1	5.00

Epoch 0: 25.07.1994
Epoch 1: 05.08.1994

Point-Number	Height change [cm/day]	Time-span [days]
1	5.7	10.98
2	4.5	10.97
3	5.1	10.97
4	5.1	10.97
5	5.5	10.94
6	5.0	10.96
7	5.2	10.93
8	5.9	10.96
9	5.1	10.92
10	5.2	10.95
11	5.8	10.92
12	5.7	10.97
13	6.7	10.93
14	6.3	10.97
15	7.3	10.93
16	*	10.97
17	7.9	10.93
18	7.3	10.96
19	8.5	10.92
20	8.4	10.96
21	8.0	10.92
22	7.4	10.96
23	8.0	10.91
24	6.3	10.95
25	7.1	10.91
26	7.0	10.96
27	6.8	10.91
28	6.2	10.96
29	5.2	10.88
30	6.0	10.96
31	6.6	10.91

Epoch 0: 20.07.1995
Epoch 1: 28.07.1995

Point-Number	Height change [cm/day]	Time-span [days]
1	3.9	8.18
2	3.9	8.20
3	4.8	8.15
4	4.9	8.13
5	5.5	8.10
6	4.3	8.07
7	4.9	7.20
8	4.3	8.00
9	5.1	6.09
10	4.9	7.94
11	5.3	7.14
12	4.3	7.12
13	4.4	7.09
14	6.3	7.07
15	6.2	7.05
16	5.4	7.02
17	5.4	7.00
18	6.6	6.97
19	6.3	6.95
20	5.5	6.92
21	6.4	5.97
22	4.3	6.88
23	6.5	5.77
24	5.1	6.83
25	5.8	5.76
26	4.3	5.84
27	4.7	5.76
28	3.5	5.80
29	5.2	5.75
30	3.8	5.75
31	6.1	5.74

Epoch 0: 28.07.1996
Epoch 1: 06.08.1996

Point-Number	Height change [cm/day]	Time-span [days]
1	4.0	9.19
2	3.4	8.64
3	3.9	9.17
4	3.3	8.65
5	5.2	9.15
6	3.8	8.66
7	3.7	9.14
8	4.0	8.67
9	4.1	9.12
10	3.3	8.69
11	*	9.11
12	3.4	8.70
13	4.7	9.09
14	4.9	8.71
15	5.5	9.08
16	5.6	8.72
17	5.8	9.08
18	5.2	8.73
19	5.9	9.06
20	4.9	8.74
21	*	9.05
22	5.1	8.75
23	5.4	9.04
24	4.5	8.76
25	*	9.01
26	3.8	8.78
27	*	8.99
28	3.8	8.79
29	3.5	8.97
30	3.2	8.80
31	3.6	8.96

Profile V

SW-Branch Taku Glacier

Epoch 0: 21.07.1992
Epoch 1: 28.07.1992

Point-Number	Height change [cm/day]	Time-span [days]
1	3.8	6.94
2	4.1	6.94
3	3.8	6.94
4	4.5	6.94
5	4.3	6.94
6	3.9	6.94
7	3.3	6.94
8	3.7	6.94

Epoch 0: 18.07.1993
Epoch 1: 27.07.1993

Point-Number	Height change [cm/day]	Time-span [days]
1	3.8	8.67
2	3.9	8.71
3	5.0	8.74
4	3.6	8.78
5	4.8	8.82
6	4.7	8.86
7	4.5	8.90
8	4.1	8.94
9	5.3	8.97
10	4.6	9.00
11	4.8	9.04
12	4.3	9.08

Epoch 0: 27.07.1994
Epoch 1: 04.08.1994

Point-Number	Height change [cm/day]	Time-span [days]
1	6.8	7.90
2	5.2	7.90
3	5.1	7.89
4	5.4	7.89
5	4.9	7.89
6	4.7	7.90
7	4.7	7.89
8	5.9	7.89
9	4.7	7.89
10	5.5	7.88
11	5.4	7.88
12	5.9	7.88

Epoch 0: 23.07.1995
Epoch 1: 29.07.1995

Point-Number	Height change [cm/day]	Time-span [days]
1	4.9	6.00
2	5.6	5.99
3	3.4	5.99
4	4.6	5.98
5	5.3	5.96
6	6.0	5.95
7	5.9	5.93
8	5.8	5.92
9	7.3	5.93
10	6.8	5.95
11	7.1	5.96
12	5.0	5.98

Epoch 0: 30.07.1996
Epoch 1: 05.08.1996

Point-Number	Height change [cm/day]	Time-span [days]
1	3.6	5.96
2	*	5.95
3	*	5.94
4	*	5.94

Point-Number	Height change [cm/day]	Time-span [days]
5	*	5.92
6	3.8	5.91
7	4.9	5.90
8	4.4	5.90

Point-Number	Height change [cm/day]	Time-span [days]
9	3.8	5.89
10	3.1	5.88
11	*	5.88
12	4.4	5.87

Profile VI

NW-Branch Taku Glacier – Echo Mountain

Epoch 0: 22.07.1992
Epoch 1: 30.07.1992

Point-Number	Height change [cm/day]	Time-span [days]
1	4.0	8.01
2	3.8	8.01
3	3.7	8.01

Point-Number	Height change [cm/day]	Time-span [days]
4	4.1	8.01
5	5.0	8.01
6	4.6	5.08

Point-Number	Height change [cm/day]	Time-span [days]
7	4.5	6.08
8	4.2	6.08
9	5.5	6.08

Profile VIa

NW-Branch Taku Glacier – Taku D

Epoch 0: 21.07.1993
Epoch 1: 28.07.1993

Point-Number	Height change [cm/day]	Time-span [days]
1	5.1	7.01
2	4.7	7.01
3	5.1	7.01
4	4.8	7.01
5	5.2	7.02
6	5.4	7.02

Point-Number	Height change [cm/day]	Time-span [days]
7	5.3	7.02
8	5.3	7.03
9	6.1	7.04
10	6.9	7.04
11	5.7	7.04

Point-Number	Height change [cm/day]	Time-span [days]
12	6.1	7.04
13	6.4	7.04
14	6.4	7.05
15	6.1	7.05
16	5.9	7.03

Epoch 0: 26.07.1994
Epoch 1: 06.08.1994

Point-Number	Height change [cm/day]	Time-span [days]
1	*	10.69
3	10.5	10.79
4	10.8	10.82
5	*	10.85
6	10.9	10.89

Point-Number	Height change [cm/day]	Time-span [days]
7	10.4	10.92
8	10.8	10.96
9	8.9	11.02
10	10.1	11.06
11	9.8	11.09

Point-Number	Height change [cm/day]	Time-span [days]
12	9.8	11.12
13	9.6	11.16
14	9.6	11.19
15	10.0	11.22
16	8.9	11.25

Epoch 0: 18.07.1995
Epoch 1: 28.07.1995

Point-Number	Height change [cm/day]	Time-span [days]
1	5.4	9.92
2	5.4	9.92
3	6.1	9.92
4	5.5	9.92

Point-Number	Height change [cm/day]	Time-span [days]
5	5.6	9.92
6	6.0	9.92
7	6.1	9.92

Point-Number	Height change [cm/day]	Time-span [days]
8	6.4	9.92
9	5.4	9.92
10	5.3	9.93

Epoch 0: 29.07.1996
Epoch 1: 07.08.1996

Point-Number	Height change [cm/day]	Time-span [days]
1	2.3	8.85
2	3.7	8.85
3	3.3	8.85
4	3.5	8.85
5	3.8	8.85

Point-Number	Height change [cm/day]	Time-span [days]
6	3.8	8.85
7	4.1	8.85
8	4.6	8.86
9	5.3	8.86
10	4.6	8.89

Point-Number	Height change [cm/day]	Time-span [days]
11	5.0	8.89
12	5.5	8.90
13	5.9	8.90
14	6.0	8.91

Profile VII

Lower Matthes Glacier – Camp 9

Epoch 0: 31.07.1996
Epoch 1: 07.08.1996

Point-Number	Height change [cm/day]	Time-span [days]
1	3.3	8.16
2	3.1	8.12
3	2.9	8.09
4	2.7	8.06
5	2.4	8.03
6	2.8	7.99

Point-Number	Height change [cm/day]	Time-span [days]
7	3.5	7.96
8	3.8	7.92
9	4.0	7.89
10	4.8	7.83
11	4.2	7.80

Point-Number	Height change [cm/day]	Time-span [days]
12	3.2	7.76
13	4.0	7.72
14	3.6	7.69
15	3.1	7.65
16	2.7	7.61

Profile VII a

Lower Matthes Glacier – Taku C

Epoch 0: 22.07.1993
Epoch 1: 29.07.1993

Point-Number	Height change [cm/day]	Time-span [days]
1	*	6.83
2	*	6.83
3	5.8	6.83
4	5.7	6.83
5	5.2	6.73

Point-Number	Height change [cm/day]	Time-span [days]
6	5.9	6.70
7	7.4	6.84
8	9.2	6.88
9	7.0	6.91
10	7.0	6.95

Point-Number	Height change [cm/day]	Time-span [days]
11	7.9	6.98
12	7.9	7.02
13	6.7	7.06
14	7.1	7.10

Epoch 0: 26.07.1994
Epoch 1: 06.08.1994

Point-Number	Height change [cm/day]	Time-span [days]
1	6.7	10.94
2	8.1	10.96
3	8.7	10.96
4	8.8	10.97
5	9.1	10.97

Point-Number	Height change [cm/day]	Time-span [days]
6	10.0	10.98
7	10.1	10.98
8	11.1	10.99
9	11.7	10.99
10	11.7	10.99

Point-Number	Height change [cm/day]	Time-span [days]
11	11.2	10.98
12	11.4	10.98
13	10.9	10.98
14	10.2	10.98

Epoch 0: 19.07.1995
Epoch 1: 26.07.1995

Point-Number	Height change [cm/day]	Time-span [days]
1	5.3	6.86
2	5.5	6.90
3	6.4	6.93
4	6.2	6.97

Point-Number	Height change [cm/day]	Time-span [days]
5	5.7	7.00
6	6.6	7.04
7	5.9	7.05
8	6.9	7.90

Point-Number	Height change [cm/day]	Time-span [days]
9	8.1	7.90
10	7.2	7.85
11	6.7	7.90
12	6.0	7.94

Epoch 0: 29.07.1996
Epoch 1: 06.08.1996

Point-Number	Height change [cm/day]	Time-span [days]
1	4.3	6.98
2	4.7	6.98
3	5.8	6.97
4	5.3	6.97
5	5.3	6.96

Point-Number	Height change [cm/day]	Time-span [days]
6	4.6	6.96
7	5.8	6.95
8	5.6	6.95
9	4.9	6.94
10	4.7	6.94

Point-Number	Height change [cm/day]	Time-span [days]
11	4.3	6.93
12	4.3	6.93
13	4.7	6.92
14	4.2	6.91

Profile VIII

Upper Matthes Glacier

Epoch 0: 01.08.1993
Epoch 1: 05.08.1993

Point-Number	Height change [cm/day]	Time-span [days]
1	5.4	3.93
2	5.0	3.93
3	4.5	3.93
4	4.9	4.03
5	4.7	4.05

Point-Number	Height change [cm/day]	Time-span [days]
6	4.6	4.09
7	5.7	4.10
8	5.0	4.10
9	5.2	4.09

Point-Number	Height change [cm/day]	Time-span [days]
10	6.2	4.09
11	4.2	4.07
12	4.5	4.08
13	6.7	4.06

Epoch 0: 06.08.1995
Epoch 1: 10.08.1995

Point-Number	Height change [cm/day]	Time-span [days]
1	6.0	4.02
2	4.6	3.99
3	6.3	3.96
4	6.1	3.93

Point-Number	Height change [cm/day]	Time-span [days]
5	5.4	3.90
6	4.3	3.86
7	2.9	4.02
8	4.3	3.96

Point-Number	Height change [cm/day]	Time-span [days]
9	3.9	3.93
10	4.6	3.90
11	3.8	3.87
12	4.6	3.84

Epoch 0: 02.08.1996
Epoch 1: 10.08.1996

Point-Number	Height change [cm/day]	Time-span [days]
1	0.5	7.97
2	0.5	7.97
3	1.3	7.97
4	5.2	7.97

Point-Number	Height change [cm/day]	Time-span [days]
5	5.3	7.97
6	5.0	7.98
7	0.3	7.99
8	0.4	7.99

Point-Number	Height change [cm/day]	Time-span [days]
9	0.4	7.99
10	0.9	8.00
11	5.5	8.01
12	-1.4	8.01

Profile VIIIa

Matthes / Vaughan-Lewis Glacier Divide

Epoch 0: 05.08.1995
Epoch 1: 11.08.1995

Point-Number	Height change [cm/day]	Time-span [days]
1	4.9	5.97
3	5.0	6.04
4	5.0	5.91

Point-Number	Height change [cm/day]	Time-span [days]
5	5.3	5.95
6	4.2	5.88
7	5.4	5.88

Point-Number	Height change [cm/day]	Time-span [days]
8	5.5	5.89
9	5.0	5.89

Profile IX

Upper Vaughan-Lewis Glacier

Epoch 0: 03.08.1996
Epoch 1: 09.08.1996

Point-Number	Height change [cm/day]	Time-span [days]
1	0.9	5.86
2	0.1	5.86
3	3.8	5.85

Point-Number	Height change [cm/day]	Time-span [days]
4	1.0	5.85
5	0.7	5.85
6	-0.3	5.85

Point-Number	Height change [cm/day]	Time-span [days]
7	0.6	5.85
8	-2.7	5.85

Profile X

Matthes / Llewellyn Glacier Divide

Epoch 0: 05.08.1995
Epoch 1: 14.08.1995

Point-Number	Height change [cm/day]	Time-span [days]
1	*	9.06
2	2.9	9.03
3	2.8	8.99
4	2.5	8.93
5	3.1	8.90

Point-Number	Height change [cm/day]	Time-span [days]
6	2.5	8.86
7	2.5	8.83
8	2.7	8.80
10	2.4	8.74
11	2.2	8.71

Point-Number	Height change [cm/day]	Time-span [days]
12	2.1	8.68
13	2.9	7.98
14	2.4	7.98
15	2.0	6.77
16	2.7	6.73

Epoch 0: 04.08.1996
Epoch 1: 10.08.1996

Point-Number	Height change [cm/day]	Time-span [days]
16	-1.6	6.01
17	-1.2	6.01
18	-1.0	6.00
19	-1.5	6.00
20	-0.8	6.00

Point-Number	Height change [cm/day]	Time-span [days]
21	-0.8	6.00
22	-0.8	6.00
23	-0.7	5.909
24	-1.1	5.98
25	-1.1	5.98

Point-Number	Height change [cm/day]	Time-span [days]
26	0.0	5.98
27	-0.3	5.97
28	-1.3	5.97
29	0.0	5.97

Profile XI

Llewellyn Glacier

Epoch 0: 07.08.1995
Epoch 1: 13.08.1995

Point-Number	Height change [cm/day]	Time-span [days]
1	4.9	6.23
2	3.1	6.19
3	4.2	6.16
4	3.1	6.12

Point-Number	Height change [cm/day]	Time-span [days]
5	2.6	6.08
6	*	6.05
7	3.3	6.01
8	4.4	5.97

Point-Number	Height change [cm/day]	Time-span [days]
9	4.0	5.94
10	4.0	5.90
11	5.5	5.86

Appendix D

Long-Term Height Changes

The following tables show the long-term height changes of various profiles for the years 1952 to 1996:

- Profile IV
  Taku Glacier (Camp 10)
  - 1993/1994
  - 1994/1995
  - 1995/1996
- Profile V
  SW-Branch Taku Glacier
  - 1995/1996
- Profile VIII
  Upper Matthes Glacier
  - 1952/1993
  - 1995/1996
- Profile IX
  Upper Vaughan-Lewis Glacier
  - 1995/1996

Profile IV

Taku Glacier – Camp 10

Epoch 0: July 25, 1993
Epoch 1: July 25, 1994

Point-No.	Height change [m]
1	- 0.14
2	0.09
3	0.14
4	0.26
5	0.12
6	0.13
7	0.23
8	0.33
9	0.40
10	0.36
11	0.61
12	0.23
13	0.10
14	0.27
15	- 0.01
16	0.35
17	0.34
18	0.00
19	0.10
20	0.44
21	0.19
22	0.09
23	- 0.31
24	0.19
25	0.29
26	0.65
27	0.06

Epoch 0: July 25, 1994
Epoch 1: July 25, 1995

Point-No.	Height change [m]
1	- 0.63
2	- 0.95
3	- 0.75
4	- 0.96
5	- 0.87
6	- 0.99
7	- 0.85
8	- 0.79
9	- 0.83
10	- 1.12
11	- 0.86
12	- 1.04
13	- 1.01
14	- 1.24
15	- 1.31
16	- 1.41
17	- 1.41
18	- 1.58
19	- 1.38
20	- 1.38
21	- 1.28
22	- 1.24
23	- 1.69
24	- 1.22
25	- 1.46
26	- 0.77
27	- 1.17
28	- 1.23
29	- 0.95
30	- 1.37
31	- 1.02

Epoch 0: July 25, 1995
Epoch 1: July 25, 1996

Point-No.	Height change [m]
1	- 0.75
2	- 0.81
3	- 0.70
4	- 0.86
5	- 0.45
6	- 0.89
7	- 0.84
8	- 1.12
9	- 1.05
10	- 1.06
11	- 0.66
12	- 0.64
13	- 0.97
14	- 0.64
15	- 0.78
16	- 0.50
17	- 0.59
18	- 0.20
19	- 0.41
20	- 0.36
21	- 0.48
22	- 0.42
23	- 0.18
24	- 0.67
25	- 0.38
26	- 0.85
27	- 0.69
28	- 0.71
29	- 0.67
30	- 0.70
31	- 0.67

Profile V

SW-Branch Taku Glacier

Epoch 0: July 29, 1994
Epoch 1: July 29, 1995

Point-No.	Height change [m]
1	- 1.08
2	- 1.17
3	- 1.15
4	- 1.27

Point-No.	Height change [m]
5	- 1.05
6	- 1.13
7	- 1.35
8	- 1.27

Point-No.	Height change [m]
9	- 1.36
10	- 1.34
11	- 1.34
12	- 1.34

Profile VIII

Upper Matthes Glacier

Upper Matthes Glacier Height Profile

Epoch 0: August, 1952
Epoch 1: August, 1993

Point-No.	Height change [m]
1	- 1.7
2	- 0.5
3	- 0.3
4	1.8
5	4.3
6	11.3

Point-No.	Height change [m]
7	18.8
8	19.3
9	17.5
10	11.4
11	13.0

Point-No.	Height change [m]
12	15.7
13	14.1
14	13.5
15	- 2.1
16	- 6.1

Profile VIII – Upper Matthes Glacier

Epoch 0: August 10, 1995
Epoch 1: August 10, 1996

Point-No.	Height change [m]
1	- 0.86
2	- 0.88
3	- 0.70
4	- 1.04

Point-No.	Height change [m]
5	- 1.06
6	- 1.23
7	- 0.92
8	- 0.86

Point-No.	Height change [m]
9	- 0.78
10	- 0.66
11	- 0.87
12	- 1.11

Profile IX

Upper Vaughan-Lewis Glacier

Epoch 0: August 9, 1995
Epoch 1: August 9, 1996

Point-No.	Height change [m]
1	- 1.48
2	- 1.42
3	- 1.20

Point-No.	Height change [m]
4	- 1.27
5	- 0.96
3	- 0.53

Point-No.	Height change [m]
7	- 0.54
8	- 0.70

Appendix E

Strain Rates

The following tables show the strain rates on various profiles:

- Profile IV
  Taku Glacier (Camp 10)
  - 1993
  - 1994
  - 1995
  - 1996
- Profile A
  Gilkey Trench (Unnamed Glacier)
  - 1990
- Profile B
  Gilkey Trench (Trench Traverse)
  - 1990
- Profile C
  Gilkey Trench (Gilkey Glacier Curve)
  - 1990
- Profile D
  Gilkey Trench (Gilkey Glacier)
  - 1990
- Profile E
  Gilkey Trench (Little Vaughan-Lewis Glacier)
  - 1990
- Profile F
  Gilkey Trench (Vaughan-Lewis Glacier)
  - 1990

The abbreviations in the tables stand for:

$\dot{e}_1$ = Maximum principal strain rate (horizontal)

$\dot{e}_2$ = Minimum principal strain rate (horizontal)

Θ = Bearing of the maximum strain rate

Profile IV

Taku Glacier – Camp 10

July 20 – July 25, 1993

Triangle Points			$\dot{e}_1$ [μ strain/day]	$\dot{e}_2$ [μ strain/day]	Θ [gon]
1	2	3	20.8	- 16.8	131.36
2	3	4	25.0	- 40.9	166.32
3	4	5	162.7	- 76.4	113.22
4	5	6	176.9	- 184.0	197.94
5	6	7	262.2	- 234.5	112.74
6	7	8	273.3	- 303.0	198.76
7	8	9	349.7	-350.8	108.16
8	9	10	350.8	-389.0	195.67
9	10	11	279.6	- 291.7	109.86
10	11	12	280.3	- 181.2	192.62
11	12	13	127.4	- 136.6	113.06
12	13	14	151.8	- 125.2	183.72
13	14	15	65.0	- 82.2	119.87
14	15	16	83.6	- 50.1	171.45
15	16	17	56.3	- 58.8	143.58
16	17	18	44.5	- 64.0	168.35
17	18	19	- 9.6	- 33.3	100.96
18	19	20	13.1	- 10.4	91.78
19	20	21	11.3	- 37.1	196.49
20	21	22	54.1	- 37.9	109.45
21	22	23	81.0	-34.2	20.67
22	23	24	88.6	- 30.9	105.81
23	24	25	112.6	- 163.9	11.57
24	25	26	245.5	- 159.7	101.72
25	26	27	289.4	- 245.0	8.63

July 25 – August 05, 1994

Triangle Points			$\dot{e}_1$ [μ strain/day]	$\dot{e}_2$ [μ strain/day]	Θ [gon]
1	2	3	46.5	- 24.3	101.37
2	3	4	39.8	- 21.9	174.41
3	4	5	124.9	- 46.9	114.03
4	5	6	157.8	- 230.4	2.21
5	6	7	343.5	- 343.6	112.77
6	7	8	339.8	- 188.0	188.75
7	8	9	255.6	- 236.4	121.47
8	9	10	352.7	- 331.1	1.58
9	10	11	158.9	- 235.0	105.90
10	11	12	159.2	- 286.0	191.99
11	12	13	433.5	- 124.6	153.02
12	13	14	163.2	- 113.9	179.33
13	14	15	82.3	- 83.9	130.50
14	15	16	71.9	- 77.1	181.43
15	16	17	3.4	- 52.0	119.60
16	17	18	12.9	- 69.2	178.40
17	18	19	29.4	- 60.0	114.33
18	19	20	32.3	23.9	35.29
19	20	21	27.8	- 40.6	8.89
20	21	22	1.0	- 42.0	112.66
21	22	23	4.7	- 92.0	0.51
22	23	24	117.3	- 94.2	97.53
23	24	25	127.8	- 166.7	19.00
24	25	26	255.8	- 150.5	100.41
25	26	27	304.1	- 277.8	9.01
26	27	28	267.5	- 291.8	92.34
27	28	29	272.9	- 242.3	15.99
28	29	30	149.2	- 243.2	83.34
29	30	31	65.3	- 91.3	15.67

July 22 – July 28, 1995

Triangle Points			$\dot{e}_1$ [μ strain/day]	$\dot{e}_2$ [μ strain/day]	Θ [gon]
1	2	3	66.6	36.1	10.16
2	3	4	40.4	- 91.4	193.96
3	4	5	138.4	- 76.0	97.69
4	5	6	130.7	- 224.3	0.82
5	6	7	246.5	40.0	111.17
6	7	8	253.0	- 204.2	199.17
7	8	9	355.7	- 336.8	113.47
8	9	10	352.7	- 331.1	1.58
9	10	11	158.9	- 235.0	105.90
10	11	12	159.2	- 286.0	191.99
11	12	13	63.7	- 196.0	95.15
12	13	14	81.1	- 190.7	192.20
13	14	15	127.7	- 164.6	104.28
14	15	16	128.0	58.9	193.89
15	16	17	84.0	- 60.1	168.39
16	17	18	75.5	- 66.1	140.45
17	18	19	34.7	- 88.9	197.86
18	19	20	12.0	- 92.5	113.54
19	20	21	11.9	- 57.0	192.96
20	21	22	15.8	- 76.7	67.16
21	22	23	30.8	- 128.1	31.95
22	23	24	189.0	- 106.1	97.62
23	24	25	209.3	- 245.2	10.80
24	25	26	387.0	- 238.3	102.16
25	26	27	413.3	- 289.3	5.55
26	27	28	296.2	- 291.1	98.67
27	28	29	304.6	- 261.1	10.27
28	29	30	198.9	- 250.9	89.71
29	30	31	165.1	- 135.1	15.82

July 28 – August 06, 1996

Triangle Points			$\dot{e}_1$ [μ strain/day]	$\dot{e}_2$ [μ strain/day]	Θ [gon]
1	2	3	71.0	- 40.0	88.50
2	3	4	45.9	- 60.9	177.73
3	4	5	143.9	- 129.2	122.22
4	5	6	165.9	- 62.1	1.68
5	6	7	295.7	- 151.4	115.45
6	7	8	301.2	- 272.3	188.16
7	8	9	435.0	- 334.7	116.09
8	9	10	441.6	- 214.5	190.59
9	10	11	198.1	- 293.9	141.69
10	11	12	86.9	- 113.8	185.63
11	12	13	126.4	- 51.0	85.71
12	13	14	177.9	- 124.0	180.41
13	14	15	77.4	- 59.3	121.44
14	15	16	120.0	- 65.8	165.75
15	16	17	99.1	- 46.3	139.16
16	17	18	100.4	- 41.1	165.26
17	18	19	74.3	- 36.0	143.65
18	19	20	106.9	- 11.7	154.06
19	20	21	208.4	- 133.3	153.44
20	21	22	396.5	- 42.2	131.19
21	22	23	378.9	- 15.6	196.02
22	23	24	208.0	- 37.6	123.56
23	24	25	207.7	- 258.9	199.11
24	25	26	271.4	- 261.6	98.55
25	26	27	318.6	- 620.7	5.00
26	27	28	364.9	- 682.9	88.84
27	28	29	460.5	- 249.6	33.67
28	29	30	177.3	- 214.8	87.98
29	30	31	120.3	- 80.6	13.15

Profile A

Gilkey Trench – Unnamed Glacier

July 10 – July 16, 1990

Triangle Points			$\dot{e}_1$ [μ strain/day]	$\dot{e}_2$ [μ strain/day]	Θ [gon]
1	2	3	- 7.9	- 154.7	161.31
2	3	4	103.1	- 236.0	63.63
3	4	5	32.3	- 141.8	121.01

Profile B

Gilkey Trench – Trench Traverse

July 11 – July 16, 1990

Triangle Points			$\dot{e}_1$ [μ strain/day]	$\dot{e}_2$ [μ strain/day]	Θ [gon]
1	2	3	549.2	- 543.9	22.32
2	3	4	408.7	- 416.6	89.57
3	4	5	285.1	- 335.9	184.45
4	5	6	200.9	- 85.1	103.03
4	6	8	160.6	- 410.2	84.58
6	7	8	34.7	- 184.5	99.12
7	8	9	83.1	- 9.0	115.35
8	9	10	28.6	143.2	114.05
9	10	11	- 15.2	- 161.6	5.15
10	11	12	- 44.3	- 148.5	69.79
11	12	13	5.9	- 96.4	154.37
12	13	14	- 0.2	- 75.0	14.51
13	14	15	57.2	- 177.1	111.25

Profile C

Gilkey Trench – Gilkey Glacier Curve

July 11 – July 16, 1990

Triangle Points			$\dot{e}_1$ [μ strain/day]	$\dot{e}_2$ [μ strain/day]	Θ [gon]
1	4	5	272.6	- 393.5	51.33
1	2	5	305.2	- 197.0	26.64
2	3	5	333.2	- 515.3	53.45
3	5	6	522.8	- 490.6	3.80

Profile D

Gilkey Trench – Gilkey Glacier

July 11 – July 16, 1990

Triangle Points			$\dot{e}_1$ [μ strain/day]	$\dot{e}_2$ [μ strain/day]	Θ [gon]
1	2	3	142.0	- 758.9	174.17
2	3	4	331.6	- 182.5	151.80
3	4	5	451.7	- 130.6	66.69
4	5	6	73.0	- 977.8	174.26
5	6	7	1,022.9	- 406.7	120.69
6	7	8	1,152.0	- 210.4	54.53
7	8	9	- 58.7	- 857.8	195.12

Profile E

Gilkey Trench – Little Vaughan-Lewis Glacier

July 11 – July 16, 1990

Triangle Points			$\dot{e}_1$ [μ strain/day]	$\dot{e}_2$ [μ strain/day]	Θ [gon]
1	2	3	614.5	- 285.1	81.03

Profile F

Gilkey Trench – Vaughan-Lewis Glacier

July 11 – July 16, 1990

Triangle Points			$\dot{e}_1$ [μ strain/day]	$\dot{e}_2$ [μ strain/day]	Θ [gon]
1	4	5	179.1	- 863.2	106.07
1	2	5	69.1	- 487.4	22.93
2	5	6	- 109.4	- 551.4	63.43
2	3	6	338.9	- 328.5	154.06
3	6	7	111.4	- 639.3	22.97

Appendix F

Coordinate Listing of JIRP Benchmarks

The following tables show the coordinates of the benchmarks of two surveying areas:

- Camp 10 area
- Camp 18 area

The abbreviations in the tables stand for:

- ✳ = Coordinates derived from GPS measurements
- – = Transformed to GPS determined passpoints

All coordinates are conformal coordinates (JIRP projection) referring to the ITRF 93 (see p. 138).

Camp 10 area

Date of last revision: August 31, 1997

Point Name	Point No.	GPS	Easting [m]	Northing [m]	Ellipsoidal Height [m]
FFGR 19	1	✳	488001.819	6503290.614	1180.835
FFGR 19B	1.1	–	488383.812	6503660.530	1241.866
FFGR 19D	1.2	–	488260.073	6503696.172	1254.266
FFGR 19C	1.3	✳	487983.650	6503410.034	1197.999
Taku B Lower	1.4	–	488291.605	6503745.868	-
Camp 10 North	1.5	–	487953.316	6503398.642	-
SW-Taku	2	–	487333.574	6495903.938	-
SW-Taku East	2.1	–	487312.700	6495908.412	-
SW-Taku Lower	2.2	✳	487320.590	6495968.918	1133.487
Taku A	3	–	490529.133	6501653.627	1512.038
Taku B	4	–	488584.437	6504541.022	1590.036
Taku B Cairn	4.1	–	488583.775	6504540.870	-
Taku C	5	–	485696.044	6506827.041	1545.431
Taku C Lower	5.1	–	485645.149	6506713.779	1528.351
Sunday Point	6	–	490254.409	6500611.311	-
Sunday Point Cairn	6.1	–	490235.701	6500682.263	-
Taku D	7	–	482941.369	6509777.053	-
Taku D Cairn (FFGR 65)	7.1	✳	482942.071	6509779.957	1774.108
Taku D Lower	8	✳	482601.539	6509092.743	1399.212
Camp 9	9	✳	489442.431	6510665.042	1554.938
Camp 9 Cairn	9.1	–	489443.183	6510663.361	-
NW-Taku	10	✳	479186.763	6505147.717	1402.060
NW-Taku Cairn	10.1	✳	479188.345	6505144.633	1402.149
Shoehorn Peak	11	–	482657.922	6500295.567	1326.342
Juncture Peak	12	–	485056.994	6498619.047	1339.311
Juncture Peak Lower	12.1	–	485424.713	6498221.909	-
Bavaria Point	13	–	489420.666	6501375.002	-
Glacier King	14	–	474734.289	6509446.896	1481.238
Glacier King Cairn	14.1	–	474736.005	6509445.705	-
Camp 10A	15	✳	489181.351	6501882.011	1105.757
Vantage Peak	16	–	490390.615	6504291.679	1709.737
Twin Peak Geodetic	17	–	500177.078	6499821.685	-
Mount Moore	18	–	492458.688	6521225.686	2176.952

Point Name	Point No.	GPS	Easting [m]	Northing [m]	Ellipsoidal Height [m]
Mount Moore Cairn	18.1	–	492460.494	6521228.959	-
Scott	19.1	✳	487963.303	6503372.111	1189.739
Exploration Peak	-	–	487450.796	6507809.503	-

Camp 18 area

Date of last revision: August 31, 1997

Point Name	Point No.	GPS	Easting [m]	Northing [m]	Ellipsoidal Height [m]
FFGR 45 (Camp 18 - Hill)	1	✳	484309.150	6524412.394	1746.191
Camp 8	2	–	492140.788	6521149.048	-
FFGR 31 (Camp 8)	2.1	✳	492136.624	6521147.773	2051.576
FFGR 39 (Blizzard Point)	4	✳	487443.145	6524360.975	1984.385
FFGR 68 (Camp 18 - Hill)	5	✳	484425.554	6524412.335	1751.611
FFGR 24 (Camp 18 - Hill)	6	✳	484189.635	6524371.872	1733.416
FFGR 43 (Camp 18)	7	✳	483990.101	6524352.738	1703.762
FFGR 44 (Cleaver)	8	✳	483834.598	6524280.382	1669.527
FFGR 31 (Cleaver)	9	✳	483705.534	6524279.606	1623.548
FFGR 49 (Cleaver)	11	–	483244.123	6524040.612	-
FFGR 48 (Cleaver)	12	–	483375.593	6524007.974	-
Camp 19	14	–	482226.811	6522614.250	-
FFGR 18 (Camp 19)	15	–	482294.684	6522477.554	-
FFGR 12 (Camp 19)	16	✳	482221.820	6522621.728	1292.865
Mammary Peak	18	–	484896.212	6522671.400	1929.813
FFGR 63 (Camp 18 - Hill)	22	✳	484315.335	6524309.996	1723.699
FFGR 64 (Camp 18 - Hill)	23	✳	484219.214	6524334.390	1727.783
Camp 19 TL	25	–	482224.893	6522611.681	-
FFGR 04 (Cleaver)	26	✳	483309.746	6524118.094	1388.753
FFGR 53 (Camp 19)	27	✳	482195.157	6522670.922	1277.773
FFGR 42 (Cleaver)	28	–	483435.183	6524134.408	1426.096
N1 (Camp 18)	29	✳	484073.444	6524262.764	1698.457
N2 (Camp 18)	30	✳	483956.324	6524239.526	1682.217
FFGR 34 (Camp 18 - Hill)	31	✳	484554.464	6524402.905	1734.890
FFGR 62 (F 10 Point)	32	✳	492497.562	6535469.195	1860.563

Schriftenreihe des Studiengangs Vermessungswesen der Universität der Bundeswehr München

Edited Volumes:

1/78 *A. Schödlbauer:* Curriculum für den wissenschaftlichen Studiengang Vermessungswesen der Hochschule der Bundeswehr München. 53 S.; DM 10,--; vergriffen

2/78 *A. Chrzanowski and E. Dorrer (Eds.):* Proceedings "Standards and Specifications for Integrated Surveying and Mapping Systems". Workshop held in Munich, 1-2 June 1977. 181 S.; DM 20,--

3/78 *W. Caspary und A. Geiger:* Untersuchungen zur Leistungsfähigkeit elektronischer Neigungsmesser. 62 S.; DM 10,--

4/79 *E. Baumann, W. Caspary, H. Dupraz, W. Niemeier, H. Peluer, E. Kuntz, G. Schmitt, W. Welsch:* Seminar über Deformationsanalysen. 106 S.; DM 15,--

5/81 *K. Torlegård:* Accuracy Improvement in Close Range Photogrammetry. 68 S.; DM 10,--

6/82 *W. Caspary und W. Welsch (Hrsg.):* Beiträge zur großräumigen Neutrassierung. 268 S.; DM 20,--

7/82 *K. Borre and W. M. Welsch (Eds.):* Proceedings „Survey Control Networks". Meeting of FIG-Study Group 5B, Aalborg, July 7-9, 1982. 428 S.; DM 35,--

8/82 *A. Geiger:* Entwicklung und Erprobung eines Präzisionsneigungstisches zur Kalibrierung geodätischer Instrumente. 124 S.; DM 10,--

9/83 *W. Welsch (Hrsg.):* Deformationsanalysen ′83. 336 S.; DM 25,--

10/84 *W. Caspary, A. Schödlbauer und W. Welsch (Hrsg.):* Beiträge aus dem Institut für Geodäsie. 241 S.; DM 20,--

11/84 *W. Caspary und H. Heister (Hrsg.):* Elektrooptische Präzisionsstreckenmessung. 268 S.; DM. 20,--; vergriffen

12/84 *P. Schwintzer:* Analyse geodätisch gemessener Punktlageänderungen mit gemischten Modellen. 155 S.; DM 15,--

13/84 *G. Oberholzer:* Landespflege in der Flurbereinigung. 80 S.; DM 10,--

14/84 *G. Neukum mit Beiträgen von G. Neugebauer:* Fernerkundung der Planeten und kartographische Ergebnisse. 100 S.; DM 25,--

15/84 *A. Schödlbauer und W. Welsch (Hrsg.):* Satelliten-Doppler-Messungen. Beiträge zum Geodätischen Seminar 24./25. September 1984. 394 S.; DM 30,--

16/85 *M. K. Szacherska, W. M. Welsch:* Geodetic Education in Europe. 230 S.; DM 20,--; vergriffen

17/86 *B. Eissfeller, G. W. Hein:* A Contribution to 3d-Operational Geodesy, Part 4: The Observation Equations of Satellite Geodesy in the Model of Integrated Geodesy. 189 S.; DM 20,--

18/85 *G. Oberholzer:* Landespflege in der Flurbereinigung, Teil II. 114 S.; DM 12,--

19/86 *H. Landau, B. Eissfeller and G. W. Hein:* GPS Research 1985 at the Institute of Astronomical and Physical Geodesy. 210 S.; DM 20,--

20/85 *W. Welsch and L. A. Lapine (Eds.):* Proceedings "Inertial, Doppler and GPS Measurements for National and Engineering Surveys". Joint Meeting of Study Groups 5B and 5C, July 1-3 1985; 2 Bände. 630 S.; DM 50,--

21/86 *G. Oberholzer:* Landespflege in der Flurbereinigung, Teil III. 97 S.; DM 12,--

22/87 *W. Caspary, G. Hein, A. Schödlbauer (Hrsg.):* Beiträge zur Inertialgeodäsie. Geodätisches Seminar 25./26. September 1986. 388 S.; DM 30,--

23/87 *E. Dorrer und J. Peipe (Hrsg.):* Motografie. Symposium 11./12. März 1986. 280 S.; DM 30,--

24/87 *G. Neugebauer (Hrsg.):* Brenta-Monographie – Grundlagenforschung auf dem Gebiet der Hochgebirgskartographie. 188 S.; DM 30,--

25/87 *A. Perelmuter:* Beiträge zur Ausgleichung geodätischer Netze. 75 S.; DM 10,--

26/87 *W. Ellmer:* Untersuchung temperaturinduzierter Höhenänderungen eines Großturbinentisches. 105 S.; DM 12,--

27/87 *H. Heister:* Zur automatischen Kalibrierung geodätischer Längenmeßinstrumente. 210 S.; DM 20,--

28/87 *E. H. Paßberger:* Systemstudie zur Sicherung ökologischer Vorrangflächen mittels Bodenordnung in Bayern. 183 S.; DM 20,--

29/87 *H. Glasmacher:* Die Gaußsche Ellipsoid-Abbildung mit komplexer Arithmetik und numerischen Näherungsverfahren. 121 S.; DM 13,--

30/87 *Y. Zhang:* Beiträge zum Entwurf von optimalen Beobachtungsplänen für tektonische Überwachungsnetze. 145 S.; DM 15,--

31/88 *W. Lechner:* Untersuchung einer kreiselorientierten Landfahrzeug-Navigationsanlage im Hinblick auf geodätische Anwendungen und Möglichkeiten der Höhenübertragung. 159 S.; DM 15,--

32/88 *R. König:* Zur Fehlertheorie und Ausgleichung inertialer Positionsbestimmungen. 138 S.; DM 15,--

33/88 *H. Borutta:* Robuste Schätzverfahren für geodätische Anwendungen. 158 S.; DM 15,--

34/88 *H. Landau, K. Hehl, B. Eissfeller, G. W. Hein, I. W. Reilly:* Operational Geodesy Software Packages. 323 S.; DM 30,--

35/88 *G. Oberholzer, E. Paßberger:* Landespflege in der Flurbereinigung, Teil IV. 149 S.; DM 15,--

36/88 *H. Landau:* Zur Nutzung des Global Positioning Systems in Geodäsie und Geodynamik: Modellbildung, Softwareentwicklung und Analyse. 284 S.; DM 28,--

37/88 *B. Eissfeller:* Analyse einer geodätischen raumstabilisierten Inertialplattform und Integration mit GPS. 321 S.; DM 32,--

38/89 *A. Schödlbauer (Hrsg.):* Moderne Verfahren der Landesvermessung. Beiträge zum 22. DVW-Seminar 12.-14. April 1989. Teil I: Global Positioning System. 354 S.; Teil II: Nivellement, Vermessungskreisel. 194 S.; DM 50,--

39/89 *N. Kersting, W. Welsch (Hrsg.):* Rezente Krustenbewegungen. Seminar 08./09. Juni 1989. 303 S.; DM 30,--

40/89 *G. Oberholzer:* Ländliche Kulturgeschichte und Landentwicklung. 210 S.; DM 20,--

41/90 *G. W. Hein, K. Hehl, B. Eissfeller, M. Ertel, W. Jacoby, D. Czerek:* On Gravity Prediction Using Density and Seismic Data. 148 S.; DM 15,--

42/92 *N. Kersting:* Zur Analyse rezenter Krustenbewegungen bei Vorliegen seismotektonischer Dislokationen. 246 S.; DM 25,--

43/92 *K. Hehl:* Bestimmung von Beschleunigungen auf einem Träger durch GPS und digitale Filterung. 215 S.; DM 20,--

44/92 *W. Oswald:* Zur kombinierten Ausgleichung heterogener Beobachtungen in hybriden Netzen. 128 S.; DM 13,--

45/93 *Institut für Geodäsie (Hrsg.):* Das Global Positioning System im praktischen Einsatz der Landes- und Ingenieurvermessung. Beiträge zum Geodätischen Seminar 12.-14. Mai 1993. 314 S.; DM 30,--

46/94 *K. Brunner und J. Peipe (Hrsg.):* Festschrift für Prof. Dr.-Ing. Egon Dorrer zum 60. Geburtstag. 254 S.; DM 20,--

47/94 *K.-H. Thiemann:* Die Renaturierung strukturarmer Intensivagrargebiete in der Flurbereinigung aus ökologischer und rechtlicher Sicht. Band 1: Kapitel 1-3, 420 S.; Band 2: Kapitel 4-5, 220 S.; DM 50,--

48/94 *Chr. Schwiertz:* Experimente zur GPS-gestützten Aerotriangulation unter besonderer Berücksichtigung systematischer Einflüsse. 189 S.; DM 20,--

49/95 *R. Scheuring:* Zur Qualität der Basisdaten von Landinformationssystemen. 122 S.; DM 13,--

50/97 *W. M. Welsch, M. Lang and M. M. Miller (Eds.):* Geodetic Activities, Juneau Icefield, Alaska, 1981-1996. 268 S.; DM 28,--